

**Landscape response to glacial-interglacial  
cycles: insights from a southern North Sea  
offshore wind farm dataset**

Stephen James Eaton

Submitted in accordance with the requirements of the degree  
of Doctor of Philosophy

The University of Leeds  
School of Earth and Environment

March 2021



## Declaration

The candidate confirms that the work submitted is his own, except where work which has formed part of jointly authored publications has been included. The contribution of the candidate and the other authors to this work has been explicitly indicated below. The candidate confirms that appropriate credit has been given within the thesis where reference has been made to the work of others.

The work in chapter 3 is published in *Journal of Quaternary Science*:

Eaton, S.J., Hodgson, D.M., Barlow, N.L., Mortimer, E.E. and Mellett, C.L., 2020. Palaeogeographical changes in response to glacial–interglacial cycles, as recorded in Middle and Late Pleistocene seismic stratigraphy, southern North Sea. *Journal of Quaternary Science*, 35(6), pp.760-775. <https://doi.org/10.1002/jqs.3230>

As lead author, Stephen James Eaton was responsible for data analysis, interpretation, and manuscript and figure preparation. The role of other co-authors was limited to discussion of results and manuscript editing.

This copy has been supplied on the understanding that it is copyright material and that no quotation from the thesis may be published without proper acknowledgement.

The right of Stephen James Eaton to be identified as Author of this work has been asserted by Stephen James Eaton in accordance with the Copyright, Designs and Patents Act 1988.

## **Acknowledgements**

I would like to thank my supervisors. David Hodgson for providing support and enthusiasm throughout this project, always being available to discuss the wonders of sedimentology, whilst providing guidance, mentoring and a sense of realism to ensure I achieved my goals. Natasha Barlow, for her constant support and faith, and for enabling me to develop into a Quaternary geologist that will prove invaluable to my future career. Thanks to Estelle Mortimer for guidance with seismic during the early stages of this research.

To Claire Mellett whose knowledge of coastal and landscape evolution proved invaluable, and for providing access to, and advice in the interpretation of sediment cores and palaeoenvironmental data that have proved crucial to this research.

Many thanks to Vattenfall, my industrial sponsor, who gave access to this wonderful dataset, and in particular Andrew Galbraith who has always endeavoured to help in any way he can, and to provide enthusiasm for the research.

To Wessex Archaeology for providing access to their core store and facilities, and their employees for a unique insight into the world of archaeology.

The School of Geography labs and the Cohen labs are also thanked for assistance with sample preparation and analysis. In particular Rachel Gasior and David Ashley who often bumped my samples to the front of the queue and enabled my research to stay on track.

To Catherine, Ophelia, Camilla, and Josephine who have always had faith in me and remained constantly enthusiastic – Thank you.

## Abstract

Landscape evolution during periods of Quaternary climate change can be reconstructed using integrated subsurface datasets acquired by the offshore wind industry. Reconstruction of landscapes that evolved during changes in past climates aid understanding the responses to future changes in climate. The bathymetry of the southern North Sea region makes it an attractive location for wind farm developments. The integration of a dense 2D grid of seismic reflection data, with sedimentological and geotechnical data, allow detailed documentation of depositional environments and landscape evolution from the Middle Pleistocene to present day over a 1040 km<sup>2</sup> area.

The stratigraphic architecture records multiple phases of transgression and regression linked to multiple glacial-interglacial cycles and relative sea-level change. Middle Pleistocene stratigraphy (MIS 19-13) reveals a predominantly fluvial depositional environment, with northward draining river valleys that are filled with a seismic architecture that support changing depositional environments from terrestrial to marginal marine. North-south orientated tunnel valleys provide evidence for subglacial conditions and southwards drainage, most likely during the Anglian stage (MIS 12). During the late Pleistocene (MIS 5d-2), a regressive stratigraphy is preserved, with geomorphology and stratigraphy recording multiple fluctuations in relative sea level in an overall low energy setting. Late Devensian postglacial stratigraphy reveals a terrestrial landscape with southward draining fluvial networks contemporaneous with peats that formed in freshwater wetlands. Early Holocene geomorphological features record marine transgression across a low relief coastal plain. Carbon stocks of postglacial peats are estimated and upscaled for the southern North Sea (726 Mt). The peats crop out on the seabed, and their susceptibility to reworking is considered.

The landscape evolution of the study area has revealed abrupt and opposing drainage directions, subglacial conditions, and postglacial marine transgression. Subtle topographic relief is a primary control on sedimentary process, and stratigraphic preservation. Improved 3D understanding of the subsurface has direct commercial application to the offshore wind industry, and for informing understanding of landscape response to changing climate.

# Contents

<b>Declaration</b> .....	<b>iii</b>
<b>Acknowledgements</b> .....	<b>iv</b>
<b>Abstract</b> .....	<b>v</b>
<b>List of tables</b> .....	<b>x</b>
<b>List of Figures</b> .....	<b>xi</b>
<b>Chapter 1 - Introduction</b> .....	<b>1</b>
1.1. Motivation.....	1
1.2. Southern North Sea Region.....	2
1.2.1. The southern North Sea - a unique geological setting.....	2
1.2.2. Deep-time and Early Pleistocene geological history southern North Sea.....	2
1.2.3. North Sea glaciation history.....	4
1.2.4. Postglacial landscapes of the southern North Sea .....	8
1.2.5. Carbon stores in coastal plain environments .....	8
1.3. Research questions .....	9
1.3.1. How has the preservation and distribution of rivers changed from Middle Pleistocene to present day in the southern North Sea region? .....	9
1.3.2. Are buried and submerged postglacial peats a carbon sink or source, and should they be a consideration in carbon stock estimates? .....	11
1.3.3. How does inherited stratigraphic architecture influence present-day seabed sediment and bedform configuration in the southern North Sea? .....	12
1.3.4. How do low relief landscapes respond to/record changes in relative sea-level changes? .....	13
1.4. Thesis structure.....	15
<b>Chapter 2 - Methods</b> .....	<b>17</b>
2.1. Geophysical data .....	17
2.1.1. Acquisition and resolution .....	17
2.1.2. Interpretation .....	22

2.1.3.	Mapping and GIS .....	23
2.2.	Vibrocores .....	24
2.2.1.	Acquisition and storage.....	24
2.2.2.	Interpretation .....	25
2.3.	Geotechnical logs.....	26
2.3.1.	Acquisition .....	26
2.3.2.	Interpretation .....	27
2.4.	Geophysical and sedimentological correlation .....	27
2.5.	Sediment samples and organic carbon analysis.....	28
2.5.1.	Sampling .....	28
2.5.2.	Sample preparation and bulk density measurement.....	28
2.5.3.	Carbon analysis .....	29
2.6.	Applications of methods to data.....	31
<b>Chapter 3 - Palaeogeographic changes in response to glacial-interglacial cycles, as recorded in Middle and Late Pleistocene seismic stratigraphy, southern North Sea .....</b>		<b>32</b>
3.1.	Introduction.....	32
3.2.	Study area .....	34
3.3.	Geological setting.....	34
3.4.	Data collection.....	38
3.4.1.	Seismic data acquisition and interpretation.....	38
3.4.2.	Vibrocoring and cone penetration tests .....	38
3.5.	Results.....	39
3.5.1.	Seismic stratigraphy.....	40
3.5.2.	Synthesis of lithology and CPT data with seismic stratigraphy.....	48
3.5.3.	Vibrocores and CPT control.....	48
3.6.	Regional seismic stratigraphic context .....	51
3.7.	Discussion .....	52
3.7.1.	MIS ~19 to 13 (L4) depositional environments.....	52
3.7.2.	MIS 12 (L3) depositional environments.....	54
3.7.3.	MIS 5d to 2 (L2) depositional environments .....	55
3.7.4.	Opposing sediment transport directions .....	60
3.8.	Conclusions.....	60
<b>Chapter 4 - Postglacial landscapes of the southern North Sea .....</b>		<b>62</b>
4.1.	Introduction.....	62

4.2.	Setting .....	64
4.3.	Methods.....	65
4.3.1.	Seismic data.....	65
4.3.2.	Bathymetry data .....	65
4.3.3.	Vibrocores .....	67
4.4.	Results .....	67
4.4.1.	Seismic stratigraphic interpretation .....	67
4.4.2.	Vibrocore interpretation.....	79
4.4.3.	Cone penetration tests interpretation .....	83
4.5.	Palaeoenvironmental analysis .....	84
4.5.1.	NV WEST (cores VC074, 76 and 85).....	85
4.5.2.	Boreas (VC028, 32 and 39) .....	86
4.6.	Radiocarbon dating .....	86
4.6.1.	NV West radiocarbon dates.....	88
4.6.2.	Boreas radiocarbon dates.....	88
4.7.	Sedimentary environments .....	89
4.8.	Discussion.....	90
4.8.1.	Postglacial fluvial processes.....	90
4.8.2.	Origin and age of incisional features (IU) .....	91
4.8.3.	Relict tidal drainage channels.....	92
4.8.4.	Relict tidal ponds.....	96
4.8.5.	Peatland palaeoenvironment, morphology, chronology and preservation .....	99
4.9.	Conclusion.....	101
<b>Chapter 5 - Submerged postglacial peat carbon stocks, in the southern North Sea .....</b>		<b>102</b>
5.1.	Introduction.....	102
5.2.	Study area.....	103
5.3.	Seismic analysis.....	104
5.3.1.	Seismic facies and stratigraphy .....	104
5.3.2.	Seismic anomaly SAU .....	106
5.3.3.	Seismic unit L1.....	106
5.4.	Vibrocore and Cone Penetration Test (CPT) analysis .....	108
5.4.1.	Core lithofacies and stratigraphic contacts.....	109
5.5.	Palaeoenvironmental interpretation.....	114



5.6. Core analysis.....	114
5.6.1. Bulk density and carbon analysis .....	114
5.6.2. Peat classification and quantification methods. ....	114
5.7. Results.....	119
5.7.1. SAU thickness.....	119
5.7.2. Dry bulk density and organic carbon .....	124
5.7.3. Volumetrics.....	128
5.7.4. Sediment mass and carbon stock quantification.....	128
5.8. Discussion .....	129
5.8.1. Carbon stock estimates and methods .....	129
5.8.2. Holocene coastal evolution - implications for carbon storage in postglacial peats .....	130
5.8.3. Peat distribution southern North Sea region – upscaled carbon stocks .....	133
5.9. Conclusion.....	136
<b>Chapter 6 - Discussion and conclusions .....</b>	<b>137</b>
6.1. How does integrated subsurface data required for offshore windfarms improve understanding of Quaternary palaeo-drainage networks feeding into the southern North Sea basin? .....	137
6.1.1. Glacial-interglacial delta plain landscape (~MIS 19-13).....	139
6.1.2. Subglacial terrestrial landscape (~MIS 12).....	140
6.1.3. Interglacial terrestrial to marine (transgressive) (~MIS 2)..	142
6.1.4. Opposing drainage directions .....	144
6.2. Are buried and submerged postglacial peats a carbon sink or source, and should they be a consideration in carbon stock estimates? .....	148
6.3. How does inherited stratigraphic architecture influence present-day seabed sediment and bedform configuration in the southern North Sea? 152	
6.4. How do low relief landscapes respond to and record changes in relative sea-level? .....	155
6.5. Application of research .....	157
6.5.1. Offshore wind farms.....	157
6.5.2. National carbon capital .....	157
6.6. Future work .....	158
6.6.1. Peat thickness classification using CPTs – pitfalls and limitations. ....	158
6.6.2. Provenance of Middle Pleistocene fluvial channel fills.....	158

6.7. Conclusions.....	159
6.7.1. How does integrated subsurface data required for offshore windfarms improve understanding of Quaternary palaeo-drainage networks feeding into the southern North Sea basin? .	159
6.7.2. Are buried and submerged postglacial peats a carbon sink or source, and should they be a consideration in carbon stock estimates? .....	160
6.7.3. How does inherited stratigraphic architecture influence present-day seabed sediment and bedform configuration in the southern North Sea?.....	161
6.7.4. How do low relief landscapes respond to/record changes in relative sea-level changes? .....	161
6.7.5. Concluding statement .....	162
<b>Reference .....</b>	<b>164</b>
<b>Appendix 1 – Bulk density analysis data.....</b>	<b>201</b>
<b>Appendix 2 – Total carbon analysis data.....</b>	<b>202</b>
<b>Appendix 3 - Organic carbon analysis data.....</b>	<b>205</b>

## List of Tables

Table 3.1. Summary of seismic facies identified and the seismic stratigraphic unit/surface they are associated with. Seismic descriptors used to characterize the facies are shown and seismic survey used to identify and characterize the facies are listed. Yellow is used to highlight seismic facies and the S2 surface is shown in blue.....	42
Table 3.2. Classification and interpretation of sedimentary facies according to lithological composition.....	49
Table 4.1. The classification scheme used in this study to characterise subaqueous dunes (after Ashley, 1990).....	67
Table 4.2. Accelerator Mass Spectrometry (AMS) radiocarbon dates for organic rich peat (Pt) intervals in six vibrocores across the NV West and Boreas sites. Depth of samples are shown in mbsf and mLAT. <sup>14</sup> C dates are calibrated using IntCal20 (Stuiver et al., 2020) and reported at the 2-sigma range. General position in peat interval and material dated are shown. ....	87
Table 5.1. A summary of the two principal seismic facies attributed to the L1 unit and SAU in NV West and Boreas.....	108
Table 5.2. List of CPTs and VCs used in this study (locations on figure 5.1) to investigate L1, SAU and L2 with the different data types available for each unit.....	108

Table 5.3. A summary of the SAU unit thickness at each vibrocore location defined using the M-V method. Where brackets have been used indicates that there are multiple SAU unit intervals within the vibrocore. * indicates where core photos have been used to define thickness. Depths relative to seabed.....	119
Table 5.4. A summary of the SAU unit thickness at each vibrocore location defined using the M-OC method. Depths relative to seabed. ....	120
Table 5.5. Mean DBD and OC values for both the SAU corresponding to methods M-V and M-OC. The mean DBD and OC for each vibrocore and the mean for each survey area and combined are shown with standard deviation.....	124
Table 5.6. SAU anomaly surface area and volume estimates for NV West, Boreas, and combined sites. Peat volume estimates have been calculated according to M-V and M-OC methodologies. ....	128
Table 5.7. Calculated peat mass following M-V and M-OC methodologies for NV West, Boreas and combined. Mean %OC for survey areas with M-V and M-OC methods applied. Calculated carbon stock for all survey areas with M-V and M-OC methods applied.....	128
Table 5.8. Carbon stocks upscaled and constrained by modelled palaeocoastlines at 11 ka and 9 ka. ....	136

## List of Figures

Figure 1.1. Drainage basin and delta of the Miocene–Pliocene–Early Pleistocene Eridanos river system, with a depiction of the former terrestrial environment in Middle-Pleistocene-glacial excavated areas that are nowadays seas. Black arrows indicate the former Eridanos fluvio-deltaic system and blue arrows show contributing fluvial systems from North West Europe (from Cohen et al., 2014). ....	4
Figure 1.2. Chronostratigraphical chart for the Middle to present-day showing the marine isotope stages and regional stage/substage divisions for NW Europe and Britain (after Gibbard and Cohen, 2008). ....	6
Figure 1.3 A compilation map showing the ice limits of the three main glaciations that occurred throughout the Middle to Late Pleistocene. In addition, published tunnel valleys that are associated with the three main glaciations are shown. These are the primary input to define ice limits in the offshore environment (Graham et al., 2011 (left and center maps); Ottesen et al., 2020 (right map)). ....	7
Figure 1.5. Previously defined terrestrial drainage networks identified in the southern North Sea region (Postglacial: Fitch et al. (2005), Gibbard (2007), Hepp et al. (2012) Gupta et al. (2017), Hepp et al. (2019), Prins et al. (2019), Emery et al. (2020); Anglian/Elsterian: Gibbard, (2007, Cohen et al. (2017); and Middle Pleistocene: Gibbard, (1988), Moorlock et al. (2002), and Busschers et al. (2007)). ....	11

Figure 1.6. Examples of the different antecedent topographical controls on transgressive deposits and the rate of transgression (Cattaneo et al., 2003).	13
Figure 1.7. Schematic models of coastal and shoreface products of marine transgression in cold-temperate (mid-latitude) and high-latitude shelf settings (Forbes et al., 2014).	15
Figure 2.1. Seismic reflection data coverage. Sub bottom profile and Ultra High Resolution seismic reflection data is available to the study over Norfolk Vanguard West, Boreas, and the Cable Route. Regional bathymetry data also shown, courtesy of (EMODnet Bathymetry Consortium, 2018).	17
Figure 2.2. Dense 2D grid of seismic reflection data is available to this study, with inlines orientated NW-SE and cross-lines orientated NE-SW. The inlines have a line spacing of 100 m, whilst the cross-lines have a spacing of 1 km.	18
Figure 2.3. Coverage of regional and site specific MBES data over Norfolk Vanguard West and Boreas. Regional surveys were acquired in 2010, and full coverage site surveys in 2015 and 2017.	19
Figure 2.4. Seabed seismic multiple present in UHR data in Norfolk Vanguard. The multiple obscures a key stratigraphic surface at Middle Pleistocene level (Top Yarmouth Roads Fm.).	20
Figure 2.5. Where large submarine bedforms (dunes and/or sand banks) are present, the underlying seismic (SBP) stratigraphy is poorly imaged.	20
Figure 2.6. Possible shallow gas anomalies present in both UHR and SBP seismic surveys.	21
Figure 2.7. The mobility of seabed sediments influences surface gridding. Data from inline M631 (15- 09-2016), xline X820 (29-10-2016) and the corresponding surface. Sediment movement occurring between inline and xline surveys creates artefact in gridded surface (Fugro, 2016).	21
Figure 2.8. Seismic facies descriptors used in this study, based on Mitchum et al. (1977) and Mellett et al. (2013).	23
Figure 2.9. Example of sediment cores logged and sampled at Wessex Archaeology (Salisbury). Example of a split sediment core ready for logging, and a whole core prior to being split.	25
Figure 2.10. An example of hand drawn sedimentary log. Log sheet design by Tim Cullen.	26
Figure 2.11. Soil Behaviour Type chart (Robertson et al., 1986) based on CPT cone resistance, qt, and friction ratio, Rf.	27
Figure 2.12. Mixer Mill MM 400 used to mill dried sediment samples.	29
Figure 2.13. A flow chart showing the laboratory process used to analyse for bulk density (DBD), total carbon (TC), organic carbon (OC).	30
Figure 2.14. An example of the elemental analyser used to analyse for TC and OC. Also shown are the silver capsules that sediment samples are measured into prior to folding and analysis.	30

Figure 3.1. The Norfolk Vanguard survey areas are located within the UK sector of the southern North Sea. Norfolk Vanguard comprises three survey areas: NV West, NV East and the cable route. The Norfolk Boreas survey area sits to the north-east. Ultra-high resolution (UHR) and sub bottom profile (SBP) seismic reflection surveys acquired over NV West and the cable route survey areas that are used in this paper. Locations for twenty-eight vibrocores and cone penetration tests (CPT) over the NV West and cable route survey areas. ....	34
Figure 3.2. Stratigraphic correlation framework for the Quaternary of the study area. (a) Marine isotope stages (Lisiecki and Raymo, 2005), (b) Global sea level estimates (Spratt et al., 2016), (c) British and European Stages (italics) (Based on Gibbard and Cohen, 2012), (d) Quaternary framework for the North Sea basin (based on Stoker et al., 2011a).....	36
Figure 3.3. Composite map showing maximum ice extents for three major Pleistocene glaciations (Anglian and Wolstonian - Hijma et al. (2012) and references there in, Devensian – Ehlers and Wingfield (1991) and Sejrup et al. (2016)). Tunnel valleys associated with the three major glaciations (Graham et al. 2011). Glacial lake formed between 400,000 to 450,000 years ago and dammed to the north by ice extending from the north (adapted from Cohen et al., 2017; Gibbard, 2007). ....	37
Figure 3.4. Summary of seismic stratigraphic surfaces and units in the survey areas. A. Type UHR seismic section with seismic stratigraphic surfaces interpreted. S4 is only partially interpreted due to a seabed multiple. B. Summary table of seismic stratigraphic units, their distribution, form, seismic facies present, environmental interpretation and the British Geological Survey (BGS) regional stratigraphic framework equivalent to seismic units.....	39
Figure 3.5. Seismic reflection profile and interpreted panels illustrating seismic facies character and association with seismic stratigraphic units and surfaces. Panel (i) shows the L4 unit and bounding surfaces S4 and S2. Surface S4 mostly obscured by a seabed multiple. Upper L4 unit valley fill (V1 and V2) shown. Panel (ii) shows L3 unit and bounding surfaces S3 and S2. Note the truncation of Middle to Late Pleistocene stratigraphy by the L3 unit. Seismic reflection profile A and B. taken from UHR survey. For location of seismic reflection profiles see inset map .....	44
Figure 3.6. L3 and L4 fills. A. Depth map of the base valley-fills (V1, V2 and V3) present in the L4 unit with position and orientation of example seismic panels and interpretation (1-1', 2-2'). B. Depth map of the S3 surface (base L3 unit fill) and position and orientation of an example seismic panel (3-3')..	45
Figure 3.7. Seismic reflection profile and interpreted panels illustrating seismic facies character and association with seismic stratigraphic units and surfaces. Panel i shows sf10 associated with depressions in the S2 surface and sf8, the dominant seismic facies in L2 unit, draping the S2 surface. Panel ii shows dipping/prograding reflectors that characterise sf9 that are present in the west of the cable route survey area. Panel C and D taken from the SBP survey. For location of seismic reflection profiles see inset map. ....	46

Figure 3.8. Seismic reflection profile and interpreted panels illustrating seismic facies character and association with seismic stratigraphic units and surfaces. Panels i shows dune-scale bedforms (sf11) seen in the southwest of NV West and in the cable route survey area. Panel ii shows zoom in of inset on panel i. Note that these bedforms are bound between sf8 facies. Panel i is taken from the SBP survey. For location of seismic reflection profiles see inset map..... 47

Figure 3.9. Calibration of SBP seismic, core logs and CPT data. Vibrocore path overlain on seismic (yellow). CPT parameter (Rf) overlain on seismic in blue. Core photographs shown alongside lithological core logs. See Figure 3.1 for locations of vibracores..... 50

Figure 3.10. Palaeoenvironmental maps depicting highstand and lowstand scenarios at the time of Yarmouth Roads Fm. deposition. A. Interglacial conditions and flooding of valleys V2 and V3 and draped deposition of fine grained marine/estuarine sediments. B. Glacial conditions with northwards expansion of fluvial networks and infilling of valley V1 with coarser grained terrestrial sediments (Modified from Cohen et al., 2012; Funnell, 1996; Gibbard, 1988; Hijma et al., 2012). ..... 54

Figure 3.11. Seismic reflection profiles with CPT friction ratio (Rf) overlain and SBT plot showing data for the L2 unit interval. The SBT plot shows two distributions interpreted to support a subdivision of the L2 unit. Using the SBT plot the lower L2 unit is predicted to be predominantly clay (organic soils) and the upper L2 unit predominantly silt with clay..... 57

Figure 3.12. Flooded landscape scenarios for hypothetical stages in the Last interglacial and Early glacial (L2 unit; Eem and Brown Bank Fms., MIS 5). A. At 50m below current mean sea level the majority of the area is subaerial with small enclosed and semi enclosed lagoons, lakes and peninsulas. B. At 46m below current mean sea level a less restricted, more open marine landscape is revealed. C. At 44m below current mean sea level the survey area is predominantly flooded with the exception of the northeast with some islands. .... 59

Figure 4.1. Northwest European chronostratigraphy (Vandenberghe, 1985; Van Huissteden et al., 2001; Busschers et al., 2007). The marine isotope record (Bassinot et al., 1994). Eustatic sea-level record derived from North Atlantic and Equatorial Pacific benthic Oxygen Isotopic Data (Waelbroeck et al., 2002). Relative sea-level curve for the Rhine river-mouth area in The Netherlands (Jelgersma, 1961; van de Plassche, 1982; van de Plassche, 1995; Cohen et al., 2005; Hijma et al., 2010; Hijma et al., 2011). ..... 64

Figure 4.2. NV West and Boreas survey areas with locations and names of vibracores and CPTs. Red lines indicate the locations of the panels shown in Figure 4.4. .... 65

Figure 4.3. Multibeam bathymetric data available to this study. Full coverage bathymetric data is available in both NV West and Boreas in addition to bathymetric surveys that were acquired using a coarser grid but over a larger area extending out of the NV West and Boreas sites. The coarser gridded bathymetric survey was acquired in 2010, whilst the full coverage bathymetric surveys were acquired in 2015 (NV West) and 2017 (Boreas)... 66

Figure 4.4. Seismic reflection profile and interpreted panels illustrating seismic stratigraphic units and surfaces. This chapter focuses on Surface 1 to the modern seabed, building on work in Chapter 3. Panel (A-B) shows an example seismic line (SBP) through NV West. Seismic unit 1 (L1) is associated with sand banks and shallow marine bedforms. Where it is not identified, only a thin veneer (<20 cm) of shallow marine sand covers the Late Pleistocene sediments. Panel (C-D) shows an example seismic line through Boreas. The north-south trending sand banks are clearly visible with Late Pleistocene sediments sub cropping in between. For location of seismic reflection profiles see location map (Figure 4.2). ..... 69

Figure 4.5. Map of S1 with a channel-form and example seismic profiles of channel-form fills. A range of seismic fill types characterise the channel-fill unit. A) The CFU with cut and fill architecture and SAU partially overlying the fill. SAU is not present on the margins. B) CFU-fill example with high amplitude basal bounding seismic reflectors and cut and fill architecture. The SAU overlies the CFU and is present on the southern margin. C) The CFU with no overlying L1 unit and visible on the seabed with positive relief. D) CFU with a chaotic fill seismic character and SAU present on the southern margin. E) Depth map (m MSL) of the Surface 1 (S1) with locations of panels A, B, C and D. .... 71

Figure 4.6. VC086 penetrates CFU in the northeast of NV West. CFU here is characterised by the Ssh lithofacies (see text for description). Ssh is underlain by L2 (Slc) and overlain by L1 (Sm). The seismic character of CFU at VC086 is characterised by low to medium-amplitude seismic reflectors that are parallel and sub horizontal, draping the channel-form margins..... 72

Figure 4.7. Example seismic sections of unit SAU in NV West and Boreas. The mapped top S1A surface for NV West and Boreas is shown coloured in depth below measured sea level. Profiles A and B show examples of the SAU unit and the variation in thickness (number of seismic reflectors). In both examples, the SAU unit is overlain by a marine bedform. .... 73

Figure 4.8. Seismic sections showing examples of the incisional seismic unit. A range of seismic fill types characterise the incision-fill seismic unit. A) Seismic section shows an incision surface with a chaotic fill character and dipping reflectors. Along the northern margin of this feature is the S1A unit, which is truncated. B) Seismic section shows an incision surface that forms part of the CFU interpretation, although its irregular planform resembles IU. Dipping, sub horizontal and transparent seismic fill characterise this feature. C) The S1 surface is shown in the main map with inset maps showing location of panels. .... 75

Figure 4.9. Key seabed features interpreted from bathymetric data and SBP seismic in NV West and Boreas. The crests of the dune-scale bedforms (sediment waves) are superimposed over north-south trending sand banks. Where only a thin veneer of seabed sediment is present (blue) the L2 unit crops out at the seabed. Relict channels and scour pits associated with dunes and linear ridges are also shown. .... 77

Figure 4.10. Bathymetric data over NV West showing examples of seabed features (see figure 4.9 for interpretation) and elevation profiles associated with those features. 1) Large scour pit on the lee of a dune (>2.5 m deep) incising into underlying sediments. 2) Linear northwest-southeast trending ridges forming a positive relief (~0.4 m high) and composed of the underlying fine grained L2 unit. 3) Sinuous relict channel orientated approximately north-south. 4) Relict channel with positive relief (levee structures) extending in a northeast-southwest orientation. .... 78

Figure 4.11. A vibrocore transect from west to east through NV West showing correlation of seismic units and lithostratigraphy relative to the ordinance datum. The lithofacies codes are explained in the body text (0). .... 80

Figure 4.12. Interpreted vibrocores that penetrated the channel-fill seismic unit. VC074 is in the southwest (Figure 4.2) and samples the margin of the channel-fill unit and is characterised by organic-rich sands and peats. VC086 samples the central part of the channel-fill seismic unit in the northwest. The channel-fill here contrasts with that in VC074, which is composed of a shell-rich silty sand. .... 82

Figure 4.13. Radiocarbon dates from 6 peat layers in vibrocores from NV West and Boreas, obtained by Wessex Archaeology. Dates calibrated with IntCal20 ((Reimer et al., 2013)) and plotted relative to m OD. .... 87

Figure 4.14. Proposed conceptual morphostratigraphic model for the development of relict tidal channels and/or relict tidal pools in an established coastal marsh undergoing sea-level rise with examples from seismic data and cores in the study area to support this model. For detail on the evolutionary stages leading to development features see text. The vertical scale, and the cross-sectional scale of the creeks, are greatly exaggerated. Adapted from Allen (2000). .... 95

Figure 4.15. Analogues of modern active tidal ponds, their scale and shape compared with the incisional units documented in the study area. The Copper River Delta is largest contiguous wetlands along the pacific coast of North America and the Lena Delta is located in northeast Russia and is approximately 400 km wide. Tidal pools are common in both areas although the Lena Delta is frozen tundra for 7 months of the year. The tidal pools seen in the wetlands of the Copper River Delta are equivalent in size to incisional units observed in the study area (<2 km), whereas those identified on the Lena Delta are larger (>5 km). Aerial images taken from Google Earth. .... 96



Figure 4.16. Proposed conceptual morphostratigraphic model for the development of tidal pools in an established coastal marsh but failing to keep pace with sea-level rise. For detail on the evolutionary stages leading to development of incisional units (see text). The vertical scale, and the cross-sectional scale of the creeks, are exaggerated.....	98
Figure 4.17. Seaward facing cliff morphology in a salt marsh environment. A) Modern analogue of seaward facing cliff morphologies on a modern salt marsh in Morecombe Bay, UK. B). Seismic data example of an abrupt lateral termination in the seismic anomaly unit (SAU) common in the survey areas and interpreted to be a seaward facing cliff formed in a salt marsh setting.....	100
Figure 5.1. Location map for the three work areas documented in this study (NV West, Cable route and Boreas), and vibrocore and Cone Penetration Test (CPT) data locations. Black circles indicate the cores used for organic carbon analysis. Figure 5.2 and 5.19 panel locations shown in red.....	104
Figure 5.2. A characteristic seismic profile for the NV West (1) and Boreas (2) survey areas displaying the three seismic surfaces (Seabed, S1, S2) and the three seismic units (L1, SAU and L2) with depth in meters below measured sea level (MSL). For location of panels see Figure 5.1. ....	105
Figure 5.3. A characteristic seismic profile illustrating the seismic character of SAU and the underlying and overlying seismic units (L2 and L1). The zoomed image shows the typical character of SAU as a package of high amplitude seismic reflectors. The number of seismic reflectors that characterise SAU varies across the survey areas. ....	106
Figure 5.4. Gridded depth maps for top SAU in NV West and Boreas.....	107
Figure 5.5. Photographs of the 4 lithofacies observed in cores that are associated with SAU. Descriptions of lithofacies can be found in text.....	110
Figure 5.6. Core panels from NV West showing SAU and the underlying (L2) and overlying (L1) sediments. Also shown are sampling points with values for Dry bulk density and % organic carbon. Descriptions of lithofacies can be found in text and photographs in Figure 5.5. The red filled section represents all organic carbon values >25% (M-OC). The radiocarbon dates shown were obtained by Wessex Archaeology, 2018 (Chapter 4). Inset map shows location of panel. ....	111
Figure 5.7. Core panels from Boreas showing the SAU unit and underlying and overlying sediments of L2 and L1, respectively. Also shown are sampling points with values for DBD and %OC. Descriptions of lithofacies can be found in text (4.1.1). The red filled section represents all organic carbon values >25% (M-OC). The radiocarbon dates shown were obtained by Wessex Archaeology, 2018 (Chapter 4). Inset map shows location of panel.....	112

Figure 5.8. Calibration of Cone Penetration Test (CPT) Friction ratio (Rf) parameter against seismic and Soil Behaviour type (SBT) plot. A. Correlation panel of three CPTs calibrated to seismic data. Interpreted seismic units are overlain and clearly correspond to deflections in CPT Rf parameter. B. A SBT plot showing CPT parameters (Cone resistance and Rf) for three CPTs shown in A. The CPT parameters calibrated to SAU fall within region 2, typical of organic-rich soils/sediments. For location of CPTs see Figure 5.1..... 113

Figure 5.9. Data types used to classify peat and calculate peat thickness. SBP seismic is used to map the spatial distribution of the peat, which correspond to SAU. Sediment cores are logged with top and base peat identified based on visual inspection. The sediment/soil mechanical property friction ratio (Rf), as gained from the CPT, is a property used for identifying peat in the subsurface, with the top and base of peat units clearly marked by Rf deflections. OC analysis of samples across the peat interval, including above and below the visual defined contacts, enable classification of peat based on % OC. Each method results in different thickness ranges for the peat interval..... 115

Figure 5.10. Scatter plot of all DBD and OC analysis for 9-sampled cores. Those sample points visually identified as organic-rich are marked with green circles and brown crosses, and form the SAU. The black markers are those samples that are above (L1) or below (L2) SAU and are visually identified as non-organic and primarily composed of sands, silts and clays. The green markers represent those samples that are identified as organic-rich but contain visible plant remains (fragments of wood) and are more classically described as peats. The 25% OC line is displayed, and this coincides with the boundary between organic rich and organic rich with plant remains visible. .... 117

Figure 5.11. Vibrocore panel showing the different thickness ranges generated using the M-V, M-OC and CPT data. The core used as the input to M-V with the interval defined shown as an orange bar. OC analysis point are shown with a red fill indicating those analysis point that have >25% OC and with the defined SAU according to M-OC shown as a green bar. The CPT data has not been used as input to SAU thickness but has been shown here to contrast the ranges generated for SAU thicknesses using different classification methods. No CPT data is available over SAU for CPT039. Inset map shows the location of the panels ..... 121

Figure 5.12. Interpolated grids showing SAU thickness across both survey areas using M-V methods, with vibrocores used to define thickness shown. Note different scales used for the two areas to highlight variations. .... 122

Figure 5.13. Interpolated grids showing SAU thickness across both survey areas using M-OC methods, with vibrocores used to define thickness shown. .... 123

Figure 5.14. DBD and OC values for each core corresponding to the SAU defined using both M-V and M-OC methods. Mean OC for each vibrocore is indicated by the orange line..... 125

Figure 5.15. Interpolated grid using mean DBD measurements peat from 6 vibrocores. A. Mean DBD values calculated over SAU according to M-V methodology. B. Mean DBD values calculated over SAU according to M-OC methodology.....	126
Figure 5.16. Interpolated grid using mean %OC measurements from sediment core peat intervals. A. M-V methodology applied. B. M-OC methodology applied.....	127
Figure 5.17. Seismic profile examples from NV West and Boreas showing eroded L2 unit supported by truncated L2 seismic reflectors and termination of the SAU anomaly coincident with erosion of the L2 unit. C) In the west of NV West, L2 unit reflectors are truncated and overlain by a thin veneer of marine sands (<30 cm), or L2 crops out at the seabed. SAU terminates laterally coincident with termination of L2 reflectors. D) Boreas has a highly variable seabed bathymetry with seabed highs associated with north-south trending sand banks. Coincident with the troughs between the sandbanks, L2 unit reflectors and SAU terminate against L1. See Chapter 3 for information on the L4 seismic unit. See Figure 5.1 for locations of panels. .	132
Figure 5.18. An example of mobile seabed sediments and active scour of the seabed in NV West. 1. Repeat bathymetry surveys acquired in 2010 and 2015 showing a large bedform with a scour pit on its steep lee-side. 2. A seismic section (2015) through the large bedform and scour pit shown in 1. Overlain are terrain profiles from the repeat bathymetric surveys. Interpreted are truncated L2 seismic reflectors (white lines) and a relict scour surface. An abrupt termination of SAU corresponds with the relict scour surface. 3. Terrain profiles from repeat bathymetry surveys. ....	133
Figure 5.19. Palaeocoastlines at 10 ka and 9 ka as modelled by Sturt et al .(2013). Where the palaeocoastline is coloured as a line fill marks the area not modelled by Sturt et al. (2013) and for the purpose of this study has been extended to the Dutch coast. The inset map shows the NV West and Boreas survey areas with aerial extents of SAU, which account for 22% of the survey areas. Crosses indicate the approximate locations of published postglacial peats identified in the southern North Sea (published peats on Dogger Bank not shown). ....	135
Figure 6.1. Interpreted drainage networks from Middle Pleistocene to present day within Norfolk Vanguard West. The arrows indicate the interpreted drainage directions.....	138
Figure 6.2. Approximate shoreline positions for the Ur-Frisia Delta in response to marine transgression. Maximum extent of the Ur-Frisia Delta extends beyond the Outer Silver Pit where marine delta-top and inter- and sub-tidal delta front facies have been described in BGS cores. The approximate general thickness of the Yarmouth Roads Fm. as defined by BGS cores. Delta shoreline positions and Yarmouth Roads Fm. thickness contours adapted from Cameron et al. (1992). ....	141

Figure 6.3. Subglacial conditions in the study area during the Anglian glaciation. Tunnel valleys documented in this study and those published earlier are predominantly north-south orientated supporting a southward flow of meltwater towards the ice sheet front (black arrows). Rivers from southeast England and mainland Europe retreated westwards and southwards due to a large proglacial lake covering the southern North Sea region. Drainage from the proglacial lake was likely through the Dover Strait. River drainage (purple) and proglacial lake (adapted from Gibbard, 2007; Cohen et al., 2017). ..... 142

Figure 6.4. A composite map of the southern North Sea with a land-sea distribution ~11 ka with the palaeocoastline being based on the -50 m bathymetric contour line (modified from Warnke, 2015). Studies that have documented Late Devensian to Early Holocene channels networks are shown alongside those documented in this study, with approximate drainage directions. An approximate position for an important drainage divide north of the study area is shown. The interpreted extent of large palaeovalleys are shown with their tributaries. The maximum ice extent during MIS 2 is shown (Dogger Bank subglacial) and the ice extent during the deglaciation phase between 18.5-17 ka (southern North Sea fully deglaciated). North Sea Palaeolandscape Project (NSPP) data set adapted from University of Birmingham (2011). ..... 144

Figure 6.5. Present-thickness maps of compacted Quaternary stratigraphy. A) 1.94 to 1.09 Ma. B) 1.09-0 Ma. Throughout the Quaternary the North Sea depocenter moved progressively northwards. The study area sits on the southwestern edge of the North Sea basin. Thickness maps adapted from Lamb et al. (2018). ..... 145

Figure 6.6. The southern North Sea and English Channel drainage networks following the LGM. South-eastern England and continental European rivers drained southwards through the Dover Strait into the Atlantic. A palaeovalley has been extended northwards from the English Channel (based on bathymetric interpretation) that drained rivers identified in this study. A series of megafloods during the Anglian/Elsterian glaciation and again during the Wolstonian/Saalian lead to a breach of the land-bridge between England and continental Europe (Dover Strait), and subsequent diversion of rivers southwards into the Atlantic. River networks (black lines) adapted from Gibbard (2007) and Gupta et al. (2017) ..... 147

Figure 6.7. Map illustrating the emergent parts of the continental shelves worldwide during the last glacial maximum. An assumed glacial eustatic lowstand of 120m below present sea level, with no glacially induced flexural uplift in high-latitude regions adjacent to large ice sheets or neotectonic (Holocene) uplift or subsidence taken into account (from Fitch et al., 2007). 149

Figure 6.8. Position and orientation of Holocene sandbanks and Anglian/Elsterian tunnel valleys, and propagation direction of southern North Sea tidal regime. A) Approximately north-south trending sandbanks (red) overlain by older tunnel valleys. The position, extent, and orientation of the sand banks and tunnel valleys is very similar. B) Present-day bathymetry with position and orientation of sand banks, and present-day propagation direction of tidal wave in the southern North Sea. .... 153



# Chapter 1 - Introduction

## 1.1. Motivation

The characterisation of the shallow subsurface (0-50 m is the depth of engineering consideration (Malhotra, 2007)) and seabed in the North Sea is important as i) a means of developing a critical geological understanding to aid in the continued successful deployment of renewable energy infrastructure; namely offshore wind farms, and ii) as an analogue for palaeoenvironmental change under models of sea-level rise.

Global climate change (IPCC, 2013), energy supply and the cost of energy are becoming increasingly important for governmental authorities and society (Díaz et al., 2020). In the last decade, growing efforts have been made to reduce CO<sub>2</sub> emissions and other pollutants that have exacerbated global warming effects. International protocols such as the 2015 Paris Agreement (UN, 2015) have led to changes in national energy framework protocols to help mitigate the adverse effects of emissions on climate. These include a binding target of 40% reduction in CO<sub>2</sub> emissions and a binding target of 27% renewable energy (Díaz et al., 2020). For the United Kingdom, in order to achieve this renewable energy quota, and decarbonisation of the energy supply, a wide and varied energy mix will have to be adopted. Geosciences play a key role in helping to address the challenges posed by the energy transition (Stephenson et al., 2019). One of the key tools in this energy transition will be offshore wind (Bull, 2019). Here geosciences can provide detailed understanding of the subsurface conditions, leading to more efficient and cost-effective developments in the short and long term. Geoscience also plays an important role in understanding the landscape and sedimentary process response to changing environmental conditions in response to rising sea levels (Meadows, 2012). Through understanding the palaeolandscape and sedimentary process responses to relative sea-level change, geosciences can help mitigate risks associated with future sea levels rise in the form of coastal defence planning, improved understanding of drainage network evolution, and the long-term fate of coastal plain environments and sequestered carbon associated with them following sea-level rise.

The aim of this study is to document a sedimentary sequence from Middle Pleistocene to present-day through use of a comprehensive, high-resolution dataset. The study aims to understand landscape and sedimentary process response to multiple glacial-interglacial cycles, with a focus on transitions in environment from terrestrial to marine

through multiple phases of marine transgression. Through use of a world class offshore subsurface dataset, including seismic reflection data, sedimentary cores, geotechnical logs and core samples, four research questions will be addressed:

1. How has the preservation and distribution of rivers changed from Middle Pleistocene to present day in the southern North Sea region?
2. Are buried and submerged postglacial peats a carbon sink or source, and should they be a consideration in carbon stock estimates?
3. How does inherited stratigraphic architecture influence present-day seabed sediment and bedform configuration in the southern North Sea?
4. How do low relief landscapes respond to/record changes in relative sea-level changes?

## **1.2. Southern North Sea Region**

### **1.2.1. The southern North Sea - a unique geological setting**

The geographical position, configuration, and the high density of geophysical and sedimentary core data from both terrestrial and marine settings, make the southern North Sea region particularly special for palaeogeographical reconstructions of Quaternary landscapes (Cohen et al., 2014). Over a relatively short time period there is extensive heterogeneity in the depositional environments that characterise the Quaternary stratigraphic record. The geographic position with respect to multiple phases of glaciation offers the opportunity to study evolving palaeolandscapes over multiple glacial-interglacial cycles. In addition, the low relief shelf environment (analogous to the modern-day coastal plain that characterises the Netherlands) that has characterised the southern North Sea from the Middle Pleistocene to present-day offers the opportunity to investigate the landscape and sedimentary process response to changes in relative sea level in a low gradient setting.

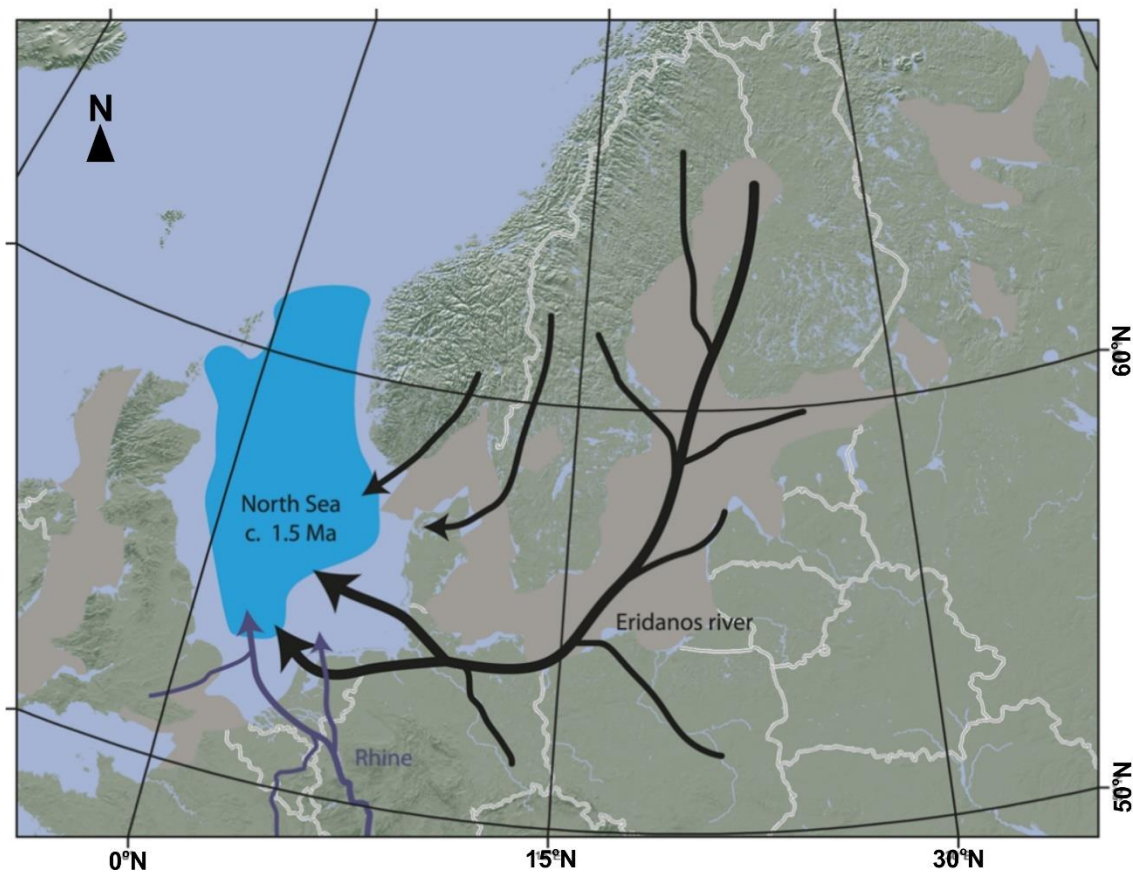
### **1.2.2. Deep-time and Early Pleistocene geological history southern North Sea**

The North Sea has a complex geological history that culminated in the present day structural rifted architecture that characterises the basin at depth today. Rifting commenced in the Permian and culminated in the Late Jurassic (Ziegler, 1992). Following rifting, thermal subsidence in the basin resulted in increased accommodation



space and the deposition of sediments ranging from Cretaceous to present day (Zanella et al., 2003). Of these sediments, in excess of 800 m are Quaternary, with the thickest packages being in the Central Graben (Gatliff et al., 1994; Lamb et al., 2017). The stratigraphic framework currently used for the southern North Sea was developed through the integration of onshore lithostratigraphic and biostratigraphic observations with offshore seismic. Through this integration, a seismic stratigraphic framework was developed through which Quaternary sediments are described (Cameron et al., 1987).

Throughout the Middle Miocene and Pliocene sedimentation in the southern North Sea was dominated by the expansion of deltaic systems that were associated with Baltic rivers that drained the Fennoscandian Shield (Figure 1.1) (Gibbard, 1988). From Early Pleistocene, relatively minor deltas built out that were associated with drainage from mainland European rivers (Rhine, Meuse, Scheldt) and minor British rivers (Zagwijn, 1974). The build-out of these minor deltas helped to deflect the principal direction of delta growth (Ur-Frisia Delta) from south-west to north-west (Cameron et al., 1993). The Early Pleistocene Quaternary sediments fall within the southern North Sea Deltaic Group. The depositional environment throughout the Early Pleistocene in the southern North Sea was predominantly marine and characterised by a relatively stable climate (Limpenny et al., 2011). By Middle Pleistocene most of the North Sea basin was filled and was occupied by a fluvio-deltaic coastal plain. With the onset of the Middle Pleistocene climatic instability caused major changes in regional drainage patterns, which lead to a widespread reduction in sediment input to the basin (Gibbard, 1988)



**Figure 1.1. Drainage basin and delta of the Miocene–Pliocene–Early Pleistocene Eridanos river system, with a depiction of the former terrestrial environment in Middle-Pleistocene-glacial excavated areas that are nowadays seas. Black arrows indicate the former Eridanos fluvio-deltaic system and blue arrows show contributing fluvial systems from North West Europe (from Cohen et al., 2014).**

### 1.2.3. North Sea glaciation history

The middle Pleistocene was a period of heightened climatic instability (Ehlers et al., 2007), driving regional scale falls in relative sea level, river drainage configurations, and glacial cycles (Lee et al., 2006). Throughout the Middle to late Pleistocene at least three major glacial advances have extended into the southern North Sea (Figure 1.2 and 1.3) (Bowen et al., 1986; Long et al., 1988; Ehlers, 1990; Ehlers et al., 1991; Carr et al., 2006; Graham et al., 2011). These glacial advances have contributed to the episodic erosion and infill of the basin (Graham et al., 2011). Locally these glacial advances are known as the Anglian/Elsterian (Marine Isotope Stage (MIS) 12), Wolstonian/Saalian (MIS 10(?)–6), and the Devensian/Weichselian (~MIS 3 to 2) (Figure 1.3). The Anglian glaciation was the most extensive of these glaciations, extending into the southern North Sea Basin below 52°N (Cameron et al., 1992; Clark et al., 2004; Streif, 2004). The Anglian glaciation is the oldest event that has left behind till deposits throughout northwest Europe. The southern outer limits of the ice sheet are

not yet clear, particularly in the Netherlands and Northwest Germany, due to it being subsequently overridden by the Wolstonian glaciation, and much of the evidence having been destroyed (Ehlers et al., 2008). The southern limits in the offshore setting have been defined using discrete sets of tunnel valleys (Figure 1.3), delimiting the broader submarginal extents (Graham et al., 2011). Tunnel valleys are defined in this study as incisions with undulating thalwegs and widths less than 5 km that formed under ice sheets (Vegt et al., 2012). The duration of the Wolstonian glaciations are less well defined, with an initial cold non-glacial phase, followed by ice sheets that extended into north Germany and the Netherlands (Ehlers et al., 2008). The extents of the Wolstonian glaciation in the Netherlands (westward limit) is defined by push end moraines (Busschers et al., 2008). The extent of the Wolstonian ice sheets in the North Sea basin is not well known, but it is likely that British and continental ice were confluent during this time (Carr, 2004). A consequence of the confluence of the British and continental ice sheets was the formation of an ice dammed lake was formed in the southern North Sea basin at this time (Busschers et al., 2008; Ehlers et al., 2008). There is evidence for a least two phases of extensive Devensian ice sheet growth in the North Sea, during the Early Devensian (MIS 4) and the late Devensian (MIS 3-2) (Carr et al., 2006; Graham et al., 2007). Tunnel valleys provide evidence onshore Britain for the early stage Devensian ice sheet although there is less definitive evidence offshore for a limit. 3D seismic has provided well preserved morphological evidence for ice sheet limits and these may correspond with early Devensian limits (Graham et al., 2007). During the Late Devensian glacial stage it is now widely accepted that the British and Fennoscandian ice sheets coalesced (Roberts et al., 2018), with a southern ice sheet limit coincident with tunnel valley limits at approximately 56°N. The North Sea became ice free after approximately 17 ka with the deglaciation of the British Irish Ice Sheet (Clark et al., 2012).

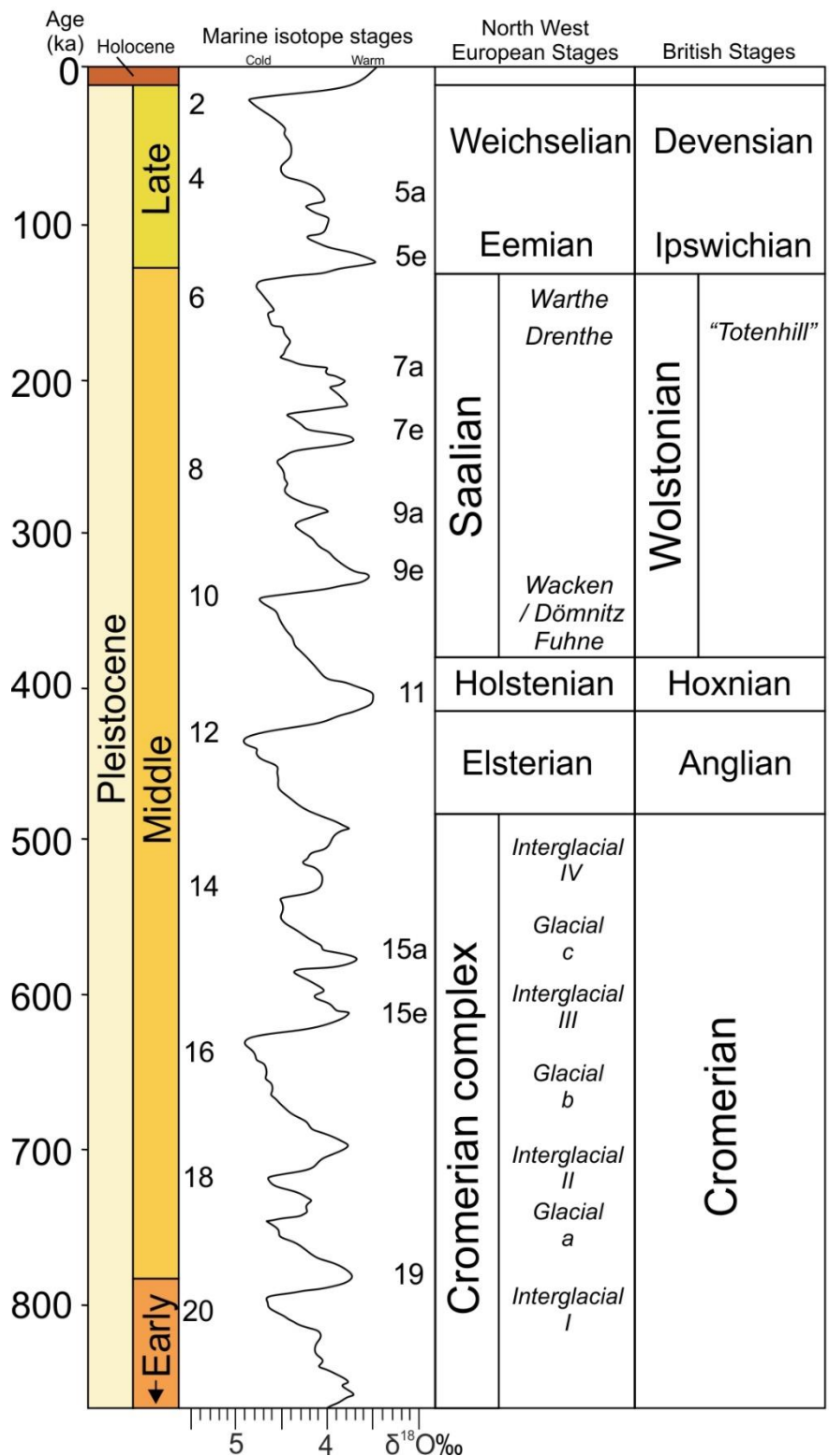
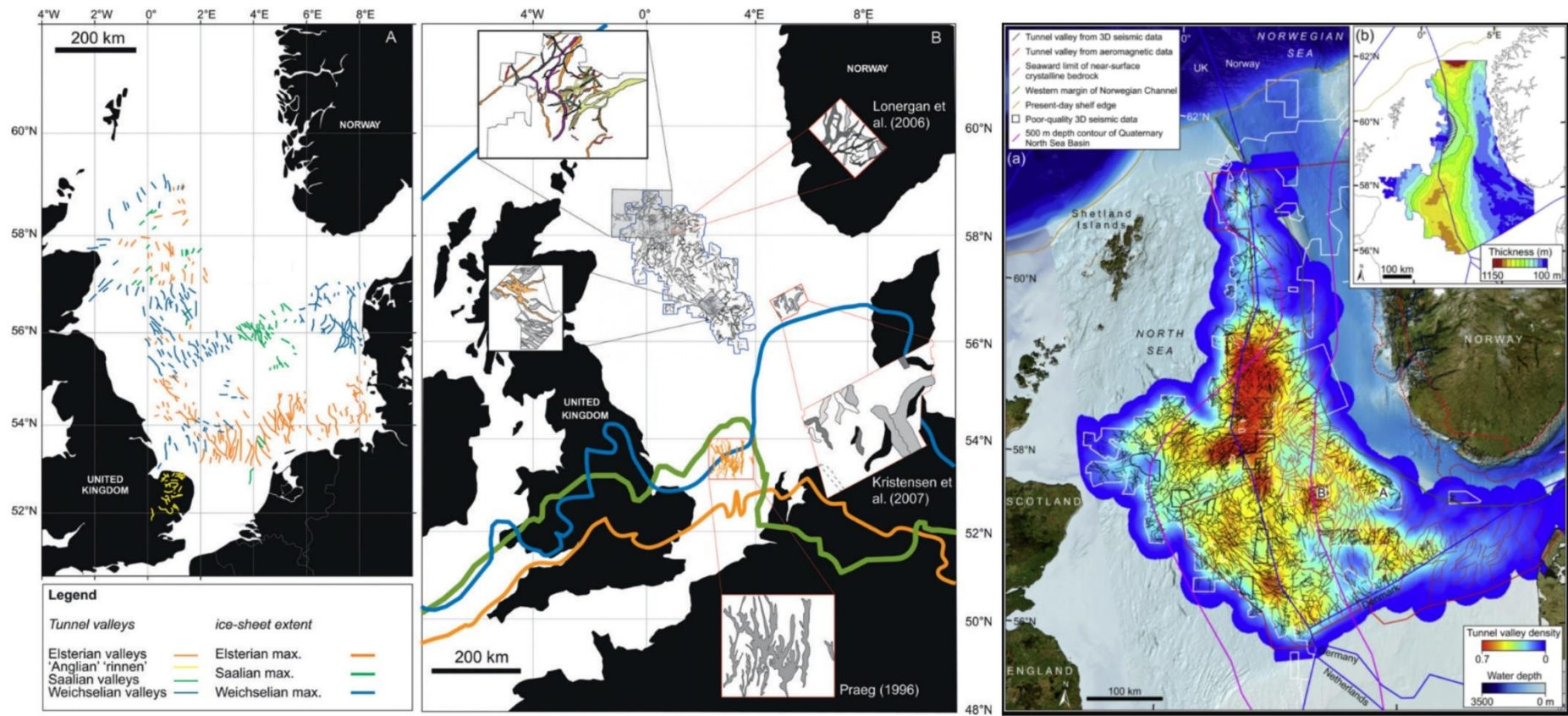


Figure 1.2. Chronostratigraphical chart for the Middle to present-day showing the marine isotope stages and regional stage/substage divisions for NW Europe and Britain (after Gibbard and Cohen, 2008).



#### **1.2.4. Postglacial landscapes of the southern North Sea**

The postglacial landscape of northwest Europe changed rapidly during the period from the Last Glacial Maximum (LGM; 26.5 to 19 ka) when sea level was at its lowest (>100 m below current mean sea-level (MSL)), to the late Devensian (12.5 to 10.15 ka) when sea level was approximately 30 to 55 m below current MSL (Spratt et al., 2016). By end of the Early Holocene (~7.9 ka) sea levels had risen to approximately 12 m below current MSL (Hijma et al., 2011). The marked change in landscape and climate from late Devensian to present has been the focus of a broad range of investigations from ice marginal, periglacial environments (Kolstrup, 1986; Murton et al., 2003; Bateman et al., 2014; Cotterill et al., 2017; Ballin, 2017; Emery et al., 2019), fluvial system response (Briant et al., 2004; Busschers et al., 2007), human occupation and archaeological preservation (Fitch et al., 2005a; Missiaen et al., 2017; Brown et al., 2018), to the timing and magnitude of relative sea-level rise (Beets et al., 2000; Shennan et al., 2000; Behre, 2007; Hijma et al., 2010; Baeteman et al., 2011; Sturt et al., 2013).

Palaeolandscape reconstruction during this postglacial period have largely been driven by studies investigating the migratory patterns and dwellings of humans during this period (Brown et al., 2018). Interest in submerged palaeolandscapes was largely driven by work on Doggerland (Coles, 1998), and also in response to increasing commercial interest in the offshore setting (aggregates, oil and gas exploration, and wind farm developments) (Bicket et al., 2015; Brown et al., 2018). Although reconstructions of the palaeogeography of submerged areas has become increasingly detailed (Fitch et al., 2005b; Sturt et al., 2013; Van Heteren et al., 2014), there is poor chronological control on postglacial sedimentary units, due to the lack of good quality dating on suitable sediments (Tappin et al., 2011). In recent years, extensive channel networks have been identified, leading to targeted sampling programmes using vibrocores, leading to palaeoenvironmental reconstructions, with the aim of targeting habitats suitable for humans (Brown et al., 2018). The low relief landscape that characterised the postglacial landscape prior to submergence is analogous to the present-day Dutch coastal plain. The gradient of the postglacial landscape in the study is typically <1°, similar to that which characterises the Dutch coast.

#### **1.2.5. Carbon stores in coastal plain environments**

Submerged postglacial landscapes are analogous to modern-day mid-latitude coastal plain landscapes, which are predominantly freshwater to marginal marine wetland environments. These wetland environments are often peat based or contain significant

stores of organic carbon within sediments (McLeod et al., 2011). This zone at the interface between terrestrial and marine is often termed 'blue carbon' wetland (Nelleman et al., 2009; Macreadie et al., 2019). Blue carbon wetlands have been shown to be important global repositories of organic carbon, with an estimated 126.2 Mt of organic carbon buried annually (Duarte et al., 2005; Smeaton et al., 2017). Blue carbon environments are now a critical research theme, given that they are at direct risk from climate change, through rising sea levels, and also as a result of anthropogenic activity, including construction of dikes, coastal defences, docks, and pipelines (Henman et al., 2008; Chambers et al., 2014). Studies that investigate the relationships between sea level and carbon storage suggest that during the Early Holocene (12-8 ka), marine transgression had a significant impact on postglacial increases in atmospheric CO<sub>2</sub> (Montenegro et al., 2006). Given the threat of future rising sea level on coastal environments, researchers are beginning to focus on quantifying the carbon stored in coastal environments and the potential for the release of carbon (Chmura, 2013; Pearsall et al., 2005). The increase in activity in offshore shelf environments for commercial aggregate projects or the development of wind farms, means more subsurface datasets are becoming available. This is particularly the case for the southern North Sea, where water depths and seabed morphology are considered optimal for offshore windfarm developments. This data will allow the characterisation of postglacial landscapes and the carbon-rich peats associated with them, leading to a better understanding and accounting of carbon stocks held within these submerged and buried palaeoenvironments.

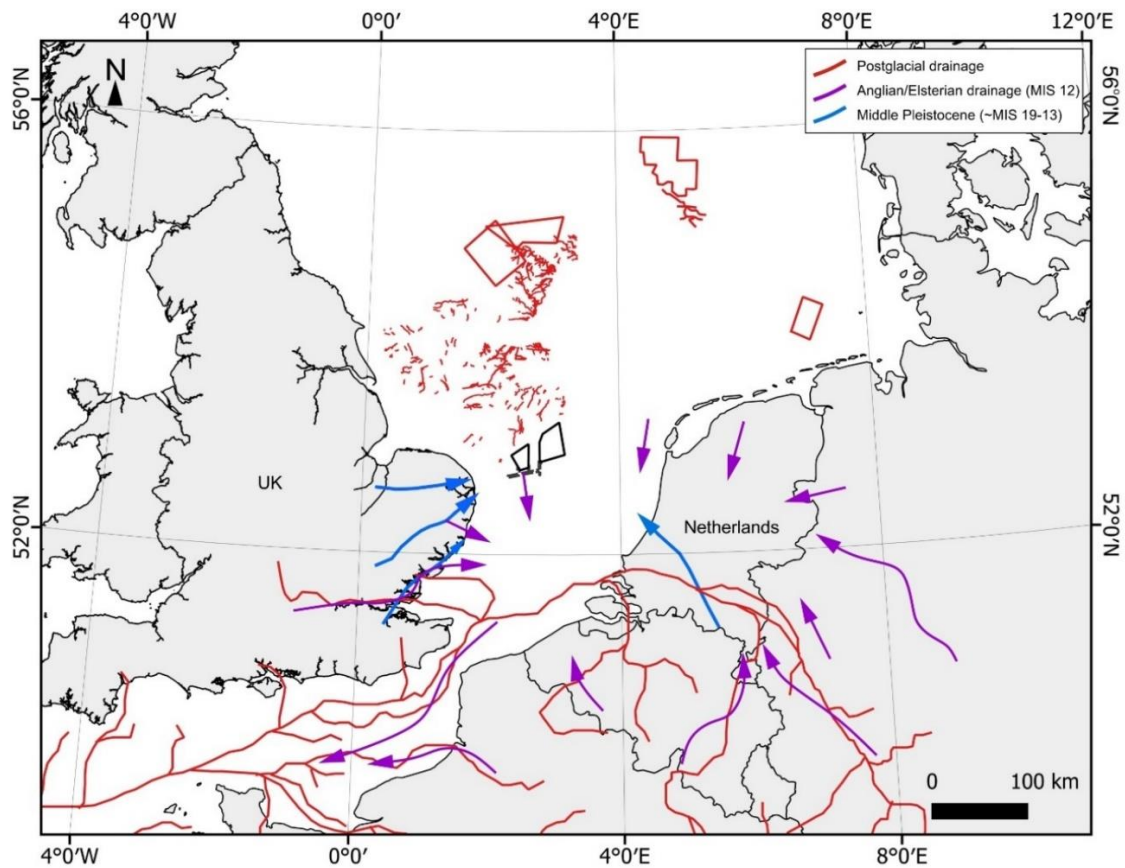
### **1.3. Research questions**

#### **1.3.1. How has the preservation and distribution of rivers changed from Middle Pleistocene to present day in the southern North Sea region?**

Palaeogeographical reconstructions in high-relief settings make the reasonable assumption that catchments and adjacent sedimentary basins maintain simple source-to-sink configurations, and that overall sediment transport directions do not change, even if sediment flux varies significantly through time (e.g. Castellort and Van Den Driessche, 2003; Sadler and Jerolmack, 2015; Romans et al., 2016). However, in low-relief continental shelf settings this assumption needs to be treated with caution. This is particularly true in ice-marginal settings where major and abrupt change in sediment transport direction can occur, which complicates estimates of sediment flux and provenance studies.

Pleistocene fluvial records offer important archives for improved understanding of the effects of external forcing on fluvial systems in north-western Europe (Busschers et al., 2007). Numerous studies (Guiot et al., 1989; Siddall et al., 2003; NGICP, 2004; Ménot et al., 2006) including ice cores, marine, and terrestrial records, show that rivers during this period experienced periodical, strong negative amplitude changes in climate and sea-level, largely in response to the multiple phases of extension and retreat of the Scandinavian and British ice-masses (Clark et al., 2004; Busschers et al., 2007). The evolution and distribution of fluvial systems is poorly studied relative to the onshore setting, where Pleistocene and Holocene fluvial systems are more well understood (Gibbard, 1988; Moorlock et al., 2002; Hijma et al., 2012). This is largely due to the relative ease in which sedimentary records can be accessed. Evidence for the expansion and retreat of these fluvial systems into the southern North Sea have been documented through sediment sampling showing delta front and marine lithofacies at various positions in the basin, indicating the migration of shorelines. However, no geomorphological records (channel morphologies) have been documented that support fluvial expansion and retreat into the basin. In contrast, southern North Sea postglacial drainage networks have been documented far more extensively (Figure 1.4), in the most part due to focused acquisition of seismic and vibrocores for palaeoenvironmental reconstructions (Brown et al., 2018). This increase in data characterising the shallow subsurface presents the opportunity to reconstruct postglacial fluvial drainage networks across the southern North Sea region. Investigation of buried and submerged fluvial systems in the southern North Sea offers the opportunity to compare and contrast with those studies focused on near shore records of fluvial systems draining into the southern North Sea basin and investigate the allogenic controls and autogenic factors driving the preservation and distribution of middle Pleistocene to present day fluvial systems.





**Figure 1.4. Previously defined terrestrial drainage networks identified in the southern North Sea region (Postglacial: Fitch et al. (2005), Gibbard (2007), Hepp et al. (2012) Gupta et al. (2017), Hepp et al. (2019), Prins et al. (2019), Emery et al. (2020); Anglian/Elsterian: Gibbard, (2007, Cohen et al. (2017); and Middle Pleistocene: Gibbard, (1988), Moorlock et al. (2002), and Busschers et al. (2007).**

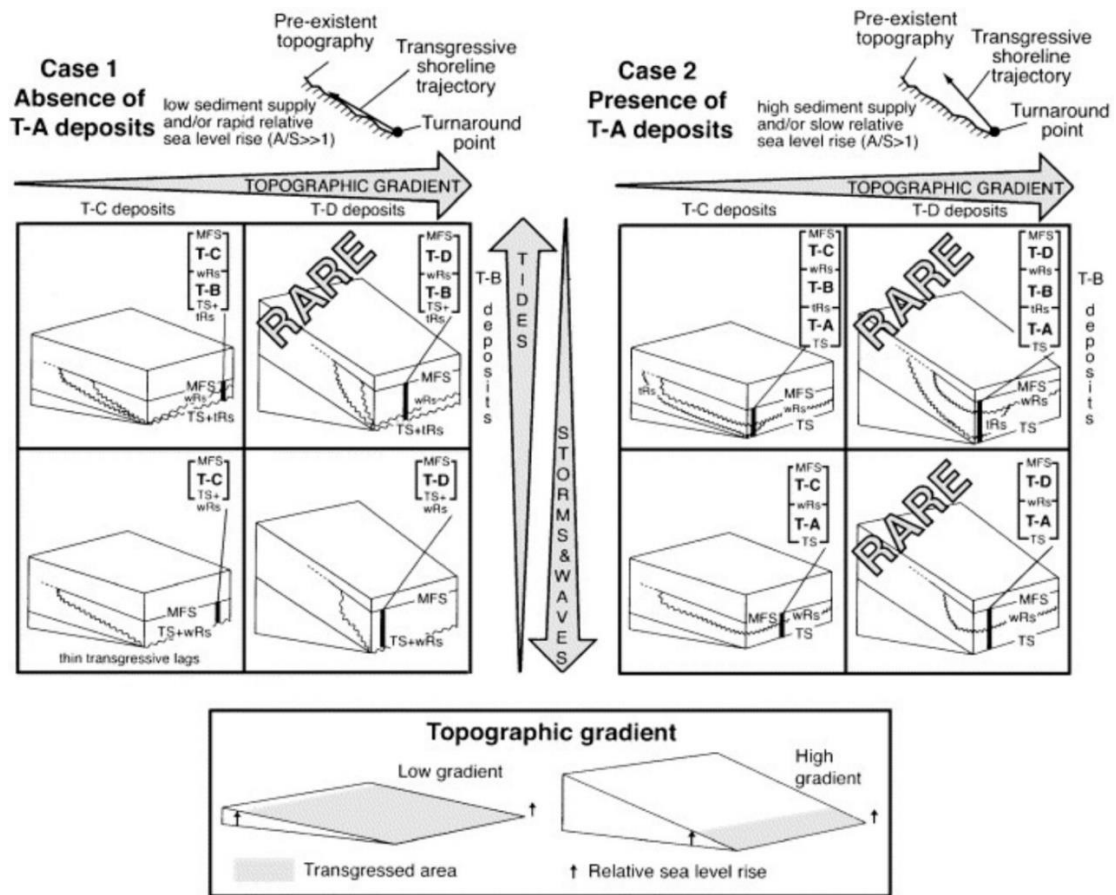
### **1.3.2. Are buried and submerged postglacial peats a carbon sink or source, and should they be a consideration in carbon stock estimates?**

Wetland environments in which peats form are important in the global carbon cycle (Tarnocai et al., 2012; Yu et al., 2010; Limpens et al., 2008), with approximately 600 Gt of carbon sequestered continuously since the Last Glacial Maximum (Charman et al., 2013). Recent studies investigating the relationship between sea level and carbon storage suggest that during the Early Holocene (~12-8 ka), marine transgression of terrestrial ecosystems had a significant impact on postglacial increases in atmospheric CO<sub>2</sub> (Montenegro et al., 2006). The buried and submerged postglacial peatlands of the southern North Sea are under increased scrutiny by researchers who are interested in marine archaeology and landscape reconstruction (Missiaen et al., 2020; Fitch et al., 2005a), however understanding the processes responsible for the evolution of coastal peatland from a carbon sink to a carbon source, and the implications for continued erosion and liberation of carbon after burial remain poorly understood.

High resolution mapping of buried and submerged postglacial peats and improved understanding of the postglacial evolution of depositional and erosional processes to present day will help further understand the vulnerability of carbon stocks held in coastal plain deposits under models of sea-level rise. In addition, the continued mapping and characterisation of postglacial peats, combined with improved understanding of the impacts associated with installation of offshore infrastructure (e.g. wind turbines, cables) on the seabed, will help improve our understanding of the impact infrastructure projects have on buried carbon stocks. Through this improved understanding, the long-term stability of buried peats, its importance as a blue carbon source and inclusion in national carbon accounts (Office for National Statistics, 2016), their potential vulnerability can be better appreciated, and ultimately included in offshore infrastructure projects environmental impact assessments.

### **1.3.3. How does inherited stratigraphic architecture influence present-day seabed sediment and bedform configuration in the southern North Sea?**

The antecedent topography and substrate are known to control sediment distribution, supply, and morphology. On a coastal plain setting the slope of the antecedent topography has important connotations for the interaction between the palaeo-shelf/coastal plain and the rising wave base during marine transgression (Cattaneo et al., 2003; Green et al., 2018). Steep shelves, where antecedent substrate is exposed to the same unit of time of relative sea-level rise, the effects of erosion are far greater than on low relief shelves, with implications for preservation of the sedimentary record (Figure 1.5). The effects of antecedent topographic controls on depositional environment and sediment supply have been investigated for many years, and are known to have a strong control on stratigraphic evolution (Dillenburg et al., 2000; Cattaneo and Steel, 2003; Green et al., 2018; Emery et al., 2019), with antecedent slope angle known to influence barrier morphology (Dillenburg et al., 2000), the location and initiation of landforms (Cooper et al., 2012), and the sedimentary architecture associated with regressive/transgressive sequences on a shallow marine shelf (Ainsworth et al., 2017). However, the effect of antecedent substrate type is not well studied in siliciclastic systems. In contrast, antecedent substrate have been investigated in carbonate systems where antecedent substrate, in combination with topography has controlled reef morphology and evolution (Grossman et al., 2006; Hineostrova et al., 2016).



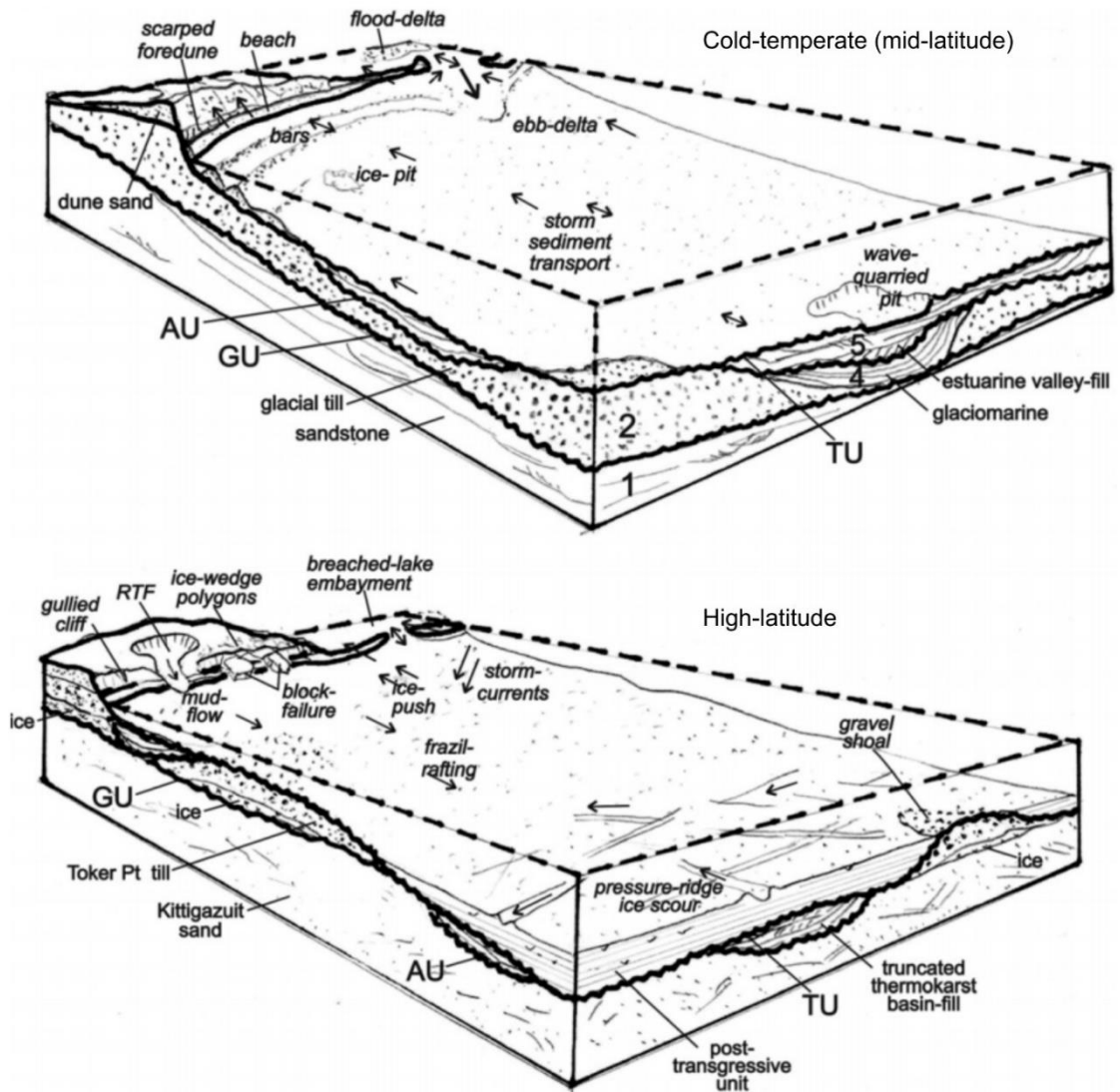
**Figure 1.5. Examples of the different antecedent topographical controls on transgressive deposits and the rate of transgression (Cattaneo et al., 2003).**

Studies have long focused on antecedent topographic control on present day depositional environment, morphology and sediment supply, typically in marine settings with steep slopes (Dillenburg et al., 2000; Cattaneo et al., 2003; Green et al., 2018; Emery, Hodgson, Barlow, Carrivick, Cotterill, Mellett, et al., 2019). The southern North Sea offers an opportunity to investigate the effects of antecedent topography as well as substrate on the distribution of present-day sediment and geomorphological record, in a low relief, marine transgressive setting, over multiple cycles of relative sea-level rise and fall.

#### 1.3.4. How do low relief landscapes respond to/record changes in relative sea-level changes?

Coastal plain landscapes that have been submerged and preserved can provide insight into the coastal response to relative sea-level change. The preservation of geomorphological features and their continued evolution in relation to antecedent topography (Green et al., 2018), and sediment supply (Mellett et al., 2012), relay important information on coastal evolution in time and space in the context of

postglacial sea-level change. Preservation of coastal landforms on continental shelves is rare due to their susceptibility to reworking and erosion as the shoreline migrated landward during transgression (Shaw, 2005; Mellett et al., 2012). However, on rocky coastlines relative sea-level changes are often recorded by erosive features such as shore platforms, which in some cases may have formed under multiple phases of relative sea-level change, with shore platforms inheriting previously formed platforms (Trenhaile, 2010). Geomorphological features formed under regression are commonly described as they are more likely to survive than in a transgression phase, with examples including coastal lagoons (Sander et al., 2016) and beach ridges (Hede et al., 2015). The effect of eustatic sea level on low relief coastal plains is often compounded by effects of subsidence (Davis, 1987), and the way in which a coastal landscape responds to relative sea-level change is often highly dependent on sediment supply. Fluvially influenced coastal plains may expect to receive sufficient sediment to keep pace with relative sea-level rise, but those that have little sediment supply will often degrade (Reed, 1990). However, coastal processes are often more complex, with rapid relative sea-level rise often associated with an increase in deposition of organic sediments, and slow sea-level rise associated with decreased sedimentation (Mudd et al., 2009). The latitude of the coastal plain environment also plays a role in the formation and/or preservation of geomorphological features formed in response to marine transgression (Forbes et al., 2014), with a broad diversity of geomorphological features developing in broadly similar transgressive coastal settings but with contrasting climatic conditions (Figure 1.6). In addition, the gradient of shelf landscapes has implications for glacial process, given that erosive processes are often selective (along valleys) on high relief terrain, and less erosive on low relief surfaces (Sugden, 1968; Hall et al., 2013), and understanding the relationship between process response and shelf gradient can inform ice sheet models. The preserved stratigraphic record of the low relief southern North Sea shelf offers the opportunity to investigate the evolution of geomorphological features in the context of sea-level rise.



**Figure 1.6. Schematic models of coastal and shoreface products of marine transgression in cold-temperate (mid-latitude) and high-latitude shelf settings (Forbes et al., 2014).**

## 1.4. Thesis structure

The thesis is structured so that each results chapter addresses the research questions. Results chapters 3 and 4 are ordered stratigraphically, with the oldest and deepest stratigraphy first. Chapter 5 focuses on the same stratigraphic units as chapter 4 but with a focus on postglacial peats. Chapter 2 is an extended methodology, describing the dataset and techniques for interpretation and analysis. Chapter 3 is the first results chapter and discusses changes in sediment process and drainage evolution recorded in the Middle to Late Pleistocene stratigraphy over glacial-interglacial cycles. Chapter 4 discusses the postglacial landscape evolution following the Late Glacial Maximum. Chapter 5 focuses on the postglacial buried peats, their evolution and the carbon stocks associated with them. Chapter 6 is the thesis discussion and synthesises the

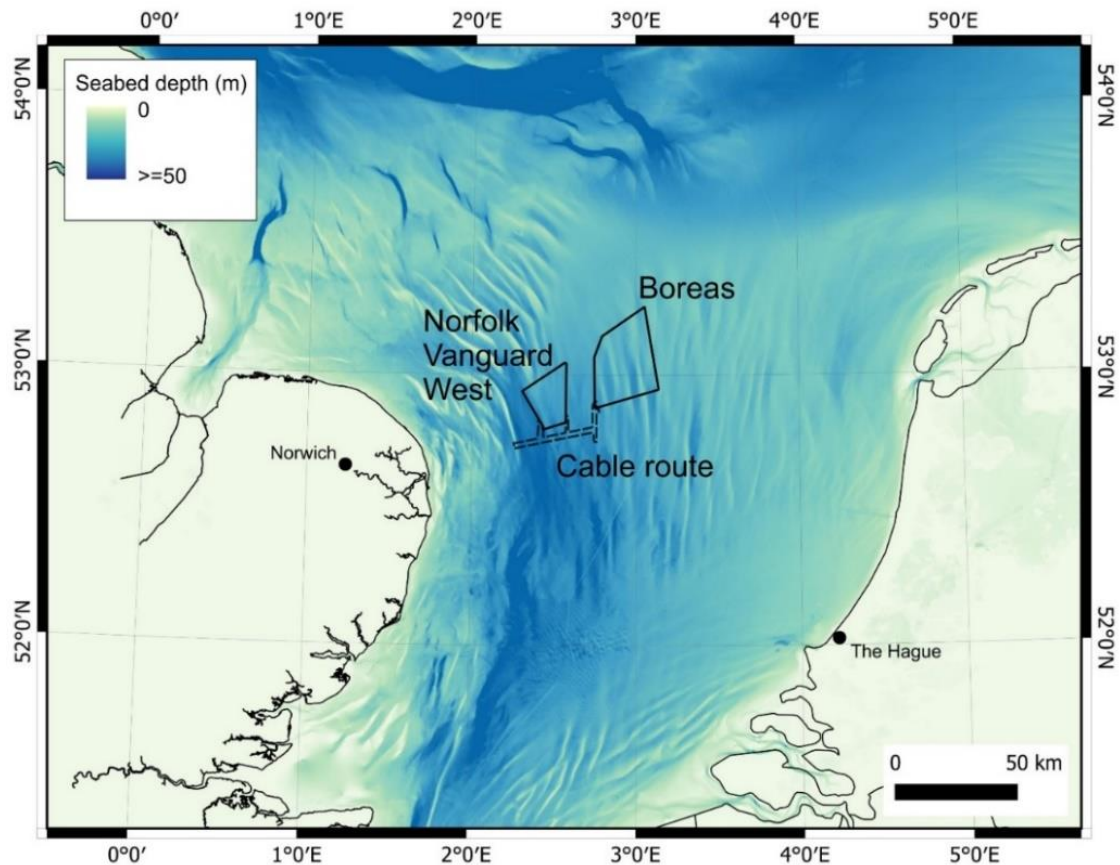
three results chapters together and presents a reconstruction of the landscapes from Middle Pleistocene to present-day. In addition, a more detailed discussion on the evolution of drainage networks over a low relief landscape is presented, as well as the evolution of the southern North Sea coastal plain in response to changes in relative sea level. Finally, the destruction and/or preservation of postglacial wetlands is discussed in the context of carbon sink and source, and the vulnerability of present-day carbon stocks held in offshore buried peats.

As stated in the declaration, Chapter 3 has been published in the *Journal of Quaternary Science* (Eaton et al., 2020).

## Chapter 2 - Methods

### 2.1. Geophysical data

Geophysical data was acquired by Vattenfall as part of the Norfolk Vanguard and Boreas windfarm projects (Figure 2.1). These data have been shared with this study, with information provided by both Fugro and Vattenfall on data acquisition techniques and processing history.



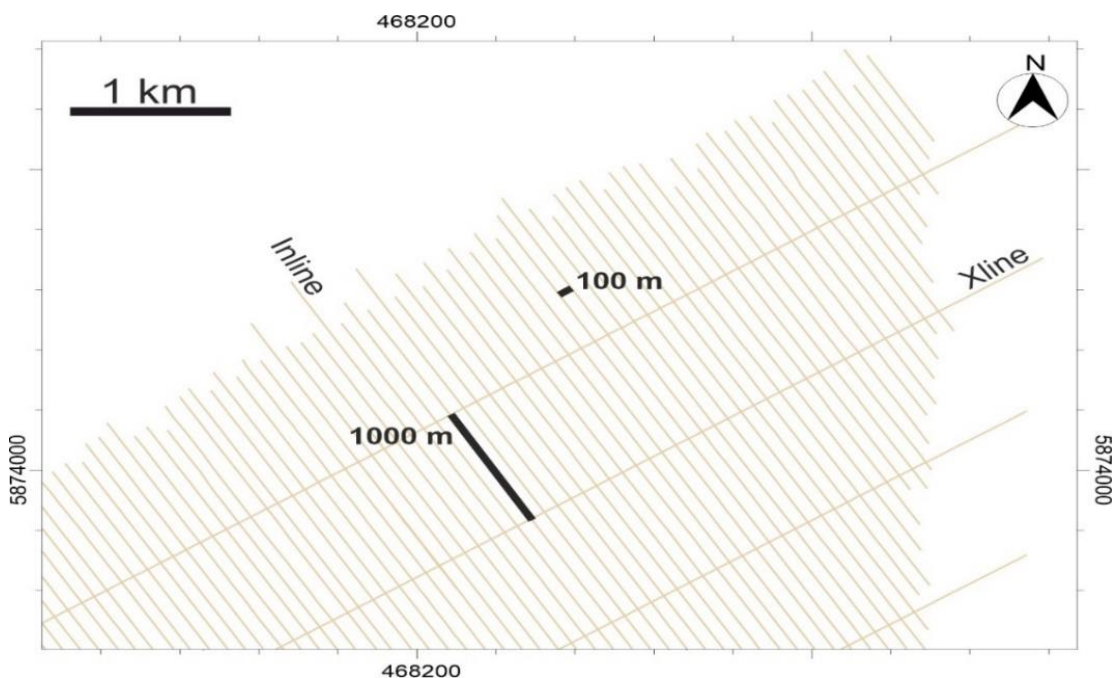
**Figure 2.1. Seismic reflection data coverage. Sub bottom profile and Ultra High Resolution seismic reflection data is available to the study over Norfolk Vanguard West, Boreas, and the Cable Route. Regional bathymetry data also shown, courtesy of (EMODnet Bathymetry Consortium, 2018).**

#### 2.1.1. Acquisition and resolution

Collection of seismic reflection data over the three survey areas (Figure 2.1) was completed using the same acquisition and processing techniques. The projected coordinate system used for all surveys analysed in this project is ETRS89 / UTM zone 31N (EPSG: 25831). Two types of seismic data were acquired concurrently in Norfolk Vanguard West (2015) and Boreas (2017) and included sub-bottom profiler (SBP) and

Ultra-high resolution seismic (UHR). In all survey areas, the spacing of seismic lines is the same, with the inlines spaced at 100 m and cross-lines spacing 1 km (Figure 2.2). The SBP data were acquired using a hull-mounted pinger. The average velocity of water was 1517 m/s. The pinger used a high frequency (4.5 kHz) and therefore provided relatively high-resolution data, with a vertical resolution between 0.1 to 0.2 m (Fugro, 2016; Fugro, 2017). The application of high-frequency comes at the expense of reduced penetration depth, with maximum investigation depths down to ~30 m below seabed. The UHR data were acquired with a sparker source. The sparker source was higher energy than that used for SBP and therefore achieved a greater depth of penetration (300 m) but with a lower vertical resolution than seen in the SBP data (Fugro, 2016; Fugro, 2017).

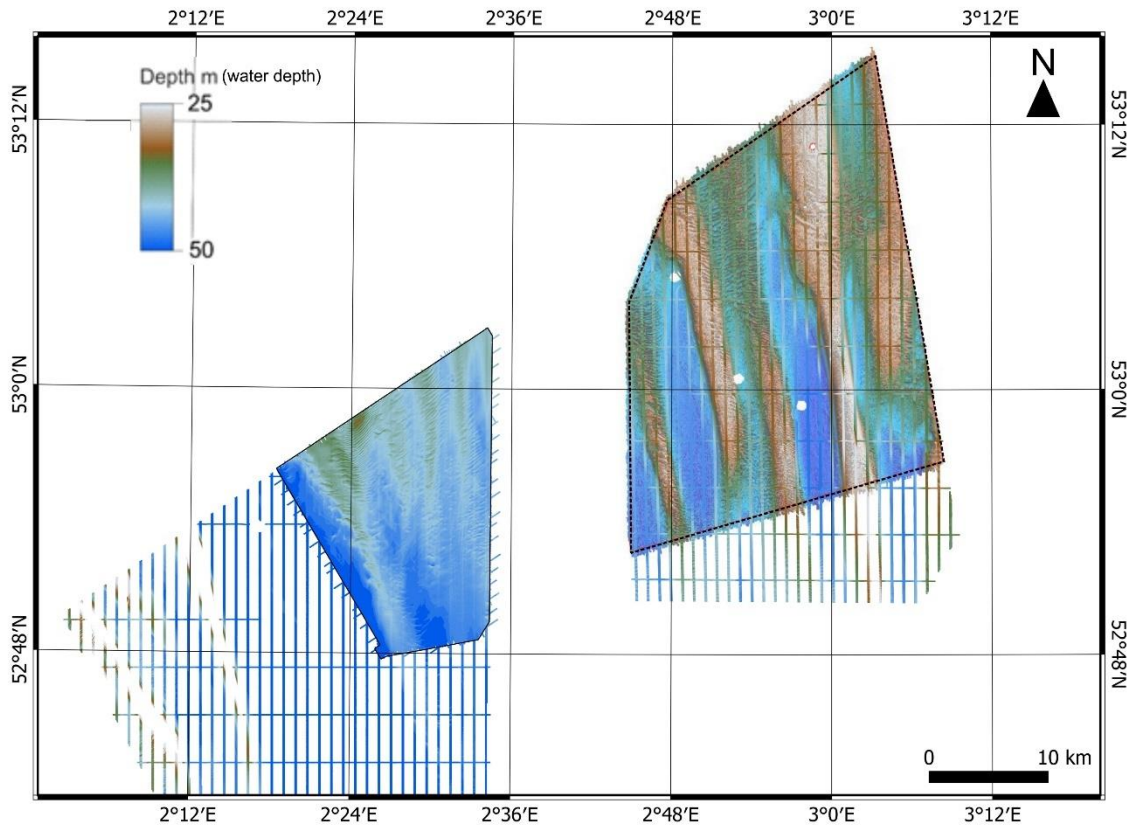
Depth conversion of all seismic data was completed by Fugro. The SBP data were converted from time to depth using a seismic velocity of 1600 m/s. The accuracy of the seismic velocity used for depth conversion is confirmed by a generally very good fit between the cone penetration test profiles and the depth converted sections. The UHR seismic were converted with a velocity field derived during seismic processing.



**Figure 2.2. Dense 2D grid of seismic reflection data is available to this study, with inlines orientated NW-SE and cross-lines orientated NE-SW. The inlines have a line spacing of 100 m, whilst the cross-lines have a spacing of 1 km.**



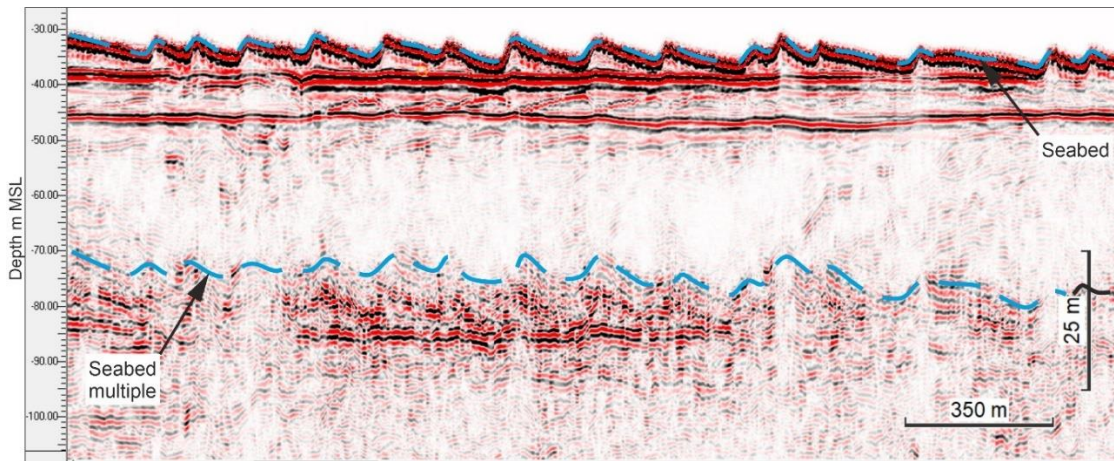
Complementing the 2D seismic data, multibeam echo sounder (MBES) bathymetry data were collected (Figure 2.3). The MBES bathymetry data were acquired using a Kongsberg EM 2040, with a frequency of 400 kHz. A regional MBES survey was acquired in 2010 that was approximately 31% coverage, whilst in 2015 (Norfolk Vanguard West and Cable Route) and 2017 (Boreas) full coverage MBES surveys were acquired.



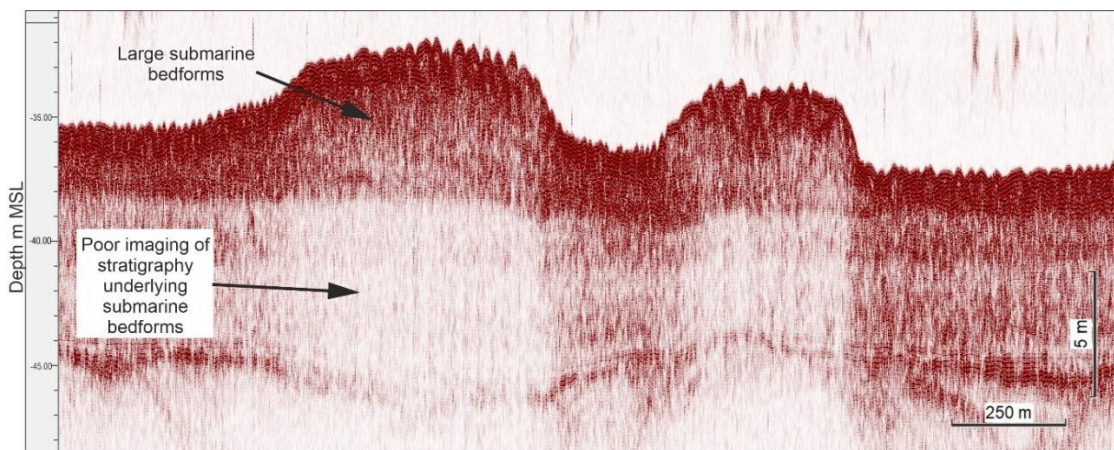
**Figure 2.3. Coverage of regional and site specific MBES data over Norfolk Vanguard West and Boreas. Regional surveys were acquired in 2010, and full coverage site surveys in 2015 and 2017.**

The quality of UHR seismic reflection data is very good and generally presents no problems for interpreting seismic stratigraphy and facies. A prominent seismic seabed multiple obscures a key stratigraphic surface at Middle Pleistocene level (Figure 2.4) and appears as a band of seismic noise that is present over the entire Norfolk Vanguard West area. The change in seismic facies above and below this level mean an approximate surface for the obscured level can be mapped, albeit with lower confidence in subtle changes in surface morphology. The quality of the SBP seismic is also good, but interpretation is affected by the relatively hard and irregular seabed throughout the study areas. Along the western margin of Norfolk Vanguard West, the data continuity is good, but elsewhere large dune-scale bedforms create strong

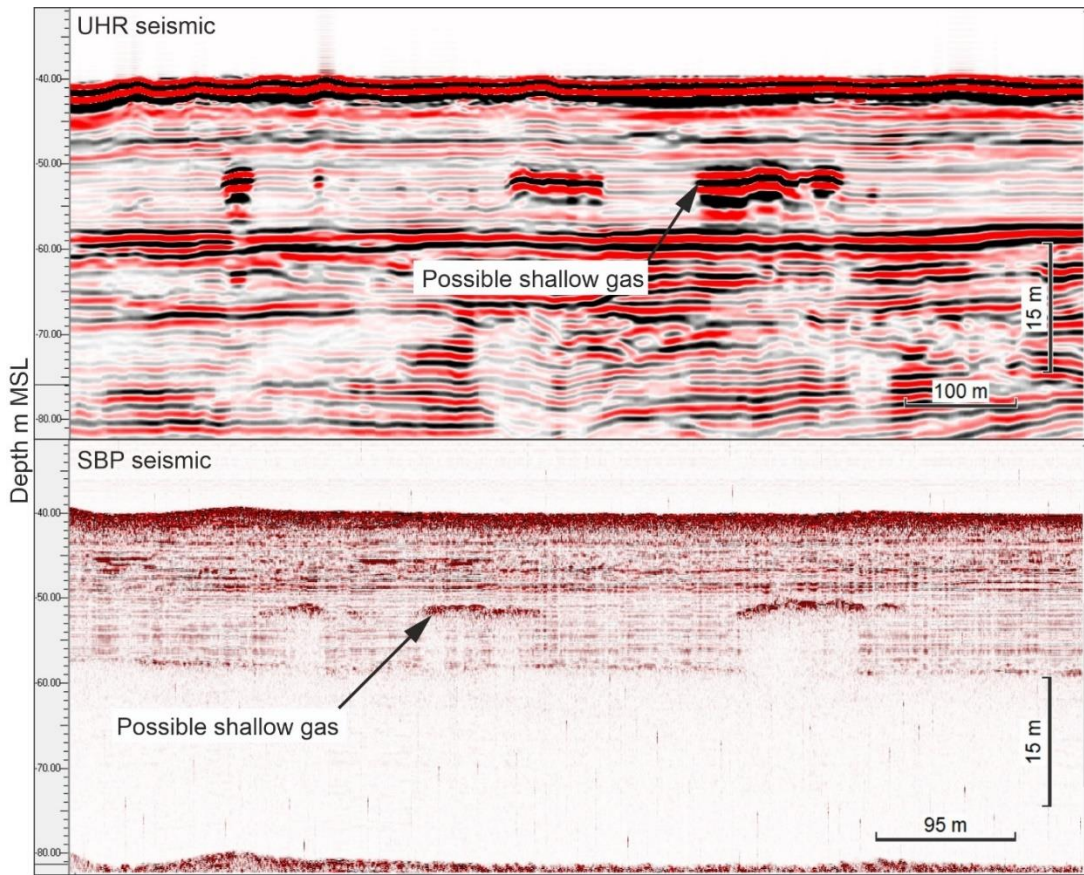
negative amplitude seismic diffractions and induce a 'wobble' on the data that cannot be fully removed by processing and has subsequently led to poor imaging of the underlying stratigraphy (Figure 2.5). Possible shallow gas anomalies obscure the seismic character in the west of Norfolk Vanguard West (Figure 2.6). These gas anomalies are present in both UHR and SBP seismic, with the character of the anomalies reflecting the differing resolution of the two datasets.



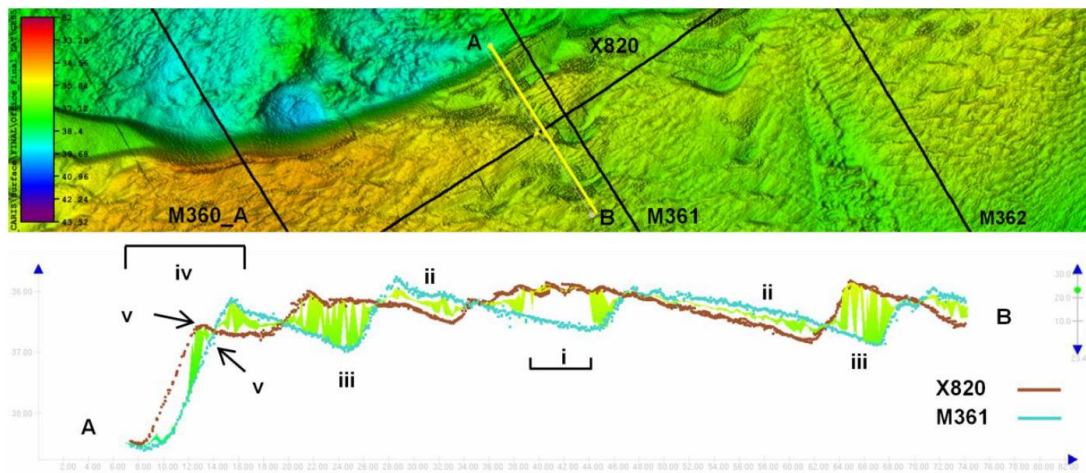
**Figure 2.4. Seabed seismic multiple present in UHR data in Norfolk Vanguard. The multiple obscures a key stratigraphic surface at Middle Pleistocene level (Top Yarmouth Roads Fm.).**



**Figure 2.5. Where large submarine bedforms (dunes and/or sand banks) are present, the underlying seismic (SBP) stratigraphy is poorly imaged.**



**Figure 2.6. Possible shallow gas anomalies present in both UHR and SBP seismic surveys.**







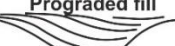


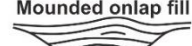
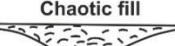
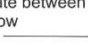
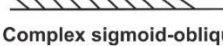



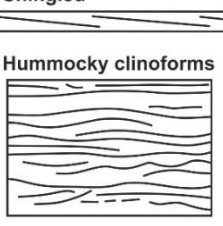



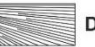
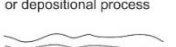


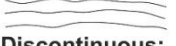

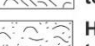
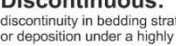

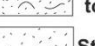


**Figure 2.7. The mobility of seabed sediments influences surface gridding. Data from inline M631 (15- 09-2016), xline X820 (29-10-2016) and the corresponding surface. Sediment movement occurring between inline and xline surveys creates artefact in gridded surface (Fugro, 2016).**

The MBES data is considered good quality but there are 'noisy' patterns in the final depth terrain model. The noise is considered the product of relatively rapid migration of marine bedforms, leading to meaningful changes in the seafloor topography, when two adjacent or intersecting swaths are surveyed with a long intervening time period (Figure 2.7).

### **2.1.2. Interpretation**

Using the IHS Kingdom software, all available inlines and cross-lines have been interpreted in depth across the Norfolk Vanguard West and Boreas study areas. The seismic stratigraphy has been characterised using a range of approaches. Firstly, major boundaries are traced based on discordant stratal relationships and unconformities. These bounding surfaces are interpreted along either a trough or peak of the seismic wavelet, depending on which has the greatest absolute value. Using a seed interpretation method, a seismic reflection event was traced as far as possible laterally in both directions along a xline, and then using the intersection with inlines to complete interpretation of the surface. Interpretation of seismic horizons in a geologically plausible fashion was achieved using loop correlation, whereby seismic horizons are tied consistently from line to line in a grid. Seismic interpretation misties between lines were identified using contour maps, whereby misties became evident by groups of unreasonable contours. Secondly, seismic facies were interpreted to discriminate other bounding surface where no obvious reflector or stratal terminations are obvious. Seismic facies were identified following Mitchum et al. (1977) and Mellett et al. (2013) by identifying distinct seismic facies, based on seismic amplitude, frequency, and geometry and termination style of reflectors (Figure 2.8), areas with similar facies could be identified across the study areas, allowing a seismic stratigraphy for the study areas to be built-up.

Prograding clinoforms	Channels and fills		Reflector configuration	
			Frequency	Amplitude
<b>Sigmoid</b> 	<b>Channel belt</b> 	<b>Channel complex</b> 	<b>High</b>  Thin bedding or highly variable	<b>High:</b> Large changes in density of sediment indicating mixed composition
<b>Oblique tangential</b> 	<b>Onlap fill</b> 	<b>Prograded fill</b> 	<b>Medium</b>  Intermediate between high and low	<b>Medium:</b> Intermediate between high and low
<b>Oblique parallel</b> 	<b>Mounded onlap fill</b> 	<b>Chaotic fill</b> 	<b>Low</b>  Thicker bedding or low variability	<b>Low:</b> Small changes in density of sediment indicating relative homogeneity
<b>Complex sigmoid-oblique</b> 	<b>Divergent fill</b> 	<b>Complex fill</b> 		
<b>Shingled</b> 	<b>Patterns</b>		<b>Continuity</b>	<b>Terminations</b>
<b>Hummocky clinoforms</b> 	 <b>Parallel draped</b>	 <b>Wavy</b>	<b>Continuous:</b> continuity in bedding strata or depositional process	<b>Onlap:</b> aggradation of younger sediments onto a surface
	 <b>Sub-parallel</b>	 <b>Divergent</b>	 <b>Discontinuous:</b> discontinuity in bedding strata or deposition under a highly variable energy regime	<b>Downlap:</b> progradation of younger sediments onto a surface
	 <b>Parallel</b>	 <b>Hummocky to oblique</b>		<b>Truncation:</b> erosion of older strata
	 <b>Sigmoid to oblique</b>	 <b>Hummocky to chaotic</b>		
	 <b>Parallel oblique</b>	 <b>Structurless</b>		

**Figure 2.8. Seismic facies descriptors used in this study, based on Mitchum et al. (1977) and Mellett et al. (2013).**

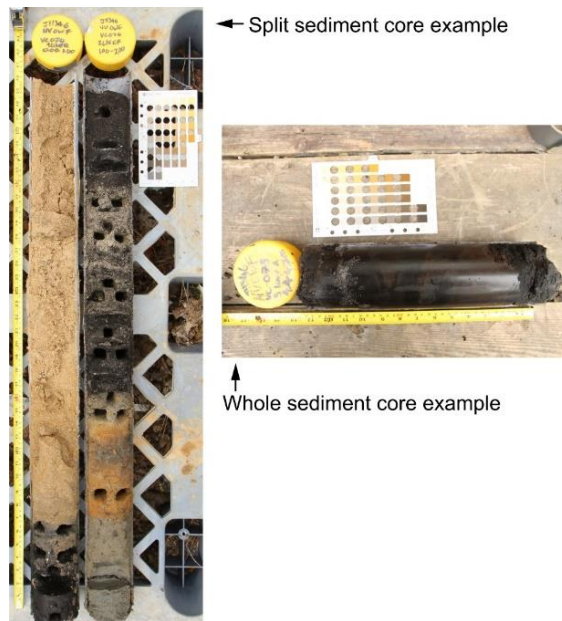
### 2.1.3. Mapping and GIS

Following interpretation of a seismic horizon along all available seismic lines, the horizon was gridded using the IHS Kingdom software. The x, y and z points that define points interpreted along a line are spaced at approximately 1 m intervals. This results in an uneven point density, with the nearest points on a different line being approximately 100 m away. In order to generate maps from interpreted horizons, these points require gridding and interpolation. Due to the difference in point density, traditional interpolation methods such as kriging or nearest neighbour produce geologically unrealistic maps. The Flex Gridding algorithm available in IHS Kingdom software reduces this by applying a plate spline and a smoothing spline to fit to the data, producing more geologically plausible maps. Isopach maps were used for interpreting changes in seismic unit thickness across the study areas. Isopach maps were generated by calculating the depth difference between the top and base depth surface (maps) of the seismic unit of interest. The gridded horizons were exported as comma separated value (.csv) files as x and y positions in ETRS89 / UTM zone 31N (EPSG: 25831) and in z in metres relative to the ETRS89 geoid. The .csv files were imported into QGIS as vector shapefiles, and converted to raster files using `gdal_rasterize`, using the same grid size as that used for gridding in Kingdom.

## **2.2. Vibrocores**

### **2.2.1. Acquisition and storage**

Seventy-nine vibrocores was acquired across Norfolk Vanguard West, the Cable Route, and Boreas. The vibrocore sampling operations were performed using Fugro's high performance corer. The barrel length of the corer was 6.5 m and uses a motor to generate optimum frequency and vibration amplitude to penetrate sediments. In general, vibrocores were sampled without issue but on occasion where full penetration (6 m) was not achieved, the core barrel was redeployed. Insufficient penetration occurred as a result of unforeseen subsurface conditions, such as stiff sediment or boulder obstruction. If poor penetration continued, the sampler was moved to another specified location (typically less than 10 m) until full penetration was achieved. The majority of the cores were taken onshore for geotechnical sampling and testing. These cores were destructively sampled and have not been physically logged in this study. However, high resolution photographs were taken prior to sampling and these photos have been available to this study and have been used in combination with cone penetration data to digitally log the cores. A number of cores were retained for geoarchaeological assessment by Wessex Archaeology (Figure 2.9). Eight cores have been physically logged for this study. The condition of these cores has been generally good and sufficient for interpretation, with cores split and stored in their plastic liners in a cool dark environment. Some sections of cores were missing due to palaeoenvironmental sampling carried out by Wessex Archaeology but in general these samples were only taken from one half of the core.



**Figure 2.9. Example of sediment cores logged and sampled at Wessex Archaeology (Salisbury). Example of a split sediment core ready for logging, and a whole core prior to being split.**

### **2.2.2. Interpretation**

Sedimentary core logs were drafted after measurement and description of vibrocores (Figure 2.10). The logging of vibrocores recorded changes in grain size and shape using a grain-size comparator card, visual estimates of sorting, textural changes (brittle, friable, plastic), and colour according to the Munsell colour scale. Where sedimentary structures, plant remains, or shells were observed, they were recorded. The core observations were then used to build sedimentary facies, which were assigned lithofacies codes.

# SEDIMENTARY CORE LOG

Coarse Clastics

PS - Preserved Sample  
 RB - Unloggable rubble  
 MI - Missing  
 BG - Bagged

$\phi$  = log<sub>10</sub> d/D<sub>50</sub> (in mm)  
 -10 = 1024mm  
 -9 = 512mm  
 -8 = 256mm  
 -7 = 128mm

Tim Cullen (t.m.cullen1@leeds.ac.uk)	
Well	VE076
Field	NW West
Date	20.2.2017
Project	PLD
2 of 2	

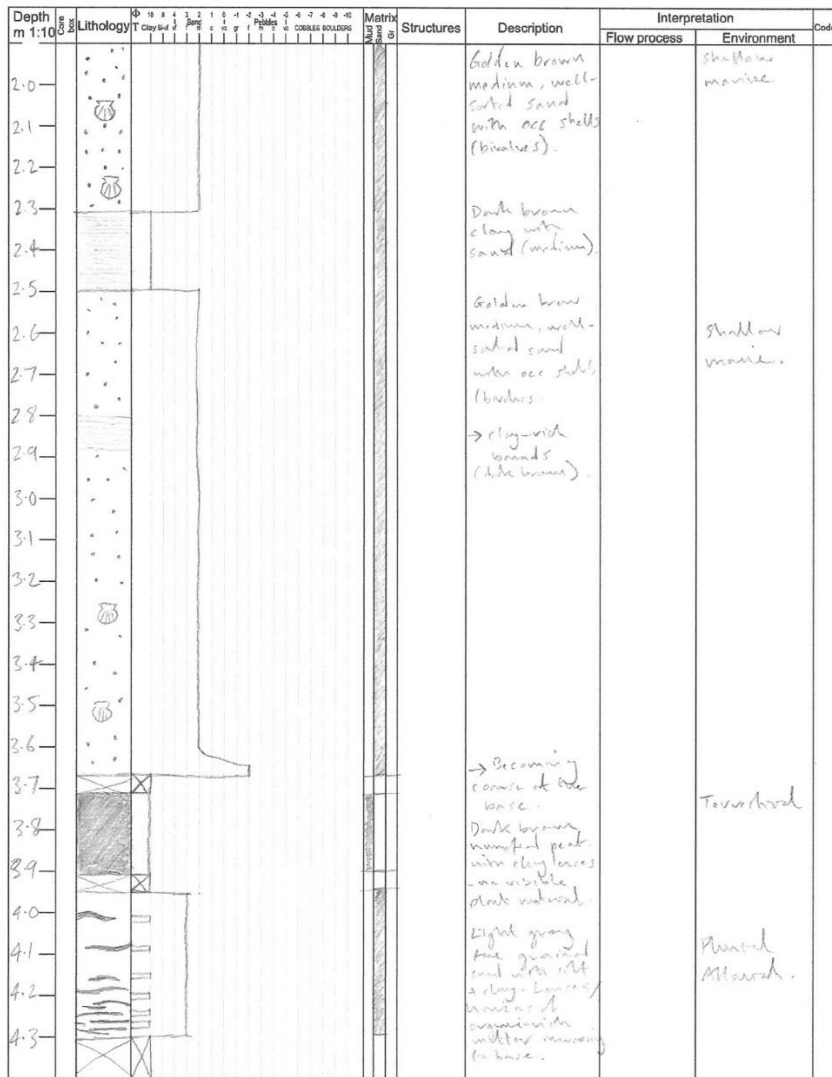


Figure 2.10. An example of hand drawn sedimentary log. Log sheet design by Tim Cullen.

## 2.3. Geotechnical logs

### 2.3.1. Acquisition

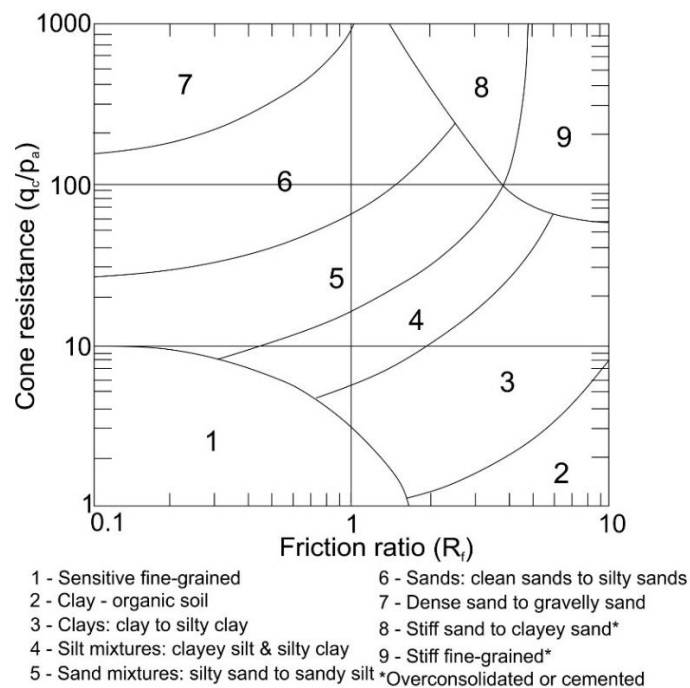
As part of the Norfolk Vanguard and Boreas site surveys 79 cone penetration tests (CPTs) were acquired by Fugro. These CPT tests were taken at the same locations as the vibrocores mentioned previously. CPT sampled to a maximum depth of 50 m below seafloor in Norfolk Vanguard West and Boreas survey areas, and down to a maximum of 7 m below seafloor in the cable route survey area. Measurements recorded during the CPT include cone resistance, sleeve friction, pore water pressure and cone



inclination. The vertical resolution of the CPTs is two metres. CPT were made available to the project pre-loaded into IHS Kingdom Suit.

### 2.3.2. Interpretation

The CPT measures of cone resistance ( $q_c$ ) and sleeve friction ( $f_s$ ) have been used to derive friction ratio (Rf). Rf is the ratio between the local sleeve friction and the cone resistance. The friction ratio has been used here as an indicator of soil/sediment type (grain size). Using the Soil Behaviour Type chart (SBT, Figure 2.11), predictions of sediment type have been made. Although no firm interpretation of lithofacies can be made from CPT logs, interpretations of depositional environment can be made when correlated with seismic facies.



**Figure 2.11. Soil Behaviour Type chart (Robertson et al., 1986) based on CPT cone resistance,  $q_t$ , and friction ratio, Rf.**

## 2.4. Geophysical and sedimentological correlation

The interpretation of depositional environments was based on correlation of seismic facies and lithofacies, relative to stratigraphic position and morphology. Where sedimentary cores were not available (>6.5 m below seafloor), seismic facies character and the position with the stratigraphic framework, were used to infer environments of deposition. In the shallow subsurface, interpreted sedimentary cores were overlain on depth converted seismic reflection data alongside CPTs and visually compared to establish a relationship between lithofacies and seismic facies character.

## **2.5. Sediment samples and organic carbon analysis**

### **2.5.1. Sampling**

Sampling of cores was completed at Wessex Archaeology's core store. The sampling program was designed to capture high-resolution changes in carbon content across organic-rich intervals of postglacial origin. Samples were taken from 9 cores across the Norfolk Vanguard West and Boreas study areas. The sampling interval was 5 cm throughout the organic-rich interval, with an additional two samples at 5 cm intervals, taken in the overlying and underlying sediments bounding the organic-rich interval. At each sample point, two 2 cm<sup>3</sup> volumetric samples were taken using volumetric sampling rings. This tube was driven into the soil/sediment either by hand or using a mallet if the soil/sediment was particularly stiff. The sample was then extruded from the volumetric sampler into a plastic sealed bag and labelled with a sample code, type, core number, and date. In addition, at each 5 cm sampling point, a 1 cm slice bulk sample was taken. This was stored in a plastic sealed bag and labelled accordingly. The samples were transported to the University of Leeds and stored in a refrigerator (approximately 4°C) until required for laboratory analysis.

### **2.5.2. Sample preparation and bulk density measurement**

Bulk density of samples was determined using a standard gravimetric method (Dadey et al., 1992). Samples were weighed to determine the wet bulk density (WBD), and then dried for 48 hrs at 105°C, until a constant weight was achieved. From the dried samples a dry bulk density (DBD) was calculated. The dried samples were then milled to a fine powder (~ 100 um) using a mixer mill MM 400 (Figure 2.12) and stored in sealed plastic bags until required for carbon analysis.



**Figure 2.12. Mixer Mill MM 400 used to mill dried sediment samples.**

### **2.5.3. Carbon analysis**

The process used to determine total carbon (TC) and organic carbon (OC) is summarised in Figure 2.13. TC and OC were determined in two stages due to the destructive nature of the method used to analyse for TC. To determine TC an aliquot of  $4 \pm 0.2$  mg of sample was placed in a silver capsule. The silver capsule (Figure 2.14) was folded into an approximate cube, being sure to remove as much air as possible. The samples were then measured for TC on the University of Leeds, School of Geography Elemental Vario Micro analyser (Figure 2.14) and calibrated with sulfanilic acid. Standard reference material B2150X and B2152X (high organic content standard from Elemental Microanalysis, UK) were used to estimate the precision of analysis. To analyse for OC, the same approach was used but with some additional steps. In order to calculate OC, the inorganic carbon (IC) components have to be removed from the sample (e.g. calcite, dolomite and siderite). Removal of the inorganic carbon was achieved by adding hydrochloric acid (HCl) to the sample (within the silver capsule). The HCl was then removed by drying at  $105^{\circ}\text{C}$  for 24 hrs or until a constant weight was achieved. It was found after analysing for OC in the elemental analyser that OC values were not realistic. It was assumed that drying was incomplete prior to analysis and excess chlorides remained in the sample from the addition of HCl, on top of the initial high natural chloride content associated with the samples. To try and remove excess chloride the new batch of samples were freeze-dried for one week. After freeze drying, the samples were run in the elemental analyser and analysed for OC. The IC was

calculated from the difference between the TC and the OC measurements. The methods used for calculation of TC and OC followed a combined approach of Smeaton et al. (2016) and the University of Leeds, School of Geography, with the exception of the freeze drying step, which was devised for the purposes of this study.

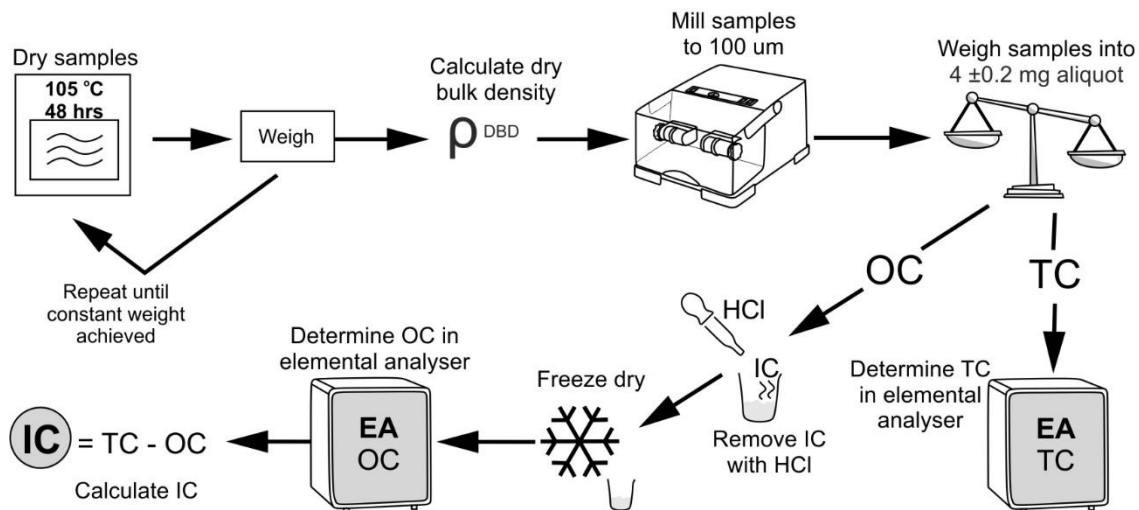


Figure 2.13. A flow chart showing the laboratory process used to analyse for bulk density (DBD), total carbon (TC), organic carbon (OC).



Figure 2.14. An example of the elemental analyser used to analyse for TC and OC. Also shown are the silver capsules that sediment samples are measured into prior to folding and analysis.

## **2.6. Applications of methods to data**

The integration of seismic, sediment core and CPT data has enabled a stratigraphic framework to be constructed for this area of the southern North Sea and then placed in the wider published framework. This robust stratigraphic framework was the basis for the interpretation of the results in the following chapters, and enabled the interpretation depositional environments and geomorphological features. The individual seismic units were correlated with lithofacies from vibrocores to determine relative timing and depositional environments. Where available radiocarbon dates and palaeoenvironmental analysis data has helped to develop chronostratigraphic relationships and further refine the timings that changes environments of deposition occurred. This workflow was used in the following results chapters and discussion chapter, and enabled interpretation of palaeogeographic environments and the process response to these changing palaeoenvironments.

## **Chapter 3 - Palaeogeographic changes in response to glacial-interglacial cycles, as recorded in Middle and Late Pleistocene seismic stratigraphy, southern North Sea**

Eaton, S.J., Hodgson, D.M., Barlow, N.L., Mortimer, E.E. and Mellett, C.L., 2020. Palaeogeographical changes in response to glacial–interglacial cycles, as recorded in Middle and Late Pleistocene seismic stratigraphy, southern North Sea. *Journal of Quaternary Science*, 35(6), pp.760-775. <https://doi.org/10.1002/jqs.3230>

As lead author, Stephen James Eaton was responsible for data analysis, interpretation, and manuscript and figure preparation. The role of other co-authors was limited to discussion of results and manuscript editing.

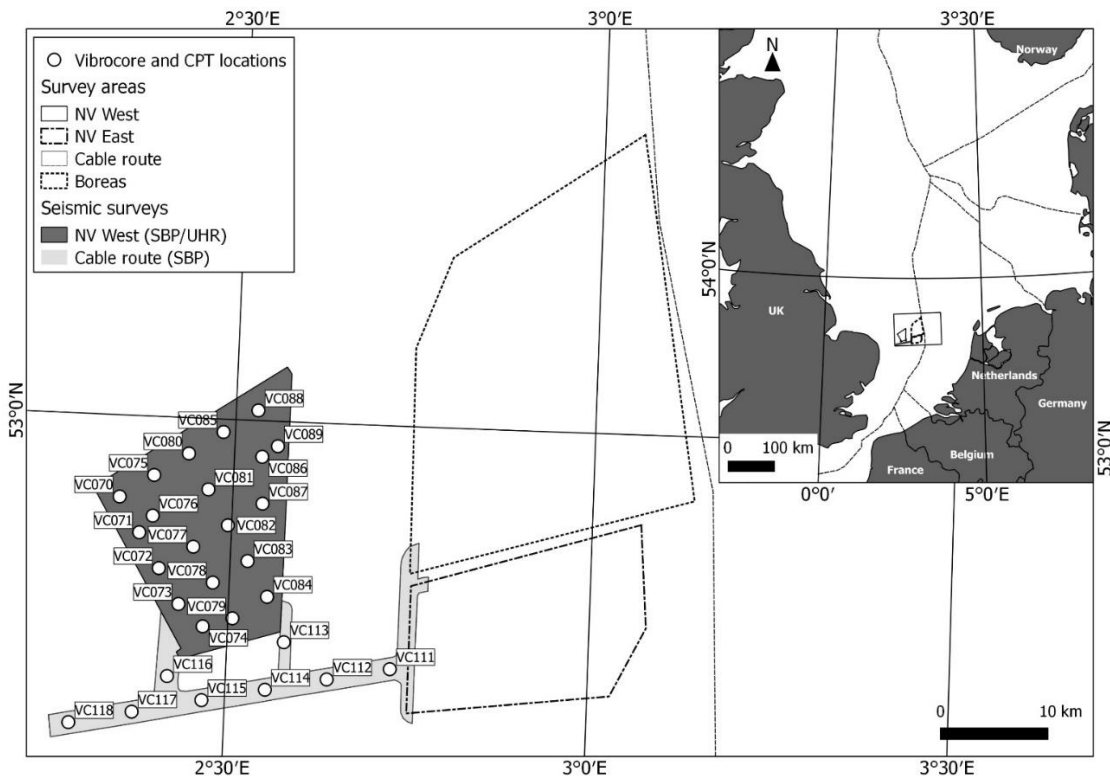
### **3.1. Introduction**

Throughout the Pleistocene, shallow continental shelves were periodically exposed and submerged in response to repeated glacial-interglacial cycles, respectively (Shennan et al., 2000; Smith et al., 2011; Bridgland, 2002; Busschers et al., 2007; Hijma et al., 2012). The resulting periods of terrestrial-marine-terrestrial transitions have resulted in a complicated stratigraphic record of depositional and erosional processes (Emery et al., 2019; Mellett et al., 2013; Scourse et al., 1998; Head and Gibbard, 2015). The Pleistocene basin-fill of the southern North Sea continental shelf is a valuable archive that has been used to reconstruct changes in palaeolandscapes (Gibbard, 1988; Cameron et al., 1992; Funnell, 1996; Busschers et al., 2007; Parfitt et al., 2010; Hijma et al., 2012; Murton et al., 2012; Cohen et al., 2014; Peeters, 2018). Studies have highlighted periods of North Sea glaciation resulting in mapped ice-sheet limits (Praeg, 1996; Scourse et al., 1998; Beets et al., 2005; Carr et al., 2006; Davies et al., 2011; Murton and Murton, 2012; Cotterill et al., 2017; Emery et al., 2019), developed palaeogeographical maps (Bicket and Tizzard, 2015; Fitch et al., 2005; Funnell, 1996; Hijma et al., 2012), and reconstructed the evolution of northwest European drainage networks (Peeters et al., 2015; Gibbard, 1988; Bridgland et al., 1995). Despite this, arriving at robust reconstructions of successive landscape responses to glacial-interglacial cycles has remained a challenge due to the fragmentary nature of evidence (Lee et al., 2006), sparse boreholes and limited 2D-seismic reflection profiles. Advances in offshore submarine technologies and increased availability of high-resolution commercial data has greatly improved the potential to understand submerged and buried landscapes, and their evolution during the Middle and Late

Pleistocene. Empirical evidence derived from these datasets of changing physiography can help to inform landscape evolution models.

Palaeogeographic reconstructions in high-relief settings make the reasonable assumption that catchments and adjacent sedimentary basins maintain simple source-to-sink configurations, and that overall sediment transport directions do not change, even if sediment flux varies significantly through time (e.g. Castelltort and Van Den Driessche, 2003; Romans et al., 2016; Sadler and Jerolmack, 2015). However, in low relief continental shelf settings this assumption needs to be treated with caution. This is particularly true in ice marginal settings where major and abrupt change in sediment transport direction can occur, which complicates estimates of sediment flux and provenance studies. With sufficiently high-resolution 3D data over large areas, sediment transport pathways can be mapped through time leading to more meaningful palaeogeographic reconstructions, particularly in low-relief landscapes that have been subject to a complex changes in climate and base level over relatively short periods of time.

This study aims to document a geologically constrained Middle to Late Pleistocene sedimentary sequence in the Vanguard wind farm zone offshore East Anglia, UK using a densely-spaced grid of 2D seismic reflection data, borehole samples and geotechnical cone penetration tests (CPT) acquired for industrial purposes (Figure 3.1). We compare our detailed regional results with the current stratigraphic framework for the wider southern North Sea (Figure 3.2d - Stoker et al., 2011) to assess spatial and temporal similarities and differences. This paper sets out to analyse the seismic facies and interpret the depositional environments through coroboration with core and CPT data; integrate our descriptions of marine, fluvial and glacial sequences to better understand the regional landscape response to climatic fluctuations; and embed these results into wider-scale reconstructed palaeogeographies for the Middle to Late Pleistocene in the southern North Sea.



**Figure 3.1. The Norfolk Vanguard survey areas are located within the UK sector of the southern North Sea. Norfolk Vanguard comprises three survey areas: NV West, NV East and the cable route. The Norfolk Boreas survey area sits to the north-east. Ultra-high resolution (UHR) and sub bottom profile (SBP) seismic reflection surveys acquired over NV West and the cable route survey areas that are used in this paper. Locations for twenty-eight vibrocores and cone penetration tests (CPT) over the NV West and cable route survey areas.**

### 3.2. Study area

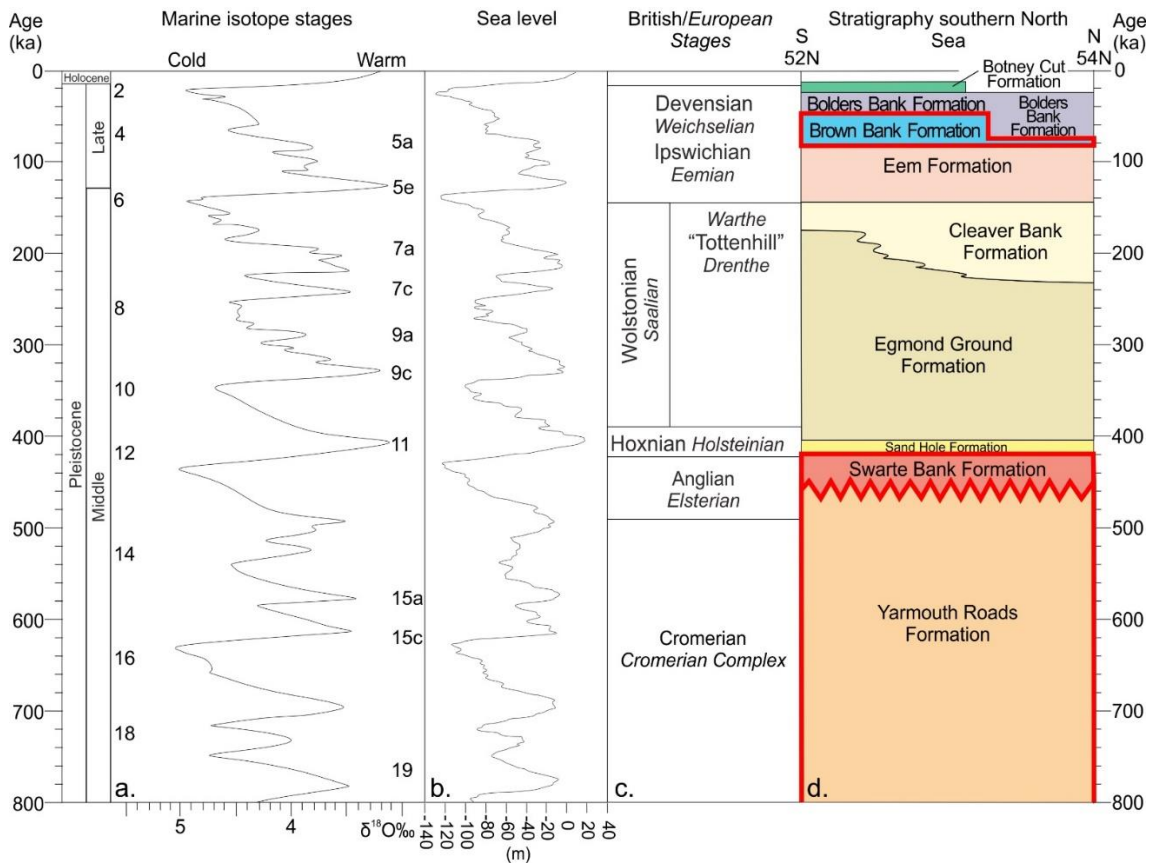
The study area is 401 km<sup>2</sup> and comprises the Norfolk Vanguard West (NV West), cable route, Norfolk Vanguard East (NV East) and Norfolk Boreas survey areas, and is in shallow water (<50 m) approximately 47 km east of the East Anglia coastline (Figure 3.1). Local variations in seabed topography are mainly attributed to the presence of large sand banks that are interpreted to have formed during the late Holocene (Dyer et al., 1999; Liu et al., 2007; Van Der Molen et al., 2001), or are relic features formed during a transgressive hydrodynamic regime (Van Landeghem, et al., 2009; Cameron et al., 1992; Uehara et al., 2006).

### 3.3. Geological setting

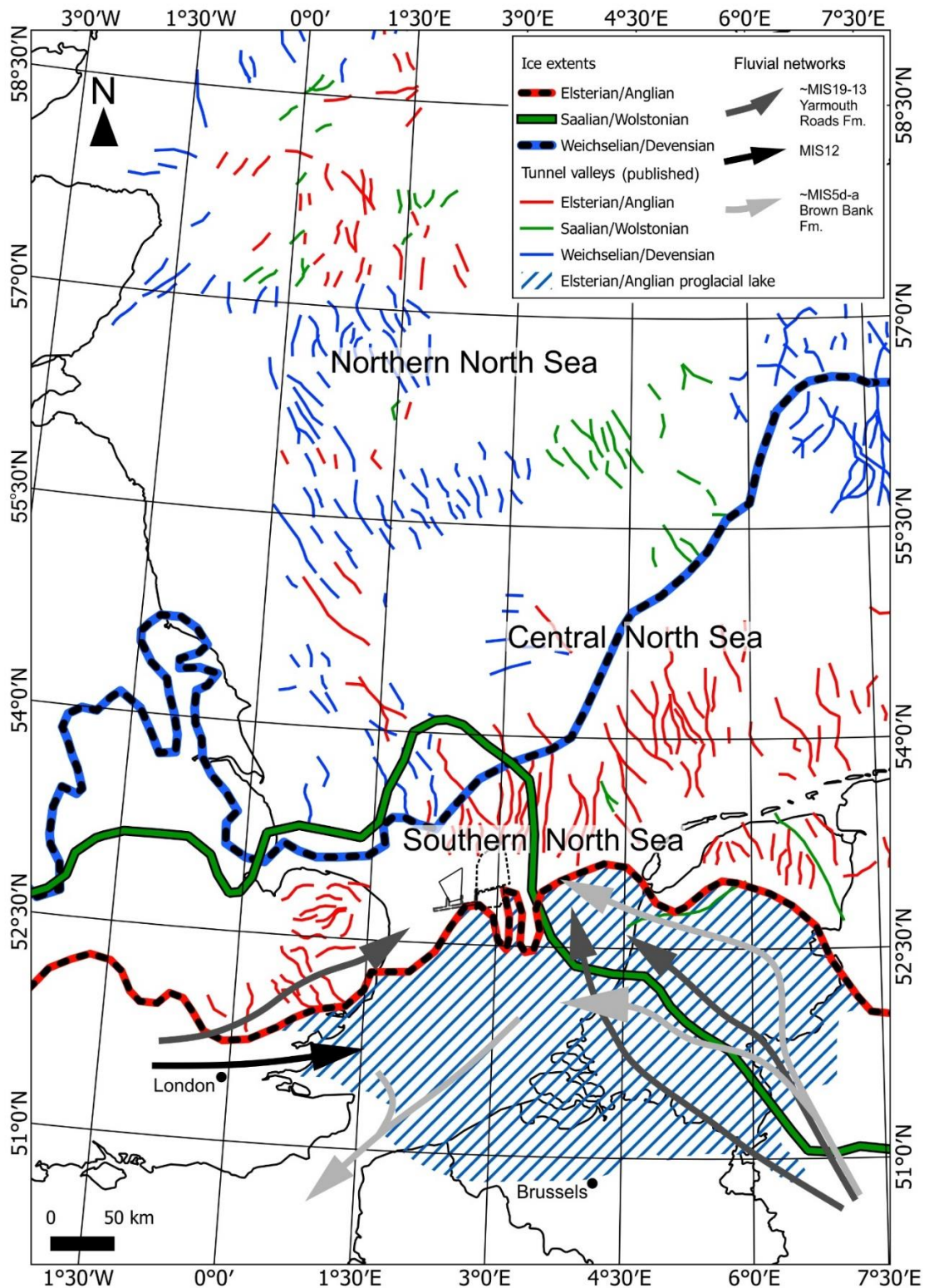
The Quaternary succession within the study area provides a record for which landscape response to climatic and base level fluctuations can be investigated. The present day configuration of the North Sea Basin is largely a result of Late Jurassic and



Early Cretaceous rifting (Glennie et al., 1998). Since the Late Cenozoic, there have been up to 3000 m of sediments deposited, of which 800 m was deposited during the Quaternary (Gatliff et al., 1994; Lamb et al., 2018). The Early Pleistocene sedimentation within the study area was dominated by shallow marine facies (Cameron et al., 1989). The Middle Pleistocene (MIS 19-13 –Figure 3.2) was a period of heightened climatic instability (Ehlers et al., 2007), driving regional-scale falls in relative sea level (RSL), river drainage configurations, and glaciation cycles (Lee et al., 2006). At least three major glacial advances have extended into the southern North Sea (Graham et al., 2011; Carr et al., 2006; Ehlers et al., 1991; Bowen et al., 1986; Long et al., 1988; Ehlers, 1990). The Anglian Stage (MIS 12) glaciation (Figure 3.3) marks the most extensive of these glaciations (Cameron et al., 1992; Clark et al., 2004; Streif, 2004). The Hoxnian interglacial followed the Anglian Stage glaciation, a period (likely correlating to both MIS 11 and 9) in which the southern North Sea was flooded (Cohen et al., 2014; Streif, 2004; Bogemans et al., 2016). During the Wolstonian Stage (MIS 10-6) there were several ice sheet advances likely during MIS 10, 8 and 6 (Graham et al., 2011; Toucanne et al., 2009; Beets et al., 2005; Pawley et al., 2008; Moreau et al., 2012), however these did not extend as far south as the study area (Figure 3.3 – maximum ice limit). The Ipswichian interglacial (MIS 5e) followed the final Wolstonian Stage, during which the North Sea was inundated, with marine influence reaching extents similar to today (Konradi et al., 2005; Streif, 2004). The subsequent Devensian Stage (Figure 3.3 – maximum ice limit)), was characterised by cycles of RSL rise (through MIS 5d-a, 4 and 3) and fall before final subaerial exposure by the time of the Last Glacial Maximum (LGM) within MIS 2 (Hijma et al., 2012; Bicket et al., 2015).



**Figure 3.2. Stratigraphic correlation framework for the Quaternary of the study area. (a) Marine isotope stages (Lisiecki and Raymo, 2005), (b) Global sea level estimates (Spratt et al., 2016), (c) British and European Stages (italics) (Based on Gibbard and Cohen, 2012), (d) Quaternary framework for the North Sea basin (based on Stoker et al., 2011a).**



**Figure 3.3. Composite map showing maximum ice extents for three major Pleistocene glaciations (Anglian and Wolstonian - Hijma et al. (2012) and references there in, Devensian – Ehlers and Wingfield (1991) and Sejrup et al. (2016)). Tunnel valleys associated with the three major glaciations (Graham et al. 2011). Glacial lake formed between 400,000 to 450,000 years ago and dammed to the north by ice extending from the north (adapted from Cohen et al., 2017; Gibbard, 2007).**

### **3.4. Data collection**

#### **3.4.1. Seismic data acquisition and interpretation**

Seismic reflection data was acquired by Fugro on behalf of Vattenfall Wind Power UK (Figure 3.1), and along with data acquisition reports, have been provided to the University of Leeds for an independent research project. A hull-mounted pinger (Massa TR-1075 pinger array, referred to here as Sub Bottom Profile (SBP)), and a towed multichannel Ultra-High-Resolution (UHR) seismic system has been used to image the shallow subsurface. The SBP seismic has a depth of investigation down to ca. 30 m below seabed (bsb) and uses a relatively high frequency (4.5 kHz), which equates to a vertical resolution of 0.1 to 0.2 m. SBP seismic has been acquired in both the NV West and cable route survey areas. In the NV West survey area, the SBP seismic has inline spacing of 100 m and xline spacing of 1 km. Along the cable route survey area, the inline spacing is variable (80 – 100 m). The UHR seismic has a depth of investigation up to ca. 300 m bsb with a frequency of 4 Hz, which equates to a 1 to 5 m vertical resolution. The seismic is minimum phase. Within the NV West survey area, UHR seismic inlines have been acquired at 100 m spacing, and xlines at 1 km spacing. UHR seismic has not been acquired along the cable route

Both the UHR and SBP seismic reflection data had been depth converted by Fugro Oceansismica SpA. A seismic velocity of  $1600 \text{ m s}^{-1}$  has been used for the SBP seismic to convert from two-way travel time (TWTT) to depths in metres, and the UHR seismic has been depth converted using a velocity field derived during seismic processing. Seismic reflection data has been interpreted on every available inline and xline by the authors using IHS Kingdom with characterisation of seismic facies and stratigraphy (see Results) following Mellett et al. (2013) and Mitchum et al. (1977). Interpreted seismic surfaces were gridded using a minimum curvature algorithm, which provides geologically plausible surfaces. The cell size used for gridding was specified based on the data resolution (25mx25m for UHR and 20mx20m for SBP) so that each cell contains no more than one point.

#### **3.4.2. Vibrocore and cone penetration tests**

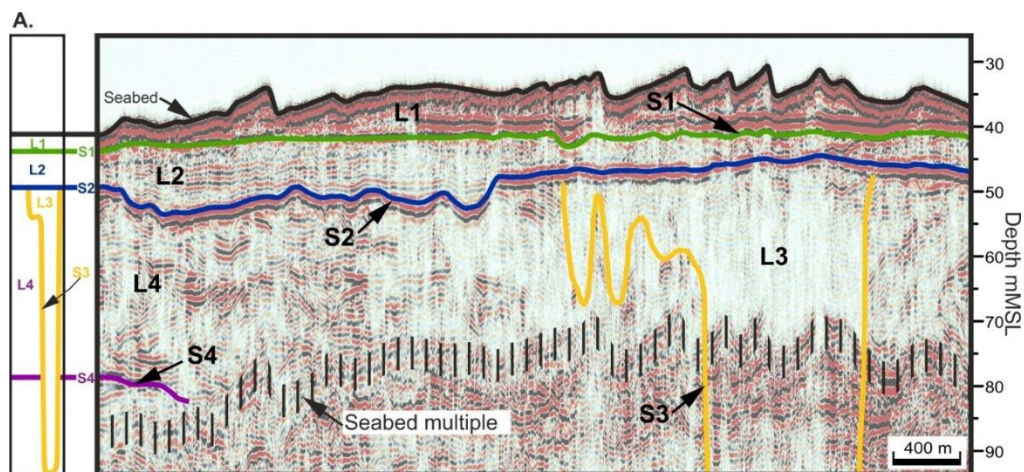
Offshore investigations within the NV West survey area by Fugro recovered 28 vibrocores (maximum penetration 6 m) and data from 28 cone penetration tests (CPT). Twenty three of these vibrocores were destructively sampled for geotechnical analysis by Vattenfall, but five cores were kept intact for geoarchaeological assessment (Wessex Archaeology, 2018). These 5 cores were independently logged for this

research project, and the remaining 23 vibrocores were logged using high resolution photographs taken by Fugro prior to destructive geotechnical sampling. CPTs penetrate to a greater depth than the vibrocores, and therefore provide data for interpretation of the geotechnical properties and lithology of deeper (>6 m) sediments. Technical information pertaining to the geotechnical investigation of Norfolk Vanguard and the cable route came from confidential reports.

The raw data and technical reporting that supports the findings of this study are not publicly available due to commercial restrictions.

### 3.5. Results

The Middle to Late Pleistocene sequence in the survey areas has been subdivided into four seismic units (L1-4) based on seismically mappable erosional surfaces/contacts (S1-4) that separate distinct seismic facies associations (Figure 3.4). These seismic facies interpretations have been corroborated with vibrocores (contacts/change in lithofacies), and changes in CPT parameters as outlined in Figure 3.4B.



**B.**

Seismic unit	Occurrence	External form	Seismic facies present	Interpretation	BGS regional stratigraphic framework equivalent
L1	Broad	Veneer	-	Shallow marine	
L2	Broad	Sheet	sf8, sf9, sf10, sf11	Marine/ lacustrine	Brown Bank Fm. Stoker et al., 2011
L3	North & central NV West	Channel fill	sf7	Glacial valley fill	Swarte Bank Fm. Stoker et al., 2011
L4	Broad	Sheet	sf3, sf4, sf5, sf6	Delta top	Yarmouth Roads Fm. Stoker et al., 2011

**Figure 3.4. Summary of seismic stratigraphic surfaces and units in the survey areas. A. Type UHR seismic section with seismic stratigraphic surfaces interpreted. S4 is only partially interpreted due to a seabed multiple. B. Summary table of seismic stratigraphic units, their distribution, form, seismic facies present, environmental interpretation and the British Geological Survey (BGS) regional stratigraphic framework equivalent to seismic units.**

### 3.5.1. Seismic stratigraphy

Eleven seismic facies (Table 3.1) have been defined based upon the seismic character, and bounding surfaces and their association. The UHR survey images down to ~300 m enabling characterisation of L4 and L3 and their bounding surfaces (S4 and S2). L1 and L2 are characterised using the SBP seismic, allowing a greater resolution of detail down to surface S2 compared with that of the UHR seismic. The seismic units and surfaces herein will be described starting with the lowermost surface and unit (S4/L4).

#### **Surface 4 (S4) and seismic stratigraphic unit 4 (L4)**

The L4 unit (average 41 m thick) is present over the entire NV West and cable route survey areas. The basal bounding surface, S4, is poorly defined across large parts of the survey area due to a coincident seabed multiple (Figure 3.5i). Where S4 is imaged (NV West western margin), it is characterised by a laterally discontinuous and high amplitude reflection, with truncated reflectors below, and is overlapped by the overlying L4 unit (sf1 – Table 3.1 and Figure 3.5i). The L4 unit is characterized by a range of seismic facies; the lower and middle L4 unit is seismically chaotic (sf3), comprising discontinuous seismic reflectors with sharp to transitional terminations (sf4). Incisional geometries are common but are more clearly defined in the upper section of L4 (sf5 and sf6, Figure 3.5i). The upper bounding surface of L4 corresponds to S2.

Three valley-fills (V1, V2 and V3) identified in the 2D sections have been mapped across the dataset (Figure 3.6A) within the upper L4 unit. These valley-fills are larger and more continuous than those observed in the Lower L4 unit. Valley-fills V2 and V3 are characterised by draped and divergent reflectors with maximum widths of 1.2 km and 4 km respectively that onlap the valley margins and are truncated at the S2 surface (sf5-Table 1, Figure 3.6A). Valley V2 is cut by V1 in the southwest of the NV West survey area. V1 is the largest (deepest and widest) of the valley-fills, is orientated approximately northeast-southwest, and has a maximum width of at least 12 km (unknown due to seismic survey limits) and a maximum valley-fill thickness of 33 m. The valley-fill comprises a series of stacked progradational reflectors (sf6), with multiple truncation surfaces, and is interpreted as a channel complex (Colombera et al., 2013). The youngest fill within V1 has a draped, divergent character. Overall, the valley axis for V1 deepens to the northeast.

### **Surface 3 (S3) and seismic stratigraphic unit 3 (L3)**

The L3 unit is bounded laterally and at its base by surface S3, and at its upper surface by S2. Locally, surface S3 is truncated by S2 (Figure 3.5ii and Figure 3.6B). L3 is confined to linear erosional features defined by S3, orientated approximately north-south, with one exception that is orientated approximately east-west. Locally, S3 extends to ~290 m below MSL, with a maximum width of ~1.5 km and thickness of ~165 m. The flanks of these linear features are steep (~40°) with an undulating thalweg depth. The flanks of the L3 fill are defined as truncated L4 reflectors adjacent to the structureless L3 but in places becomes uncertain due to seismic blanking. The seismic character of unit L3 is largely structureless and/or chaotic (sf7), although locally the seismic character is masked by two seabed multiples (Figure 3.5ii).

**Table 3.1. Summary of seismic facies identified and the seismic stratigraphic unit/surface they are associated with. Seismic descriptors used to characterize the facies are shown and seismic survey used to identify and characterize the facies are listed. Yellow is used to highlight seismic facies and the S2 surface is shown in blue.**

Seismic facies	Unit/surface association	Seismic survey	Frequency	Amplitude	Continuity	Reflector termination	Structure or fill	Seismic example
Sf1	S4	Ultra high resolution (UHR)	Low	High	Discontinuous	Abrupt or masked by seabed multiple	Surface	
Sf2	S2	Ultra high resolution (UHR)	Low	High	Continuous	Not seen in survey area	Surface	
Sf3	L4	Ultra high resolution (UHR)	High to low	High to low	Discontinuous	Abrupt and transitional	Hummocky to chaotic	
Sf4	L4	Ultra high resolution (UHR)	High to low	High to low	Discontinuous	Abrupt and transitional	Parallel	
Sf5	L4	Ultra high resolution (UHR)	Medium to low	Medium to low	Continuous	Onlap	Channel with Parallel draped and divergent	
Sf6	L4	Ultra high resolution (UHR)	High to low	Medium to low	Continuous and discontinuous	Onlap, downlap and truncation	Channel complex with complex fill	
Sf7	L3	Ultra high resolution (UHR)	Low	Low	Not applicable	No applicable	Structureless	
Sf8	L2	Sub bottom profile (SBP)	High to low	High to low	Continuous	Onlap and truncation	Parallel	
Sf9	L2	Sub bottom profile (SBP)	Medium to low	Medium to low	Continuous	Base: downlap Top: truncation	Prograding, oblique parallel	
Sf10	L2	Sub bottom profile (SBP)	Medium to low	High to low	Discontinuous	Onlap and transitional	Hummocky and chaotic	
Sf11	L2	Sub bottom profile (SBP)	Medium to low	Low	Continuous	downlap	Mounded structure with foresets	



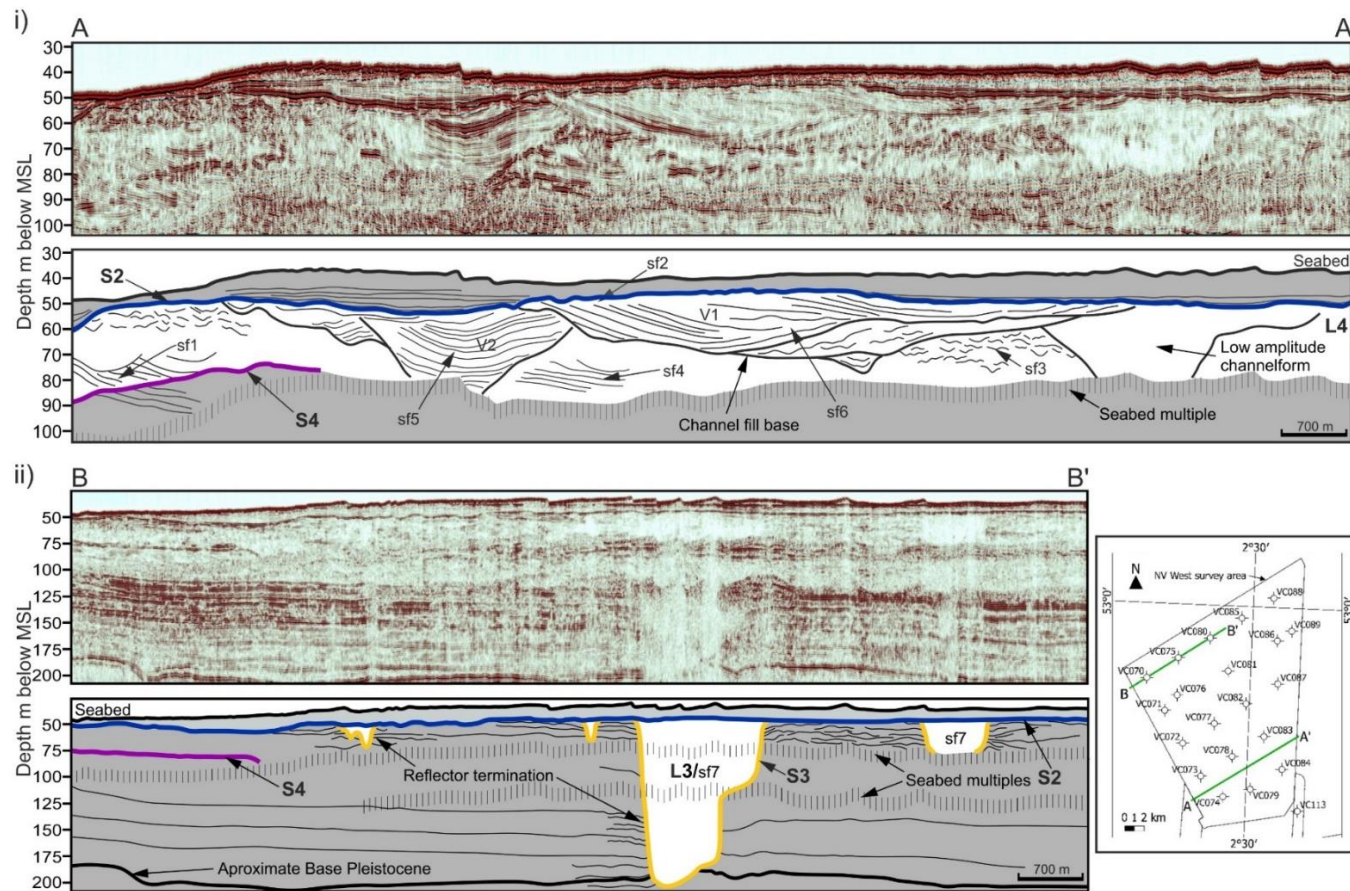
## **Surface 2 (S2) and seismic stratigraphic unit 2 (L2)**

The L2 is present over the NV West and cable route survey areas, ranging in thickness from 17 m to <0.5 m, with the exception of the southwest of NV West where the unit thins below seismic resolution. The basal bounding surface, S2, is a continuous, high-amplitude, reflector, truncating underlying L4 and L3 reflectors. L2 has a variable thickness, largely attributed to the relief of the S2 surface. The L2 unit comprises laterally continuous, parallel dipping, draped, low to high amplitude, medium to high frequency reflectors (sf8 – Figure 3.7i), which typically onlap on the S2 surface. Above the L2 unit, reflectors are truncated by the S1 surface. In the west of the cable route survey area, the seismic character of the L2 unit is not typical of that observed in the NV West survey area. Here, parallel reflectors (sf9 – Table 1, Figure 3.7ii) downlap onto the S2 surface and are overlapped towards the east by sf8 reflectors. At the base of the L2 unit in the NV West survey area, sf10 is present (Table 1). The distribution of this seismic facies is patchy and associated with depressions in the S2 surface (Figure 3.7i – sf10). The character of sf10 is chaotic, hummocky and discontinuous, and is draped by sf8.

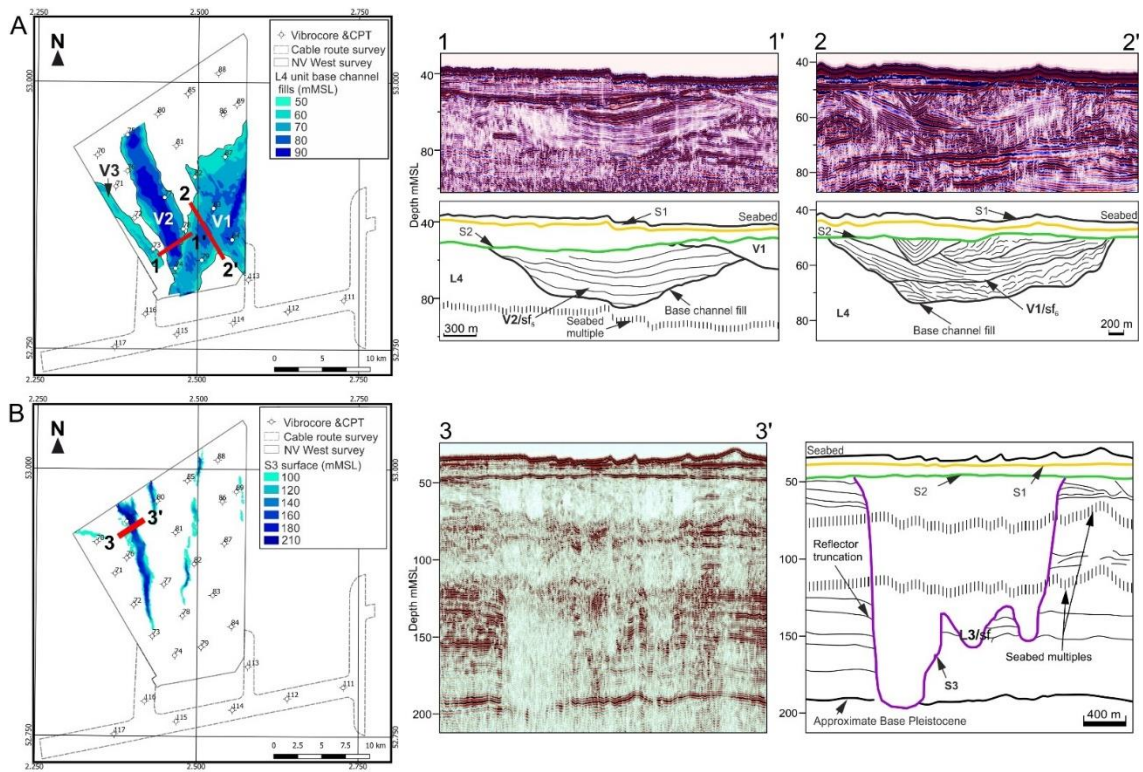
Along the western margin, and in the southwest of the NV West survey area, the typical character of L2 (sf8) is disrupted by a change in seismic facies. Here, discrete mounded structures (sf11-Table 1 and Figure 3.8) are bounded by sf8. These structures are approximately 1-3 m high (crest-to-trough) with a 20-50 m wavelength. The internal seismic character of these mounds is low frequency, low amplitude but with both planar parallel and dipping reflectors visible. The bedforms are both symmetric and asymmetric, with internal reflectors dipping southward and the crests orientated approximately east-west.

## **Surface 1 (S1) and Lithostratigraphic unit 1 (L1)**

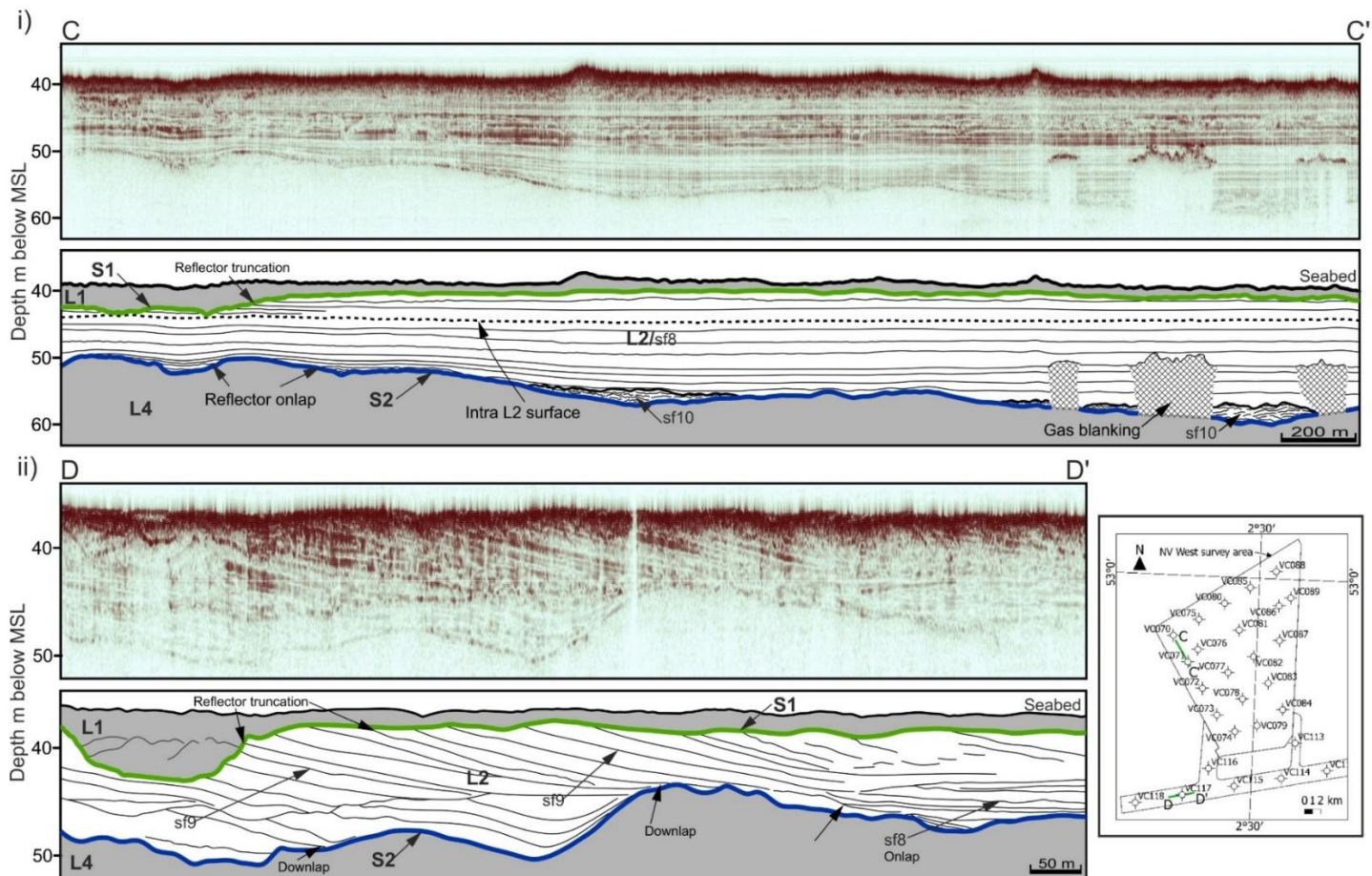
L1 is bounded at the base by the S1 surface, which is characterized by truncation of L2 reflectors and a gradational stratigraphic change from low-amplitude and low-frequency to high-amplitude and low-frequency reflectors (Figure 3.7i). The L1 unit forms a thin veneer, typically 1-2 m thick, but is locally up to 10.5 m thick where large bedforms are present on the seabed. Locally, the L1 unit is absent with the L2 unit cropping out at the seabed



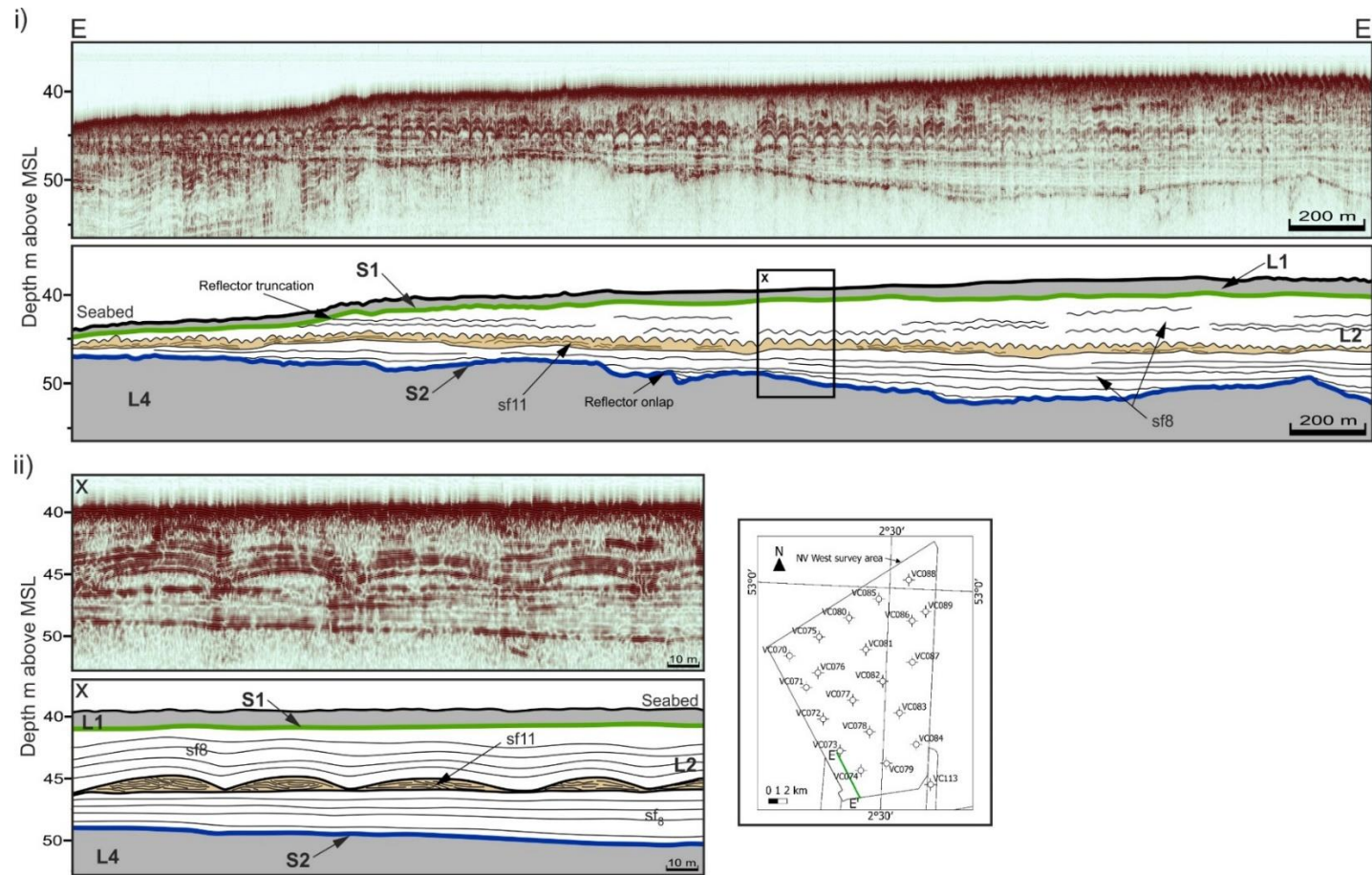
**Figure 3.5. Seismic reflection profile and interpreted panels illustrating seismic facies character and association with seismic stratigraphic units and surfaces. Panel (i) shows the L4 unit and bounding surfaces S4 and S2. Surface S4 mostly obscured by a seabed multiple. Upper L4 unit valley fill (V1 and V2) shown. Panel (ii) shows L3 unit and bounding surfaces S3 and S2. Note the truncation of Middle to Late Pleistocene stratigraphy by the L3 unit. Seismic reflection profile A and B, taken from UHR survey. For location of seismic reflection profiles see inset map**



**Figure 3.6. L3 and L4 fills. A. Depth map of the base valley-fills (V1, V2 and V3) present in the L4 unit with position and orientation of example seismic panels and interpretation (1-1', 2-2'). B. Depth map of the S3 surface (base L3 unit fill) and position and orientation of an example seismic panel (3-3').**



**Figure 3.7. Seismic reflection profile and interpreted panels illustrating seismic facies character and association with seismic stratigraphic units and surfaces. Panel i shows sf10 associated with depressions in the S2 surface and sf8, the dominant seismic facies in L2 unit, draping the S2 surface. Panel ii shows dipping/prograding reflectors that characterise sf9 that are present in the west of the cable route survey area. Panel C and D taken from the SBP survey. For location of seismic reflection profiles see inset map.**



**Figure 3.8. Seismic reflection profile and interpreted panels illustrating seismic facies character and association with seismic stratigraphic units and surfaces. Panels i shows dune-scale bedforms (sf11) seen in the southwest of NV West and in the cable route survey area. Panel ii shows zoom in of inset on panel i. Note that these bedforms are bound between sf8 facies. Panel i is taken from the SBP survey. For location of seismic reflection profiles see inset map**

### 3.5.2. Synthesis of lithology and CPT data with seismic stratigraphy

Lithofacies have been defined for the L1 and L2 units using vibrocores and corroborated to seismic facies associated with the L1 and L2 units. In addition, cores, CPTs and seismic have been integrated to characterize the nature of the S1 surface and to better understand how and why CPT parameters vary across this surface.

### 3.5.3. Vibrocores and CPT control

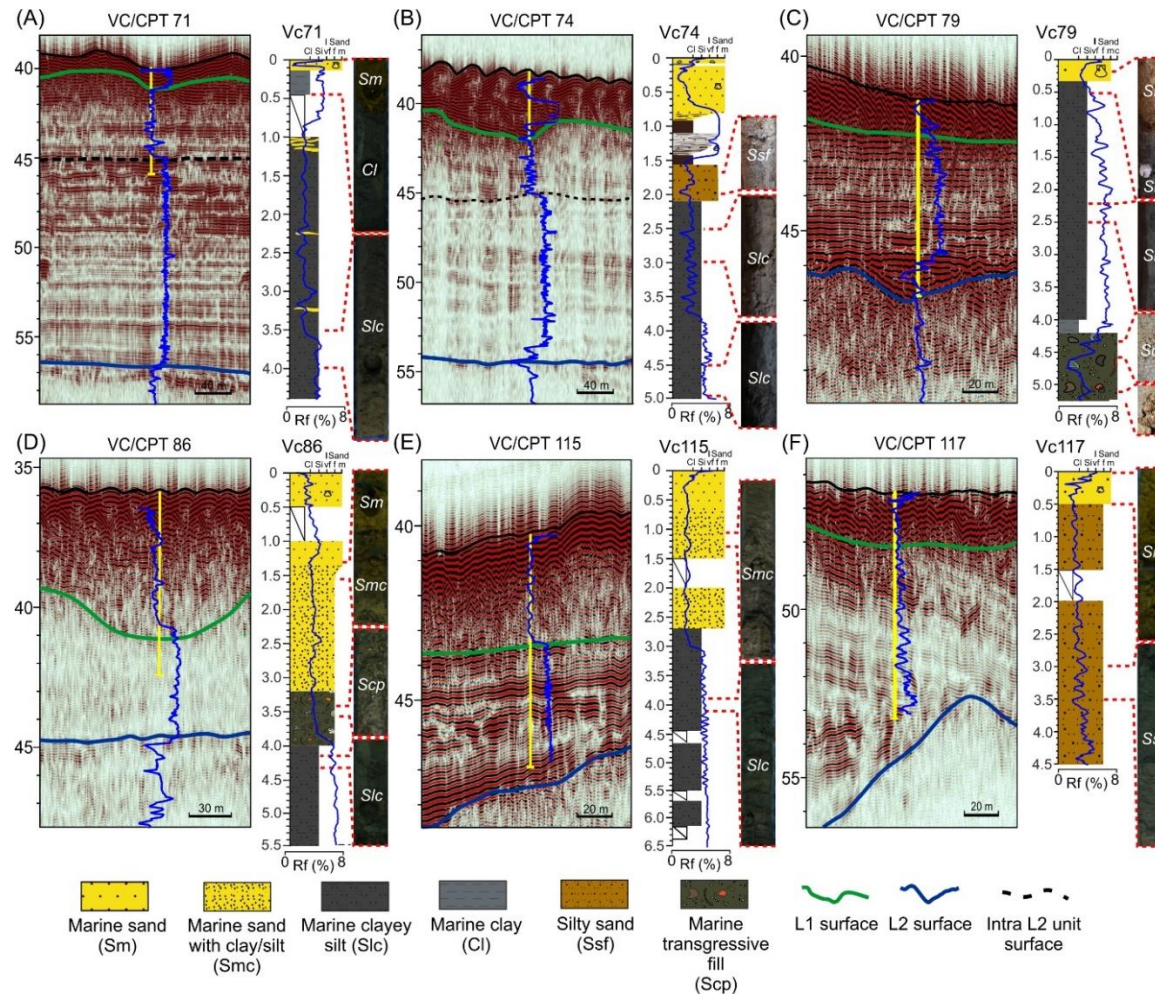
*L2 unit and S2 surface:* The L2 unit is largely characterised by clayey silt with no visible structure and rare shells (Slc –Figure 3.9 and Table 2), although in the west of the cable route survey area the L2 unit is largely characterised by sandy silt with clay (Ssf – VC117), which extends from the S1 to S2 surface. At the top and subdividing the L2 unit are silty clay intervals (<0.5 to 35 cm) with rare shells (Cl). In places, the sand content increases in the Slc towards Cl lithofacies. The contacts between Slc and Cl lithofacies are always sharp but these contacts and changes in lithofacies are not evident in the seismic reflection data, nor is there evidence in the cores for the parallel, continuous reflectors (sf8) that are characteristic of the L2 unit. This may be a result of seismic resolution. Black mottling is present in both Slc and Cl and is considered to be minerogenic as opposed to organic in origin. At the base of the L2 unit, and confined to a topographic low in the S2 surface, is a coarse to fine, poorly sorted muddy sand with subangular to subrounded pebbles (<0.5-4 cm) and abundant disarticulated and fragmented shells (Scp – VC79), which is thought to be associated with sf10. CPT parameters (friction ratio ( $R_f$ ) and cone resistance ( $q_c/p_a$ )) show that the L2 unit differs in mechanical properties. These changes in properties can be calibrated over NV West and the cable route survey areas (Intra L2 surface, Figure 3.9 (CPT71 and 74) and Figure 3.7i). Changes in CPT parameters within the L2 unit are not evident in vibrocores.

**Table 3.2. Classification and interpretation of sedimentary facies according to lithological composition.**

Lithofacies	Description	Depositional environment	Facies photographs
Sm	Well sorted, medium grained sand with occasional coarse grains and shells. Sand grains are subangular to subrounded.	Shallow marine	
Slc	Dark grey silt with sand and clay and occasional shells. Sand and clay content <15%. Homogenous with no visible structure.	Shallow marine/ intertidal/ lagoon	
Cl	Dark grey clay with occasional shells. Homogenous with no visible structure.	Shallow marine/ intertidal/lagoon	
Ssf	Dark grey sandy silt with clay. Sand grains are fine and well sorted.	Shallow marine/ intertidal/lagoon	
Scp	Dark brown grey, coarse to fine, poorly sorted sand with silt, clay and pebbles (<0.5-4 cm) and occasional shells. Pebbles are distributed throughout and are subangular to subrounded.	Transgressive marine	

Sf10 is sampled in one core (VC79 – Figure 3.9) and is characterised by lithofacies Scp, which is a poorly sorted sand with silt, clay with subangular to subrounded pebbles (<0.5-4 cm diameter) and occasional shells and overlies the S2 surface. The S2 surface is not penetrated by vibrocores, therefore characterising a change in lithofacies between L2 and L4 has not been possible. However, CPTs penetrate the S2 surface and show a clear change in CPT parameters between L4 and L2 that can be correlated across the survey areas (Figure 3.9).

*L1 unit and S1 surface:* The L1 unit is characterised by well sorted, medium grained sand with shells dispersed throughout and occasional shell rich intervals (Sm – Figure 3.9 and Table 2). In some vibrocores, the base of the L1 unit contains peats, organic rich clays and fluvial sediments. These changes in lithofacies are clearly seen in the CPTs, and the S1 surface is readily correlated across the survey areas. Correlation of the S1 surface becomes challenging where either the upper L2 lithofacies (Slc) is more sand-rich, therefore decreasing the contrast in geomechanical properties, or where the L1 unit is thin



**Figure 3.9. Calibration of SBP seismic, core logs and CPT data. Vibrocore path overlain on seismic (yellow). CPT parameter (Rf) overlain on seismic in blue. Core photographs shown alongside lithological core logs. See Figure 3.1 for locations of vibracores.**



### 3.6. Regional seismic stratigraphic context

The characterisation of the main seismic stratigraphic units identified in this study (L2 to L4) and surfaces (S4 to S1), have been used to assign depositional environments, which enables the units to be placed in a regional context within the previously defined formal lithostratigraphic framework (Figure 3.2d - Stoker et al., 2011).

The stratigraphic position of L4, which is incised by L3 and unconformably overlain by L2, supports deposition prior to the formation of the regionally extensive Anglian Stage glaciogenic unconformity (MIS 12). The L4 unit shows stacked valley-fills, reflector terminations and laterally discontinuous high-amplitude reflectors, which are typical of depositional systems dominated by fluvial activity (Mitchum et al., 1977). Therefore, L4 is interpreted to be the Yarmouth Roads Fm., which has been described by Cameron et al. (1992), Van Kolfshoten et al. (1995) and Funnell (1996), who considered this unit in this region to represent a fluvial dominated delta top environment. The Yarmouth Roads Fm. stratigraphy that is not confined to valley-fills shows truncated, discontinuous reflectors that are likely to be of fluvial, intertidal and coastal origin as previously observed in cores (Cameron et al., 1992). The uppermost parts of the Yarmouth Road Fm. are likely to have been eroded by subsequent glaciations, and proglacial and periglacial fluvial activity (Cameron et al., 1992; Cohen et al., 2012).

The L3 unit is confined to linear features, predominantly orientated approximately north-south, which incise the underlying L4 unit. Subglacial valley-fills of equivalent size and geometry have been identified north of the study area and have been assigned to the Swarte Bank Fm. (Praeg, 2003). The seismic character of the L3 unit is predominantly structureless, consistent with tunnel valley-fills assigned to the Swarte Bank Fm. elsewhere in the North Sea (Praeg, 2003; Huuse et al., 2000; Stewart et al., 2013; Vegt et al., 2012), but without an overlying draped seismic facies. The southern limit of the Anglian glaciation extends south of the study area, whereas the younger Wolstonian and Devensian glaciations do not extend to the study area, which supports formation and infilling of these tunnel valleys during the Anglian Stage (Figure 3.2 and Figure 3.3).

The L2 unit is a fine grained, low energy shallow marine deposit with a uniform seismic facies extending across the entire study area. The character of L2 is consistent with the Brown Bank Fm., which is described at multiple locations across the southern North Sea as a fine grained shallow marine deposit (Cameron et al., 1992; Limpenny et al., 2011), and dated between MIS 5 and 3 (Bicket and Tizzard, 2015; Wessex

Archaeology, 2018). No direct glaciogenic deposits nor deformation structures relating to the Wolstonian stage, or confirmed shallow marine deposits relating to the marine transgressive Ipswichian stage, have been observed in the study area, supporting that deposition of L2 occurred between MIS 5 and 3, equivalent to the Brown Bank Fm.

### **3.7. Discussion**

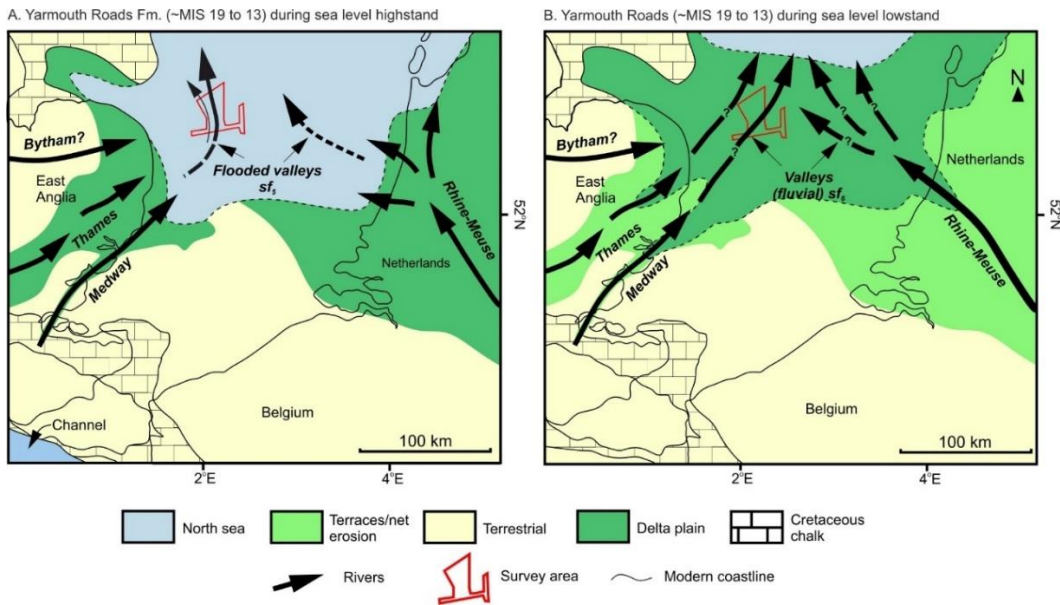
The seismic stratigraphy, sedimentology and geotechnical data provides an integrated 3D architectural framework over a 401 km<sup>2</sup> study area. Corroboration with literature supports extrapolation of this subregional architectural framework to the existing lithostratigraphic framework, chronostratigraphic ages, and sequence stratigraphic positions (Cameron et al., 1987; Stoker et al., 2011). Within the study area the chronology of this framework extends from the Cromerian Stage (~MIS 19-13) to present day, although some chronostratigraphic ages are not represented by deposits.

#### **3.7.1. MIS ~19 to 13 (L4) depositional environments**

The seismic stratigraphy of the L4 succession is interpreted as a fluvially-dominated delta top environment (Yarmouth Roads Fm.), as suggested by the presence of composite valley-fill features and adjacent, subhorizontal high amplitude reflectors that may indicate adjacent peat or salt-marsh deposits. River systems were the primary agents of sediment transport during MIS 19 to 13 in the basin, and the presence of northeast-southwest and north-south trending valleys mapped in seismic reflection data support the proposed model of the expansion and increased influence of mainland European (e.g. Rhine-Meuse) and British (e.g. Thames and/or Bytham) rivers at this time (Gibbard, 1988; Hijma et al., 2012; Moorlock et al., 2002). North and north-eastward drainage direction is supported by a deepening thalweg in V1 to the northeast. An increase in composite valley size (height and width) and preservation from base to top in L4 indicate that fluvial networks were increasing in size in the area, either due to increased precipitation (Funnell, 1996; Gibbard, 1988), or were part of an overall prograding distributive fluvial system (e.g. Hartley et al., 2010; Gulliford et al., 2014).

The age relationship between valley-fills V1 and V2 is clearly defined by cross-cutting relationships, with V1 being younger than V2, but there are no chronostratigraphic constraints to place the channel evolution more precisely in the MIS 19 to 13 period. V3 has the same fill character as V2 but an age relationship with respect to V1 and V2 is not possible to determine with this dataset. Allogenic controls on sedimentation at this time would largely have been a result of climatic instability, with cycles of

glaciation/deglaciation resulting in times of increased precipitation and changes in RSL. The difference in valley-fill types between V2 and V3 and the younger V1 (with respect to V2) support a marked change in depositional style. The draped, divergent fill characteristic of V2 and V3 are typical of a low energy environment, such as estuaries, with fine grained deposition under low energy tidal conditions (Figure 3.10A). In contrast, the multistory V1 fill suggests a higher energy depositional environment with a coarser grained sediment load and repeated cut-and-fill cycles. This change in sedimentation style may be accounted for by a regional base-level fall resulting in northward shoreline migration and increased terrestrial influence (Figure 3.10B). Alternatively, changes in climate may have resulted in increased sediment supply, and subsequent progradation of the fluvial system, leading to northwards shoreline migration and continued progradation of both the Rhine-Meuse and Thames fluvial systems (Hijma et al., 2012; Cohen et al., 2012; Funnell, 1996). Therefore, it is considered highly likely that valleys V1, V2 and V3 reflect the northwards progradation of these systems. The multiple stages of glaciation from MIS 19 to 13, resulting in several RSL cycles (Hijma et al., 2012), suggest that allogenic controls were a major influence on the sedimentary systems in the southern North Sea during this time. Alternatively, V1, V2 and V3 may support deposition during a relatively short period during the later parts of the Cromerian Stage, whereby channel style and position reflect internally generated autogenic changes. The truncation of the channel-fills at the S2 surface prohibits understanding of the age relationship between these channel systems. However, uncertainty remains as to whether allogenic or autogenic controls were the primary driver for the changes in channels fill types seen in V1, V2 and V3 due to the absence of chronostratigraphic constraints. Consequently, support for either a landscape responding to changes in the climate and base level, which drove significant increases in climate and sediment supply, and northward shoreline migration, and/or normal regression from progradation of a fluvial distributive system, remain unresolved.



**Figure 3.10. Palaeoenvironmental maps depicting highstand and lowstand scenarios at the time of Yarmouth Roads Fm. deposition. A. Interglacial conditions and flooding of valleys V2 and V3 and draped deposition of fine grained marine/estuarine sediments. B. Glacial conditions with northwards expansion of fluvial networks and infilling of valley V1 with coarser grained terrestrial sediments (Modified from Cohen et al., 2012; Funnell, 1996; Gibbard, 1988; Hijma et al., 2012).**

### 3.7.2. MIS 12 (L3) depositional environments

The structureless character of the seismic facies infilling the deep narrow erosion surfaces constituting the L3 unit are consistent with the Swarte Bank Fm. (Stoker, et al., 2011a), which have been widely documented in the North Sea Basin (e.g. Praeg, 2003; Davies et al., 2011; Graham et al., 2011). The fill character in conjunction with the geomorphological characteristics of the deep erosive bounding surfaces (asymmetric and steep sides (>40°)), over-deepened and irregular thalwegs are consistent with tunnel valleys (O’Cofaigh, 1996; Stewart et al., 2012) and their fills. These are common features northward of 53°N (Figure 3.3; Graham et al., 2011). However, we document the most southerly tunnel valley-fills for this time period in the offshore domain. The orientation (north-south) of the tunnel valleys, the east-west trending fill (Figure 3.3 and 6B), the depth of incision, and their position with respect to the upper and lower units is consistent with tunnel valley-fills that formed during the Anglian glaciation elsewhere in the region (Huuse et al., 2000; Praeg, 2003; Graham et al., 2011), and support previous estimates of MIS 12 ice sheet limits in the southern North Sea (Graham et al., 2011; Laban, 1995; Laban et al., 2004). In many cases in the North Sea, the Swarte Bank Fm. tunnel valley-fills comprise multiple seismic facies (Praeg, 2003; Mellett et al., 2019). Typically, a lower structureless unit is overlain by a layered unit, which have

been interpreted to be basal glaciofluvial sands and/or glacial diamicts that transition into lacustrine muds (Balson et al., 1990; Praeg, 2003; Long et al., 1988; Cameron et al., 1989). Within the NV West survey area, the tunnel valley-fills comprise a single structureless seismic facies. This may indicate a predominantly glacio-fluvial sand and/or diamict-fill. However, a structureless seismic facies could be the result of both lithology and/or seismic blanking. Where the Swarte Bank Fm. is present, the overlying L2 unit shows no increased thickening, in contrast to documented thickening of sediments overlying tunnel valley-fills north of the survey area (Cameron et al., 1992). This suggests that either the tunnel valleys were filled or that the S2 surface represents an erosion surface that planed off the L3 unit tunnel valley shoulders and neighbouring L4 delta top palaeosurfaces. Given that the tunnel valley-fills are always truncated by S2, we interpret a major planar erosion surface that removed some Swarte Bank Fm. stratigraphy, likely a result of polycyclic events (ice marginal-proglacial-transgression) culminating in marine transgression. The lithology and the infilling history of the tunnel-valleys remains unclear, due to both the limits of seismic imaging (blanking and structureless character) and the absence of core and CPT data penetrating the fills. However, given the diversity and complexity of fills documented to the north (Praeg, 2003), and to the northwest (Mellett et al., 2019) of the study area it would be unwise to assign a fill history and lithology to these tunnel-valley fills based on the data available.

### **3.7.3. MIS 5d to 2 (L2) depositional environments**

The L2 unit blankets the study area and is predominantly composed of clayey-silt and silty-clay lithologies, which are consistent with the interpretation of the Brown Bank Fm. (Stoker et al., 2011; Cameron et al., 1992). The Brown Bank Fm. has been subdivided by previous workers into an upper and lower unit (Bicket et al., 2015 and references therein), with the lower unit being sandier and associated with topographic lows, and the underlying marine transgressive Eem Fm. (Limpenny et al., 2011). The fine-grained lithology, the seismic character, and the flat nature to S2 suggests that only the upper Brown Bank Fm. is present in the study area. The core sedimentology and faunal assemblages (Wessex Archaeology, 2018) support deposition under a low energy, shallow marine and/or lagoonal environment in which regional changes in relative sea level may be superimposed (Figure 3.2a and b). However, given that the study area is located towards the northern limits of where the Brown Bank Fm. deposits are distributed (Cameron et al., 1992), it may suggest that Brown Bank Fm. deposits seen in the study area are of a slightly different genesis and age than seen in the Belgian, British and Dutch areas south of the study area.

The CPT data calibrated to seismic reflection data provide compelling evidence for subdivision within the Brown Bank Fm. Soil Behavior Type plots (SBT) reveal that the fine-grained lithofacies that characterise the upper Brown Bank Fm. have two distinct distributions (Figure 3.11), with geomechanical parameters predicting a silt-dominated lithology overlain by a clay-dominated lithology. This subdivision is further supported by seismic reflection data where a marked change in seismic facies is coincident with a change in CPT character. The change in CPT character supports a change in sediment supply and/or energy regime as a result of RSL change. Evidence for a multi-stage fill is not supported by all CPT tests. This may be explained by erosive processes and/or spatial variability in contemporaneous sedimentary depositional environments.

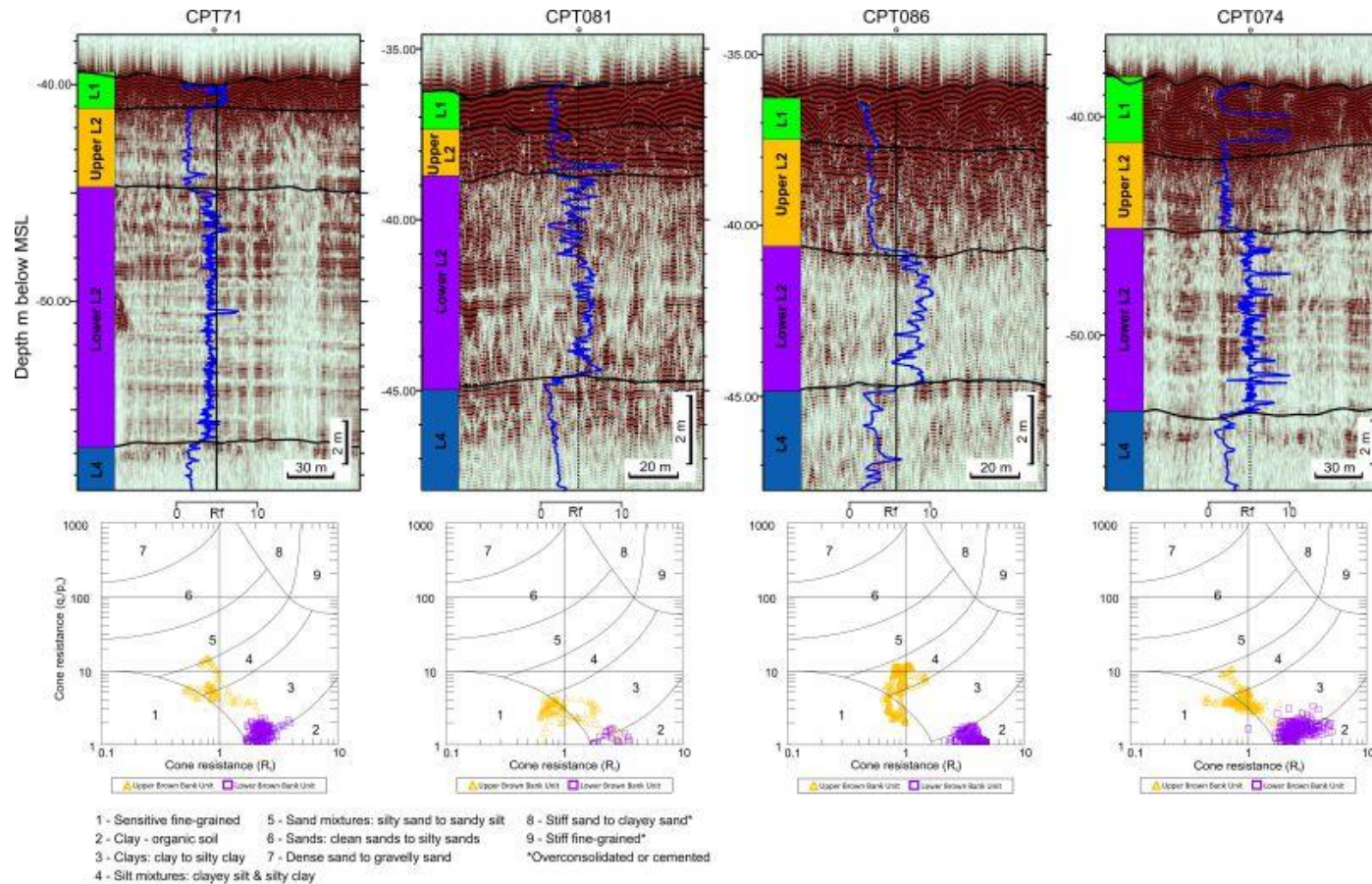


Figure 3.11. Seismic reflection profiles with CPT friction ratio (Rf) overlain and SBT plot showing data for the L2 unit interval. The SBT plot shows two distributions interpreted to support a subdivision of the L2 unit. Using the SBT plot the lower L2 unit is predicted to be predominantly clay (organic soils) and the upper L2 unit predominantly silt with clay.

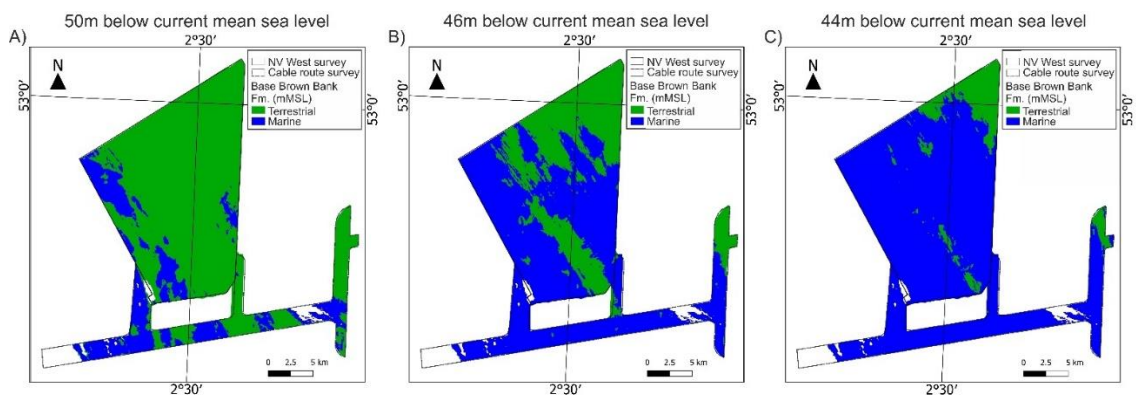
The Brown Bank Fm. has been interpreted to represent a widespread lagoon-type system, with limited connection to open marine conditions, which extended across the southern North Sea, and became increasingly restricted during the early Devensian (Cameron et al., 1989; Laban, 1995). Seismic and core data in the study area support regional deposition of fine-grained sediments onto a gently undulating lower bounding surface (S2), though likely during a time of fluctuating RSL. Figure 3.12 estimates the position of the palaeo coastlines, with the overlying sediment fill stripped back. When sea level is 50 m below present (Figure 3.12A), the majority of the study area is subaerial with only enclosed and semi-enclosed lagoons. However, when RSL is approximately 46 m below present (Figure 3.12B) a more complex coastal configuration is revealed. At 44 m below present the area is predominantly flooded, with a small area in the northeast remaining subaerial. These flooding and exposure scenarios suggest that minor changes in RSL would have resulted in major shifts from open marine through estuarine to restricted lagoonal conditions and challenges the idea of a long-lived and widespread lagoonal environment. Cores from the study area support periods of submersion and exposure with iron sulphide indicative of a restricted marine and/or subaerially exposed landscape. Work by Wessex Archaeology (2018) on changes in faunal assemblages in the region add further support to the idea of restriction and/or isolation of water bodies through time.

Further evidence for an environment controlled by localized topography and RSL change are the dune-scale bedforms (symmetric and asymmetric, 1 -3 m high (crest-to-trough) with a 20-50 m wavelength) present in the southwest of the study area. The bedforms are not channel-confined, which discounts a fluvial or estuarine origin. Given the uniform crest-line orientation and scale of the bedforms, and their stratigraphic position between marine fines, a tidal origin on an open shelf is the preferred interpretation. Examples of similar bedforms are identified both on modern shelf environments (Passchier et al., 2005) and in the stratigraphic record (Brew, 1996). An aeolian origin is unlikely given their size, preservation and bounding by marine fines. The net southward-migration direction would support an overall east-to-west trending contemporary shoreline with available sand supply. Their patchy distribution is likely due to be a combination of the S2 surface topography, grain-size availability, and water depth. The symmetric and asymmetric geomorphology of the tidal bedforms could support an interpretation of an estuarine environment where ebb and flood tides were both symmetrical and asymmetrical (Reynaud, 2012). However, without core calibration their composition and process origin remain equivocal. A rising and falling RSL during MIS 5 (Zagwijn, 1983; Long et al., 2015) presents one scenario for bedform



development. In this scenario, the landscape would fluctuate from open marine to increasingly restricted, with estuarine processes becoming more dominant during periods of lower sea level. During RSL fall tidal processes could become more dominant, and sand supply increase, leading to the development of tidal bedforms. Subsequent RSL rise led to burial of the tidal bedforms by fine-grained marine sediments. The exceptional preservation of these tidal bedforms suggests that burial was rapid and under relatively low energy conditions.

The detailed timing of Brown Bank Fm. deposition has remained a subject of discussion and chronological evidence is scarce. The Brown Bank Fm. drapes the S2 surface, which is coincident with the top of the Swarte Bank Fm. In rare exceptions, for example in VC79, coarse-grained marine sediments overly the S2 surface. These coarse-grained marine sediments are considered to represent a marine transgressive lag (i.e. a wave ravinement surface), likely deposited during the Ipswichian transgression, and therefore part of the Eem Fm. Dates obtained by Limpenny et al. (2011) and the stratigraphic position of the Brown Bank Fm. fill (overlying MIS 12 stratigraphy and suspected Eem Fm. transgressive sediments) support a time of deposition between MIS 5d and 3, with the S2 surface representing major erosion and/or a hiatus of approximately 0.4 Ma. Any sediment accumulation in the study area most probably occurred during the Hoxnian interglacial (Figure 3.2), followed by a hiatus and/or erosion during the following Wolstonian glaciations (Figure 3.3 – maximum ice extent), with eroded sediment likely transported south away from the ice front (Toucanne et al., 2009).



**Figure 3.12. Flooded landscape scenarios for hypothetical stages in the Last interglacial and Early glacial (L2 unit; Eem and Brown Bank Fms., MIS 5). A. At 50m below current mean sea level the majority of the area is subaerial with small enclosed and semi enclosed lagoons, lakes and peninsulas. B. At 46m below current mean sea level a less restricted, more open marine landscape is revealed. C. At 44m below current mean sea level the survey area is predominantly flooded with the exception of the northeast with some islands.**

#### **3.7.4. Opposing sediment transport directions**

Over short timescales, most catchments and adjacent sedimentary basins have a simple source-to-sink configurations driven by the direction of slope, meaning the net direction of sediment flux does not change. During the Middle to Late Pleistocene, the southern North Sea underwent major changes in sedimentary process regime under the influence of glacial and interglacial cycles. Associated with these changes are marked shifts in the primary direction of sediment flux. During Yarmouth Roads Fm. deposition the primary sediment transport direction was to the north (Figure 3.10A and B), with sediment transported from catchments to the West (England) and Southeast (mainland Europe) (Figure 3.3). During the Anglian glaciation, northward fluvial and westward ice-marginal glaciofluvial transport of sediment was towards a proglacial lake (Figure 3.3) and the previously fluvial-dominated landscape became glaciated with evidence for subglacial conditions preserved in the stratigraphy as tunnel-valley fills (Figure 3.3), with net sediment transport to the south via meltwater conduits (Gibbard et al., 2009). Significant erosion and/or a hiatus took place prior to marine transgression during the Eemian period (though the direction of this erosion is unknown) and following this, marine sediments including those of the Brown Bank Fm. were deposited in a highly dynamic low relief environment that was highly responsive to cycles of RSL. This environment likely shifted from open marine to more restricted, with embayments and lagoons being the main environments of deposition. During deposition of the Brown Bank Fm. sediments are considered to come from the West, a result of the Rhine delta progradation into the basin (Hijma et al., 2012; Peeters et al., 2016). These marked changes in sediment transport directions over relatively short-time periods reflect the low relief continental shelf environment and proximity to an ice marginal setting. The low relief physiography in the study area contrasts with more typical high-relief source-to-sink configurations. The results caution against applying simple estimates of sediment flux and provenance signals even over short durations, particularly in ice marginal continental shelf settings.

### **3.8. Conclusions**

The availability of high-resolution seismic reflection data acquired for the offshore windfarm industry alongside a complimentary dense network of cores and CPTs allows the development of a detailed and integrated view of the stratigraphy and depositional environments of the middle and late Pleistocene in a 401 km<sup>2</sup> area of the southern North Sea, 47 km off the coast of East Anglia. The patterns of deposition are strongly related to periods of glacial/interglacial cycles but record a far more spatial and

temporally complex fill rather than a simple record of alternating warm and cool climate periods.

Imaged within the lower units are the topsets associated the Yarmouth Roads Fm. Changes in valley-fill architecture and scale record changes in the influence of terrestrial, fluvial and marine depositional environments during the Cromerian period (MIS ~19-13), as a result of allogenic controls (climate and base level change) and/or autogenic control. The expansion and increasing influence of European and British rivers are the predominate control on the north-south orientation of the fluvial network, which drained northwards.

The extensive Anglian glaciation (MIS 12) altered the mode of sediment erosion and deposition by 180 degrees, with north-south trending sub-glacial tunnel valleys under a southward advancing ice sheet (the Swarte Bank Fm.). Currently, the tunnel valley-fills mapped here are the most southern sub-glacial expression of the extensive MIS 12 ice sheet documented in the southern North Sea. Following MIS 12, a stratigraphic hiatus of approximately 0.4 Myr is marked by an unconformity that is overlain by sediments closely related to the upper Brown Bank Fm. (Cameron et al., 1989).

Shallow marine/estuarine sediments form the latter part of MIS 5 record a phase of fluctuating RSL, within a low relief shelf setting. Dune-scale bedforms, preserved within these fine-grained sediments are interpreted as tidal in origin, and suggest at least one phase of lower or stable relative sea level, likely during cool conditions approaching the onset of the Devensian glaciation (MIS 4-2). Previously, Brown Bank deposits have been thought to represent a single estuarine phase at the culmination of the sea-level highstand following the Last Interglacial. However our analysis shows that there were periods of alternating sediment deposition suggesting change in RSL and sediment suppl

## Chapter 4 - Postglacial landscapes of the southern North Sea

As lead author, Stephen James Eaton was responsible for data analysis, interpretation, and manuscript and figure preparation. The role of other co-authors (Hodgson, D.M., Barlow, N.L., Mortimer, E.E. and Mellett, C.L.) was limited to discussion of results and manuscript editing.

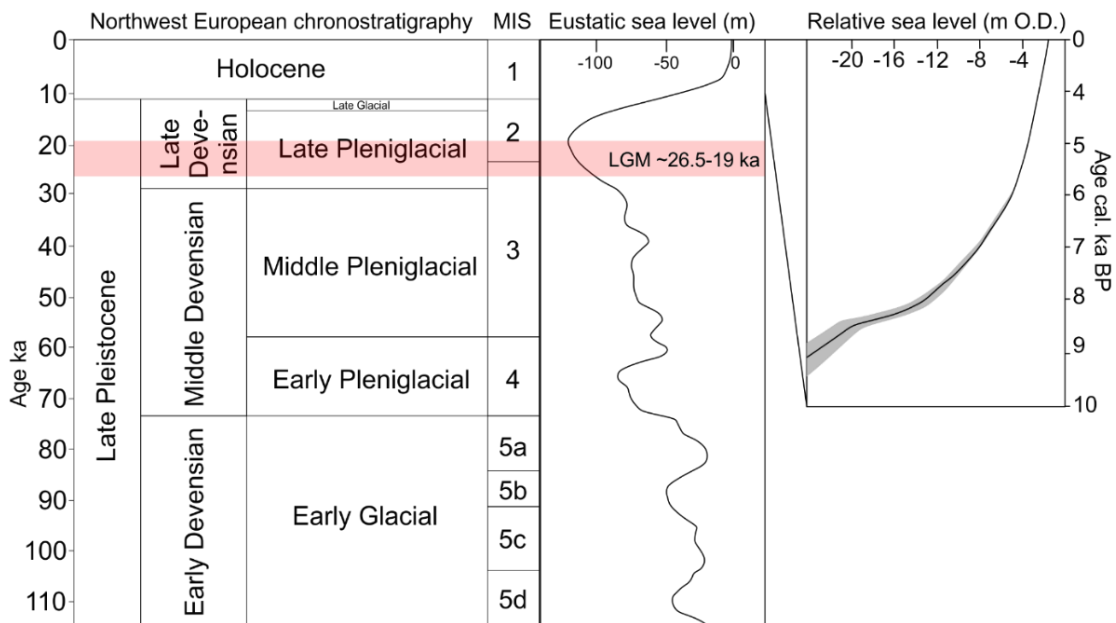
### 4.1. Introduction

The postglacial landscape of northwest Europe changed rapidly during the period from the Last Glacial Maximum (LGM; 26.5 to 19 ka) when sea level was at its lowest (>100 m below current mean sea-level (MSL)), to the late Devensian (12.5 to 10.15 ka) when sea level was approximately 30 to 55 m below current MSL (Spratt et al., 2016) (Figure 4.1). By end Early Holocene (~7.9 ka) sea levels had risen to approximately 12 m below current MSL (Hijma et al., 2011). The marked change in landscape and climate from late Devensian to present has been the focus of a broad range of investigations from ice marginal, periglacial environments (Kolstrup, 1986; Murton et al., 2003; Bateman et al., 2014; Cotterill et al., 2017; Ballin, 2017; Emery et al., 2019), fluvial system response (Briant, et al., 2004; Busschers et al., 2007), human occupation and archaeological preservation (Fitch et al., 2005a; Missiaen et al., 2017; Brown et al., 2018), to the timing and magnitude of relative sea-level rise (Beets et al., 2000; Shennan et al., 2000; Behre, 2007; Hijma et al., 2010; Baeteman et al., 2011; Sturt et al., 2013) .

Understanding the landscape response in coastal plain environments to changes in sea level during the Holocene period is fundamental to our understanding of how coastal landscapes will respond to future sea level and climatic changes (McGowan et al., 2014; Sloss et al., 2018). The low relief configuration of the shelf of the southern North Sea region makes its landscapes particularly susceptible to relatively minor changes in relative sea level. An assumption that the preservation potential of coastal plain geomorphological features during marine transgression is limited (Shaw, 2005) has been challenged in recent years with documentation of well-preserved geomorphological features from the emerged landscape of the early postglacial period (Fitch et al., 2005a; Gaffney et al., 2007; Storms et al., 2008; Hijma et al., 2011; Missiaen et al., 2020; Emery et al., 2020). Onshore around the southern North Sea, the relative ease of data acquisition, compared with offshore, has led to detailed documentation of Late Devensian and Holocene landscapes. In England and the

Netherlands, the response of fluvial systems to changes in climate following the LGM have been a main research topic (Coope et al., 1997; Briant et al., 2004; Kerney et al., 1982; Stouthamer et al., 2011; Peeters et al., 2015; Hijma et al., 2012; van Asselen et al., 2017) alongside ice marginal and periglacial landscapes and processes (Bateman, 1998; Lowe et al., 1999; Kolstrup, 1986; Pissart, 1987; Huijzer et al., 1997). The development of widespread offshore infrastructure over the past decade, particularly in the renewable energy sector, has increased the availability of data used to characterise the seabed and shallow subsurface. High resolution, comprehensive data sets are available that allow characterisation of buried geomorphological features with high confidence. In addition, the drive to preserve archaeological heritage including relicts and palaeolandscapes in the offshore environment has led to increased interest and frequency of research focusing on the postglacial landscapes of the southern North Sea (Brown et al., 2018; Bicket et al., 2015; Limpenny et al., 2011; Missiaen et al., 2020; Fitch et al., 2005a).

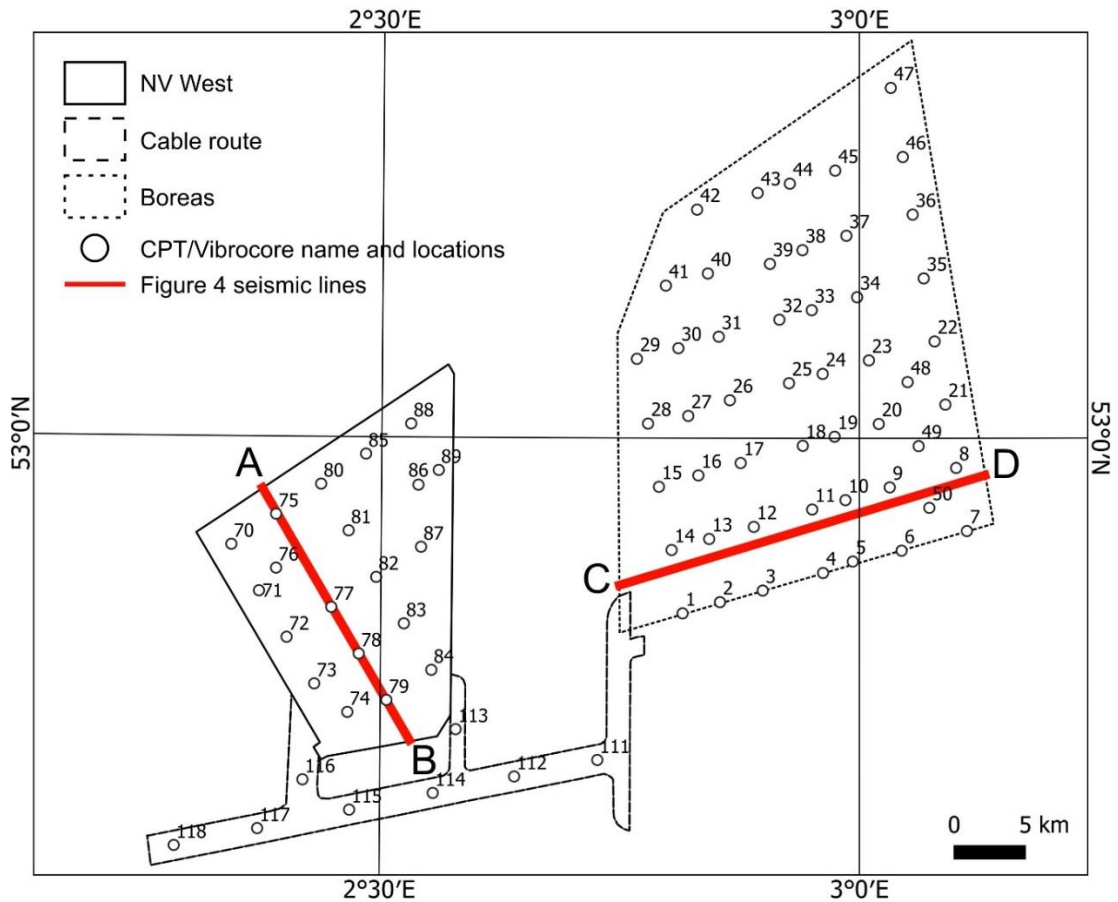
In this study, the Late Devensian and Holocene stratigraphic record is examined to deduce the landscape response to a warming climate following ice retreat and rising sea level. The aim is to determine the sedimentary process response and shifts in depositional environment through investigation of postglacial sediments and stratigraphy. Using palaeoenvironmental data, radiocarbon dates, and sedimentary and stratigraphic information the evolution of the coastal system is investigated under models of relative sea-level rise.



**Figure 4.1. Northwest European chronostratigraphy** (Vandenberghe, 1985; Van Huissteden et al., 2001; Busschers et al., 2007). **The marine isotope record** (Bassiot et al., 1994). **Eustatic sea-level record derived from North Atlantic and Equatorial Pacific benthic Oxygen Isotopic Data** (Waelbroeck et al., 2002). **Relative sea-level curve for the Rhine river-mouth area in The Netherlands** (Jelgersma, 1961; van de Plassche, 1982; van de Plassche, 1995; Cohen et al., 2005; Hijma et al., 2010; Hijma et al., 2011).

## 4.2. Setting

The Norfolk Vanguard West, cable route, and Norfolk Boreas study areas are located approximately 47 km east of the East Anglia coastline (Figure 4.2). The study areas is approximately 401 km<sup>2</sup> and in shallow water of <50 m, with variations in bathymetry attributed to north-south trending sand banks.



**Figure 4.2. NV West and Boreas survey areas with locations and names of vibrocores and CPTs. Red lines indicate the locations of the panels shown in Figure 4.4.**

### 4.3. Methods

#### 4.3.1. Seismic data

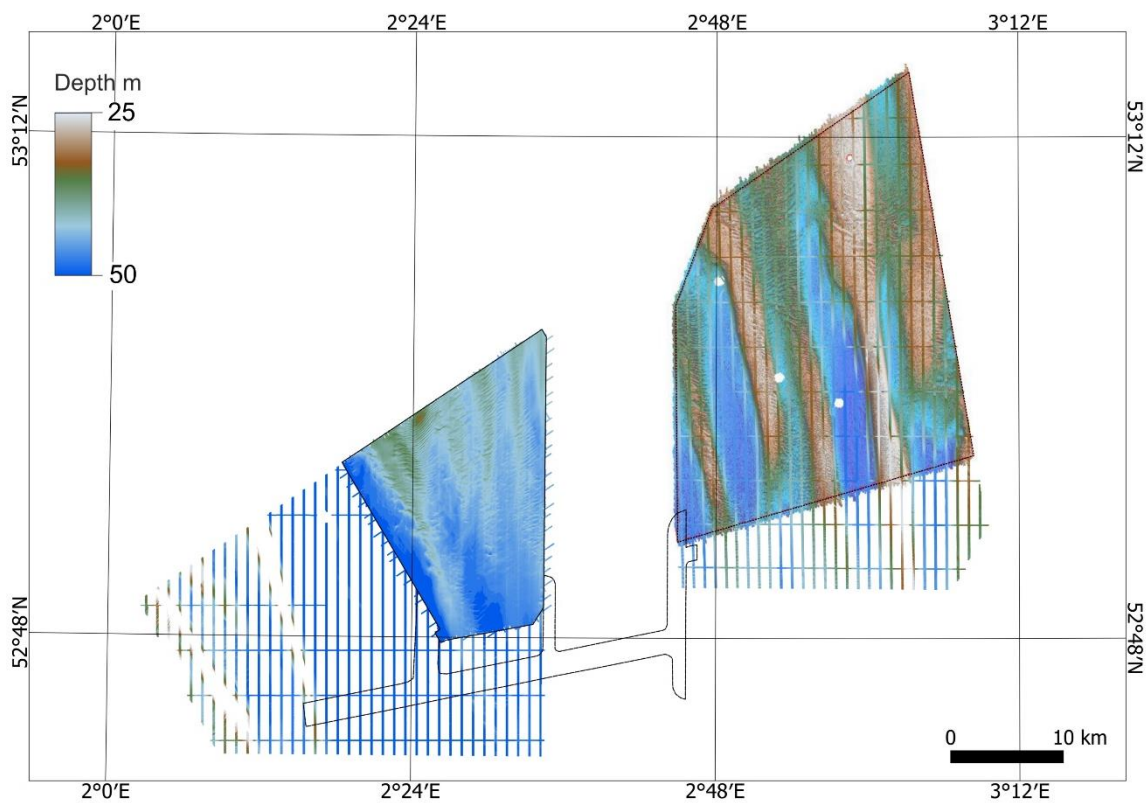
For information on seismic acquisition, processing and limitations refer to Chapter 3 where these have been documented in full. For the purposes of this study Sub Bottom Profile (SBP) seismic data have been used primarily to interpret stratigraphic and geomorphological features. In cases where the SBP seismic data were not of sufficient quality (poor imaging), the Ultra High Resolution (UHR) seismic data has been used where possible.

#### 4.3.2. Bathymetry data

#### Acquisition

Multibeam echo sounder (MBES) bathymetric data were collected as both regional surveys and as site specific surveys (Figure 4.3). The MBES bathymetric data were

acquired using a Kongsberg EM 2040, with a frequency of 400 kHz. A regional MBES survey was acquired in 2010 that was approximately 31% coverage, whilst in 2015 (Norfolk Vanguard West and Cable Route) and 2017 (Boreas) full coverage MBES surveys were acquired. The projected coordinate system used for these surveys is ETRS89 / UTM zone 31N (EPSG: 25831). The quality of the bathymetry surveys is generally good and more than adequate for interpretation of seabed features. In places there are 'noisy' patterns in the final depth terrain model. The noise is considered to be the product of relatively rapid migration of marine bedforms, leading to meaningful changes in the seafloor topography, when two adjacent or intersecting swaths are surveyed with a long intervening time period.



**Figure 4.3. Multibeam bathymetric data available to this study. Full coverage bathymetric data is available in both NV West and Boreas in addition to bathymetric surveys that were acquired using a coarser grid but over a larger area extending out of the NV West and Boreas sites. The coarser gridded bathymetric survey was acquired in 2010, whilst the full coverage bathymetric surveys were acquired in 2015 (NV West) and 2017 (Boreas).**

## Interpretation

Seabed morphology was characterised using the full coverage surveys acquired over NV West and Boreas. Classification of shallow marine bedforms has been done



according to the Ashley's (1990) classification scheme for subaqueous dunes (Table 4.1). The geometric characterisation of shallow marine bedforms was achieved using a GIS terrain profile tool (QGIS Development Team, 2020). To characterise areas of seabed scour and places where underlying sediments subcrop at the seabed, both the SBP seismic data and bathymetric data were used.

**Table 4.1. The classification scheme used in this study to characterise subaqueous dunes (after Ashley, 1990)**

Subaqueous Dune				
First order descriptors				
Size				
Term	Small	Medium	Large	Very large
Spacing	0.6-5 m	5-10 m	10-100 m	>100 m
Height	0.075-0.4 m	0.4-0.75 m	0.75-5 m	>5 m
Shape				
2-Dimensional	Straight-crested, little or no scour in trough			
3-Dimensional	Sinuous, catenary or linguoid/lunate, deep scour in trough			
Second order descriptors				
Superposition				
Simple	No bedforms superimposed			
Compound	Smaller bedforms superimposed			

#### 4.3.3. Vibrocores

For information on acquisition of vibrocores refer to Chapter 3 and Figure 4.4. In this study, 7 vibrocores have been used to investigate stratigraphy and lithofacies with the primary focus being postglacial sediments and geomorphological features. Logging and interpretation of vibrocores was done according to methods outlined in Chapter 2 and those used in Chapter 3.

## 4.4. Results

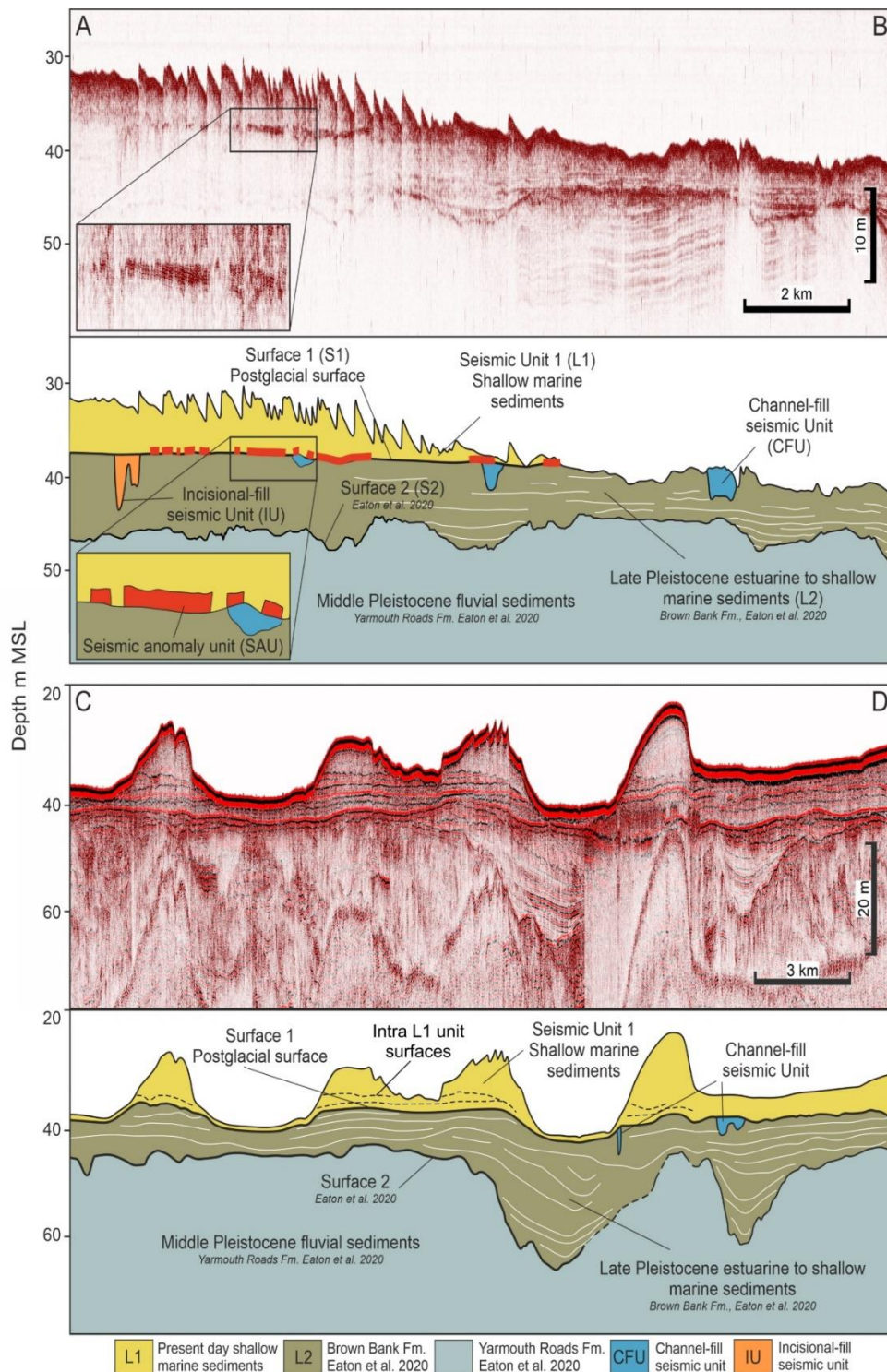
### 4.4.1. Seismic stratigraphic interpretation

Three seismic units have been mapped, which demarcate the contacts between the seismic units. Surface 1 (S1) is a prominent surface that can be mapped across the study areas. Underlying S1 is the L2 seismic unit (Brown Bank Fm.), which comprises the Middle to Late Pleistocene stratigraphy documented in (Eaton et al., 2020)

#### Surface 1 (S1)

Surface 1 (S1) is present across the entire study area and is marked by multiple erosion surfaces indicating it is a composite surface. S1 is poorly imaged where it is overlain by a thick (several metres) succession of shallow marine depositional

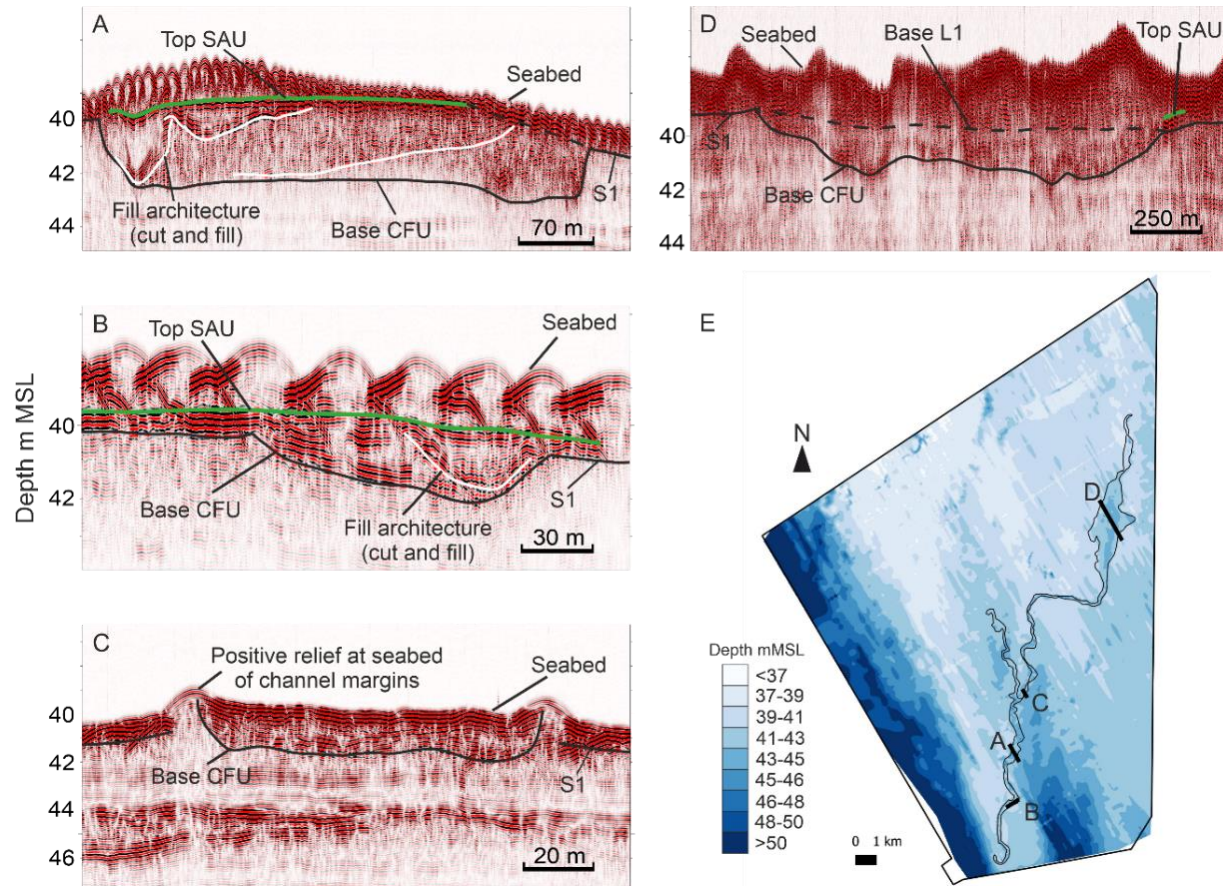
bedforms (dunes, sediment waves, banks). These bedforms cause attenuation of the seismic signal leaving the underlying units poorly resolved. Typically, where only a thin veneer of seabed sediments is present, the underlying units are well imaged. The seismic character of the surface is variable across the study area. In the central and northern regions of NV West and Boreas, S1 is characterised by both high-amplitude, low-frequency seismic reflectors (S1A) and low-amplitude, low-frequency seismic reflectors (Figure 4.4). In some areas, S1 loses reflectivity and is only distinguishable by the stratigraphic change in seismic facies character between the underlying L2 and overlying L1 units (defined in Chapter 3). In the underlying L2 unit, seismic reflectors are both parallel with and truncated by S1. Truncation of unit L2 coincides with where unit L1 thins to < 0.5 m. S1 is incised by channel-forms and incisional features, which are distinguishable from unit L2 by changes in seismic reflector amplitude at the base and seismic facies character overlying the erosion surfaces.



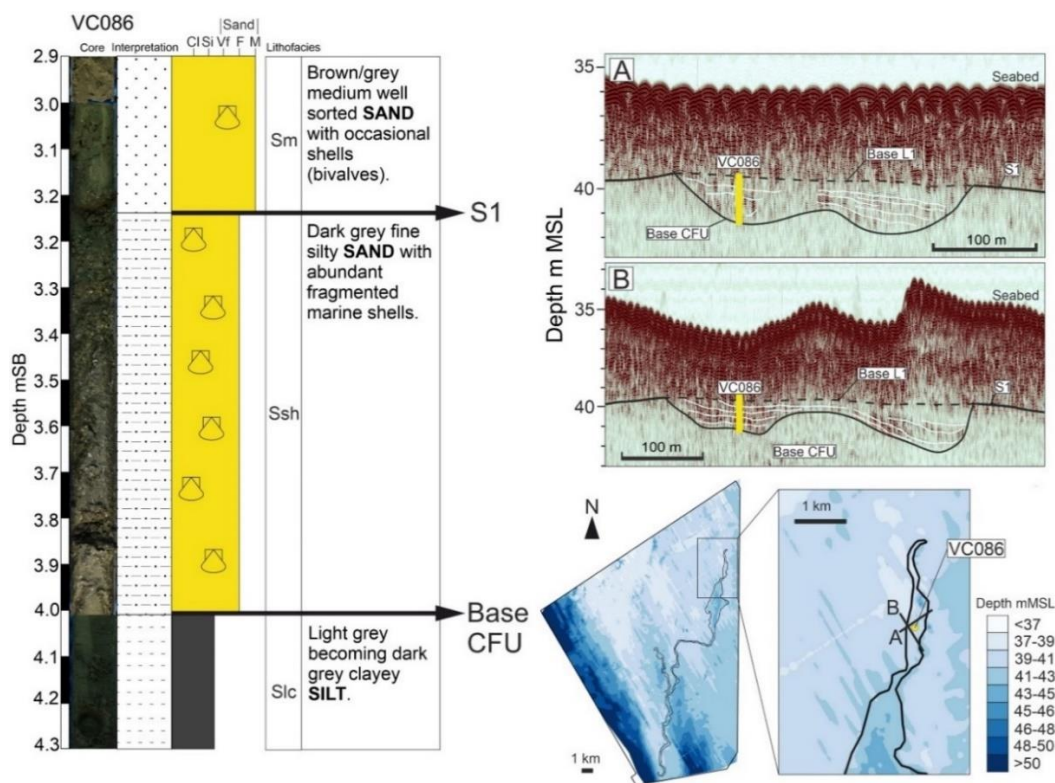
**Figure 4.4. Seismic reflection profile and interpreted panels illustrating seismic stratigraphic units and surfaces. This chapter focuses on Surface 1 to the modern seabed, building on work in Chapter 3. Panel (A-B) shows an example seismic line (SBP) through NV West. Seismic unit 1 (L1) is associated with sand banks and shallow marine bedforms. Where it is not identified, only a thin veneer (<20 cm) of shallow marine sand covers the Late Pleistocene sediments. Panel (C-D) shows an example seismic line through Boreas. The north-south trending sand banks are clearly visible with Late Pleistocene sediments sub cropping in between. For location of seismic reflection profiles see location map (Figure 4.2).**

## **Channel-fill seismic unit (CFU)**

The base of the channel-fill seismic unit (CFU) incises down from approximately S1 (~40 m below LAT) and is overlain by a range of seismic facies. The channel-forms are imaged in the UHR seismic data, and the channel-fill in the SBP seismic data. The fill shows a range of architectural styles, although where the channel is overlain by a thick L1 unit (> 3 m thick) the channel-fill has less reflectivity. The base of the channel-form is characterised by the contrast in seismic facies (high-amplitude, low-frequency) between the channel fill and underlying L2 unit. The stratigraphic transition from channel-fill to unit L1 is not easily defined. Where unit L1 <0.5 m, the top of the channel-fill is characterised by high-amplitude, low-frequency seismic reflectors. The channel-fill is characterised by a range of seismic facies extending along the channel form, from northeast to southwest (Figure 4.5). Stacked channel-fills are common and characterised by dipping and draped reflectors, and truncation of channel-fill by incision surfaces. The seismic-fill character of CFU changes towards the northeast with parallel, sub horizontal and draped seismic reflectors dominating (Figure 4.5 D and Figure 4.6 D). Where only a thin veneer (< 0.5 m thick) of unit L1 is present, the flanks of the channel-form are pronounced and form a positive seabed relief (Figure 4.5 C). In the southwest of NV West, the channel-form is clearly truncated and evident at the seabed.



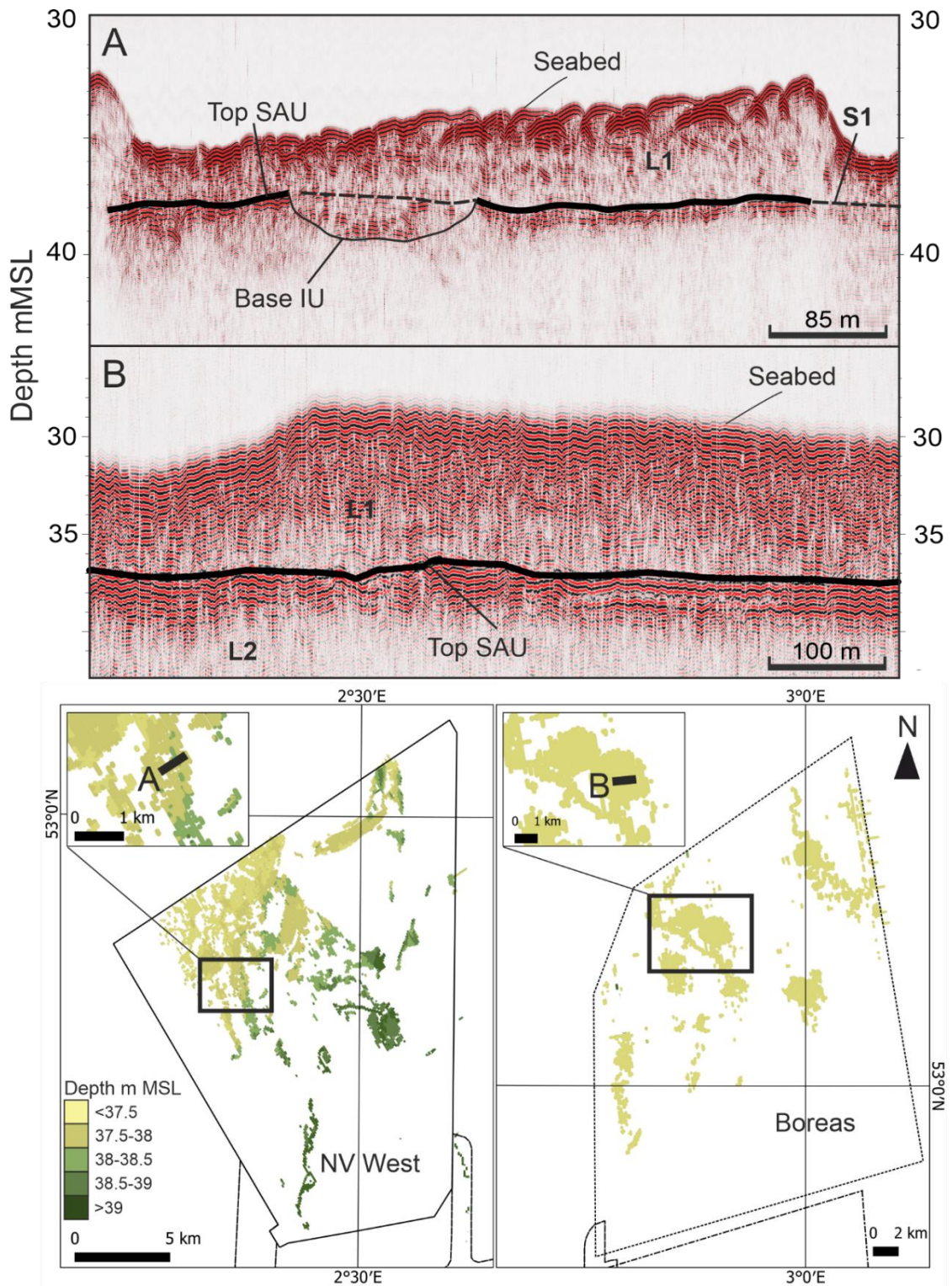
**Figure 4.5. Map of S1 with a channel-form and example seismic profiles of channel-form fills. A range of seismic fill types characterise the channel-fill unit. A) The CFU with cut and fill architecture and SAU partially overlying the fill. SAU is not present on the margins. B) CFU-fill example with high amplitude basal bounding seismic reflectors and cut and fill architecture. The SAU overlies the CFU and is present on the southern margin. C) The CFU with no overlying L1 unit and visible on the seabed with positive relief. D) CFU with a chaotic fill seismic character and SAU present on the southern margin. E) Depth map (m MSL) of the Surface 1 (S1) with locations of panels A, B, C and D.**



**Figure 4.6. VC086 penetrates CFU in the northeast of NV West. CFU here is characterised by the Ssh lithofacies (see text for description). Ssh is underlain by L2 (Slc) and overlain by L1 (Sm). The seismic character of CFU at VC086 is characterised by low to medium-amplitude seismic reflectors that are parallel and sub horizontal, draping the channel-form margins.**

### Seismic anomaly unit (SAU)

SAU overlies unit L2, is closely associated with S1, and is present in NV West and Boreas with a patchy distribution (Figure 4.7). The depth to the top of the SAU relative to mean sea level (MSL) ranges from 37.5 to 40 m, with the SAU unit deepening towards the southeast in NV West, and with no clear depth trend in the Boreas area. Locally, the SAU unit is characterised by multiple high-amplitude, low-frequency seismic reflectors. The number of reflectors range from 2 – 8. No clear trend in SAU thickness is observed across the study area. SAU reflectors are parallel to seismic reflectors in the underlying unit (L2, Figure 4.7). The L1 unit overlies the SAU unit, with the thickest areas of unit L1 coincident with the presence of the SAU (Figure 4.4). Commonly, the SAU is associated with the margins of incisional features, either channel-forms that can be mapped across the study area, or laterally discontinuous incisional features. The SAU either partially or completely overlies channel-forms but does not overlie, and is truncated by, the incisional seismic unit.

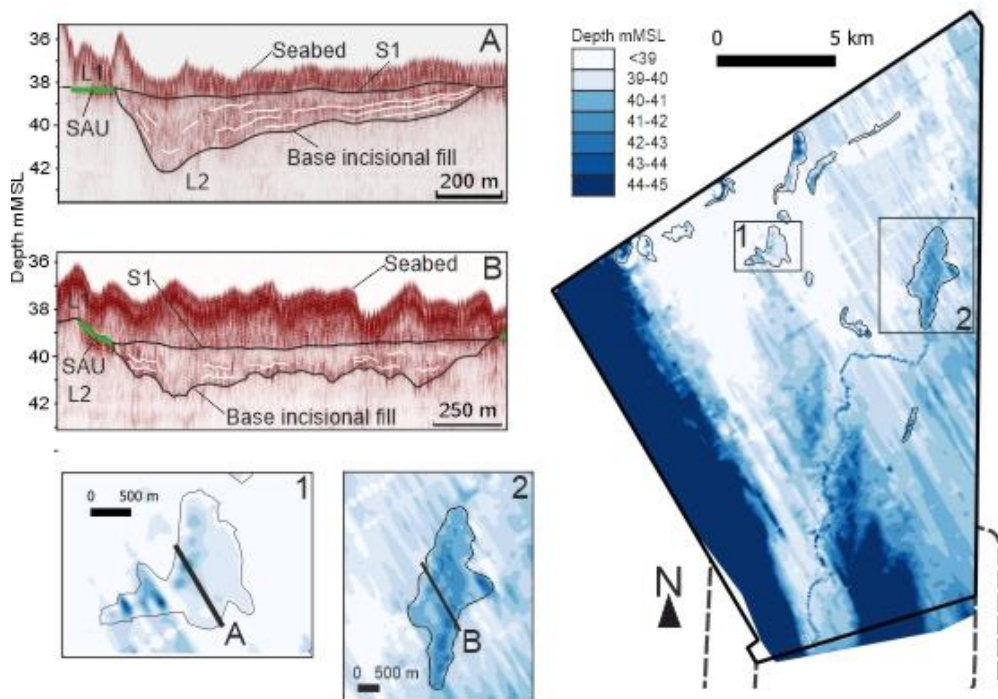


**Figure 4.7. Example seismic sections of unit SAU in NV West and Boreas. The mapped top S1A surface for NV West and Boreas is shown coloured in depth below measured sea level. Profiles A and B show examples of the SAU unit and the variation in thickness (number of seismic reflectors). In both examples, the SAU unit is overlain by a marine bedform.**

## **Incision-fill seismic unit (IU)**

The incisional seismic units (IU) differ from the channel-fill seismic units, in both fill character and planform geometry. In NV West, the incisional seismic units are irregular in planform (ranging from strongly elongate to sub-circular), with widths <2.4 km. In Boreas, differentiating between the incision-fill seismic unit and channel-fill seismic units is more challenging as there is little reflectivity, and the distribution of the two seismic units is more complex. Furthermore, low aspect ratio channel-forms widen then narrow along their length to locally resemble the irregular planforms of the IU (Figure 4.8). Where the incision-fill seismic unit is clearly defined it extends from S1. The incisional seismic unit is distinguished from the overlying L1 unit by an abrupt change in seismic facies character and/or truncation reflectors characterising the fill. Multiple seismic facies characterise the infill of the incisional seismic units (Figure 4.8). Where prograded fills are observed, the reflectors tend to dip southward. Complex fills are seen in NV West (Figure 4.8 A) and Boreas, where seismic facies are stacked and comprise prograded, draped and transparent fills. Features with similar seismic characteristics to IU have been observed in the SBP seismic data in NV West, but these are associated with the troughs of dune-scale bedforms (Figure 4.9).





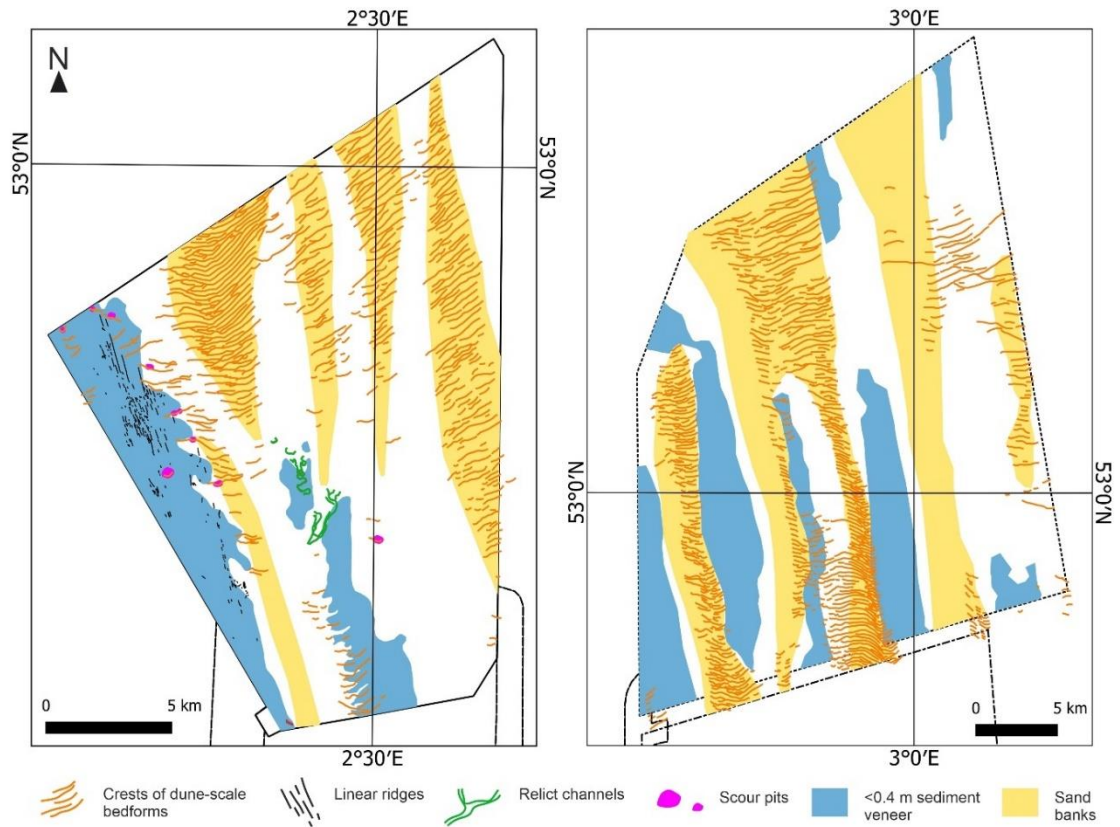
**Figure 4.8. Seismic sections showing examples of the incisional seismic unit. A range of seismic fill types characterise the incision-fill seismic unit. A) Seismic section shows an incision surface with a chaotic fill character and dipping reflectors. Along the northern margin of this feature is the S1A unit, which is truncated. B) Seismic section shows an incision surface that forms part of the CFU interpretation, although its irregular planform resembles IU. Dipping, sub horizontal and transparent seismic fill characterise this feature. C) The S1 surface is shown in the main map with inset maps showing location of panels.**

### Seismic unit 1 (L1)

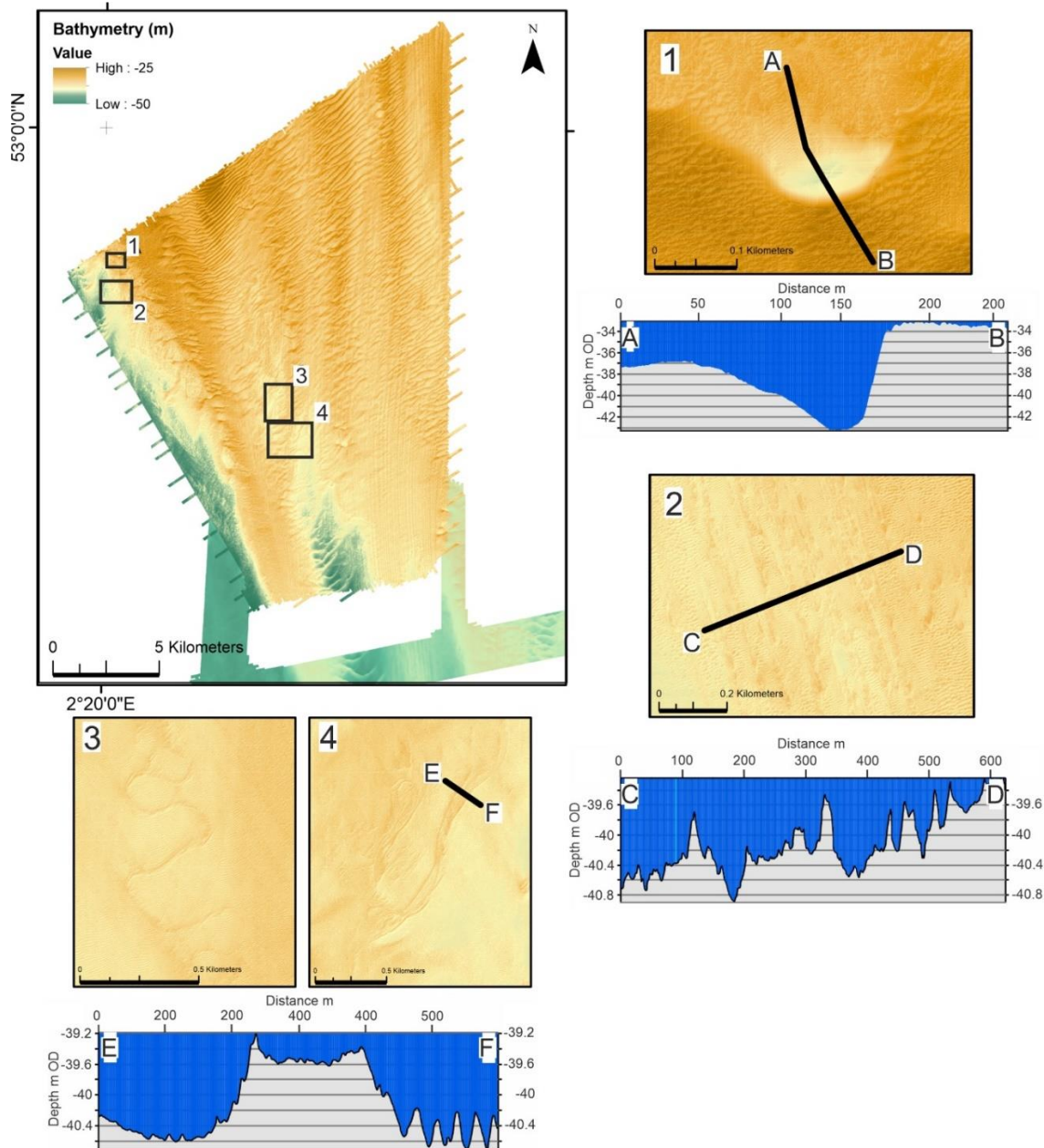
Seismic unit L1 is bound at the base by S1 and at the top by the seabed (S0) and is the youngest seismic stratigraphic unit in the study area. The thickness of the L1 unit is highly variable across the study areas. Where S1 is coincident with the seabed, seismic unit L1 is either not present or below seismic resolution. S1 crops out at seabed in the west and central southern areas of NV West, and in the troughs between the north-south orientated banks in Boreas. At these locations there is only a thin veneer (<0.5 m) of sediment characterised by continuous to discontinuous, high amplitude seismic reflectors. Locally, the SAU crops out at the seabed, which is typically associated with a scour pit between large bedforms. The north-south orientated banks (Figure 4.3 and 4.9) mark the thickest L1 unit (up to 8 m high) and on these banks are superimposed sediment waves (up to 4 m high). In these areas, the seismic character of L1 unit is often low-amplitude to transparent, but dipping seismic reflectors are present, coincident with the dip of the lee face of the large dune-scale bedforms.

## Seabed topography

Bathymetric data shows that seabed topography is uneven with major changes in water depth associated with large (5 and 7 m amplitude, 2.5 to 4 km wavelength) north-south trending sand banks (Figure 4.2 and 4.7). Superimposed on the sand banks are dunes (Table 4.1), the largest of these being 6 m in amplitude. The superimposed dunes show a range of geomorphological characteristics including symmetric and asymmetric in cross section, or 2D or 3D in planform. In the south-central and western edge of NV West, and between the north-south trending sand banks in Boreas, there are smaller bedforms (<0.4 m height) and some large (up to 5 m height) and very large (>5 m height) isolated bedforms. In the northwest and central western areas of NV West, linear ridges are present and are associated with areas where L1 is either thin or absent. In the southwest of NV West, there are elevated, gently-dipping flat areas that are associated with little to no unit L1 present. Associated with very large bedforms are pits on their steeper lee-side (Figure 4.9 and Figure 4.10 A). These pits range from 1 to 3 m deep, are irregular in shape and incisional. Within the central area of NV West, a channel feature with a sinuous profile and positive relief (up to 2 m) is exposed (Figure 4.10 C and D). The exposed channel is associated with areas of limited or absent unit L1. Where unit L1 thickens (towards the sand banks) the channel is no longer visible in the bathymetric data but can be mapped in the SBP seismic data. The location of this channel is coincident with the mapped CFU unit. However, the surface expression of the channel on the seabed is narrower and more sinuous compared to CFU when defined using SBP seismic data. In the west of NV West, linear ridge features (hummocky, linear texture with positive relief compared to the surrounding seabed) are present where the underlying fine grained L2 unit is exposed (Figure 4.10 B).



**Figure 4.9. Key seabed features interpreted from bathymetric data and SBP seismic in NV West and Boreas. The crests of the dune-scale bedforms (sediment waves) are superimposed over north-south trending sand banks. Where only a thin veneer of seabed sediment is present (blue) the L2 unit crops out at the seabed. Relict channels and scour pits associated with dunes and linear ridges are also shown.**



**Figure 4.10. Bathymetric data over NV West showing examples of seabed features (see figure 4.9 for interpretation) and elevation profiles associated with those features. 1) Large scour pit on the lee of a dune (>2.5 m deep) incising into underlying sediments. 2) Linear northwest-southeast trending ridges forming a positive relief (~0.4 m high) and composed of the underlying fine grained L2 unit. 3) Sinuous relict channel orientated approximately north-south. 4) Relict channel with positive relief (levee structures) extending in a northeast-southwest orientation.**

#### **4.4.2. Vibrocore interpretation**

##### **Seismic anomaly unit (SAU)**

The SAU has been sampled in seven vibrocores through NV West and Boreas and represents a clayey peat lithofacies (Pt) (Figure 4.5) that overlies the L2 unit. In vibrocores VC074 and 81, an organic-rich sand that increases in organic content upwards, underlies the Pt lithofacies. Due to the seismic resolution, it is unclear if this lithofacies contributes to SAU. In cores VC028, 32, 75, 80, 81, and 88, the Pt lithofacies is underlain by a grey to light-brown silty-clayey sand that sharply overlies the L2 unit (Figure 4.11 and 4.12). In cores VC039 and 85, the Pt lithofacies is underlain by a light-grey clayey, silty sand grading to a dark-brown sandy, silty clay. In all the cores, the peat is dark brown, humified and amorphous with no visible plant remains, with the exception of VC028 where wood fragments are present. The Pt lithofacies is overlain by a thin (<10 cm thick) organic-rich dark brown clay in cores VC028, 74 and 85. The contact between the Pt lithofacies and the overlying L1 unit is sharp in cores VC039, 75, 80 and 85, but is more convolute, in cores VC028, 74 and 76, with incorporation of organic-rich peats and/or clay into the overlying L1 unit. In VC032, Pt lithofacies transitions upwards into clayey silt with ripple cross lamination.

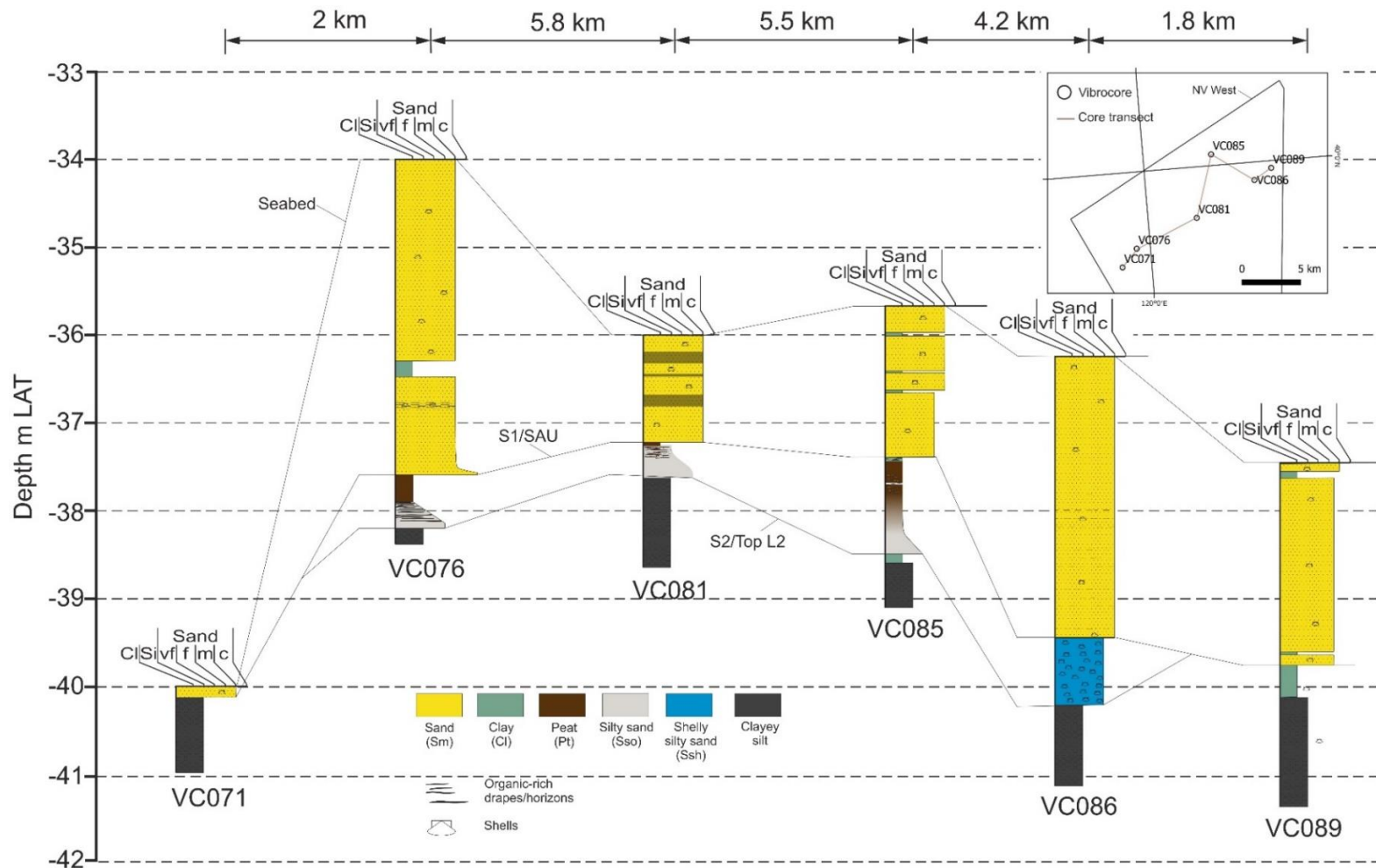
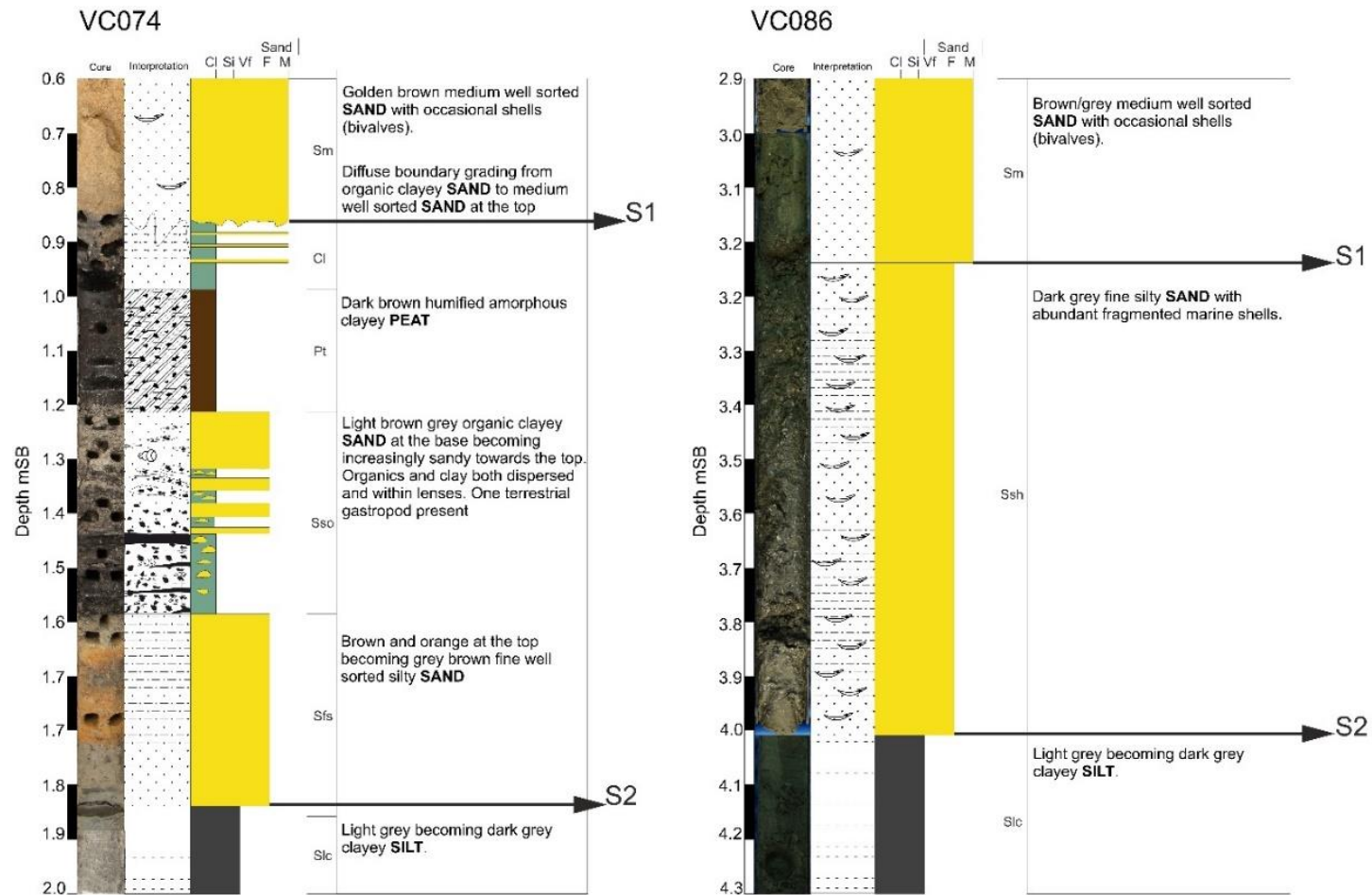


Figure 4.11. A vibrocore transect from west to east through NV West showing correlation of seismic units and lithostratigraphy relative to the ordinance datum. The lithofacies codes are explained in the body text (0).

## **Channel-fill seismic unit**

The channel-fill seismic unit has been intersected by vibrocore VC074 and VC086, with cores extending from the seabed into L2 (Brown Bank Fm.) (Figure 4.12). Two broad lithofacies are present in the cores. VC074 is characterised by lithofacies Sso (Figure 4.5), which is a fine grained organic-rich sand, with the organic component distributed as horizons and/or lenses and decreasing upwards. In contrast, VC086 is characterised by lithofacies Ssh, which is composed of dark grey fine-to-medium silty sand with abundant gravel-sized shell fragments distributed throughout. In both cores, the contact between the channel-fill and the underlying sediment is sharp. In VC086, channel-fill overlies L2, but in VC074 the channel-fill overlies a grey fine-grained silty sand, which in turn overlies the L2 unit sharply. In VC074, a clayey peat overlies the Sso lithofacies with a sharp contact and is considered to be associated with the S1A anomaly



**Figure 4.12. Interpreted vibrocores that penetrated the channel-fill seismic unit. VC074 is in the southwest (Figure 4.2) and samples the margin of the channel-fill unit and is characterised by organic-rich sands and peats. VC086 samples the central part of the channel-fill seismic unit in the northwest. The channel-fill here contrasts with that in VC074, which is composed of a shell-rich silty sand.**



## **Seismic unit 1 (L1) lithofacies**

In all cores, unit L1 corresponds with a golden-brown, well sorted medium sand with rare, fragmented shells (Sm). All vibrocores extend from the seabed, and therefore give a good control of L1 unit thickness. The thickness of unit L1 in the cores is highly variable across the study areas with the thickest unit L1 in core corresponding to sand banks and large bedforms. Along the western margin of NV West (VC071 and 72), a very thin unit L1 is present (<20 cm thick). In vibrocores VC077 and 118, no unit L1 lithofacies (Sm) is observed, with the L2 unit cropping out at the seabed. In some cores (VC070, 78, 84, 86 and 115) unit L1 contains more silt and clay at the base, with the fine-grained fraction decreasing upwards. In vibrocore VC078, a coarse-grained sand with gravel and pebbles (<4 cm diameter), which corresponds with the base of unit L1. In several vibrocores (VC081 and 85 – Figure 4.11), organic-rich clayey horizons are present within unit L1, and these correspond to dipping seismic reflectors within the large bedforms.

### **4.4.3. Cone penetration tests interpretation**

Cone Penetration Tests (CPTs) intersected the SAU, the CFU, and unit L1, but no test was taken through the IU. The CPT data provides a good calibration of soil geomechanical properties to seismic reflection data that can be used to infer a likely lithology (Chapter 3). CPTs penetrate to a maximum depth of 60 m below seabed. For the purpose of this chapter, only the top 10 m are considered.

### **CPT: Seismic anomaly unit (SAU)**

A high (>5%) friction ratio (Rf) and low (<1 MPa) cone resistance (Qc) occurs through the SAU, which corresponds to an organic-rich clay or peat (Robertson, 1990), consistent with peat observed in the vibrocores. This provides confidence that the CPTs are a useful guide to seismic interpretation of the SAU where core intersections are not available. However, the depth interval over which the SAU occurs is thicker than that recorded in the CPTs, indicating that seismic reflection data cannot be used to infer exact thickness of organic-rich peats and/or clays.

## **CPT: Channel-fill seismic unit**

Two CPTs penetrate the channel-fill seismic unit. The character of the two CPTs are markedly different, and this is supported by the core data at the two locations. CPT074 tests the margin of CFU in the southwest of NV West, and this coincides with the mapped SAU. At this location, two lithofacies (Pt and Sso) have been identified in the cores, but differentiating between these using the CPT data is challenging. There is a clear deflection in CPT parameters (friction ratio and cone resistance) at the seismically mapped base of the channel-fill unit and the top of the SAU, but the change in lithofacies is not captured. The CPT parameters support a channel-fill unit composed of silty sand to sandy silt with some organic-rich clays (Robertson, 1990), corresponding to lithofacies Sso. VC086 intersects the channel-fill unit in the northeast of NV West, and presents a marked change in CPT character compared with VC074. The channel-fill unit has low friction ratio (<1) and high cone resistance (>3) compared with VC074, and this implies a sand-rich unit. This corresponds to lithofacies (Ssh) interpreted from core as a silty sand with abundant gravel sized shell fragments.

## **Seismic unit 1 (L1)**

The thickness of the L1 unit is well-constrained using the vibrocores and CPT data, with a clear change in friction ratio and cone resistance seen at the base of unit L1 corresponding to marked changes in lithology in cores from marine sand to either peats, organic -rich clays/sands or marine silts/clays. The L1 unit generally has low friction ratio (<1) and cone resistance (<10), which implies a sand-rich unit. The character of the CPT does show some variation with small spikes in the CPT parameters (friction ratio, ~1.15). The CPTs with a variable character in unit L1 are those that penetrate large sand waves and banks. The increase in friction ratio calibrates with organic-rich clay horizons seen within the sand-rich L1 unit (Sm) in core (Figure 4.11). The clear contrast in the CPT character between L1 and L2 enables identification of those areas with no unit L1, and where L2 crops out at the seabed.

## **4.5. Palaeoenvironmental analysis**

As part of the offshore wind development, a broad-scale palaeoenvironmental assessment was undertaken by Wessex Archaeology on cores in Boreas (Wessex Archaeology, 2019b) and NV West (Wessex Archaeology, 2019c) to identify sites of archaeological significance. A summary of the results from six cores are presented below and contribute to understanding the palaeo-landscape preserved in this region.

#### 4.5.1. NV WEST (cores VC074, 76 and 85)

Diatom analysis of lithofacies fine-grained sand Sso (VC074), indicate deposition in a freshwater environment (*Aulacoseira granulate*, *A. ambigua*, *Epithemia sp.*, *E. turgida* and *Pinnularia major*), although the presence of reworked foraminifera and ostracods from the underlying Brown Bank Fm. (L2), suggests a high-energy setting. Particle-size distribution analysis (Wessex Archaeology, 2018) on Sso in VC076 showed a unimodal distribution, and transparent and well-rounded grains typical of water-lain sediments. Freshwater diatoms and ostracod are present in the clay-rich unit below the peat in VC085, however no reworked material is present.

Pollen assemblages through the peat in VC076 suggest that initial peat development occurred in an open woodland dominated by *Betula* (Birch), with wetlands forming on low-lying, open ground. The pollen assemblage is then characterised by a decline in arboreal pollen, and a switch to a tall herb swamp environment (Wessex Archaeology, 2019c), which is then replaced by a woodland assemblage dominated by *Pinus* (pine) and *Corylus* (hazel). The pollen assemblages in VC074 and 85 are also characterised by *Pinus*- and *Corylus*-dominated woodland, suggesting peat in these vibrocores corresponds with the later phase of peat development seen in VC076.

VC074 records the environmental change from terrestrial to marine conditions and is considered the most complete pollen sequence (Wessex Archaeology, 2019c). This core is situated on the margin of a palaeochannel, and the pollen assemblage is initially dominated by woodland taxa, *Pinus* and *Betula*, and later *Corylus*. The pollen of shrubs is mostly represented by *Corylus* with smaller quantities of *Salix* (willow) and occasional *Llex aquifolium* (holly). Herbaceous pollen is largely represented by *Poaceae* (grass family) with lesser amounts of a range of herb taxa, including *Cyperaceae* (sedge family), *Rosaceae* (rose family), *Filipendula* (meadowsweet). Herbaceous plants would grow on the woodland floor, and sedges and reeds in a wetland environment, likely along the margins of the palaeochannel in a freshwater environment.

In VC085, overlying the Pt lithofacies is an organic clay, silt and sand comprising marine diatoms (*Epithemia sp*, *Gyrosigma sp*), brackish ostracods (*Cyprideis torosa*), and freshwater diatoms (*Epithemia turgida*, *Pinnularia major*, *Cymbella sp*, *Surirella sp*) and ostracods (*Ilyocypris bradyi*, *Herpetocypris reptans*, *Candona neglecta*, *Limnocythere inopinata*). This mixed macrofaunal assemblage is interpreted to represent deposition in an intertidal environment, likely recording a shift in environmental conditions from freshwater to estuarine.

#### **4.5.2. Boreas (VC028, 32 and 39)**

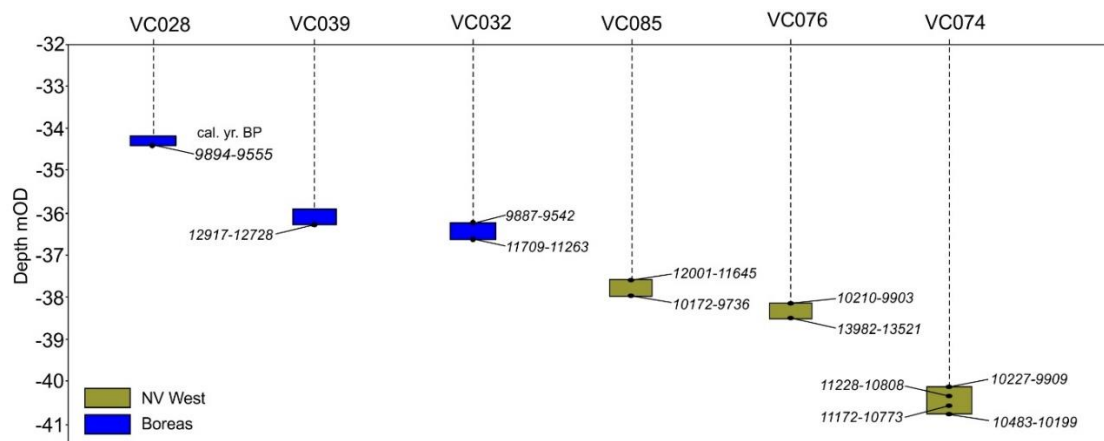
Pollen at the base of the Pt lithofacies in VC039 (SAU), and the uppermost underlying sands, includes *Betula* and grasses typical of a sub-arctic environment and sparse tree cover (Wessex Archaeology, 2019b). Ostracods support the interpretation of a freshwater cold environment. Foraminifera from this level are reworked and likely come from the underlying L2 unit (Brown Bank Fm.). Through the peat, there is an increase in *Pinus*, reflecting an increase in woodland. The same pine-dominated woodland is recorded in VC039. In VC028, the pollen assemblages at the base of the Pt lithofacies record mixed deciduous broadleaved woodland *Ulmus* (Elm) and *Quercus* (Oak) and wetland herb fens habitats (e.g. *Potamogeton natans* type *Sparganium*). The peat in VC032 is overlain by ripple-cross laminated silts. These clays and silts contain foraminifera and ostracods assemblages indicative of intertidal-brackish mudflats and creeks. Diatom assemblages in this interval include marine (*Paralia sulcata*), brackish (*Cocconeis scutellum*) and freshwater (*Grammatophora*) taxa supporting an intertidal environment. VC028, 32 and 39 all show pollen of *Chenopodiaceae* and *Aster* type in the upper Pt lithofacies, typical of a salt marsh environment.

## **4.6. Radiocarbon dating**

The timing of freshwater peat deposition represented by the SAU in seismic reflection data was constrained using <sup>14</sup>C dates taken as part of core analysis completed by Wessex Archaeology. The peat is the primary interest for archaeological remains and understanding of the landscape evolution to constrain the timing of the freshwater peat deposition. These dates provide maximum and minimum ages for the rest of the deposits defined by seismic data. The radiocarbon dates reported by Wessex Archaeology (Wessex Archaeology, 2019b; Wessex Archaeology, 2019c) for peats in the NV West and Boreas are shown in Table 4.2 and Figure 4.13.

**Table 4.2. Accelerator Mass Spectrometry (AMS) radiocarbon dates for organic rich peat (Pt) intervals in six vibrocores across the NV West and Boreas sites. Depth of samples are shown in mbsf and mLAT. <sup>14</sup>C dates are calibrated using IntCal20 (Stuiver et al., 2020) and reported at the 2-sigma range. General position in peat interval and material dated are shown.**

Laboratory code	Depth mbsf (mLAT)	14C Age, BP (no correction)	Calibrated 14C age (cal. yr. BP) INTCal20	Sample point	Material dated
<b>VC074</b>					
UB-36846	0.90 (-39.40)	8955 ± 46	10227-9909	Top peat	Seeds (Nuphar lutea 2x, Nymphaea alba 2x, Juncus sp. 1x, Cyperaceae 1/2x) + leaves (Sphagnum sp. 25x)
UBA-39469	1.18 (-39.68)	9696 ± 44	11228-10808	Mid peat	Cyperaceae, Solanum sp. and Alisma sp. seeds, Poaceae husks
UBA-39470	1.45 (-39.95)	9613 ± 39	11172-10773	Mid peat	Juncus sp., Betula sp., Caryophyllaceae, Alisma sp., Chenopodiaceae and Carex sp. Seeds
UB-36847	1.56 (-40.06)	9122 ± 49	10483-10199	Base peat	Seeds (Betula sp. 3x, Solanum sp. 2x, Chenopodium sp. 1x, Caryophyllaceae 1x, Betula sp. 5x, Lycopodium europaeus 1x, Potamogeton sp. 1x, Nymphaea alba 1x, Cyperaceae 15x), Betula sp. 1x catkin scale
<b>VC076</b>					
UB-36848	3.61-3.63 (-37.61--37.93)	8936 ± 47	10210-9903	Top peat	Seeds: Lycopodium europaeus 1x, Juncus sp 2x, Asteraceae 1x, Carex sp 2x., Ranunculus sp. 0.5
UB-36849	3.91-3.93 (-37.91--37.93)	11863 ± 55	13982-13521	Base peat	Seeds: Potamogeton sp. 5x
<b>VC085</b>					
UB-36850	1.75-1.77 (-37.15--37.17)	10192 ± 47	12001-11645	Top peat	Seeds: Ceratophyllum sp. 1x, Menyanthes trifoliata 2x
UB-36851	2.07-2.09 (-37.47--37.49)	8856 ± 48	10172-9736	Base peat	Seeds: Menyanthes trifoliata 2x
<b>VC028</b>					
UB-38188	2.59-2.62 (-33.79--33.82)	8749 ± 40	9894-9555	Base peat	Bud scales
<b>VC032</b>					
UB-38189	3.83 (-35.73)	8697 ± 45	9887-9542	Top peat	Menyanthes trifoliata seed
UB-38190	4.11 (-36.01)	9992 ± 51	11709-11263	Base peat	Bulk sediment organic sediment
<b>VC039</b>					
UB-38191	3.07 (-35.77)	10881 ± 60	12917-12728	Mid peat	Menyanthes trifoliata seed



**Figure 4.13. Radiocarbon dates from 6 peat layers in vibrocores from NV West and Boreas, obtained by Wessex Archaeology. Dates calibrated with IntCal20 ((Reimer et al., 2013)) and plotted relative to m OD.**

#### **4.6.1. NV West radiocarbon dates**

Material (seeds and leaves) for four radiocarbon dates were taken from the peat in VC074. The two mid samples proved to be out of sequence with the top and base samples and do not allow construction of an age model. However, they do help constrain the approximate depositional age (~10 k BP). The out of sequence dates may reflect formation process given the peat is located on the margin of a channel whereby carbon from the channel might have been washed in. It still remains unclear as to what sample provides a reliable date, however with all samples roughly corresponding in age peat developed between approximately 11228 and 9920 cal. BP, with initial peat development in the early Holocene.

Two dates were acquired from seeds collected in VC076 at the top and base of the peat. The dates suggest development of the peat commenced at approximately 13790-13540 cal. BP until 10220-9910 cal. BP. The dates taken from peat in VC085 are inverted and therefore unreliable, however the ages are concurrent with the ages (c. 12-9 k BP) for peat formation from the other cores.

#### **4.6.2. Boreas radiocarbon dates**

Material for only one radiocarbon age was taken in VC028 at the base of the peat, with an age of 9901 to 9564 cal. BP. The basal peat date in VC032 also record peats deposition during the early Holocene (11707 to 11264 cal. BP). However, this age is from a bulk-peat sample and therefore should be treated with some caution. Peat deposition ended at VC032 c.9884 to 9542 cal. BP. Only one sample was dated in VC039 (12895-12685 cal. BP) at the base of the peat, as the upper parts of the peat were considered disturbed as a result of coring.

Peat sampled in NV West are deeper in respect to elevation than those sampled in Boreas (Figure 4.13). This correlates with earliest age, whereby the oldest peats formed at lower elevations (NV West) and the younger peats formed at higher elevations (Boreas). The correlation between age and elevation might support evolution of peatland in response to changes in landscape (e.g. proximity to the coast and increase in marine influence).

## 4.7. Sedimentary environments

Calibration of seismic data, core and CPT data, and supporting information from  $^{14}\text{C}$  ages and palaeoenvironmental analyses, support a temporal transition through four environment types including; fluvial dominated, freshwater peatland, coastal plain marsh, and shallow marine.

S1 is a composite surface with both conformable sediments overlying the L2 unit and localised unconformable contacts represented by channel-fills and incisional units. The S1 surface is low relief with the overall depth trend deepening to the south, with incision of channel-forms in both NV West and Boreas. The longest channel-fill extends NE-SW at least 26 km, and a shorter channel extends 4.7 km, approximately N-S, merging with the longer NE-SW channel in the south (Figure 4.5). In Boreas, the channel-forms are less extensive, and are <3.5 km in length. Locally, the thickness of the channel-fill is 5 m, and typically <3 m. The main channel-form in NV West has a sinuosity (total length along channel axis/length between channel end points (Mueller, 1968)) of 1.28 over its entire preserved length but channel-forms identified within this main channel-form (Bathymetry - Figure 4.10 C and D) have a higher sinuosity (2.3). Overlying and coincident with the channel margins are peats observed both in the seismic (the SAU) and cores (Pt lithofacies), and in the central and northern areas of NV West and Boreas discontinuous peats overlie the S1 surface.

The preserved geomorphology supports the interpretation of S1 as a terrestrial surface that formed during the retreat phase of the Devensian glaciation. At the Last Glacial Maximum (~18,000 yrs BP) the study area would have been <40 km from the ice-front (Dove et al., 2017), and influenced by ice-marginal glaciofluvial processes. Sharply overlying S1 are freshwater sands, silts and clays, deposited in an alluvial/fluvial environment and seen in core as lithofacies Sso and Cl. The distribution of lithofacies Sso and Cl is patchy, as indicated by their absence in some cores, suggesting the environment of deposition over the S1 surface was dynamic and typified by both depositional and erosive processes. Peat (Pt) from c.13-9 k cal. BP (Table 4.2 and Figure 4.11) overlies both the S1 surface and the Sso and Cl alluvial/fluvial lithofacies. Contemporaneous with peat development, fluvial channels incised into underlying unit L2. The sinuous nature of the fluvial channels, coupled with peat development along their margins, suggest that they were formed under lower energy conditions over a long time period (>1000 yrs, Vandenberghe et al., 2013) as opposed to under energetic meltwater conditions (Vandenberghe, 1995; Bourillet et al., 2003; Marren et al., 2014; Prins et al., 2019; Emery et al., 2020)

Peat developed in the north of NV West and Boreas as laterally extensive sheets. In contrast, those in the south of NV West formed on the margins of channel-forms. Palaeoenvironmental data (Wessex Archaeology, 2019b; Wessex Archaeology, 2019c) support the interpretation of a transition from a landscape that supported large broad leaf trees (well drained) to a wetter fen-bog landscape, and wetland environment as a consequence of rising ground water levels.

The fine grained, clay-rich unit in VC032 with ripple-cross lamination and the presence of abundant estuarine gastropods *Hydrobia*, indicate a transition from a freshwater environment into one with increasing tidal influence. This is supported by macrofaunal assessments (Wessex Archaeology, 2019c), whereby diatom assemblages are dominated by *Polyhalobous* (marine) to *Mesolhalobous* (brackish) species at the base. This change is likely a response to relative sea-level rise in the early Holocene. (Shennan et al., 2000; Sturt et al., 2013).

The generally transparent L1 unit and the presence of a medium grained sand with marine shells in cores completes the record of marine transgression. The sharp contact with the underlying deposits marks a change in energy from a coastal plain environment with peats and intertidal drainage networks into a higher-energy shallow marine environment.

## **4.8. Discussion**

The high spatial resolution and comprehensive dataset used in this study provide unique insights into submerged postglacial landscape in the southern North Sea, which evolved as a consequence of a warming climate following the Last Glacial Maximum. The data demonstrate the importance of fluvial sedimentary processes as part of the landscape evolution in the study area, alongside the stratigraphic and landscape response to marine transgression.

### **4.8.1. Postglacial fluvial processes**

Within the southern North Sea region, studies concerning landscape evolution from Late Devensian to Late Holocene have focused on the now submerged landscape of Doggerland (Cotterill et al., 2017; Fitch et al., 2005b; Emery, et al., 2019), with few focusing on the submerged landscape south of Doggerland (Briggs et al., 2007; Missiaen et al., 2020) and often relying on either single or disparate data types. In contrast, the dataset used in this study allows us to develop a detailed, high-resolution, regional understanding of palaeo-landscape response to changing climate.



At the base of the succession is unit L2, which was most likely deposited between ~MIS 5d and 3 (Eaton et al., 2020). Sea level during MIS 3 and 2 remained low due to the presence of large ice sheets in the North Hemisphere (Peltier, 2005) leaving the southern North Sea, beyond the limit of the Devensian ice sheet, sub-aerially exposed. The results presented here shows that the late Devensian landscape in the North Sea was dominated by freshwater alluvial and fluvial sediments, which were then accompanied by peats developing alongside the margins of these channels from c. 13.9 ka BP as climate warmed. These fluvial systems are contemporaneous with those observed elsewhere in the North Sea (Prins et al., 2019; Tizzard et al., 2014). The channel-fill facies is interpreted to record a channel system evolving from fully fluvial to one subject to gradual marine flooding and subsequent deposition of marine deposits within the channel. The fluvial system flowed to the south as supported by channel thalwegs that dip to the south and likely drained into the advancing marine environment in the south. The sinuous character of the channels reflects a longer-lived fluvial system than if the channels were formed under meltwater conditions. The channel-form likely accommodated a shifting more sinuous channels as evidenced by bathymetric data and the stacked and multiple fill types identified in seismic data. The distribution of peats on the channel margin and overlying freshwater deposits supports channel avulsion and revegetation within a larger channel-form. Ultimately fluvial processes retreated during rising relative sea level and the northward migration of the shoreline with fluvial channels were overtopped by marine sands.

#### **4.8.2. Origin and age of incisional features (IU)**

The incisional features identified in seismic data (Figure 4.8) are distinctive in their planform geometry and seismic fill character compared with the channel network (Figure 4.5). Seismic data, core and palaeoenvironmental analysis of the peat supports development of the incisional unit either synchronous with or after the channel network. The origin of the incisional features is enigmatic given the limited data coverage and lack of similar features in the literature. However, their origin can be explained by a number of scenarios.

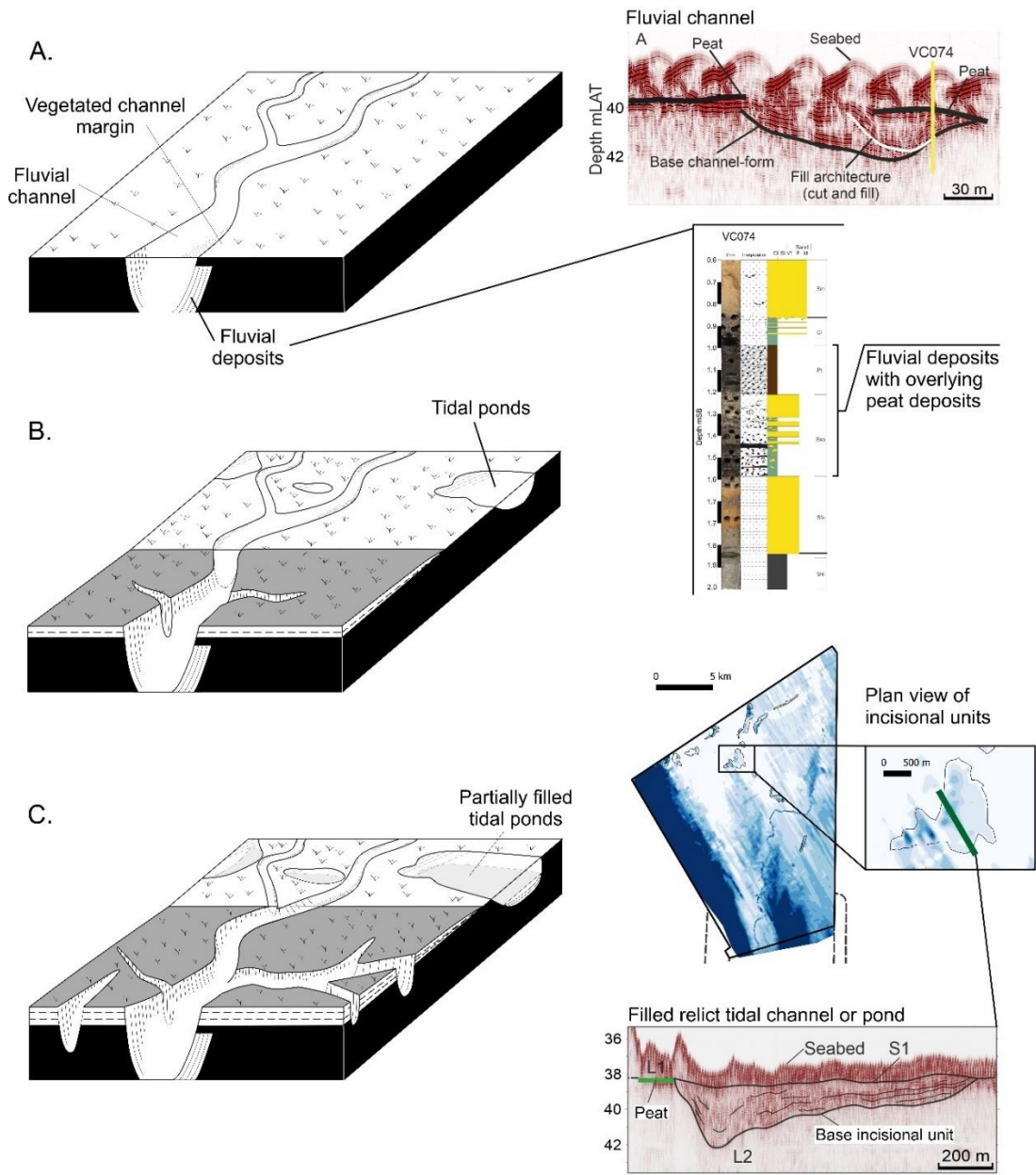
The seismic character of the incisional unit fills is marked by a change in seismic facies between the base of the incisional unit and the underlying L2 (Brown Bank Fm.). In contrast, the base of the channel network fill is marked by high amplitude seismic reflectors. The fill of the incisional unit is also generally low amplitude with little visible internal structure, whereas the fill of the channel network shows a more complex fill pattern. An exception to this is shown in Figure 4.8 B where the fill of the incisional unit

is clearly more complex (dipping, draped and truncated seismic reflectors). The channel network fill is in places overlain by peat (Figure 4.5 A and B) suggesting an age relationship both pre-dating and contemporaneous with peat formation. In contrast, the incisional features are never overlain by peat, and preserve a sharp termination of peat at their margins (Figure 4.8 A). Discriminating between the channel network and the incisional unit using seismic data to infer a depositional environment is challenging. A large range of seismic fill facies are ambiguous and do not necessarily indicate a specific environment, but rather a variety of different depositional environments (Prins et al., 2019). Furthermore, the fill character is not necessarily related to the process that eroded the feature and may infill much later. This is illustrated in cores VC074 and 86, where both vibrocores sample the channel network fill but contain different lithofacies interpreted to have been deposited in fluvial and marine environments, respectively. The geographic location and stratigraphic position of these incisional features support several possibilities for their origin and evolution, as formed under models of relative sea-level rise. Using an adapted version of Allen's (2000) conceptual morphostratigraphic model for the evolution of established coastal marshes in response sea-level rise two possible origins are discussed.

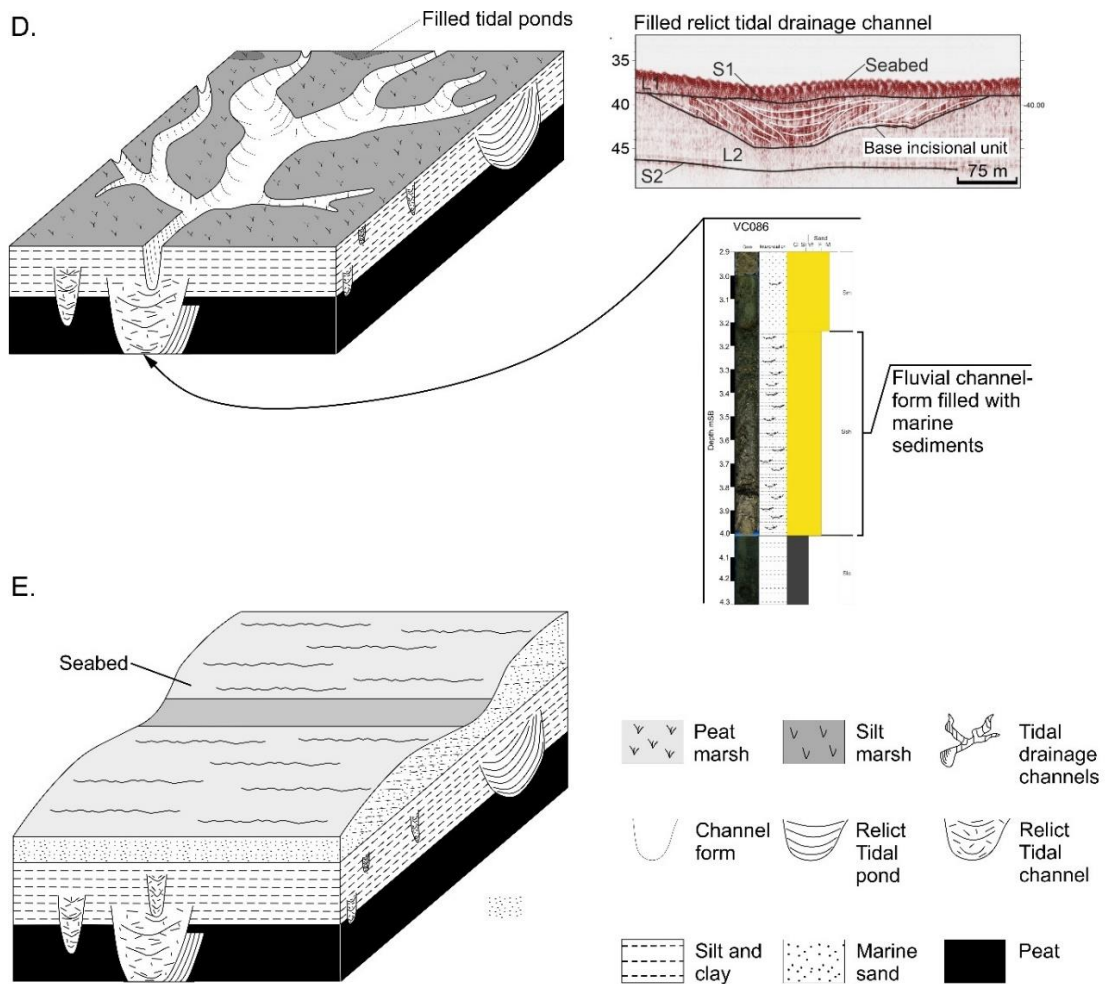
#### **4.8.3. Relict tidal drainage channels**

Channels in tidal marshes act as drainage conduits for flood and ebb waters in the marsh system. The function and form of tidal marsh channels vary throughout the marsh (Zeff, 1999). During rising relative sea levels temporal and spatial variations in physical processes would result in the development of distinct sedimentary environments (Frey et al., 1978). Within the study area at c. 9 ka BP sea levels would have risen sufficiently that part of the low-lying marsh would have been subject to marine inundation with introduction of tidal processes and development of a transgressive surface (Shennan et al., 2000), as seen in VC032 where estuarine sediments have been identified. Drainage of the supratidal marsh environment would have been through surface channels (CFU) and absorption directly through the permeable marsh surface (Figure 4.14 A). The channels at this stage would have been filled with fresh water fluvial deposits (VC074) and have migrated across the marsh landscape with colonisation of plants and development of peats on abandoned fill deposits (Figure 14 A seismic example). In the lower marsh, a minerogenic marsh was established, with deposition of silts and clays. This would migrate up dip through the marsh with continued relative sea-level rise (Figure 4.14 B). With parts of the marsh now lying just below highest astronomical tide (HAT), erosion and differential deposition initiate tidal drainage networks (Rieu et al., 2005). With further relative sea-

level rise, accretion of sediment continues on the marsh surface, and extension and incision of tidal channels increases. Pre-existing landscape features such as the channel network are either submerged and/or buried or repurposed as drainage conduits with the consequent deposition of estuarine/marine sediments in previously freshwater channels and colonisation of estuarine/marine fauna (Figure 14 D VC086). The increase in size of the tidal drainage network leads to displacement by erosion of contemporaneous and older marsh deposits including the terrestrial peat deposits. With continued relative sea-level rise, and a consequent decrease in tidal prism size (Du et al., 2018) the marsh platform accretes more slowly, and tidal drainage channels begin to silt up (Rieu et al., 2005) (Figure 4.14 D). At this stage, the down-dip sections of the drainage channels and associated over bank and peat deposits, that are below lowest astronomical tide are either silted up and buried or eroded by wave and tidal processes. With continued relative sea-level rise, the remaining drainage channels are drowned and consequently silt-up and shallow marine conditions dominant leading to deposition of shallow marine sediments over the now relict subtidal channels (IU) (Figure 4.14 E). The planimetric form of the incisional units can be explained by erosive processes leading up to full marine inundation, however the isolated nature of the incisional units remains unclear. It would be expected that some channel-form morphology would remain, particularly in a low relief shelf setting, were small rises in relative sea level would result in significant advances in transgression.

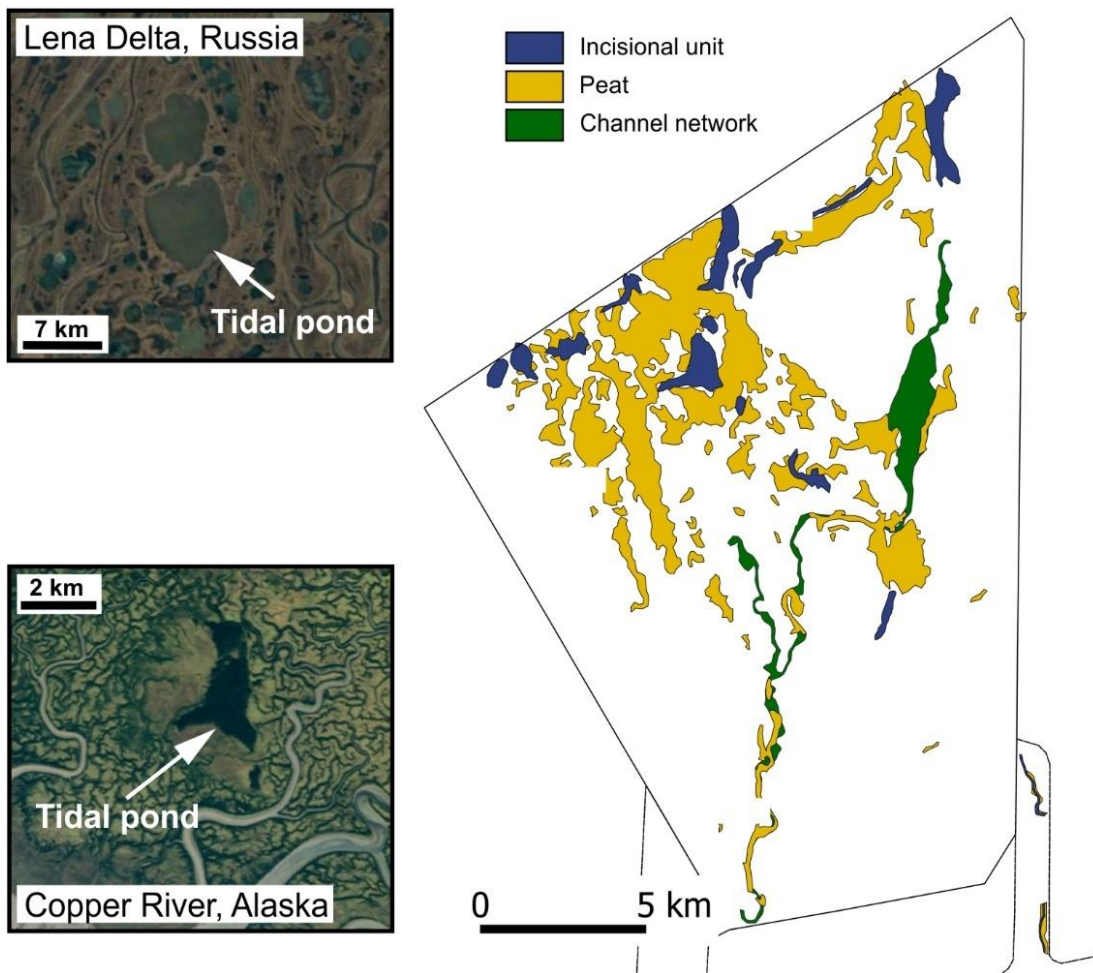


See following page for figure caption.



**Figure 4.14. Proposed conceptual morphostratigraphic model for the development of relict tidal channels and/or relict tidal pools in an established coastal marsh undergoing sea-level rise with examples from seismic data and cores in the study area to support this model. For detail on the evolutionary stages leading to development features see text. The vertical scale, and the cross-sectional scale of the creeks, are greatly exaggerated. Adapted from Allen (2000).**

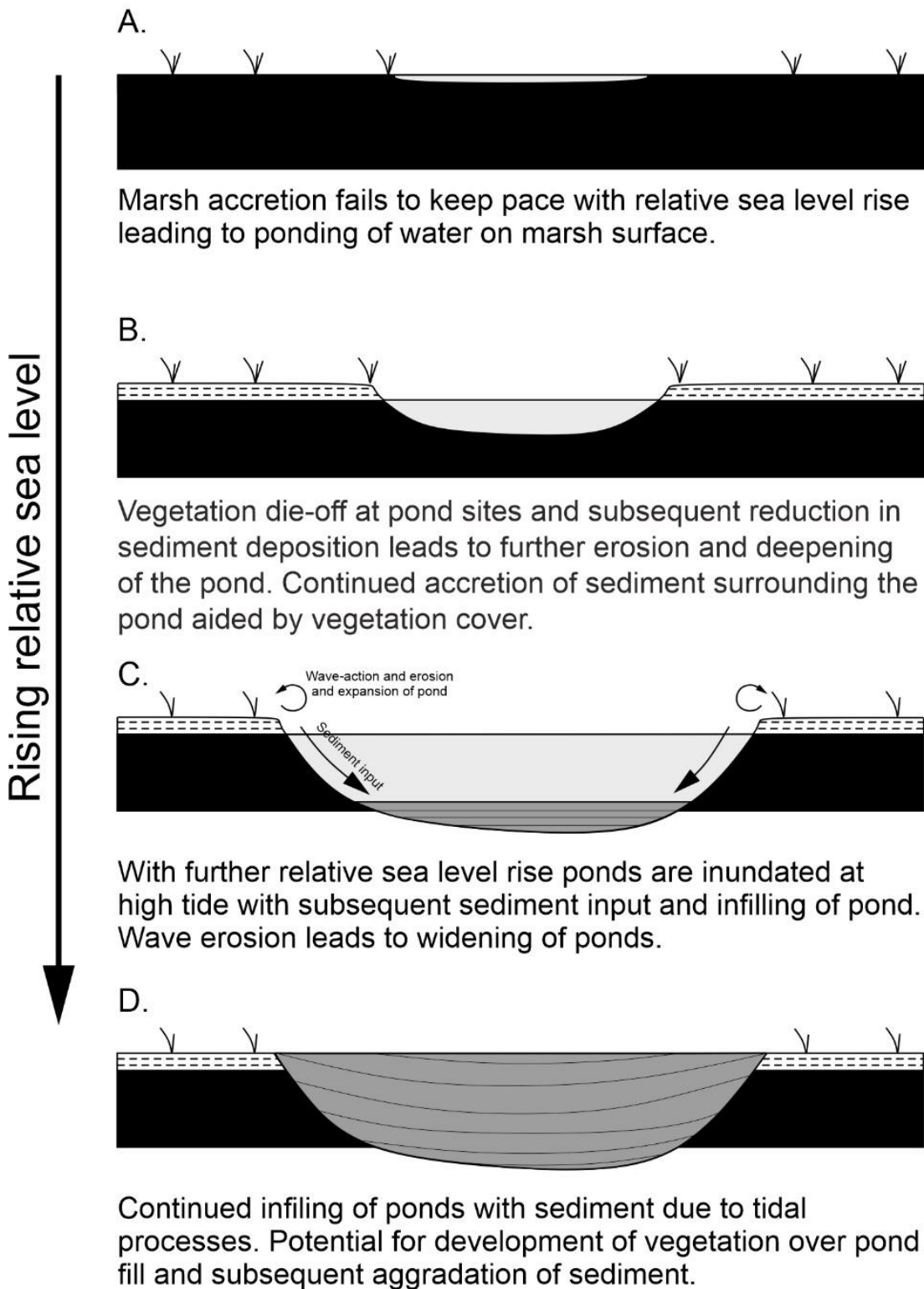
#### 4.8.4. Relict tidal ponds



**Figure 4.15. Analogues of modern active tidal ponds, their scale and shape compared with the incisional units documented in the study area. The Copper River Delta is largest contiguous wetlands along the pacific coast of North America and the Lena Delta is located in northeast Russia and is approximately 400 km wide. Tidal pools are common in both areas although the Lena Delta is frozen tundra for 7 months of the year. The tidal pools seen in the wetlands of the Copper River Delta are equivalent in size to incisional units observed in the study area (<2 km), whereas those identified on the Lena Delta are larger (>5 km). Aerial images taken from Google Earth.**

The planform geometry of incisional units are distinctive compared to other features in the study area. However, similar features are present on modern coastal marsh analogues on the Copper River delta in Alaska (Figure 4.15, Galloway, 1976), the embayed Rhode Island coastline of northeast USA (Raposa et al., 2017), and coastal New Jersey (Zeff, 1999), and the Lena Delta, Russia (Figure 4.15), which have been characterised as tidal ponds, pools or potholes. For the purposes of this discussion, these features will be referred to as tidal ponds. In general, modern tidal ponds are smaller than the IU feature, although exceptions are seen on the Copper River Delta

and Lena Delta (Figure 4.15). However, the comparatively small scale of the modern coastal marshes compared with ancient Late Devensian to Early Holocene marshes might support the existence of larger tidal ponds at that time. Furthermore, the basal surface of the IU features might be time transgressive stratigraphic surfaces rather than geomorphic surfaces. The difference in seismic character of the incisional unit compared with the channel fill unit supports a different fill lithofacies and/or sedimentary process. The closure of the incisional unit basal bounding surface at S1 in all directions also supports a marked change in origin compared to the channel fill unit that show sub-parallel erosion surface and no closure. The formation of tidal ponds is an early indicator of a marsh that is failing to keep pace with relative sea-level rise (Stevenson et al., 1985; Nyman et al., 1993), and the enlargement of tidal ponds is a fundamental component of marsh loss in submerging marshes (Schepers et al., 2017). Examples of this are seen in the Mississippi Delta (Nyman et al., 1993), Chesapeake Bay (Kearney et al., 1988) and the Venice Lagoon (Carniello et al., 2009). Here, it is proposed that the incisional unit represents relict tidal ponds that formed during the Late Holocene through failure of the marsh surface to keep pace with the rate of relative sea-level rise, resulting in vegetation loss, and denudation of the marsh surface. Figure 4.14 B and 4.16 shows the morphostratigraphic evolution of the marsh leading to the formation of tidal pools and their subsequent infill. The loss of vegetation in areas of pool formation likely decreased deposition and/or enhanced erosion (Baustian et al., 2012; Temmerman et al., 2012) (Figure 4.16 A). The relatively sparse number of incisional units in the study area compared with modern marsh tidal pool examples (tidal pool constitute 15 to 60% coverage (Koop-Jakobsen et al., 2019) may be explained by merging of pools or connection with tidal channels or drainage of pools followed by revegetation and rapid sedimentation accretion (Wilson et al., 2009; Wilson et al., 2010; Millette et al., 2010). Through these processes tidal pools can become smaller or larger or disappear. More tidal pools may have been preserved in the study area but cannot be resolved due to the limitations imposed by seismic resolution and line spacing.



**Figure 4.16. Proposed conceptual morphostratigraphic model for the development of tidal pools in an established coastal marsh but failing to keep pace with sea-level rise. For detail on the evolutionary stages leading to development of incisional units (see text). The vertical scale, and the cross-sectional scale of the creeks, are exaggerated.**



#### 4.8.5. Peatland palaeoenvironment, morphology, chronology and preservation

Following establishment of a network of channels, peats developed on a low relief coastal plain landscape from ~13.9 ka, with pollen assemblages typical of a sub-arctic environment. With continued development of peat into the Early Holocene, prior to their burial by marine sands at c. 9 ka BP, there was a decline in arboreal pollen and a switch to herb species found in wetter ground conditions, which supports a warming climate throughout the Early Holocene and increased proximity to the coast. Salt marsh taxa, e.g., *Chenopodiaceae*, are found in the upper peat of Boreas core VC032, suggesting a low energy environment or relative slow rate of relative sea-level rise, and minimal erosion of the upper peat surface in this location.

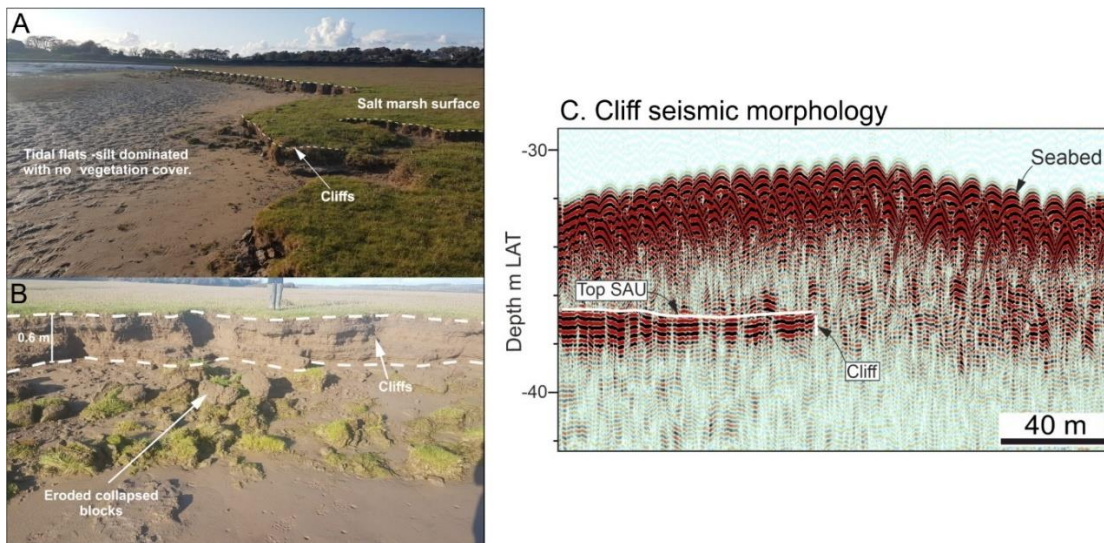
The elevations of the peat range from -40.5 to -34.5 m LAT (Figure 4.13), with some directly overlying S1 (Brown Bank Fm.) and others overlying postglacial alluvial and fluvial deposits. The majority of the peat has a discontinuous sheet-like form typical of a low relief wetland environment (Warner, 2005; Sim et al., 2019) whilst other peats are associated with channel margins.

Given the low relief landscape, the underlying clay-rich substrate and relatively large area over which the peats are found, it is likely that these now discontinuous peats were more continuous across the landscape. Within the study area there has been continuous peat development for ~4.5 kyr synchronous with a landscape dominated by fluvial processes. Evidence for reworking of the peats is seen VC074, where peat clasts are incorporated into an overlying sand dominated interval, in VC076 where peat clasts are seen in the interval overlying the peat, and in VC028 where the upper interval of the peat has sand-rich lenses distributed throughout. With this in mind, it is highly likely that peats have been reworked throughout this time. This might explain the channel margin peats in NV West that show an out of sequence chronology in VC074, which can be interpreted to be a result of reworking of older organic deposits with subsequent deposition on the channel margins.

A reduction of peat volume (degradation) can also occur as a result of normal peat processes such as decomposition, humification, and stabilization of organic matter in soils (Kalbitz et al., 2002), and also changes in climate (Milner et al., 2021).

Degradation in modern-day peats is considered to be either due to development phase processes (autogenic) (Payette, 1988) or human-induced changes in the environment (climate, land use and atmospheric pollution) (Bowler et al., 1985; Kennish, 2001). Late Devensian and Holocene peats identified in this study would have been subject to the

same autogenic processes as modern-day peats and a significant climate change, such as increased precipitation (Emery et al., 2020), which might have driven peat degradation, and therefore the distribution of the preserved buried peat. The present-day morphology of the buried peat, with abrupt lateral stepped terminations at peat margins (not associated with channels), is likely an erosive feature formed in response to fluvial processes and/or relative sea level-rise. However, geomorphological features similar to this are seen at the seaward facing margins of salt marshes and along the margins of subtidal channels in modern-day coastal peatlands (Allen, 1989; Allen, 2000; Adam, 2002) and are commonly referred to as ‘cliffs’ (Figure 4.17). With pollen data supporting a peatland succession from freshwater terrestrial through to salt marsh, and peat margin morphology analogous to modern day coastal peat setting, marine inundation due to rising relative sea levels throughout the Holocene was likely one of the primary drivers for the documented peat distribution and configuration.



**Figure 4.17. Seaward facing cliff morphology in a salt marsh environment. A) Modern analogue of seaward facing cliff morphologies on a modern salt marsh in Morecombe Bay, UK. B) Seismic data example of an abrupt lateral termination in the seismic anomaly unit (SAU) common in the survey areas and interpreted to be a seaward facing cliff formed in a salt marsh setting.**

## 4.9. Conclusion

The acquisition of a high-resolution dataset optimised to image and sample the shallow subsurface has provided a unique opportunity to investigate submerged postglacial landscapes. Sediment cores logged at a high resolution, and put into a chronological framework, have allowed sequential changes in landscape to be interpreted and then correlated using seismic stratigraphy and facies to reconstruct palaeolandscapes and their evolution over the broader area.

Following LGM this part of the southern North Sea was dominated by fluvial processes and these processes are considered to be contemporaneous with fluvial systems documented elsewhere in the North Sea. The dominance of fluvial process would have continued from Late Devensian until ~9 ka when marine transgressive processes prevailed. From ~13.9 ka, peats developed on a low relief coastal plain landscape, and continued to develop into the Early Holocene, prior to submergence and burial with the onset of marine transgression. Palaeoenvironmental data supports a succession from freshwater peatland through to salt marsh, in-line with a warming climate and relative sea-level rise throughout the Early Holocene.

Relict tidal drainage channels and tidal ponds have been proposed as two possible origins for the formation of the enigmatic incisional features documented here. Without core data to confirm the origin of incisional features it remains a challenge to assign preference to one particular origin. However, with the morphological characteristics of incisional features often not conforming with those expected of tidal channels, the tidal pond origin is preferred.

The present-day configuration and preservation of buried postglacial peats is a result of erosional and degradational processes throughout the Late Devensian and Late Holocene period. Changes in erosional and degradational processes resulted from relative sea-level rise, a consequence of a warming climate. Submerged and buried postglacial peats offer insights into the fates of modern coastal plain wetlands such as the present-day Netherlands coastal plain. Under models of relative sea-level rise, the Netherlands coastal plain is at significant risk of flooding through marine inundation. The relief of the Netherlands coastal plain is similar to that documented in this study, characterised by low-lying areas with minor changes in surface gradient. Through understanding these now submerged analogues, the evolution of modern low lying coastal plain systems can be predicted and managed.

## **Chapter 5 - Submerged postglacial peat carbon stocks, in the southern North Sea**

As lead author, Stephen James Eaton was responsible for data analysis, interpretation, and figure preparation. The role of other co-authors (Hodgson, D.M., Barlow, N.L., Mortimer, E.E.) was limited to discussion of results and chapter editing.

### **5.1. Introduction**

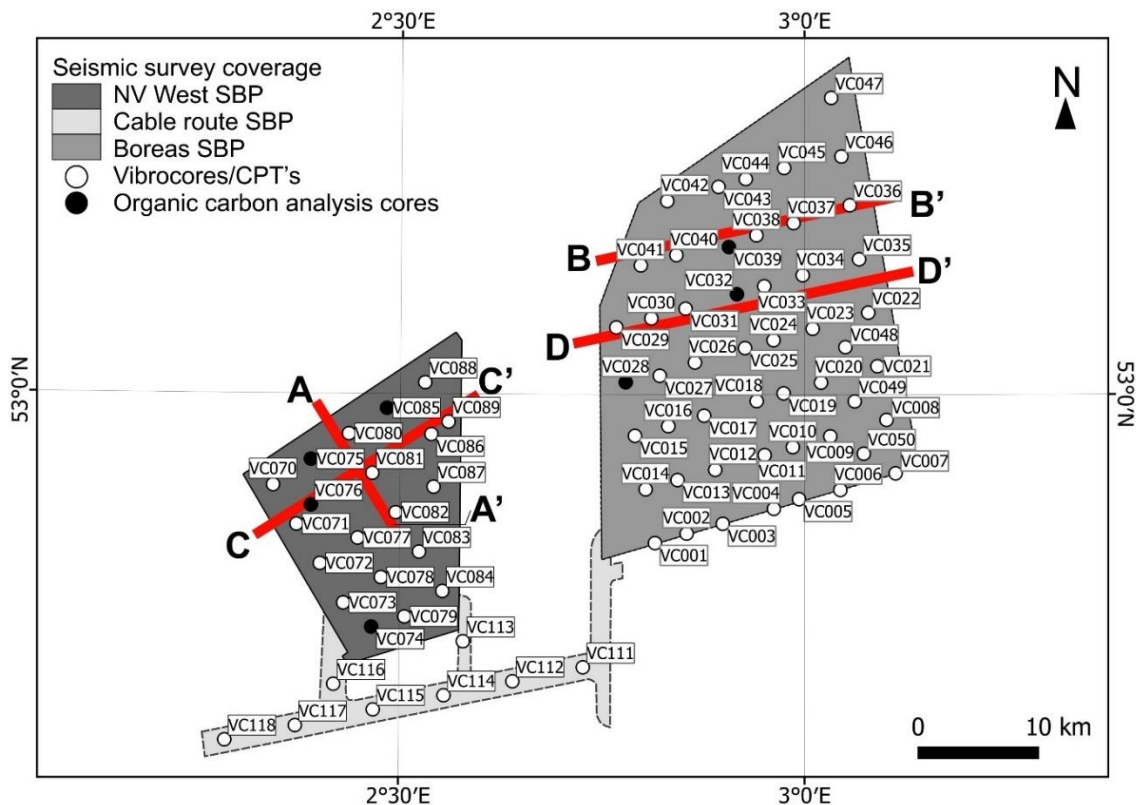
Wetland environments in which peats form are important in the global carbon cycle (Tarnocai et al., 2012; Yu et al., 2010; Limpens et al., 2008), with approximately 600 Gt of carbon sequestered since the Last Glacial Maximum (LGM) (Charman et al., 2013) and form important stocks of carbon (Dargie et al., 2017; Treat et al., 2019). Much assessment of carbon stocks in wetland environments has been disproportionately skewed to inland terrestrial environments (Yu et al., 2010). However, located seawards and often overlapping with terrestrial wetlands are 'blue carbon' wetlands (Nelleman et al., 2009). These buried wetlands are often peat-based or contain significant volumes of organic matter mixed with sediments within carbon-rich soils (McLeod et al., 2011). The continuing survival of blue carbon wetlands is at risk due to climate change, sea-level rise and direct anthropogenic pressures e.g., dikes, weirs, levees, docks, and pipelines (Henman et al., 2008; Chambers et al., 2014). Investigations that study the relationships between sea level and carbon storage suggest that during the Early Holocene (~12-8 ka) marine transgression of terrestrial ecosystems had a significant impact on postglacial increases in atmospheric CO<sub>2</sub> (Montenegro et al., 2006). The actual fate of carbon on exposed continental shelves at the LGM and during marine inundation is not fully understood given the complicated biogeochemical processes and feedbacks that occur in the water column and sediments of different geochemistry. Given the threat of future rising sea level on coastal environments, researchers are beginning to focus on quantifying the carbon stored in coastal environments and the potential for the release of carbon (Chmura, 2013; Pearsall et al., 2005). Whilst recent studies have attempted to quantify carbon stocks in fjord landscapes (Smeaton et al., 2016; Burrows et al., 2014), there are few documented studies investigating carbon stocks associated with submerged and buried ancient coastal plain environments (Montenegro et al., 2006).

Following retreat of Last Glacial Maximum ice sheets from the North Sea basin (Kristensen et al., 2007; Dove et al., 2017), the resulting postglacial terrestrial landscape provided a surface for colonisation by pioneer vegetation as climate started to warm (Crombé et al., 2011). Climate warming of ~2-3°C in the North Sea region from the end of the Younger Dryas (11.5-10.5 ka) to c.8 ka (Emery et al., 2020) culminated in the establishment of birch woodland followed by hazel (Crombé et al., 2011). As the remnants of the global LGM ice sheets melted, ongoing RSL rise initially raised groundwater levels, before full marine inundation of this woodland environment (Shennan et al., 2000; Sturt et al., 2013). Remains of this terrestrial peatland landscape are buried beneath the middle and late Holocene marine sediments, in particular within the southern North Sea (Fitch et al., 2005a; Missiaen et al., 2020). New offshore geophysical and core data from offshore wind site investigations offers the resolution required to study this peatland landscape in detail and quantify the buried carbon stocks.

This study aims to quantify the carbon stocks held within the peats and organic-rich sediments held offshore in the study area. Through interpretation of seismic, cone penetration tests (CPT) and vibrocores, the carbon stock contained within the peats and organic-rich sediments are quantified. Interpretation of seismic and vibrocores data constrain the spatial distribution and geometrical character of the peats and surrounding features. The processes which controlled the preserved spatial configuration are discussed, and evidence to support the continued erosion of the peats and organic-rich sediments are presented. Finally, the upscaled potential for carbon stocks in the wider southern North Sea region are considered with an estimate of carbon stock for postglacial peats across the southern North Sea region.

## **5.2. Study area**

The study area is located approximately 40 km offshore East Anglia and comprises three shallow water (<50 mMSL) work areas; Norfolk Vanguard West, Norfolk Boreas, and the cable route (Figure 5.1). Local bathymetric variations are due to large (up to 7.3 m high) north-south trending sand banks that either formed in response to the present day hydrodynamic regime, or are relic features following postglacial RSL rise (Dyer et al., 1999).



**Figure 5.1. Location map for the three work areas documented in this study (NV West, Cable route and Boreas), and vibrocore and Cone Penetration Test (CPT) data locations. Black circles indicate the cores used for organic carbon analysis. Figure 5.2 and 5.19 panel locations shown in red.**

### 5.3. Seismic analysis

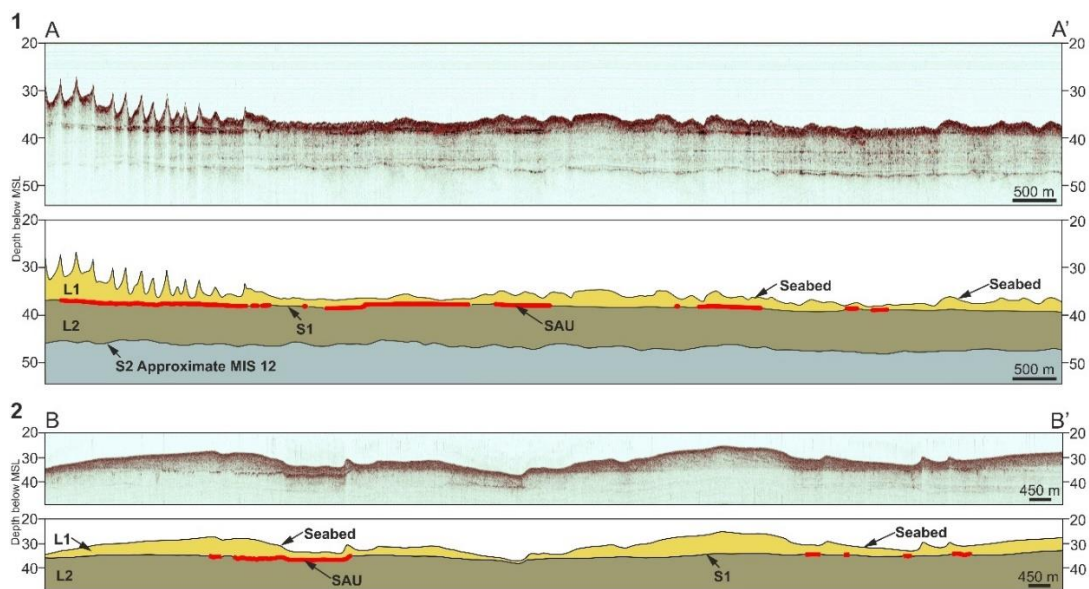
For information on seismic acquisition, processing and limitations refer to Chapter 2 where these have been documented in full. For the purposes of this study Sub Bottom Profile (SBP) seismic has been used primarily to interpret stratigraphic and geomorphological features. In case where the SBP seismic was not of sufficient quality (poor imaging), the Ultra High Resolution seismic data has been used where possible.

#### 5.3.1. Seismic facies and stratigraphy

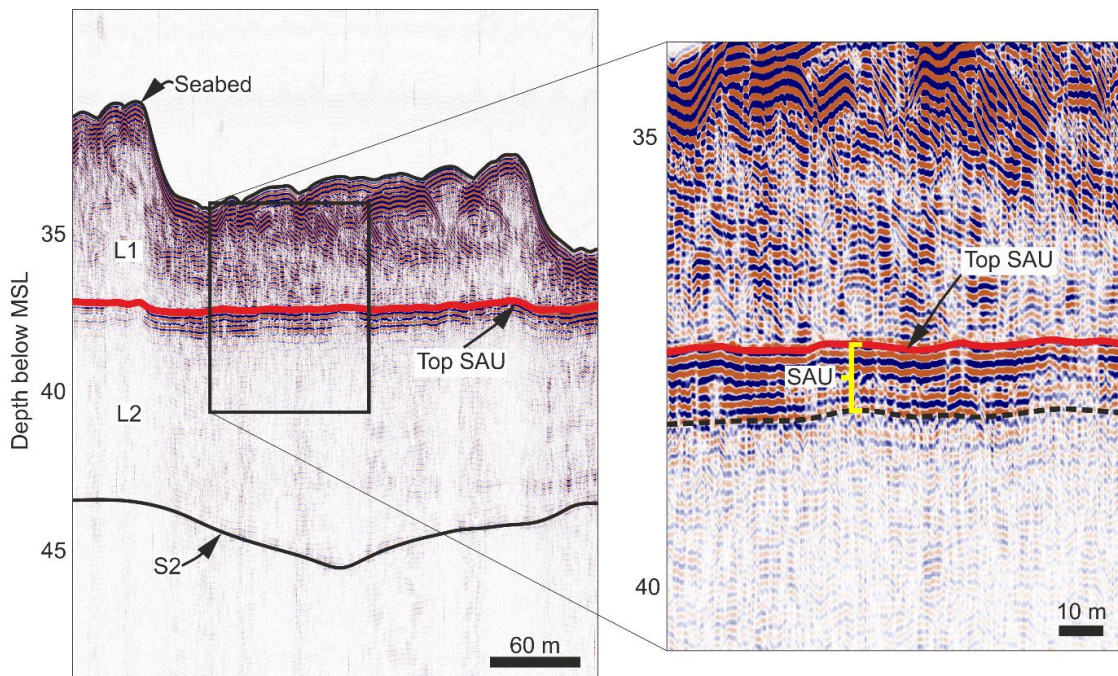
Depth converted seismic reflection data are used to interpret seismic surfaces with the exception of the seabed, which was generated through the depth conversion process utilising the multibeam echosounder data (MBES). Seismic units are packages bound by the seismic surfaces, which together have been used to establish a seismic stratigraphy in the work areas (Figure 5.2).

The interpreted seismic horizons were gridded using a minimum curvature algorithm, which provides geologically realistic surfaces. The basis for the cell size used for the gridding was data resolution (20x20 m) and each cell contains no more than one point.

Four seismic horizons have been identified that are present in both survey areas: an undulating, low gradient erosion surface (S2), the sediment-water interface (Seabed), and an intermediate horizon S1 (Figure 5.2) that define two seismic units, L2 (underlies S1), and L1 (overlies S1). Additionally a seismic anomaly (SAU) is present at S1 level (Figure 5.3). Mitchum et al. (1977) and Mellett et al. (2013), have been used to characterise L1 and SAU (Table 5.1). L2 has previously described in Chapter 3.



**Figure 5.2. A characteristic seismic profile for the NV West (1) and Boreas (2) survey areas displaying the three seismic surfaces (Seabed, S1, S2) and the three seismic units (L1, SAU and L2) with depth in meters below measured sea level (MSL). For location of panels see Figure 5.1.**



**Figure 5.3. A characteristic seismic profile illustrating the seismic character of SAU and the underlying and overlying seismic units (L2 and L1). The zoomed imaged shows the typical character of SAU as a package of high amplitude seismic reflectors. The number of seismic reflectors that characterise SAU varies across the survey areas.**

### 5.3.2. Seismic anomaly SAU

Description: SAU has a patchy distribution and is observed only in NV West and Boreas (Figure 5.4). The seismic facies of SAU are characterised by Sf13; tabular, laterally discontinuous, high amplitude, low frequency seismic reflectors (Table 5.1). The thickness of the SAU varies throughout the survey areas and can be characterised by two-to-eight high amplitude seismic reflectors. Typically, SAU is overlain by L1, but does occasionally subcrop at the seabed, where commonly scour pits are present.

Interpretation: Core observations tied to seismic mapping support that SAU is a peat horizon. Detailed interpretation of SAU based on seismic, cores and CPTs can be found in Chapter 4.

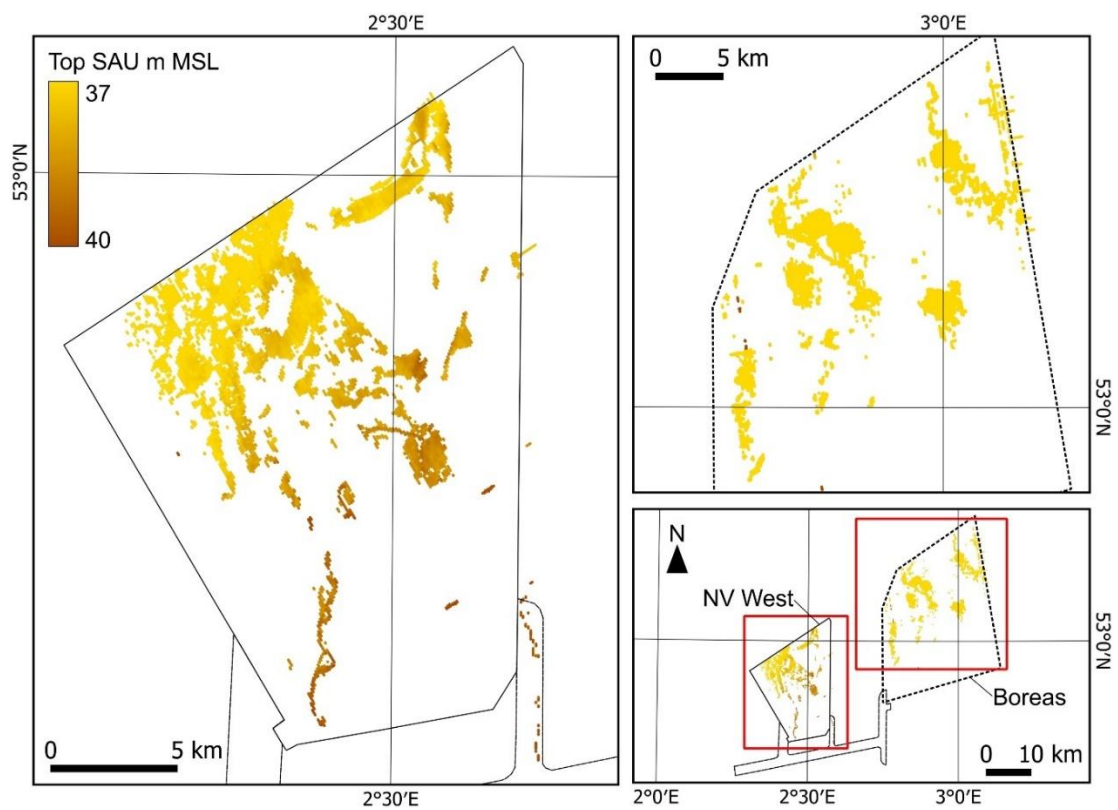
### 5.3.3. Seismic unit L1.

Description: L1 overlies S1, and therefore either L2 and SAU, depending on the spatial distribution of SAU. The thickness of L1 varies over the survey areas, from <1 m to >10 m, with the thickest deposits coinciding with modern shallow marine bedforms. Along the western margin of NV West, the thickness of L1 thins to <1 m. Seismic facies Sf12 characterises L1, which is predominantly seismically dim and structureless. Locally, the



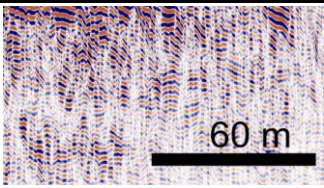
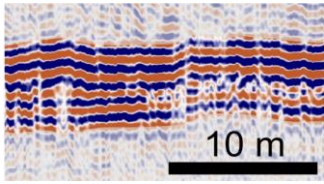
seismic character of L1 differs from Sf1, with dipping and truncated seismic reflectors. L1 overlies mapped channel-form features and incisional features where they are present (Chapter 4).

Interpretation: Truncation of L2 reflectors, channel-forms and incisional features provide evidence of widespread erosional processes associated with the base of L1 (S1). Sf12 is attributed to coarser grained shallow marine deposits, forming large bedforms. The dipping and truncated seismic reflectors are atypical of L1 and are interpreted as foresets associated with shallow marine bedforms (dunes and sediment waves (Chapter 4)).



**Figure 5.4. Gridded depth maps for top SAU in NV West and Boreas.**

**Table 5.1. A summary of the two principal seismic facies attributed to the L1 unit and SAU in NV West and Boreas.**

Seismic facies	Unit	Frequency	Amplitude	Continuity	Termination	Spatial extent	Seismic example
Sf12	L1	Medium to low	Medium to low	Discontinuous	Not applicable	Patchy	
Sf13	SAU	Low	High	Discontinuous	Lateral	Patchy	

#### 5.4. Vibrocore and Cone Penetration Test (CPT) analysis

For information on acquisition of vibrocores and cone penetration tests (CPT) refer to Chapter 2. In this study, 14 vibrocores and CPTs (Table 5.2) have been used to investigate lithology and stratigraphy with the primary focus being SAU, and a secondary focus being L1 and L2 units.

**Table 5.2. List of CPTs and VCs used in this study (locations on figure 5.1) to investigate L1, SAU and L2 with the different data types available for each unit.**

Test/Core ID	Position		Seismic units present			Site
	Latitude	Longitude	CPT	VC	Photo	
CPT/VC016	52.8	2.49	L1/L2	L1/L2		Boreas
CPT/VC028*	53.01	2.78	L1/SAU/L2	L1/SAU/L2		Boreas
CPT/VC032*	53.07	2.92	L1/SAU/L2	L1/SAU/L2		Boreas
CPT/VC039*	53.11	2.91	L1/SAU/L2	L1/SAU/L2		Boreas
CPT/VC047	53.13	3.01	L1/L2	L1/L2		Boreas
CPT/VC074*	52.49	2.27	L1/SAU/L2	L1/SAU/L2		NV West
CPT/VC075*	52.57	2.51	L1/SAU/L2	SAU	L1/SAU/L2	NV West
CPT/VC076*	52.55	2.23	L1/SAU/L2	L1/SAU/L2		NV West
CPT/VC079	52.5	2.3	L1/L2	L1/L2		NV West
CPT/VC080	52.58	2.26	L1/SAU/L2		L1/SAU/L2	NV West
CPT/VC081	52.56	2.26	L1/SAU/L2		L1/SAU/L2	NV West
CPT/VC085*	52.59	2.29	L1/SAU/L2	L1/SAU/L2		NV West
CPT/VC088	53	2.31	L1/SAU/L2		L1/SAU/L2	NV West
CPT/VC089	52.58	2.33	L1/L2	L1/L2		NV West

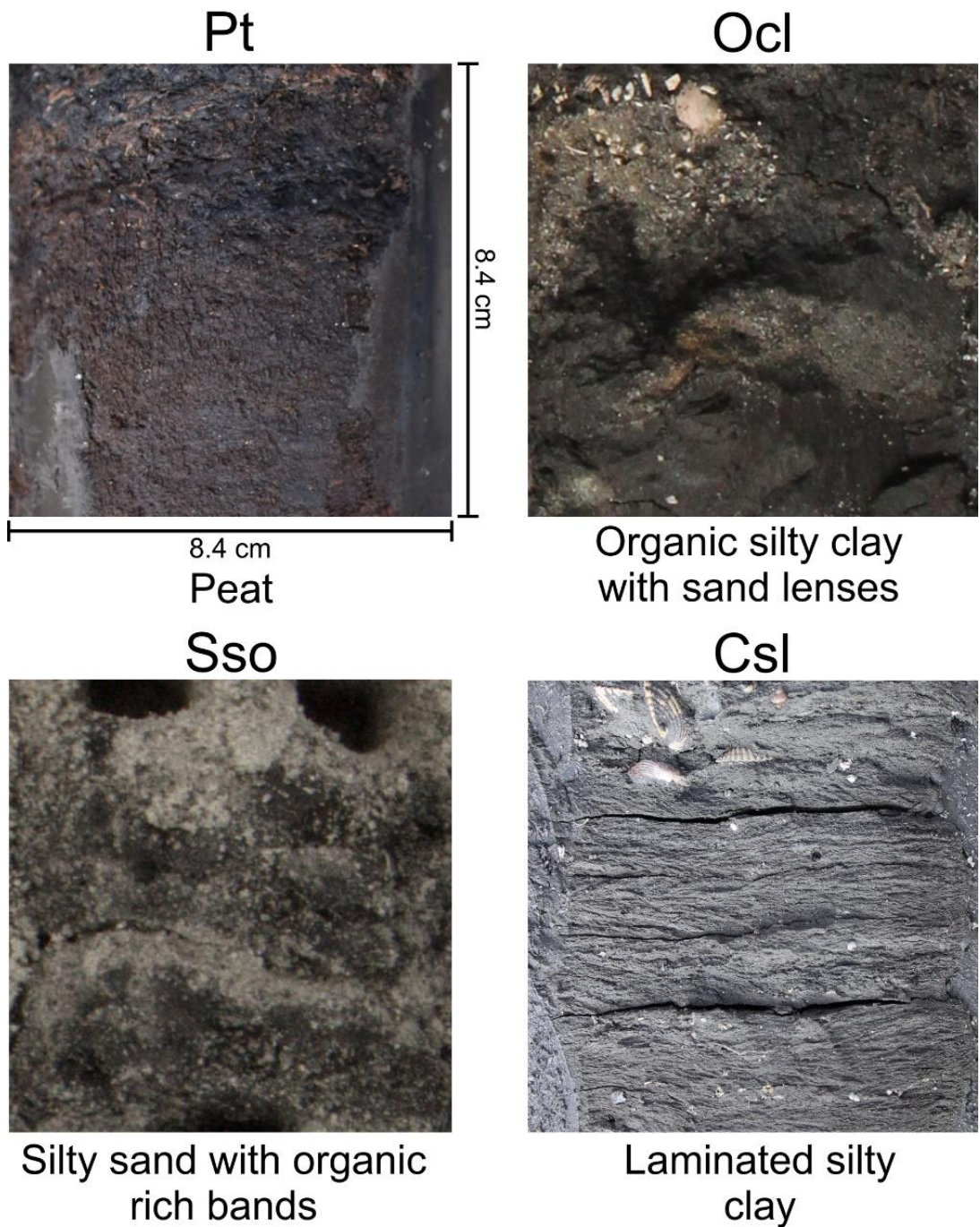
\*used in SAU thickness calculation

#### **5.4.1. Core lithofacies and stratigraphic contacts**

Detailed sedimentary logging was completed on nine available vibrocores (VC) with six lithofacies identified. The stratigraphic focus is seismic anomaly SAU that coincides with S1 (Figure 5.3), and the underlying and overlying seismic units L2 and L1, respectively. High-resolution photographs of a further 67 VCs have been used for additional core logging and comparison with seismic data. Lithofacies associated with the L1, SAU and L2 units are described in Chapter 4, however a description of SAU lithofacies are presented below for the benefit of this study.

#### **Lithofacies Pt, Ocl, Sso and Csl - SAU**

Lithofacies Pt, Ocl, Csl and Sso (Figure 5.5) all calibrate to SAU, and their presence and thickness is variable between cores. Seven of the logged cores contain lithofacies Pt, which is primarily organic-rich, brown, humified and amorphous, contains negligible quantities of sand, silt and clay, and is of varying thickness. Plant remains are rarely identifiable, but fragments of wood are identified in cores VC028 and 85 (Figure 5.6 and 7). In all logged cores, with the exception of VC039 and VC075 (Figure 5.6 and 5.7), lithofacies Pt is overlain by Ocl, which is a dark brown, organic-rich clay with silt and sand. The sand, silt and clay are dispersed throughout the matrix or concentrated in lenses that contain bivalve shell fragments. Lithofacies Sso is predominantly silty sand with organic-rich bands and is only identified in cores VC074 and 76. In core VC074, Sso separates two intervals of Pt, whereas in VC076 Sso overlies seismic unit L2 (Slc) and underlies the Pt interval. In core VC032, lithofacies Csl overlies Pt. Csl is clay-dominated with silt and rare sandy laminae with clay content increasing upwards. The Csl lithofacies contains sedimentary structures (cross-ripple lamination) and *Hydrobia* shells.



**Figure 5.5. Photographs of the 4 lithofacies observed in cores that are associated with SAU. Descriptions of lithofacies can be found in text.**

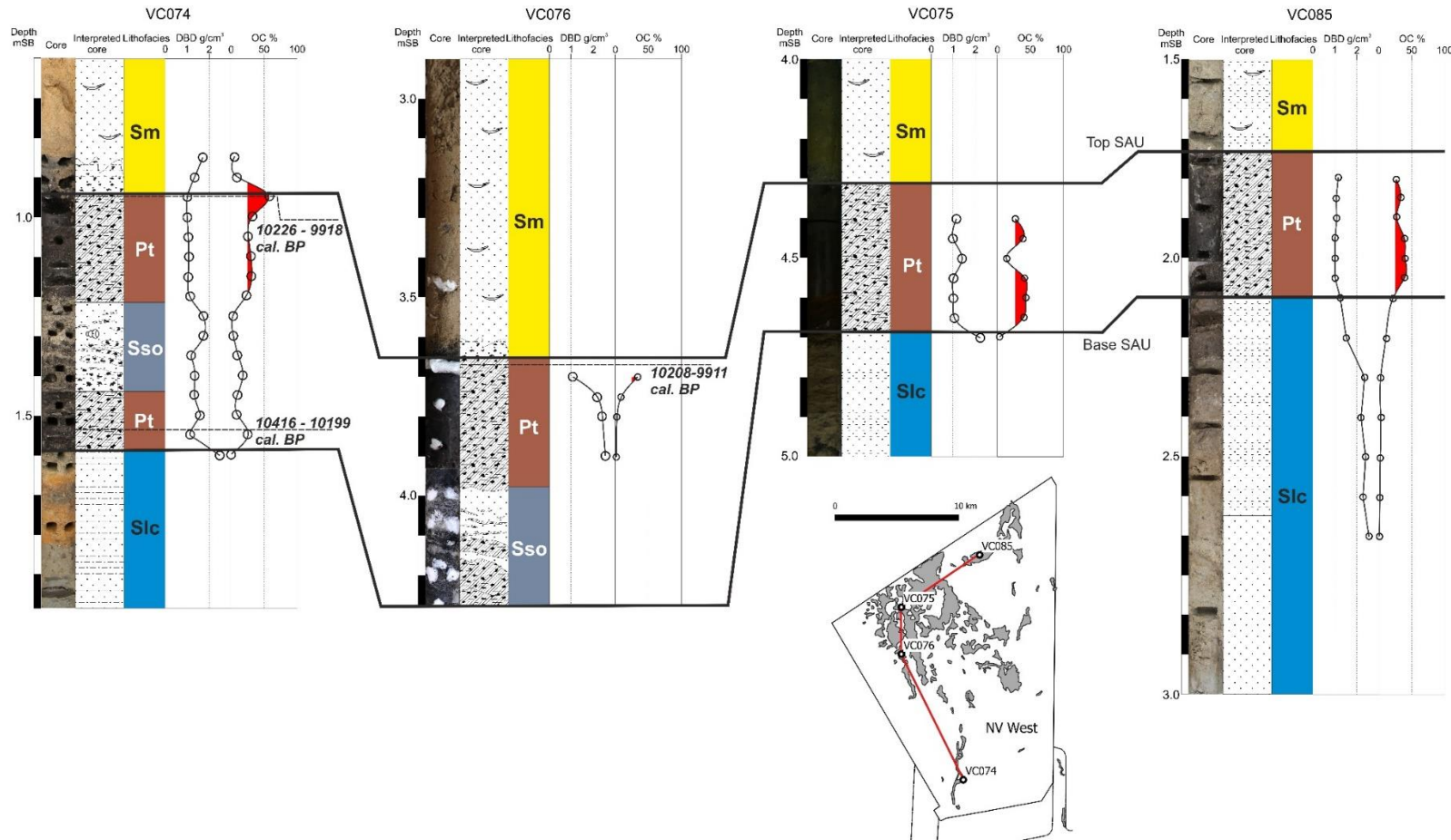


Figure 5.6. Core panels from NV West showing SAU and the underlying (L2) and overlying (L1) sediments. Also shown are sampling points with values for Dry bulk density and % organic carbon. Descriptions of lithofacies can be found in text and photographs in Figure 5.5. The red filled section represents all organic carbon values >25% (M-OC). The radiocarbon dates shown were obtained by Wessex Archaeology, 2018 (Chapter 4). Inset map shows location of panel.

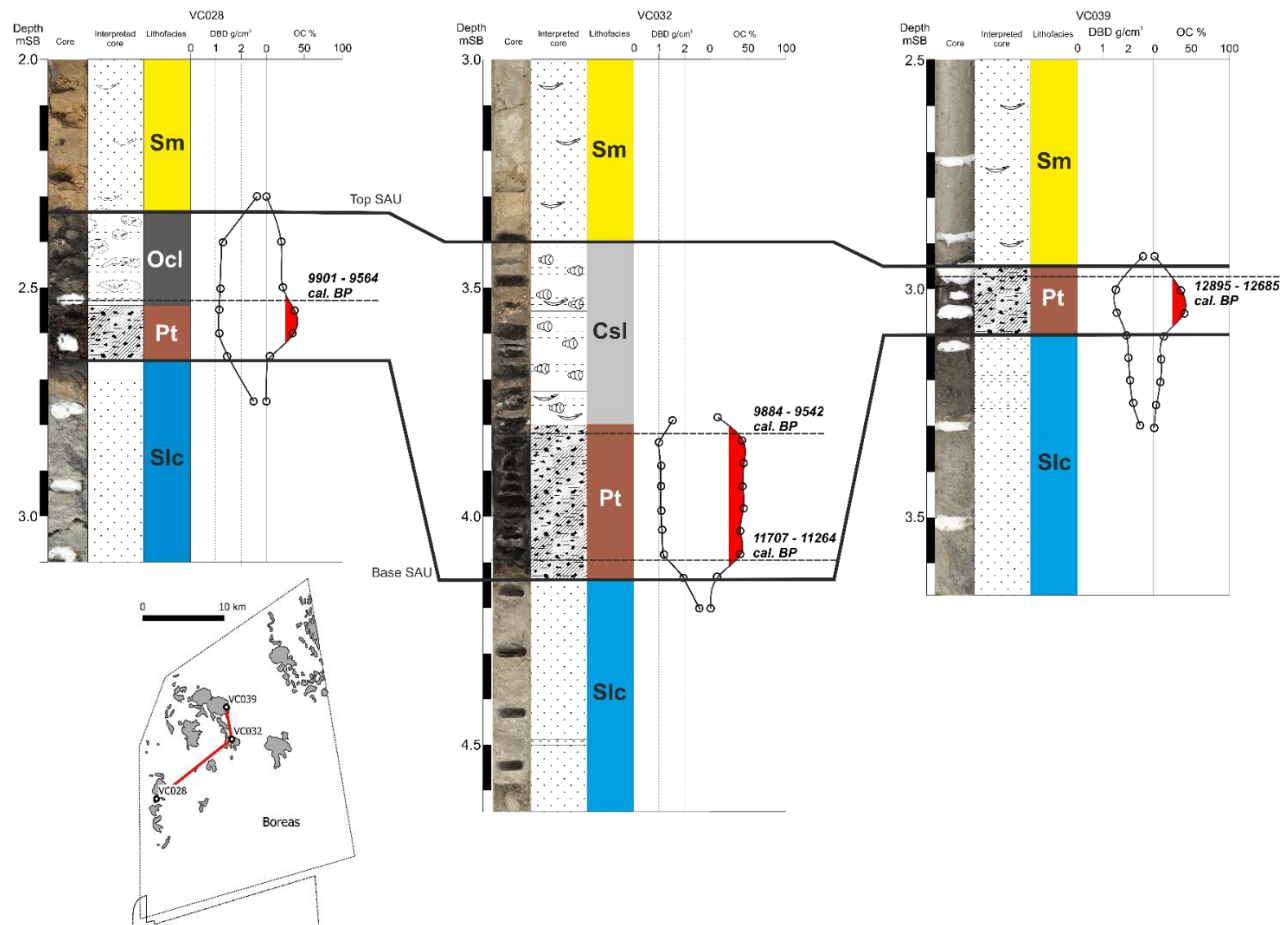
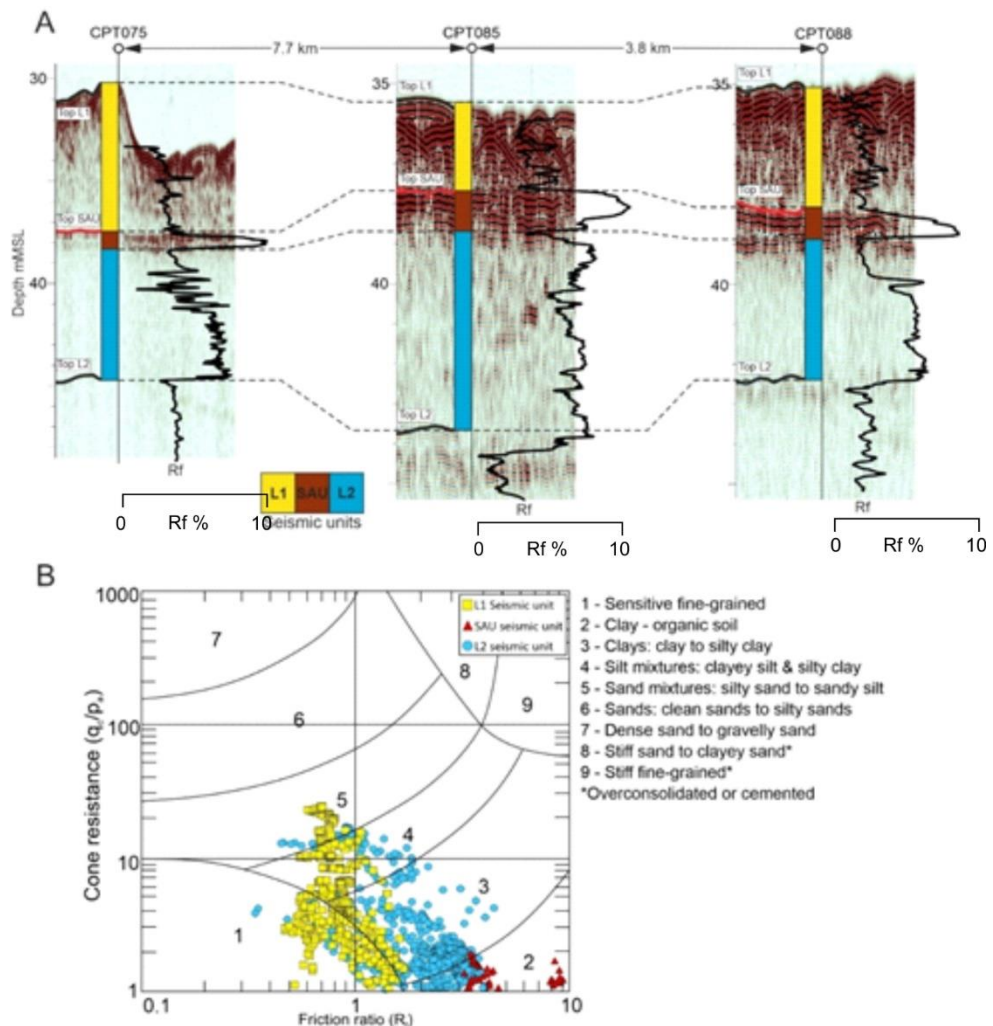


Figure 5.7. Core panels from Boreas showing the SAU unit and underlying and overlying sediments of L2 and L1, respectively. Also shown are sampling points with values for DBD and %OC. Descriptions of lithofacies can be found in text (4.1.1). The red filled section represents all organic carbon values >25% (M-OC). The radiocarbon dates shown were obtained by Wessex Archaeology, 2018 (Chapter 4). Inset map shows location of panel.

## CPT stratigraphy

CPT data are used (Friction ratio,  $R_f$ , and cone resistance,  $Q_c$ ) to investigate the differences in mechanical properties of sediment/soil across the seismic units. Seismic surfaces S1 and S2 have been calibrated to deflections in the CPT parameter  $R_f$ . SAU clearly correlates to a change in the geomechanical properties as evidence in the SBT plot (Figure 5.8 B) and corresponds to organic rich soils. This deflection in CPT parameters at the SAU level is readily correlated (Figure 5.8 A) and used to define top and base of SAU on seismic data in conjunction with seismic amplitude.



**Figure 5.8. Calibration of Cone Penetration Test (CPT) Friction ratio ( $R_f$ ) parameter against seismic and Soil Behaviour type (SBT) plot. A. Correlation panel of three CPTs calibrated to seismic data. Interpreted seismic units are overlain and clearly correspond to deflections in CPT  $R_f$  parameter. B. A SBT plot showing CPT parameters (Cone resistance and  $R_f$ ) for three CPTs shown in A. The CPT parameters calibrated to SAU fall within region 2, typical of organic-rich soils/sediments. For location of CPTs see Figure 5.1.**

## **5.5. Palaeoenvironmental interpretation**

The palaeoenvironments assigned to seismic units L2, SAU and L1 is documented in Chapter 4, which documents stratigraphic and geomorphological features calibrated to radiocarbon dates and palaeoenvironmental analysis that support interpretation.

## **5.6. Core analysis**

A methodology for core sampling and analysis are described in the following chapters but for a more comprehensive overview of methods see Chapter 2.

### **5.6.1. Bulk density and carbon analysis**

Samples were taken from the 9 logged cores at 5 cm intervals through the SAU peat unit, and one sample from above SAU in the L1 unit (lithofacies Sm, Chapter 3) and one below the base of SAU in L2 (lithofacies Slc, Chapter 3). At each depth, two 2 cm<sup>3</sup> volumetric samples were taken for bulk density analysis and 1 bulk sample (1 cm slice) for carbon analysis. Bulk density was determined using a standard gravimetric method. Samples were weighed to determine the wet bulk density (WBD), and then dried for 48 hrs at 105 °C, until a constant weight was achieved, and from this the dry bulk density (DBD) was calculated (Dadey et al., 1992).

The dried sample was milled to a fine powder. An aliquot of 4 ±0.2 mg was placed in a silver capsule, measured on University of Leeds School of Geography Elementar Vario Micro analyser (EA), and calibrated with sulfanilic acid to determine total carbon (TC). Standard reference materials B2150X and B2152X (High Organic content standard from Elemental Microanalysis, UK) were used to estimate the precision of the analysis. The process was then repeated to quantify organic carbon (OC) with the addition of hydrochloric acid (HCl) to remove the inorganic carbon (IC). Following acidification, the silver capsules were then freeze-dried to remove all HCl. The inorganic carbon (IC) was calculated from the difference between the TC and the OC measurements. To calculate TC and OC, I followed the approach Smeaton et al. (2016) who calculated TC and OC in a fjord setting.

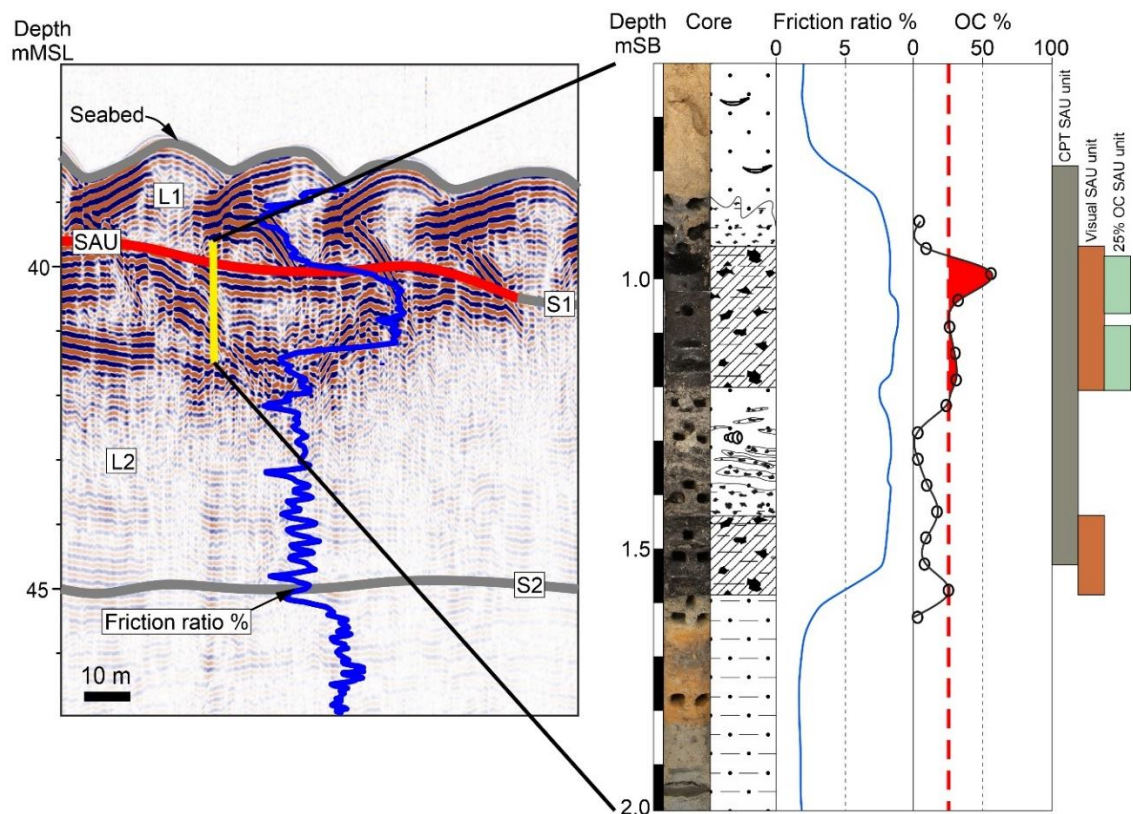
### **5.6.2. Peat classification and quantification methods.**

#### **Peat classification methods**

In this study, three data types have been used to identify and define SAU thickness: from cores, CPT data and percentage organic carbon (%OC) measured in a laboratory.



Calibration between CPT and seismic reflection data with visual inspection of the core, the SAU unit is interpreted as a peat deposit, albeit with spatially variable characteristics. Identifying peat in sediment cores is via visual logging of the cores (M-V method), whereby changes in soil/sediment over either a sharp or transitional boundary are used to define tops and bases of the peat (Figure 5.9). CPT data show changes in mechanical properties using the Rf parameter, whereby the peat represents a low-density interval contrasting with the relatively higher density sediments bounding it (Figure 5.8 – SBT plot and Figure 5.9). These deflections in the Rf value can be used to mark the top and base boundaries of the peat (Figure 5.9). Using %OC values (M-OC method) requires assigning a threshold value, whereby only soils/sediments above a certain %OC are considered peats.



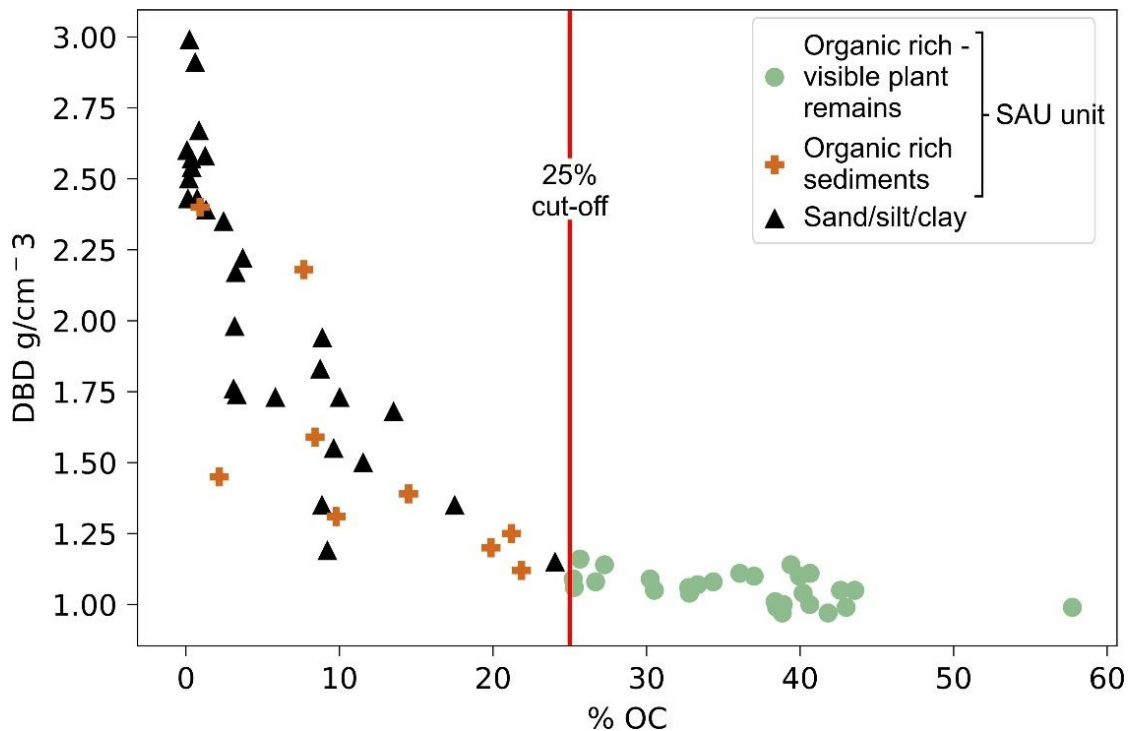
**Figure 5.9. Data types used to classify peat and calculate peat thickness. SBP seismic is used to map the spatial distribution of the peat, which correspond to SAU. Sediment cores are logged with top and base peat identified based on visual inspection. The sediment/soil mechanical property friction ratio (Rf), as gained from the CPT, is a property used for identifying peat in the subsurface, with the top and base of peat units clearly marked by Rf deflections. OC analysis of samples across the peat interval, including above and below the visual defined contacts, enable classification of peat based on % OC. Each method results in different thickness ranges for the peat interval.**

## **M-V method**

Using each data type (core, CPT and %OC) independently results in different thickness range estimates for SAU (Figure 5.8). The M-V methodology allows boundaries to be assigned to the unit in the vibrocores where clear changes in lithofacies occur. The defined SAU in core is underlain and overlain by coarser grained lithofacies (Slc and Sm respectively, Chapter 3) that contrast in texture and colour. Where the boundary between SAU and the underlying L2 and overlying L1 are transitional (VC028, 32, 85 – Figure 5.6 and 5.7) and clear changes in organic content based on colour and plant remains are seen (VC074 and 76 – Figure 5.6), defining a boundary using colour alone is possible. However, this is more challenging when the top and/or base of SAU have spatial variations of sediment/soil (undulating contact, lenses, mixing of sediment/soil types) due to the inclusion of minerogenic components with organics. This uncertainty can lead to overestimation, if SAU is considered to represent a peat, as intervals deposited under sedimentary processes might be included as opposed to those intervals formed through peat accumulation alone.

## **M-OC method**

The M-OC method uses the same peat classification as used by Natural England, with 'true' peat defined as having >25% OC. Figure 5.10 shows all sample points from the 9 vibrocores, and their respective DBD and OC values against the 25% threshold. The brown crosses and green circles fall within the SAU unit as defined by the M-V method. The brown crosses represent those intervals that have higher quantities of minerogenic components (lithofacies Ocl, Sso and Csl) but also contain visible organic matter. Those intervals that contain minor minerogenic components and clearly identified as lithofacies Pt are represented by the green circles. Those intervals outside of the M-V defined SAU unit and composed of lithofacies Sm and Slc are represented by the black triangles. The intervals composed of lithofacies Pt correspond to lower %OC threshold of 25% and those with higher quantities of minerogenic components fall below this threshold.



**Figure 5.10. Scatter plot of all DBD and OC analysis for 9-sampled cores. Those sample points visually identified as organic-rich are marked with green circles and brown crosses, and form the SAU. The black markers are those samples that are above (L1) or below (L2) SAU and are visually identified as non-organic and primarily composed of sands, silts and clays. The green markers represent those samples that are identified as organic-rich but contain visible plant remains (fragments of wood) and are more classically described as peats. The 25% OC line is displayed, and this coincides with the boundary between organic rich and organic rich with plant remains visible.**

### CPT method

The CPT provides a useful understanding of the geotechnical properties of sediments/soils in the shallow subsurface and predictions of the sediment/soil type. Calibrated to seismic, the CPT has confirmed that SAU conforms to a sharp change in geotechnical properties seen in L2 and L1. Rf values are lower in L2 and L1 compared with SAU, corresponding to a more clay-/organic-rich unit (Figure 5.8 B) and sandier L2 and L1 units. However, the CPT character throughout the SAU does not always reflect changes in lithofacies seen in core (Appendix 4) (Lunne et al., 2002; Lengkeek et al., 2018; Bruno et al., 2019). This is demonstrated in Figure 5.9, where the friction ratio shows little variation with depth throughout SAU, leading to marked discrepancies in thickness ranges compared with those defined using M-V and M-OC methodologies. For this reason, the CPT is considered a crude assessment of SAU thickness, but useful for extracting maximum thickness ranges for SAU in the absence of core data.

## Thickness and volume calculation methods

The volume of the SAU within each study area is calculated based upon the surface area of SAU, defined using the aerial extent of SAU (Figure 5.4) and thickness ranges from core according to the M-V and M-OC methods. Using the M-V and M-OC methods, two SAU thickness values have been generated at each vibrocore location (Table 5.2). The SAU thickness values are interpolated to the locations defined by SAU seismic anomaly mapping. The interpolation is done using a nearest neighbour algorithm in QGIS 3.2 (QGIS Development Team, 2020). The volume of SAU in each of the survey areas is calculated by multiplying the thickness value within each contour interval by the associated surface area.

## Dry bulk density and organic carbon interpolation methods

DBD and OC is calculated at 5 cm intervals across the SAU (as defined in core at the top and base by contacts with the L3 and L1 units). Using the range of DBD and OC values the mean DBD and OC has been calculated for SAU intervals classified according to M-V and M-OC in each core. From M-V and M-OC defined mean DBD and OC values are assigned to each survey area.

## Sediment/soil mass and Carbon stock quantification methods

The mass of soil/sediment within SAU is calculated using the SAU volume for each survey area and the mean DBD values assigned to each survey area according to the M-V and M-OC methods. The sediment/soil mass is calculated according to Equation 5.1.

Equation 5.1. Sediment mass (SM).

$$\text{M-V method:} \quad \text{SM}^{\text{M-V}} = V^{\text{M-V}} * \text{meanDBD}^{\text{M-V}}$$

$$\text{M-OC method:} \quad \text{SM}^{\text{M-OC}} = V^{\text{M-OC}} * \text{meanDBD}^{\text{M-OC}}$$

Where, V is SAU volume and meanDBD is mean dry bulk density for survey area.

The carbon stock (C) is calculated for each survey area according to the M-V and M-OC classification of SAU. To derive C, the volume of SAU, mean DBD and mean OC are required and is calculated according to equation 5.2.

Equation 5.2. Carbon stock (C)

$$\text{M-V method:} \quad C^{\text{M-V}} = \text{Volume}^{\text{M-V}} * CD^{\text{M-V}}$$

$$\text{M-OC method:} \quad C^{\text{M-OC}} = \text{Volume}^{\text{M-OC}} * CD^{\text{M-OC}}$$

Where, Volume is SAU volume and CD is carbon density (mean DBD x OC fraction) (Smeaton et al., 2016).

## 5.7. Results

### 5.7.1. SAU thickness

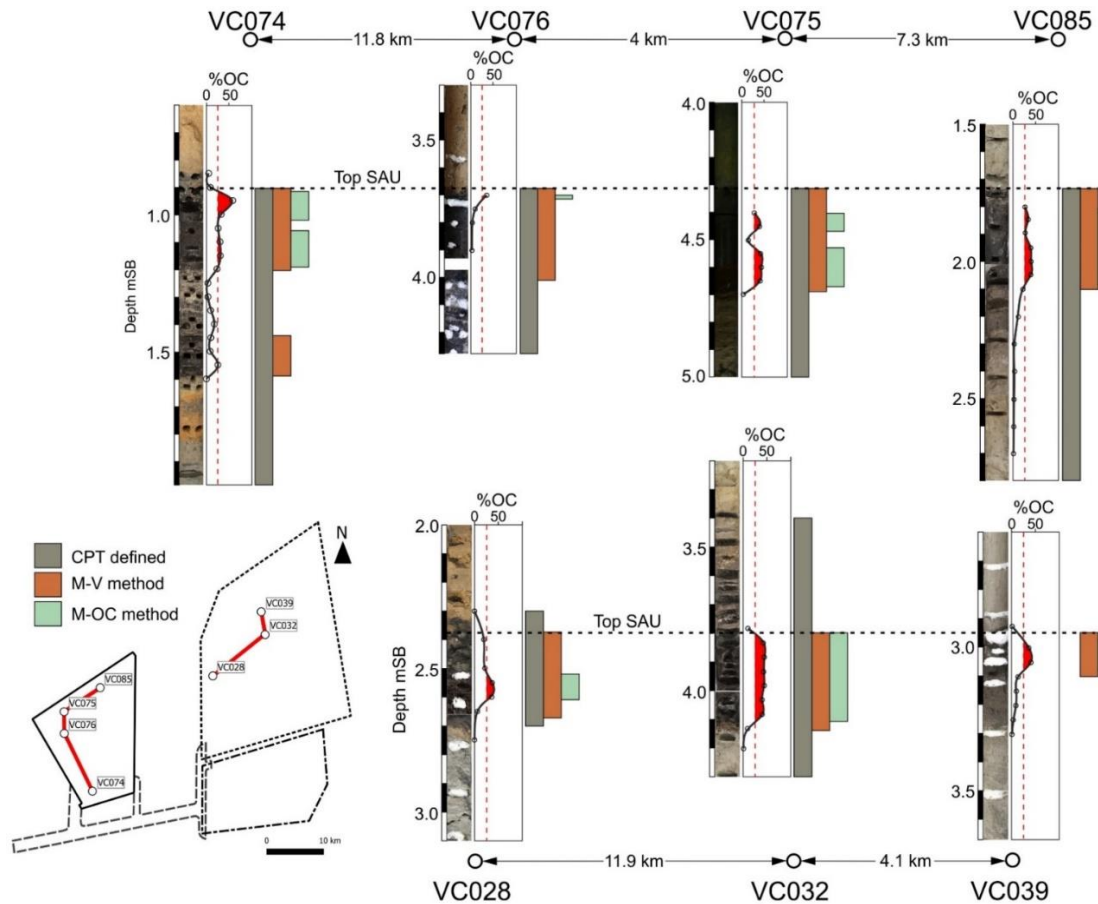
The thickness of SAU according to M-V and M-OC methods have been defined at each core location (Figure 5.11) and are documented in Tables 5.4 and 5.5. SAU thickness maps (Figure 5.12 and 5.13) have then been gridded in QGIS 3.2 using a nearest neighbour algorithm for each survey area according to M-V and M-OC methods. Three additional vibrocores have been used to define thickness ranges for the M-V method (Table 5.5 \*) using only high-resolution core photographs but could not be used as input using the M-OC method due to destructive geotechnical sampling.

**Table 5.3. A summary of the SAU unit thickness at each vibrocore location defined using the M-V method. Where brackets have been used indicates that there are multiple SAU unit intervals within the vibrocore. \* indicates where core photos have been used to define thickness. Depths relative to seabed.**

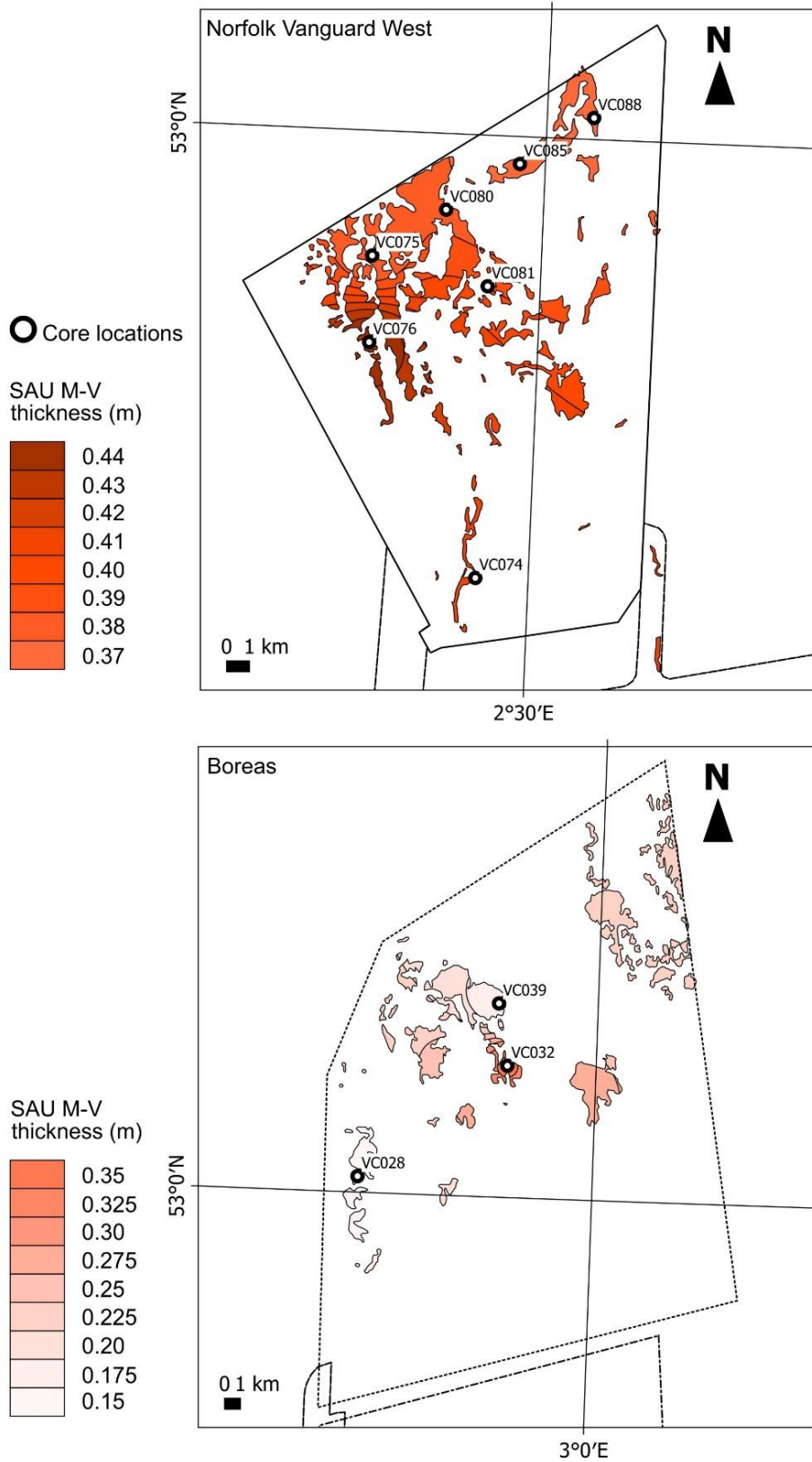
Core ID	Position		Depth (second layer)				Thickness (m)
	Lat	Long	Top (m)		Base (m)		
VC074	52.83	2.47	0.92	(1.43)	1.20	(1.57)	0.28 (0.05)
VC075	52.95	2.39	4.31		4.68		0.37
VC076	52.92	2.39	3.65		4.10		0.45
VC085	52.99	2.48	1.73		2.10		0.37
VC028	53.01	2.78	2.53		2.66		0.13
VC032	53.07	2.92	3.80		4.13		0.33
VC039	53.11	2.91	2.95		3.10		0.15
VC080*	52.97	2.44	2.00		2.10		0.10
VC081*	52.94	2.47	1.40		1.43		0.03
VC088*	53.01	2.53	3.65		3.90		0.25

**Table 5.4. A summary of the SAU unit thickness at each vibrocore location defined using the M-OC method. Depths relative to seabed.**

Core ID	Position		Depth (second layer)		Thickness (m)
	Lat	Long	Top (m)	Base (m)	
VC074	52.83	2.47	0.92	1.20	0.28
VC075	52.95	2.39	4.40	4.68	0.28
VC076	52.92	2.39	3.70	3.73	0.03
VC085	52.99	2.48	1.80	2.10	0.30
VC028	53.01	2.78	2.49	2.63	0.14
VC032	53.07	2.92	3.80	4.12	0.33
VC039	53.11	2.91	2.97	3.09	0.13

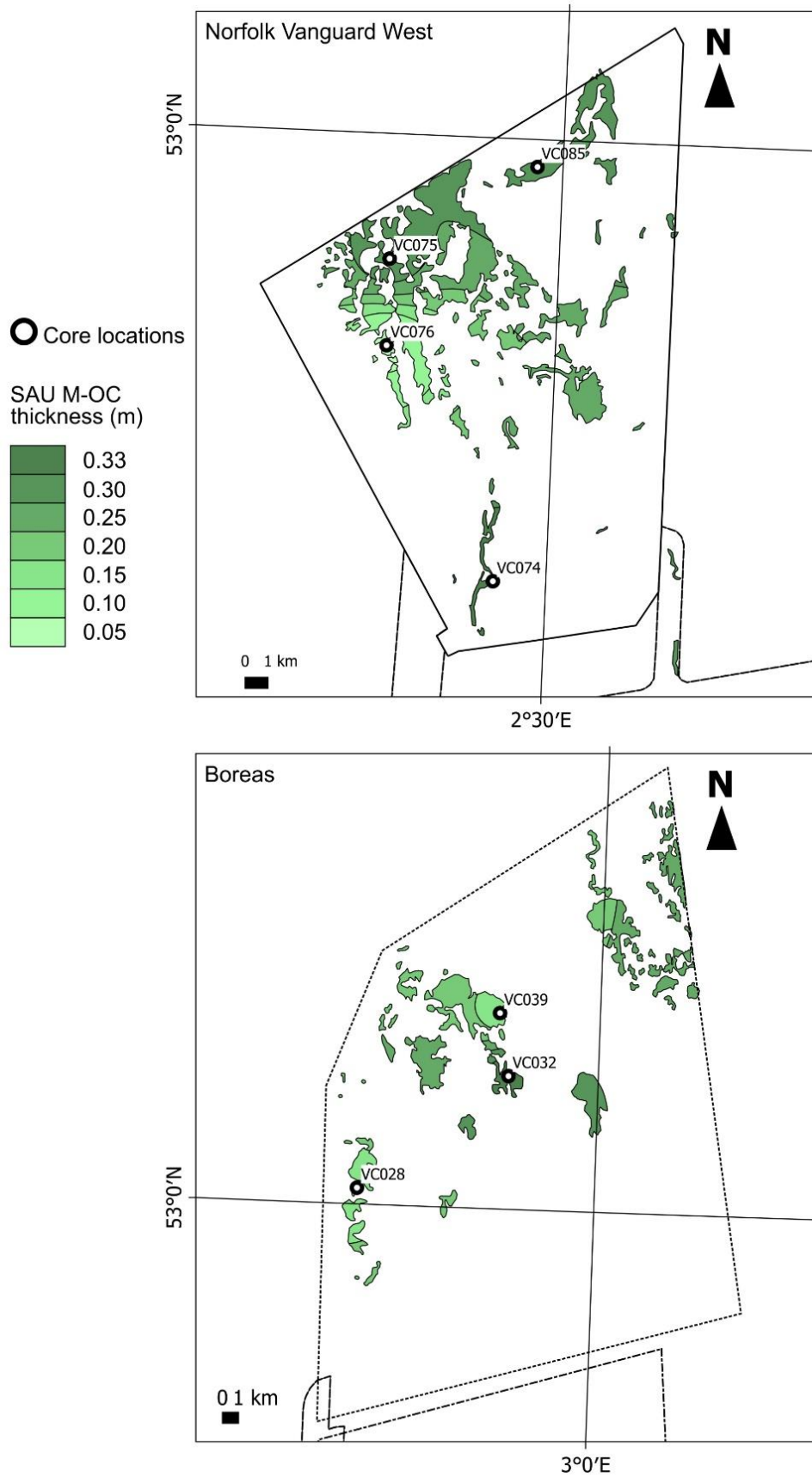


**Figure 5.11. Vibrocore panel showing the different thickness ranges generated using the M-V, M-OC and CPT data. The core used as the input to M-V with the interval defined shown as an orange bar. OC analysis point are shown with a red fill indicating those analysis point that have >25% OC and with the defined SAU according to M-OC shown as a green bar. The CPT data has not been used as input to SAU thickness but has been shown here to contrast the ranges generated for SAU thicknesses using different classification methods. No CPT data is available over SAU for CPT039. Inset map shows the location of the panels**



**Figure 5.12. Interpolated grids showing SAU thickness across both survey areas using M-V methods, with vibrocores used to define thickness shown. Note different scales used for the two areas to highlight variations.**





**Figure 5.13. Interpolated grids showing SAU thickness across both survey areas using M-OC methods, with vibrocores used to define thickness shown.**

### 5.7.2. Dry bulk density and organic carbon

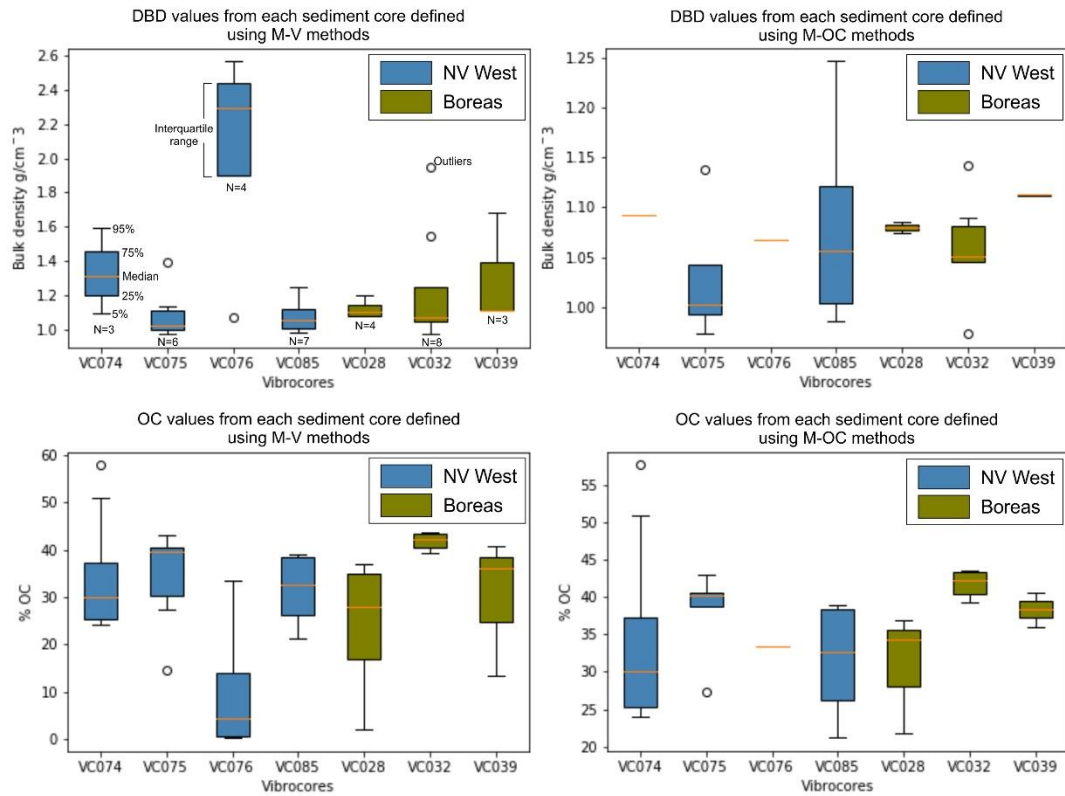
The calculated mean DBD and OC for SAU in each vibrocore and for the survey areas are shown in Table 5.6. Raw data for DBD, TC and OC can be found in Appendix 1, 2 and 3. The mean DBD across both survey areas using M-OC is  $1.07 \text{ g/cm}^3 \pm 0.03$ , and  $1.08 \text{ g/cm}^3 \pm 0.03$  when using M-V. The mean OC across both survey areas using M-OC is  $36.3\% \pm 2.40$ , and  $32.49\% \pm 7.80$  when using M-V.

**Table 5.5. Mean DBD and OC values for both the SAU corresponding to methods M-V and M-OC. The mean DBD and OC for each vibrocore and the mean for each survey area and combined are shown with standard deviation.**

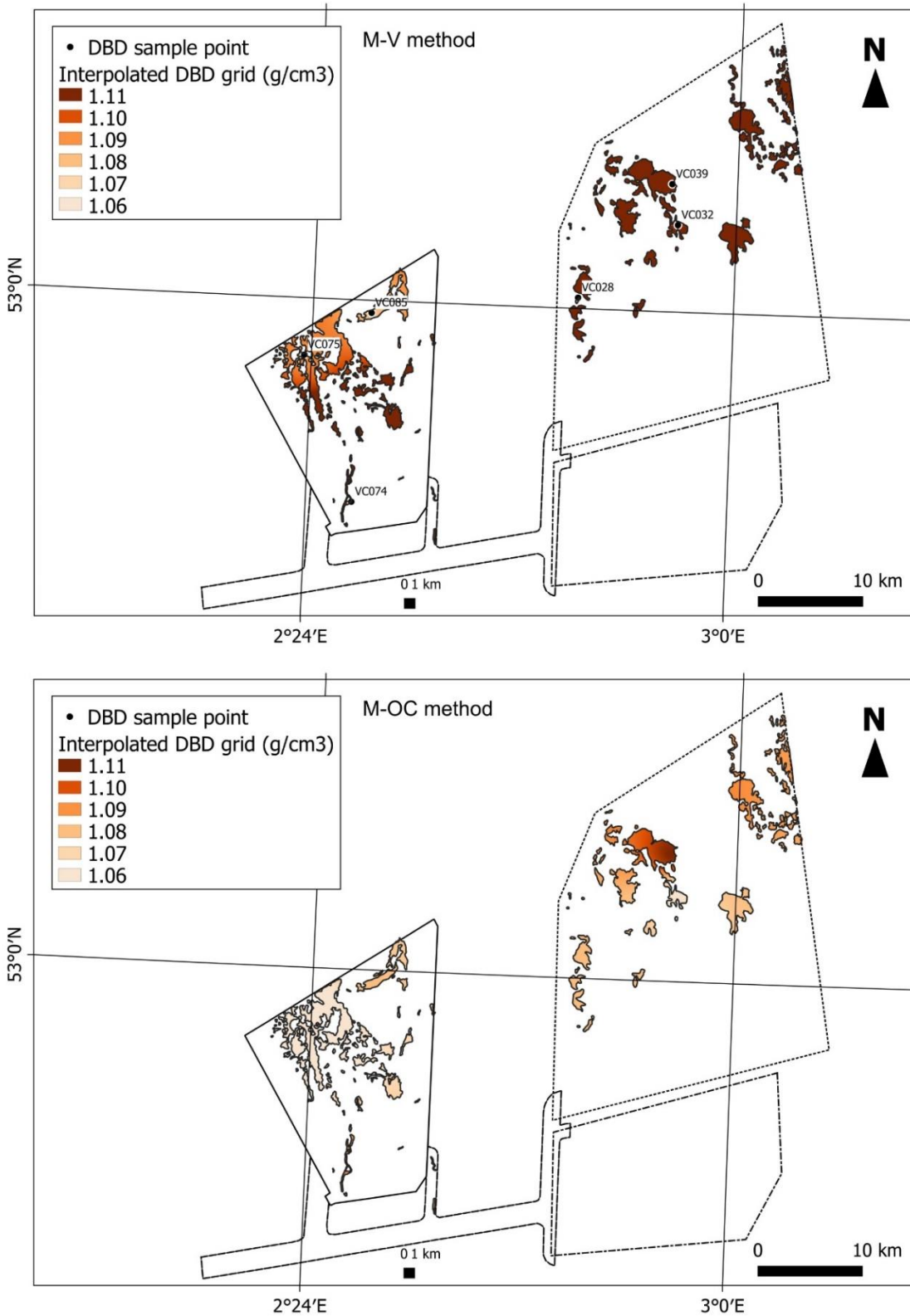
Peat ID method	Vibrocore Mean DBD $\text{g/cm}^3$						Survey area Mean DBD $\text{g/cm}^3$ [SD]		
	VC074	VC075	VC085	VC028	VC032	VC039	NV West	Boreas	Combined
M-V	1.33	1.09	1.08	1.12	1.23	1.3	$1.19 \pm 0.11$	$1.17 [\pm 0.18]$	$1.22 [\pm 0.10]$
M-OC	1.09	1.03	1.08	1.08	1.06	1.11	$1.07 \pm 0.03$	$1.08 [\pm 0.03]$	$1.07 [\pm 0.03]$
	Vibrocore Mean OC%						Survey area Mean OC% [SD]		
M-V	33.4	34.1	31.7	23.8	41.8	30.1	$33.1 [\pm 1.2]$	$31.9 [\pm 12.3]$	$32.5 [\pm 7.8]$
M-OC	33.4	37.9	33.5	35.7	41.8	38.4	$34.6 [\pm 2.3]$	$38.6 [\pm 3.1]$	$36.3 [\pm 2.4]$

There is a larger range and higher mean DBD when SAU thickness is classified using the M-V method (Figure 5.14). Overall, the DBD values are higher than typical soils described as peat with mid latitude peats often having DBD values ranging from  $0.1$  to  $0.4 \text{ g/cm}^3$  (Chambers et al., 2011) compared with  $1.06$  to  $1.11 \text{ g/cm}^3$  seen here. This relatively large difference in DBD may be a result of a peat deposit with higher than typical amount of minoregenic seiments. The mean DBD for SAU is generally higher in Boreas than in NV West, with the spatial trend being more apparent when SAU is defined using M-OC (Figure 5.15). The points sampling L2 and L1 record higher DBD values than those seen in SAU coinciding with a marked change in lithofacies.

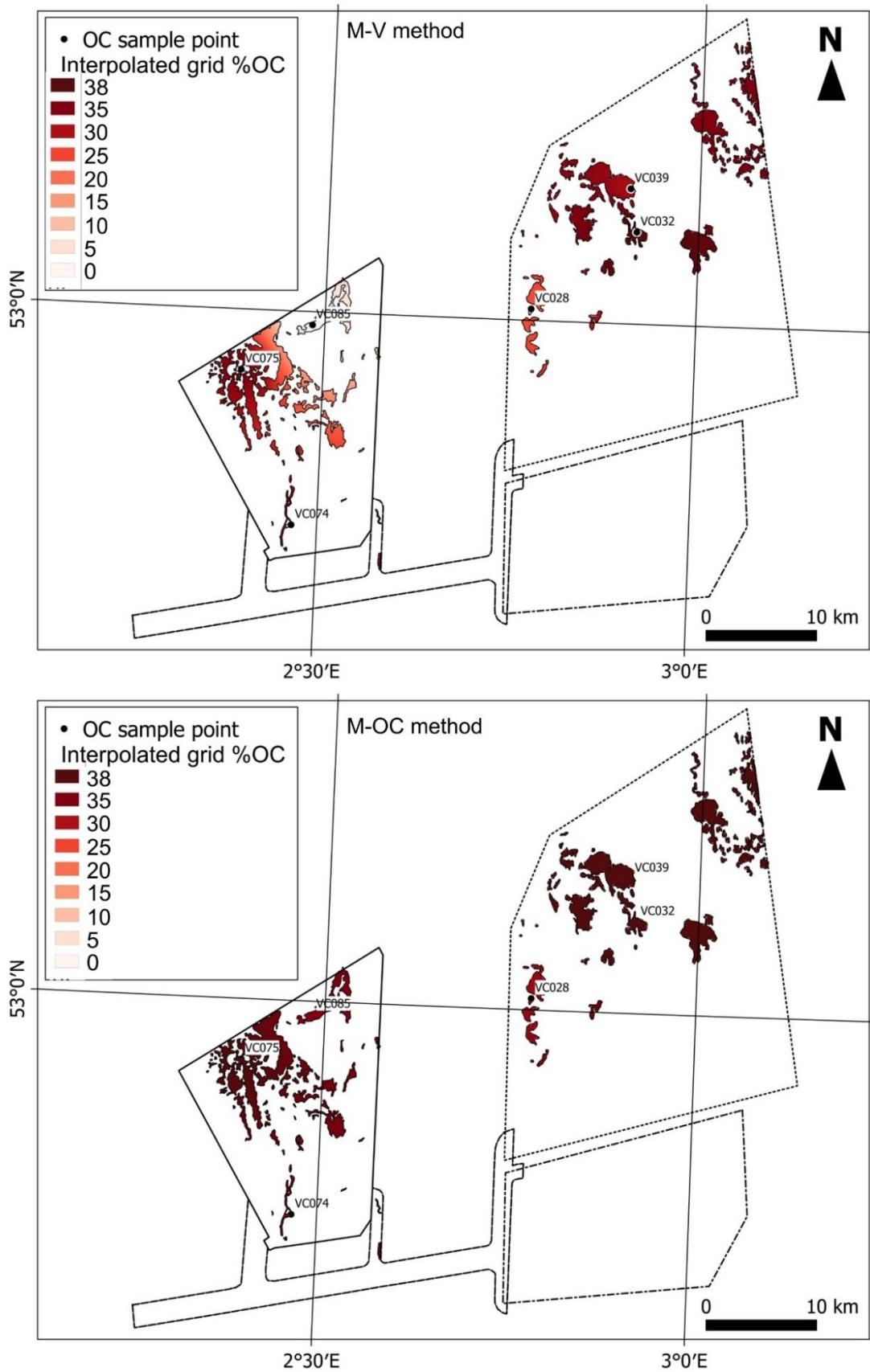
A much broader range of OC is recorded for SAU classified using M-V methods compared with M-OC (Figure 5.14). However, the mean OC is greater when SAU is classified using the M-OC method. There is no clear spatial trend in OC when SAU is defined using M-OC, with OC values between 33 and 42%. A clear spatial trend is seen in OC values over NV West when SAU is defined using M-V, with OC increasing from East to West (Figure 5.16). OC values recorded in L2 and L1 are  $<5\%$  coinciding with a marked change in lithofacies.



**Figure 5.14. DBD and OC values for each core corresponding to the SAU defined using both M-V and M-OC methods. Mean OC for each vibrocore is indicated by the orange line.**



**Figure 5.15. Interpolated grid using mean DBD measurements peat from 6 vibrocores. A. Mean DBD values calculated over SAU according to M-V methodology. B. Mean DBD values calculated over SAU according to M-OC methodology.**



**Figure 5.16. Interpolated grid using mean %OC measurements from sediment core peat intervals. A. M-V methodology applied. B. M-OC methodology applied.**

### 5.7.3. Volumetrics

The interpolation of peat thickness from sediment core data (Table 5.4 and 5.5) using M-V and M-OC methodologies provided input for volume calculation of the SAU. The surface area of peat was defined by the extent of the SAU anomaly (Figure 5.4). When comparing peat volumes across both survey areas (NV West and Boreas), we estimate 0.029 km<sup>3</sup> of peat using the M-V approach, and 0.023 km<sup>3</sup> when using M-OC (Table 5.7).

**Table 5.6. SAU anomaly surface area and volume estimates for NV West, Boreas, and combined sites. Peat volume estimates have been calculated according to M-V and M-OC methodologies.**

Survey area	Area (km <sup>2</sup> )	Volume (km <sup>3</sup> )	
		M-V	M-OC
NV West	45.37	0.018	0.011
Boreas	52.12	0.012	0.012
NV West + Boreas	97.50	0.029	0.023

### 5.7.4. Sediment mass and carbon stock quantification

The mean DBD for both M-V and M-OC was multiplied with the estimated peat volumes across NV West and Boreas survey areas in order to calculate a mass of SAU (Table 5.8); the calculated SAU mass equates to 24.61 Mt for M-OC, and 36.07 Mt for M-V.

The mean %OC values for each survey area, using both M-V and M-OC identification methods, were multiplied by the sediment mass in order to quantify the carbon stocks held with SAU. When SAU is defined using M-V contains 11.72 Mt of OC across both survey areas compared with 8.93 Mt of OC when M-OC is applied (Table 5.8).

**Table 5.7. Calculated peat mass following M-V and M-OC methodologies for NV West, Boreas and combined. Mean %OC for survey areas with M-V and M-OC methods applied. Calculated carbon stock for all survey areas with M-V and M-OC methods applied.**

Site	Mass (mean)		OC (mean)		Carbon stock	
	M-V	M-OC	M-V	M-OC	M-V	M-OC
	Mt	Mt	%	%	Mt	Mt
NV West	20.86	11.88	33.07	34.56	6.90	4.11
Boreas	14.08	12.85	31.91	38.62	4.49	4.96
NV West + Boreas	36.07	24.61	32.49	36.30	11.72	8.93

## **5.8. Discussion**

The acquisition and availability of high-resolution data over a relatively large area in the southern North Sea has enabled calculation of carbon stocks for postglacial/early Holocene peat deposits. In addition, the mapping and coring of previously unknown peats provides valuable information for the spatial distribution, thickness, and properties (texture, dry bulk density and organic carbon content), and insights into the scale of buried carbon in the offshore environment.

### **5.8.1. Carbon stock estimates and methods**

An estimated 11.72 Mt of OC has been accounted for under the M-V methods compared with 8.93 Mt under the M-OC methods. The different methods highlights the importance of understanding limitations in different data types (seismic, CPT and core) and how marked difference in the carbon stock estimates can arise. The CPT proved unsuitable for determining thickness of the SAU as it did not discriminate between peats, organic-rich clays, and organic-rich sands. The CPT was crucial for calibrating high amplitude seismic reflections to low density organic-rich units (spatial distribution estimates), particularly when no vibrocores are present, but combined with seismic alone can lead to overestimation in carbon stocks. Peats are often classified according to their organic carbon content, and when used here resulted in a notable reduction in carbon stock estimates compared with the M-V method. The M-V method used texture and colour of sediments/soils to classify the thickness of the SAU but often proved challenging, particularly in reworked intervals where clay and silt content increased but was not often visible (horizons and/or lenses) so remained unaccounted for. The calculation of carbon stock in buried peats and organic-rich sediments that formed on a coastal plain presents a unique challenge when compared with modern terrestrial peats forming environments. These peatlands are widely subject to erosive processes resulting from rising sea levels. In this study, this has resulted in a more complex sediment/soil profile, with multiple intervals of reworked peats that lead to different carbon stock estimates depending on the classification method used.

These carbon stock estimates cannot be directly compared with other studies as no similar published study has been done for mid latitude buried peats in the offshore environment, with recent offshore catalogues focusing on the top 10 cm of marine sediments (Smeaton et al., 2021). However, the global storage of carbon has been estimated within areas of salt marsh, mangrove and sea grass (McLeod et al., 2011) and the contributions of fjord sediments as major carbon storage sites for organic material transported into them (Smith et al., 2015; Smeaton et al., 2016; Burrows et al.,

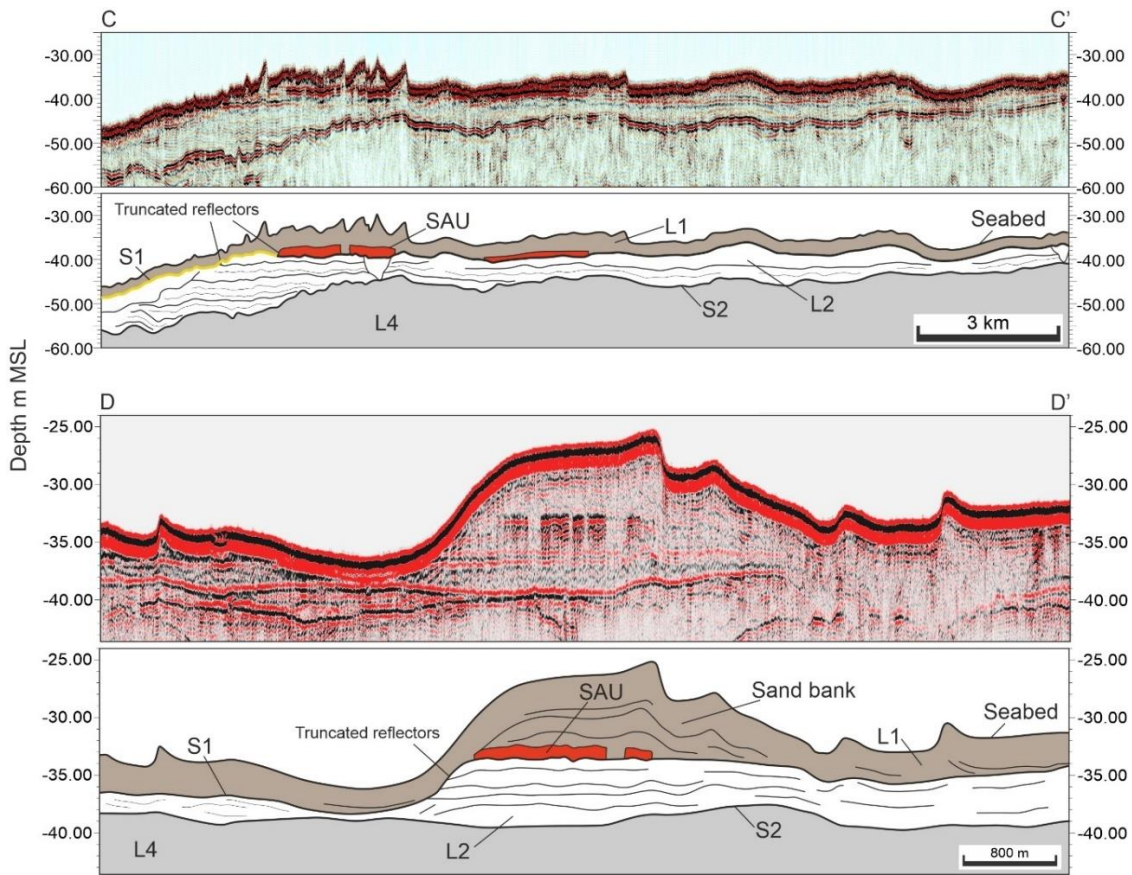
2017; Smeaton et al., 2019). Within Scottish fjords (Burrows et al., 2017; Smeaton et al., 2016; Burrows et al., 2014) a range of carbon stocks have been estimated. Burrows et al. (2014) estimated a total of 0.3 Mt of OC stored in all 110 Scottish lochs, which is in marked contrast to Smeaton et al. (2016) who estimated 11.5 Mt of OC for a single fjord (Loch Sunart). The difference in organic carbon estimates between these studies is due to an increase in the thickness of sediment estimated by improved data acquisition and different methods for carbon stock estimation. The volume of sediment/soil over which organic carbon has been calculated is approximately 40 times less in Vanguard compared with Loch Sunart by Smeaton et al. (2016) (0.03 km<sup>3</sup> and 1.13 km<sup>3</sup> respectively), but they contain a similar quantity of organic carbon. The depositional environment of Loch Sunart is not comparable to the palaeo-depositional environment over which peats and organic-rich sediments developed in the study area. The Smeaton et al. (2016) study focused on fjord environments in which organic material is brought into the fjord landscape from a surrounding drainage catchment, whereas this study focused on organic material that would have formed *in situ*, and came from the continued growth and decay of vegetation. Also, Smeaton et al. (2016) measured carbon over the entire postglacial sedimentary succession (~17 ka to present), in contrast to this study that focused on a single high amplitude seismic event over a narrower period (~13 to 9 ka). Considering the relatively small volume of peat and organic sediment containing organic carbon compared with the large volume in Loch Sunart it is striking that both contain similar quantities of organic carbon and highlights the importance of buried peatland environments as storage sites for organic carbon.

### **5.8.2. Holocene coastal evolution - implications for carbon storage in postglacial peats**

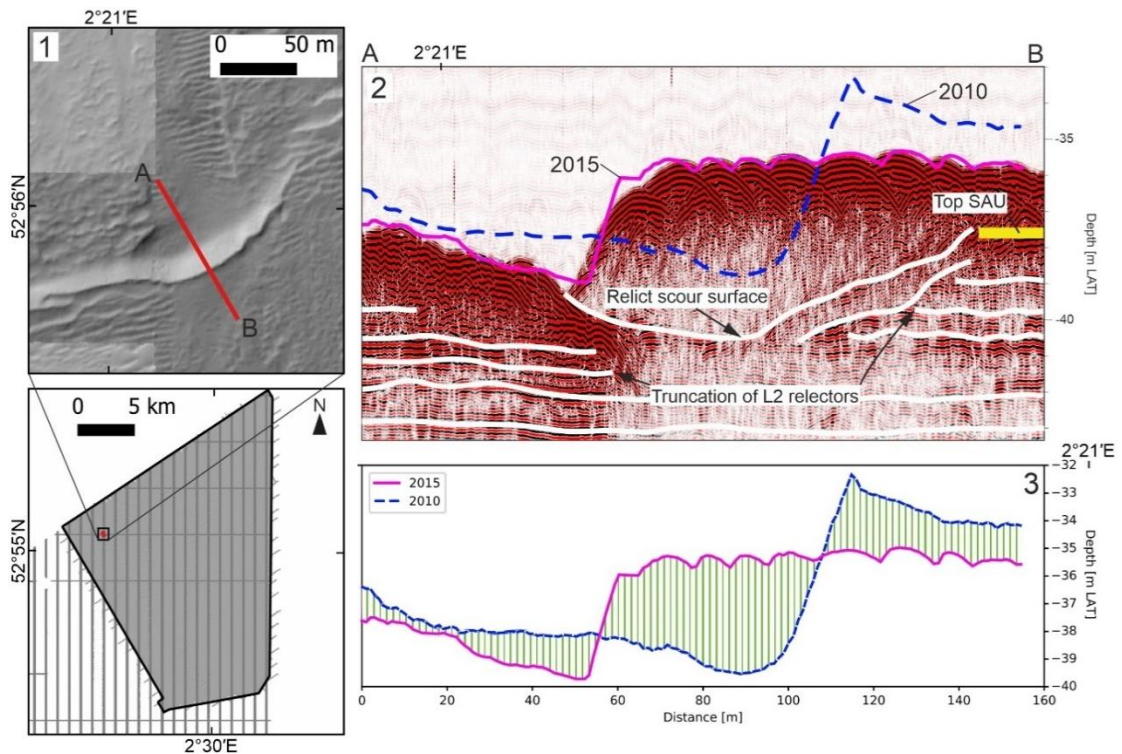
The degradation and loss of modern vegetated coastal plain ecosystems has occurred for centuries. This loss has accelerated in recent decades due to anthropogenic factors and conversion to open water due to accelerated sea-level rise and subsidence (Pendleton et al., 2012). The southern North Sea region experienced rapid RSL rise from c.12 to 8 ka, following an organic-rich, terrestrial landscape (Sturt et al., 2013) suggesting that the challenges vegetated ecosystems face today due to climate change are likely to have impacted ancient southern North Sea coastal plain environments and their sequestered carbon stocks. The present-day spatial configuration of peats and organic-rich sediments in NV West and Boreas is patchy, with laterally discontinuous peat and/or organic sediments. This spatial configuration might reflect the original area over which peat developed but, as discussed in Chapter



4 is likely strongly linked to fluvial systems present throughout the Late Devensian and Early Holocene and the coastal evolution in response to RSL rise driving marsh degradation and an increase in tidal and fluvial erosive processes, Chapter 4). This inference is supported by modern climate induced coastal habitat destruction (Kennish, 2001). Even after final submergence and burial by marine sands, it is likely that peats continued to be eroded, as supported by seismic data (Figure 5.19), where erosion of the peats corresponds to truncation of the underlying L2 unit seismic reflectors and cropping out of the SAU at the seabed. Features identified on bathymetry data (ridges and scour pits, Chapter 4) also supports continued erosion of the seabed and exposure of the underlying L2 unit, Furthermore, repeat bathymetric surveys (2010, 2015, and 2017) show evidence for a dynamic and active seabed with active scour of the seabed, eroding both postglacial deposits and those deposited prior to the Devensian glaciation (Figure 5.20), a possible mechanism for continued erosion of buried peats. With active erosive processes on the modern seabed and throughout the Holocene, postglacial peats likely remained a potential source of atmospheric carbon through oxidation as a result of erosive processes. However, it should be considered that although postglacial buried peats are still subject to erosion, the potential for them to contribute to atmospheric carbon is likely much reduced. This is because the peats underwent degradation by microbial processes prior to burial, much reducing their organic carbon content, and have since remained in an anoxic environment with limited microbial activity.



**Figure 5.17. Seismic profile examples from NV West and Boreas showing eroded L2 unit supported by truncated L2 seismic reflectors and termination of the SAU anomaly coincident with erosion of the L2 unit. C) In the west of NV West, L2 unit reflectors are truncated and overlain by a thin veneer of marine sands (<30 cm), or L2 crops out at the seabed. SAU terminates laterally coincident with termination of L2 reflectors. D) Boreas has a highly variable seabed bathymetry with seabed highs associated with north-south trending sand banks. Coincident with the troughs between the sandbanks, L2 unit reflectors and SAU terminate against L1. See Chapter 3 for information on the L4 seismic unit. See Figure 5.1 for locations of panels.**



**Figure 5.18. An example of mobile seabed sediments and active scour of the seabed in NV West. 1. Repeat bathymetry surveys acquired in 2010 and 2015 showing a large bedform with a scour pit on its steep lee-side. 2. A seismic section (2015) through the large bedform and scour pit shown in 1. Overlain are terrain profiles from the repeat bathymetric surveys. Interpreted are truncated L2 seismic reflectors (white lines) and a relict scour surface. An abrupt termination of SAU corresponds with the relict scour surface. 3. Terrain profiles from repeat bathymetry surveys.**

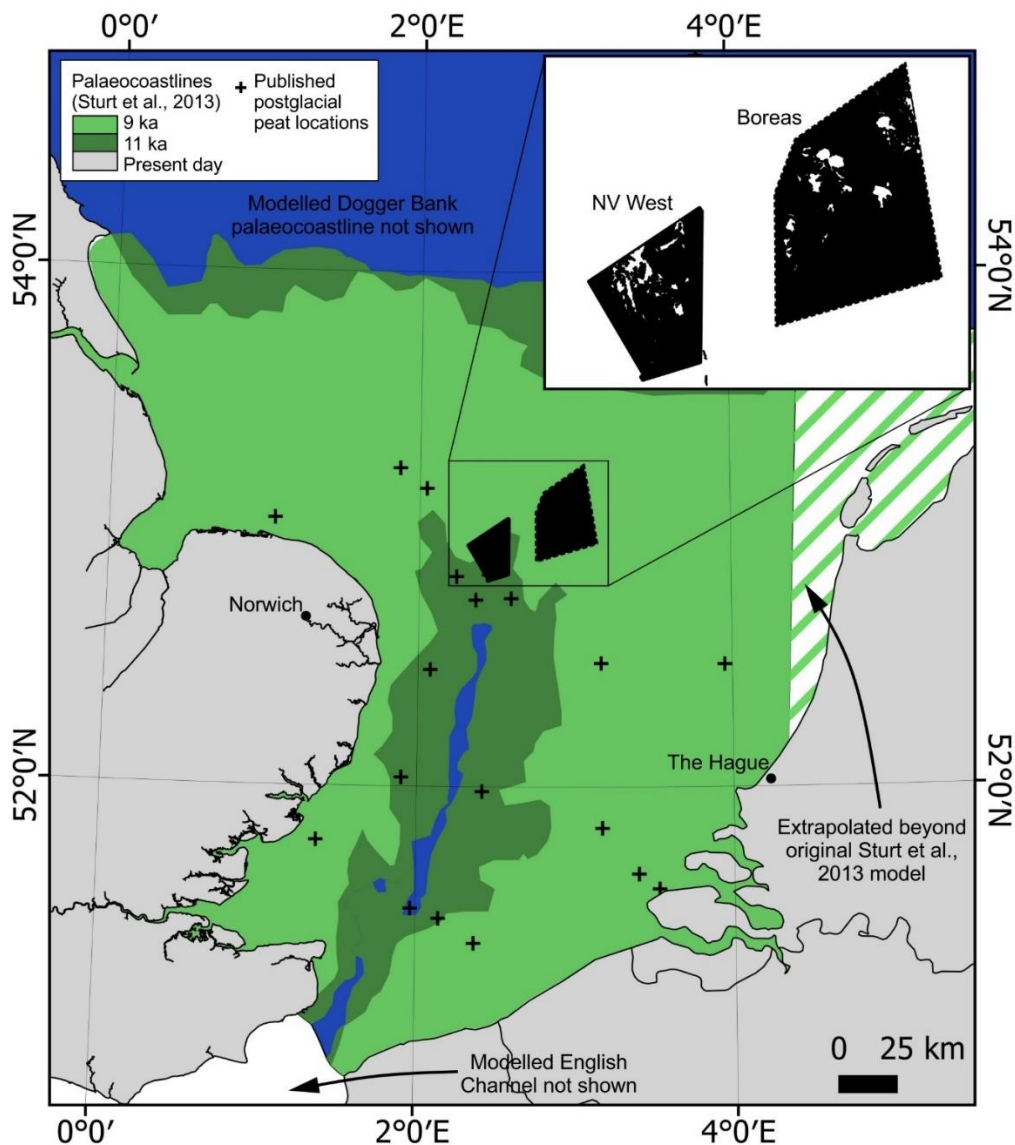
### 5.8.3. Peat distribution southern North Sea region – upscaled carbon stocks

Many modern day peatland ecosystems are considered under threat from anthropogenic pressures and by rising sea levels (Whittle et al., 2016). Palaeoenvironmental evidence suggest that peatlands have undergone similar changes in the past with records of marine transgressions under rising Holocene sea levels (Long et al., 2006; Shennan et al., 2009; Cott et al., 2012; Waller et al., 2020). Observations made in this study provide further evidence for peatland modification and/or destruction due to RSL rise and for their continued erosion through hydrodynamics processes that characterise the southern North Sea region presently. Freshwater wetland soils and tidal salt marshes are major carbon sinks and their continued preservation is an important consideration for global climate change mitigation plans. However, the importance of buried ancient coastal plain peats and their potential to hold large carbon stocks remains understudied and poorly understood when compared with modern peatland environments. The carbon stocks calculated in

this study are not included in any national carbon inventory (Office for National Statistics, 2019). Therefore the quantification of these offshore buried peats is critical to understanding the challenges and risks they pose to ongoing climate change mitigation resulting from their continued erosion and emission of carbon into oceans and/or the atmosphere (Grenfell et al., 2019; Nicholls et al., 1999).

The low gradient configuration of the southern North Sea shelf means that the peats mapped are not limited to this study area, and likely represent part of a much larger coastal plain environment. This is supported by documented postglacial peats at locations throughout the southern North Sea (Hazell, 2008) and the continuing discovery of postglacial buried peats in the southern North Sea and English channel/Le Manche (Plets et al., 2007; Missiaen et al., 2020; Mellett et al., 2019; Emery, 2019) that have similar characteristics in both seismic and core to those documented in this study. Figure 5.21 shows the modeled (Sturt et al., 2013) aerial extent of the coastal plain landscape at approximately 11 ka and 9 ka in the southern North Sea. At this time sea levels were continuing to rise leading to a continued reduction in terrestrial landscapes of the southern North Sea. Radiocarbon dates from peats in the study (Chapter 4) area indicate the preserved peats developed between 13.9 ka and 9.5 ka (Figure 5.6 and 5.7), in accordance with radiocarbon dated peats in other areas of the southern North Sea (Figure 5.21), and Ward et al. (2006) and Hazell (2008). Given the ages of the postglacial peats, it is reasonable to assume that the modelled palaeocoastline at 11 ka (Figure 5.21) represents the maximum terrestrial landscape over which peats could have formed, prior to flooding from the south at 9 ka. Under the assumption that peats developed across the entire southern North Sea region up to 9 ka (max 11 ka palaeocoastline), and were subject to the same geomorphological and erosional process as documented and discussed in Chapter 4, an upscaled estimate for carbon stocks associated with postglacial peats, based on the present-day % cover documented in the study areas (Figure 5.20 inset), can be estimated. Based on these inferences, 726 Mt of organic carbon using the M-V method and 526 Mt using the M-OC method (Table 5.9) is estimated. Although this upscaled estimate applies only to postglacial peats, the estimate could increase with further investigation of the subsurface. For example, a likely scenario is identification of older peat deposits through continued characterisation of the southern North Sea subsurface from increased development activities in the region. The 726 Mt of organic carbon (M-V) accounted for in NV West and Boreas survey areas is equivalent to 2664 Mt CO<sub>2</sub>e (carbon dioxide equivalent), which is equivalent to approximately 6 times the UKs 2019 total greenhouse emissions, estimated to have reached 435 Mt CO<sub>2</sub>e (UK government,

2019). With a projected increase in rates of sea-level rise (IPCC, 2013), and an increase in the rate of offshore seabed infrastructure developments, particularly in renewable energy, understanding the fragility of buried peats and the carbon risk associated with them becomes more pressing.



**Figure 5.19. Palaeocoastlines at 10 ka and 9 ka as modelled by Sturt et al. (2013). Where the palaeocoastline is coloured as a line fill marks the area not modelled by Sturt et al. (2013) and for the purpose of this study has been extended to the Dutch coast. The inset map shows the NV West and Boreas survey areas with aerial extents of SAU, which account for 22% of the survey areas. Crosses indicate the approximate locations of published postglacial peats identified in the southern North Sea (published peats on Dogger Bank not shown).**

**Table 5.8. Carbon stocks upscaled and constrained by modelled palaeocoastlines at 11 ka and 9 ka.**

Palaeocoastline	Area km <sup>2</sup>	Carbon stock	
		M-V Mt	M-OC Mt
Upscaled peat			
11 BP	6103	726	526
9 BP	4950	589	427

## 5.9. Conclusion

Carbon stocks associated with postglacial peat deposits have been calculated. These carbon stock estimates cannot be directly compared with other published study as no similar studies have been done for mid latitude buried peats in the offshore environment.

The peat and organic sediment within the study area contain a similar proportion of organic carbon, when compared with carbon stock studies in mid latitude fjord environments that sample much larger volumes of sediment. This highlights the importance of buried peatland environments as storage sites of organic carbon.

The present-day configuration and spatial distribution of postglacial peats likely reflects the ongoing processes of erosion (fluvial and tidal) and degradation (warming climate and marine influence) that occurred from Late Devensian until marine transgression in the Early Holocene period. Following submergence and burial, peats continued to be eroded as a result of shallow marine process and continue to be eroded to the present-day, due to continued active scour of the seabed. The continued erosion of peats from Late Devensian to present-day suggests that postglacial peats remained a source of carbon through erosive processes after burial and continue as a source of carbon presently.

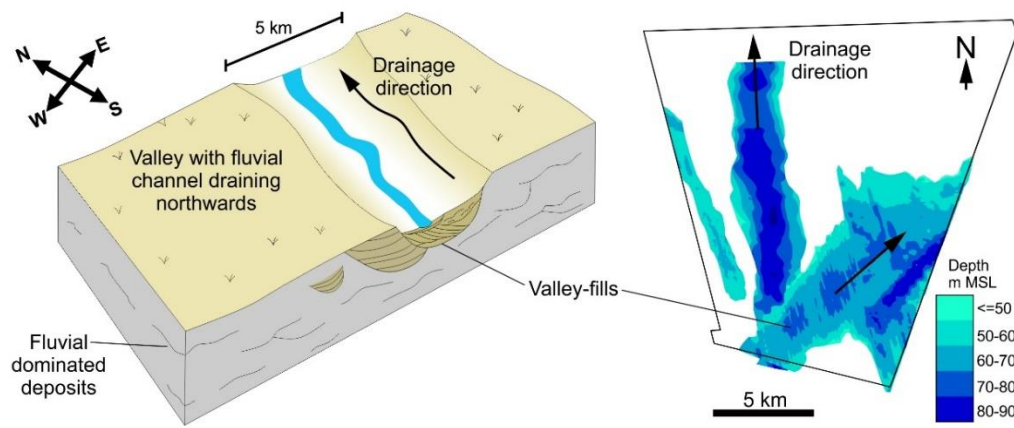
The low gradient configuration of the southern North Sea shelf, and documented peats in other published studies, support widespread distribution of postglacial peats, similar to those documented in this study. Upscaled carbon stock estimates based on predicted distribution of peat across the southern North Sea region, and organic carbon properties documented in this study area provide compelling evidence for the importance and inclusion of submerged buried peats in national carbon inventories, particularly with increases in offshore renewable energy infrastructure projects and those projected for the future.

## Chapter 6 - Discussion and conclusions

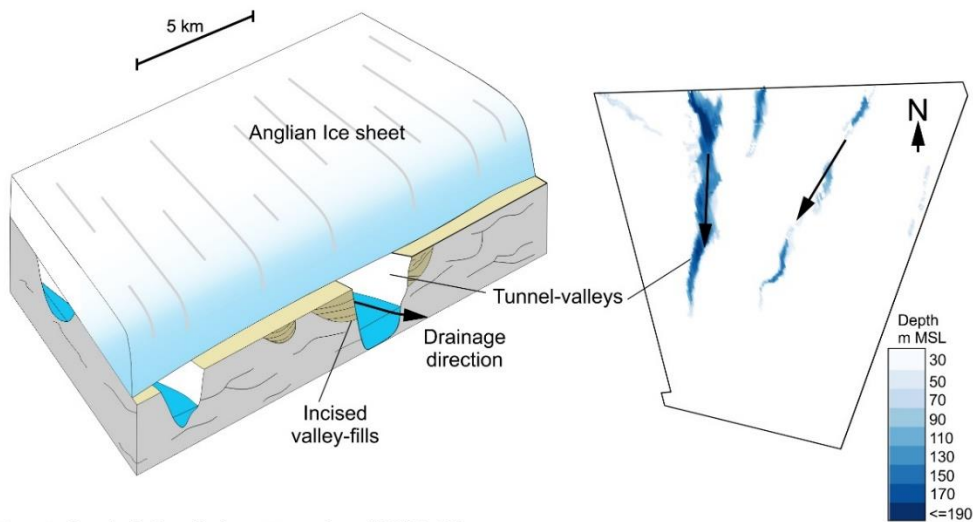
### **6.1. How does integrated subsurface data required for offshore windfarms improve understanding of Quaternary palaeo-drainage networks feeding into the southern North Sea basin?**

The opportunity to investigate the Middle Pleistocene to Holocene drainage networks on a low relief shelf over periods characterised by multiple glacial and interglacial cycles was afforded by a comprehensive, high-resolution integrated data set offered and the location of the study area. Drainage into the southern North Sea region from Britain and mainland Europe has been the focus of many studies (Rose, 1994; Funnell, 1996; Gibbard et al., 2009; Hijma et al., 2012; Prins et al., 2019). The lack of data means that the evolution and orientation of those drainage networks in the submerged southern North Sea region has received little attention. However, this study has documented major changes in the orientation and style of drainage in the study areas that can be placed into the evolution in the region. Figure 6.1 shows the landscape reconstructions for three stages of drainage evolution, from the fluvially-dominated delta plain environment of the Middle Pleistocene (MIS 19-13), through the Anglian/Elsterian glaciation (MIS 12) when the landscape was subglacial, to the postglacial coastal plain landscape (MIS 2), dominated by fluvial and wetland environments.

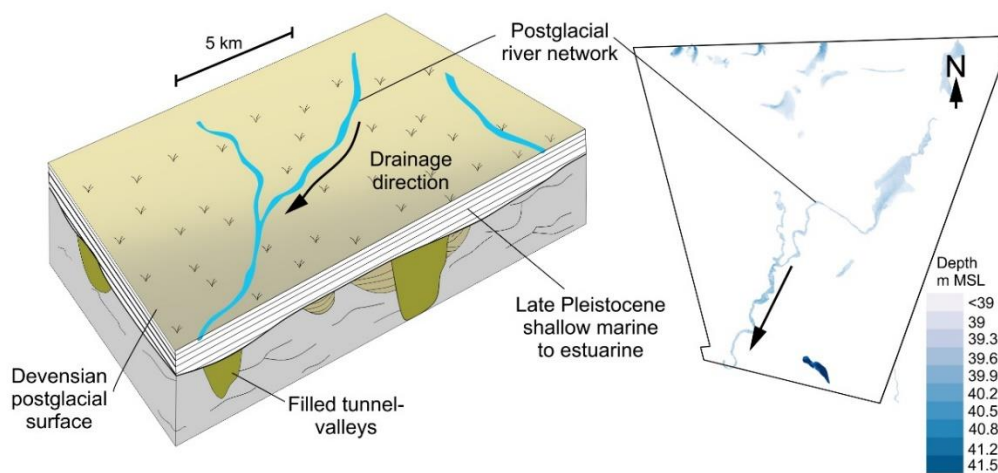
A. Middle Pleistocene fluvial networks (~MIS 19-13)



B. Anglian tunnel valleys (MIS 12)



C. Postglacial fluvial networks (MIS 2)



**Figure 6.1. Interpreted drainage networks from Middle Pleistocene to present day within Norfolk Vanguard West. The arrows indicate the interpreted drainage directions.**

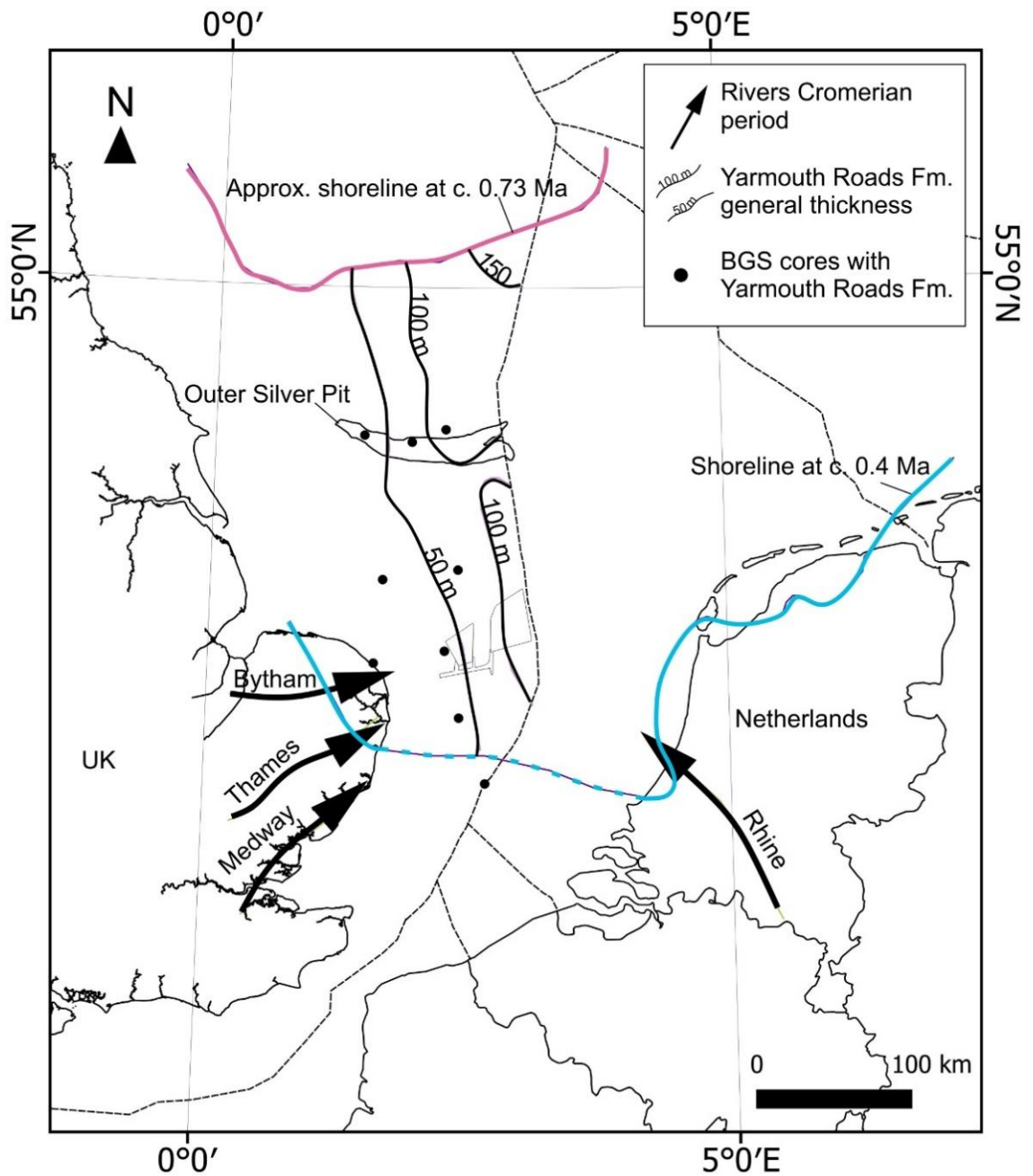


### **6.1.1. Glacial-interglacial delta plain landscape (~MIS 19-13)**

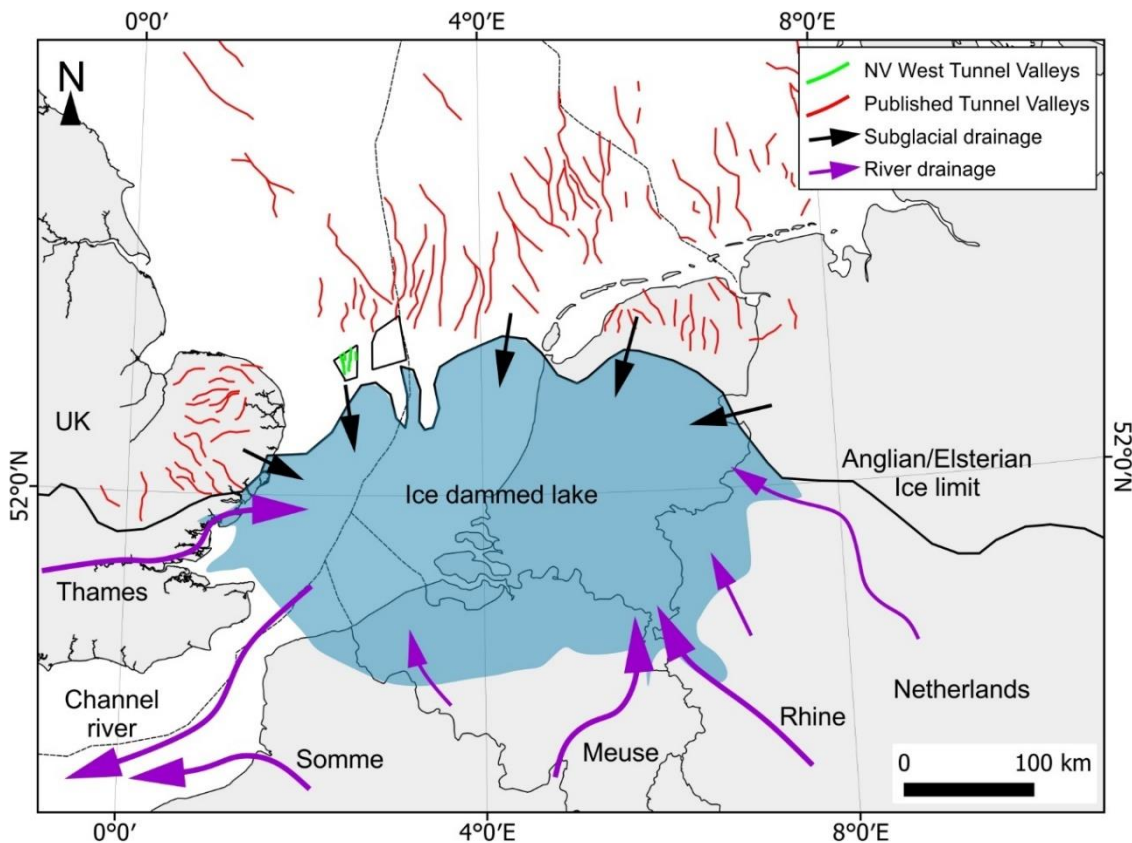
The Middle Pleistocene stratigraphy represents the earliest record of terrestrial drainage networks unveiled in this study. This stratigraphic interval is predominantly fluvial and corresponds to the Yarmouth Roads Fm., which has been documented and discussed in several studies (Cameron et al., 1987; Cameron et al., 1992; Funnell, 1996). Previously, interpretations of depositional environments for the Yarmouth Roads Fm. were based on single line, low-resolution seismic reflection data and scarce cores. Using high-resolution seismic reflection data, large south-north trending valleys have been documented with depositional architecture consistent with a fluvial origin. Drainage through these valleys is interpreted as northward, based on deepening trends. This is consistent with fluvial reconstructions for the Rhine-Meuse system (Hijma et al., 2012), river networks draining south-eastern England (Bridgland et al., 1995), and core observations from the Outer Silver Pit where marine delta-top and inter- and sub-tidal delta front facies have been described (Cameron et al., 1987), consistent with the northward expansion of the Ur-Frisia Delta (Cameron et al., 1992) (Figure 6.2). Throughout the Middle Pleistocene, rivers draining mainland Europe (e.g. the Rhine-Meuse and north German rivers) and southern-eastern England (e.g. the Bytham and Thames rivers) flowed northward into the North Sea Basin, and components of these systems are represented in the valley-fills documented in this study. However, ascribing particular valley-fills to their onshore fluvial sources remains challenging, and remains unresolved. The northward extent of the Middle Pleistocene drainage networks likely fluctuated during this period due to marine regressions and transgressions, a consequence of glacial-interglacial cycles throughout the Cromerian Stage (Figure 6.2 and Chapter 3, Figure 3.2). The change in depositional environment is supported by the seismic architecture of the valley-fills, with switches from terrestrial dominated fluvial deposits to marine influenced environments (Chapter 3), consistent with relative sea-level changes. The low relief shelf configuration during this time would have enabled extensive marine transgression to occur through relatively small rises in sea level, with consequences for the evolution of the drainage networks over relatively short periods.

### **6.1.2. Subglacial terrestrial landscape (~MIS 12)**

Of the three major Pleistocene glaciations, only the Anglian glaciation (MIS 12) extended southwards beyond the study area (Figure 6.3). This has presented an opportunity to investigate the evolution of southern North Sea drainage networks over a landscape transitioning from interglacial to subglacial environmental conditions. During the Anglian glaciation, global sea level was >100 m below present levels (Spratt et al., 2016), leaving the southern North Sea shelf subaerially exposed. The Anglian ice sheet at its maximum extended between 10 and 40 km south of the study area with multiple phases of ice sheet advance and retreat resulting in both subglacial and ice marginal conditions during MIS 12 (Davies et al., 2012). During the early stages of maximum Anglian glaciation, the development of a proglacial lake has been hypothesised that extended over the entire southern North Sea, much of Belgium and the Netherlands, and the East of England (Cohen et al., 2005; Gibbard, 2007). This lake was dammed to the North by the Anglian ice sheet, and drained southwards through the Dover Straits (Figure 6.3) (Gupta et al., 2017). River networks that extended northwards from mainland Europe and from England, draining into the North Sea during the Early and early Middle Pleistocene (MIS 19 to 13, Figure 6.2) retreated with the onset of the Anglian glaciation and drained into the proglacial lake, or diverted southwards (Figure 6.3) (Gibbard, 2007) into the channel (Gibbard, 1988; Rose, 1994; Hijma et al., 2012). Within the study area, the basal morphology of tunnel valleys is consistent with subglacial erosion by southward drainage towards the ice margin. This is further supported by other tunnel valley networks documented north (Praeg, 2003) and east (Wingfield, 1990) of the study area, which also show basal morphologies consistent with southward drainage (Figure 6.3). The Brown Bank Fm. stratigraphy overlying the tunnel valley-fills (Chapter 3, Eaton et al., 2020) records a regressive marine to estuarine environment with river drainage into the basin from the south (Hijma et al., 2012), as previously documented during MIS 19 to 13, marking a sharp change in drainage direction from a predominantly southwards to northwards drainage direction.



**Figure 6.2. Approximate shoreline positions for the Ur-Frisia Delta in response to marine transgression. Maximum extent of the Ur-Frisia Delta extends beyond the Outer Silver Pit where marine delta-top and inter- and sub-tidal delta front facies have been described in BGS cores. The approximate general thickness of the Yarmouth Roads Fm. as defined by BGS cores. Delta shoreline positions and Yarmouth Roads Fm. thickness contours adapted from Cameron et al. (1992).**

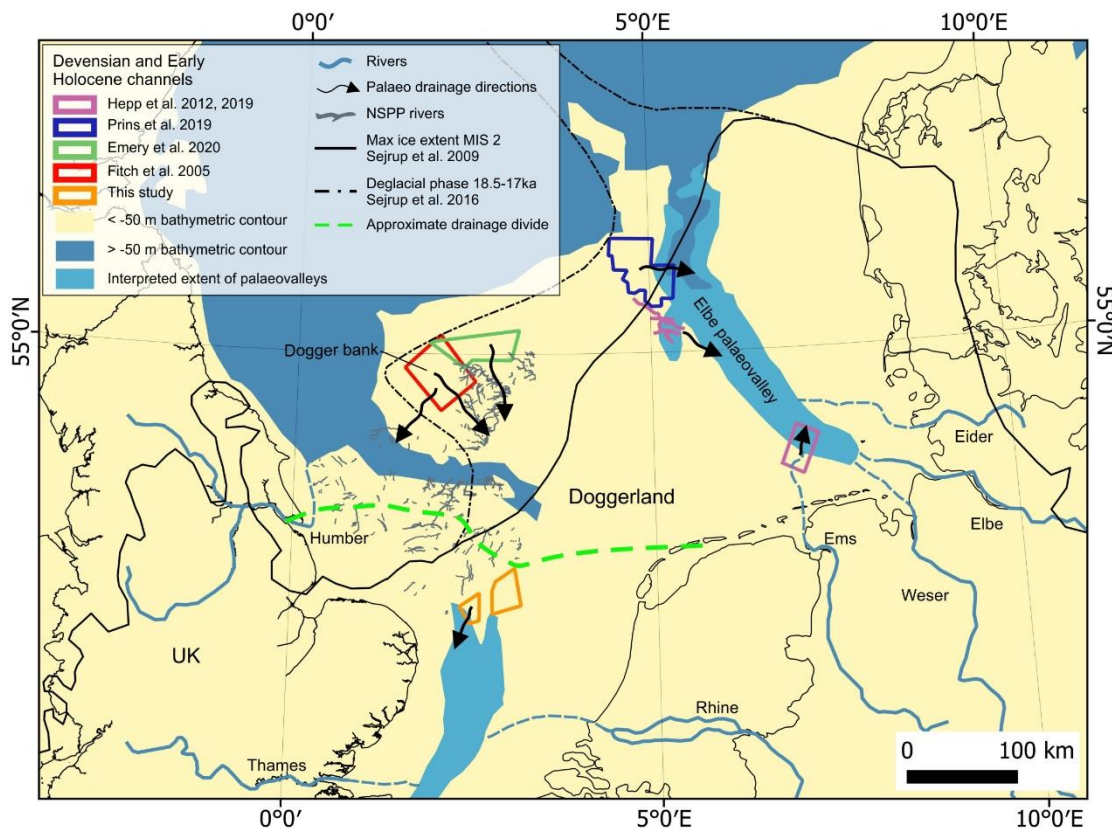


**Figure 6.3. Subglacial conditions in the study area during the Anglian glaciation. Tunnel valleys documented in this study and those published earlier are predominantly north-south orientated supporting a southward flow of meltwater towards the ice sheet front (black arrows). Rivers from southeast England and mainland Europe retreated westwards and southwards due to a large proglacial lake covering the southern North Sea region. Drainage from the proglacial lake was likely through the Dover Strait. River drainage (purple) and proglacial lake (adapted from Gibbard, 2007; Cohen et al., 2017).**

### 6.1.3. Interglacial terrestrial to marine (transgressive) (~MIS 2)

Following the LGM, the study area remained subaerially exposed until approximately 9 ka. Fluvial processes dominated the landscape during this time contemporaneous with freshwater peatland development (Chapter 4). With continued relative sea-level rise, freshwater peatland was succeeded by salt marsh with coastal and estuarine processes dominating. North of the study area, at Dogger Bank, subglacial conditions prevailed. Just south of Dogger Bank, ice marginal, periglacial conditions dominated during LGM until approximately 23 ka when Dogger Bank was fully deglaciated (Emery et al., 2020). From 23 ka onwards, the southern North Sea was dominated by fluvial processes. The variable landscapes that have characterised the southern North Sea following the LGM, combined with the low gradient shelf setting, has led to a complicated drainage history, with the origin and evolution of drainage networks

controlled by positioning in the basin. Drainage networks in the north (Dogger Bank, Figure 6.4) drained glacial meltwater from the Dogger Bank high (Fitch et al., 2005a; Prins et al., 2019; Emery et al., 2020) in the form of proglacial channels, which in some cases exploited pre-existing subglacial meltwater channels. The deglaciation of Dogger Bank then led to the formation of drainage networks, these responding to an increase in precipitation, with documented channels draining southward off the Dogger Bank high (Emery et al., 2020) and eastward into the Elbe palaeovalley (Figure 6.4, Hepp et al., 2019; Prins et al., 2019). In contrast, postglacial drainage networks documented further south in this study (Figure 6.4), developed in a comparatively low relief environment, and far from the ice front (>40 km). The two-phase evolution of drainage networks documented in the north, which formed in response to deglaciation of the region, are not observed in the study area. The fluvial networks documented in this study drained southward. This likely only reflects local drainage patterns, similar to those documented by Hepp et al. (2012), where drainage channels reflect the offshore extension of now submerged rivers (Ems, Figure 6.4). In addition, the North Sea Palaeolandscape project has identified postglacial channels over a large area west of Dogger Bank and north of East Anglia, UK (University of Birmingham, 2011 - Figure 6.4). The timing of these channels with respect to deglaciation is currently unknown. However, their presence further supports a fluvially dominated postglacial landscape throughout the southern North Sea region. The configuration of the North Sea Basin, with subtle changes in relief from south to north, the multiple river systems draining into it from the UK and continental Europe, and the complex glacial-interglacial history resulted in a complicated evolution of drainage networks with marked changes in drainage direction. The comparatively few studies documenting postglacial drainage networks in the southern areas of the southern North Sea region, compared with those on Dogger Bank, poses challenges for deciphering the link between UK and continental European river networks, and the buried and submerged drainage networks documented in this and other studies (Missiaen et al., 2020).

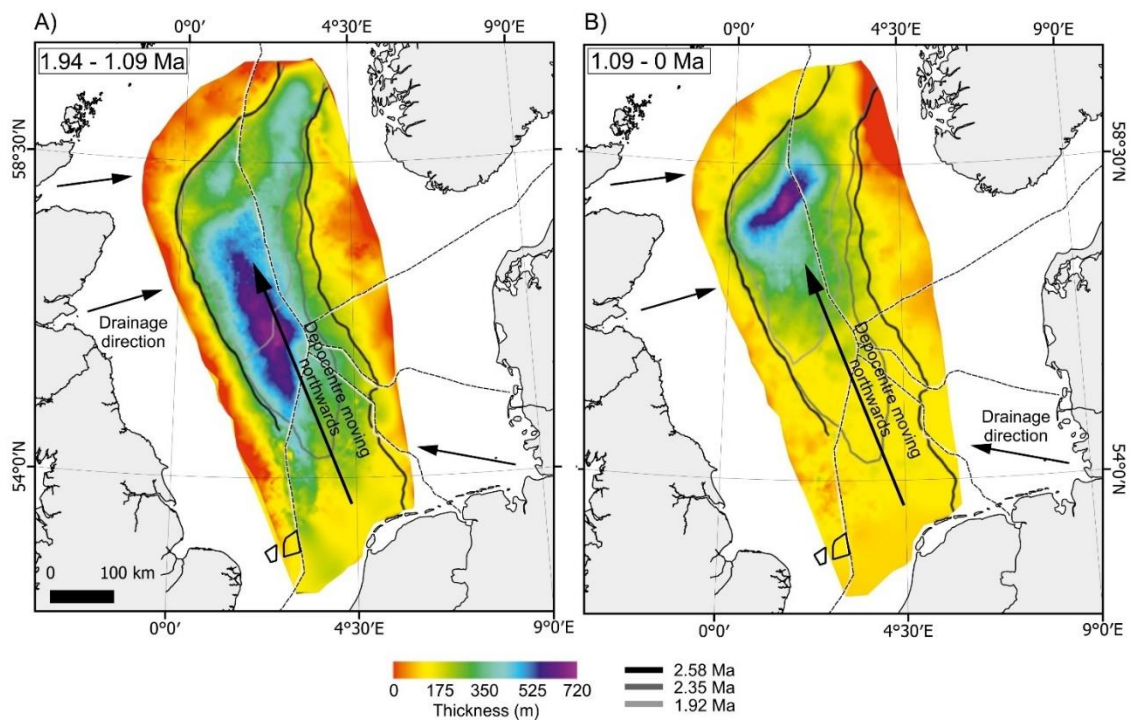


**Figure 6.4. A composite map of the southern North Sea with a land-sea distribution ~11 ka with the palaeocoastline being based on the -50 m bathymetric contour line (modified from Warnke, 2015). Studies that have documented Late Devensian to Early Holocene channels networks are shown alongside those documented in this study, with approximate drainage directions. An approximate position for an important drainage divide north of the study area is shown. The interpreted extent of large palaeovalleys are shown with their tributaries. The maximum ice extent during MIS 2 is shown (Dogger Bank subglacial) and the ice extent during the deglaciation phase between 18.5-17 ka (southern North Sea fully deglaciated). North Sea Palaeolandscape Project (NSPP) data set adapted from University of Birmingham (2011).**

#### 6.1.4. Opposing drainage directions

The southern North Sea Basin during the Pleistocene to present-day is a physiographically distinctive setting, characterised by a low relief continental shelf, and landmasses enclosing it to the south, west, and east. During the early Quaternary, rapid sediment deposition, sourced mainly from the Rhine-Meuse and Baltic river systems (Overeem et al., 2001; Busschers et al., 2007), caused infill of the North Sea basin and differential subsidence, driving a northwards migration of the basin depocenter (Figure 6.5). Throughout the Quaternary, regional drainage patterns were predominantly towards the north, and this north-to-south dispersal pattern led to a thick sedimentary succession (Lamb et al., 2018). Thickness maps for the North Sea Quaternary stratigraphy shows that the study area is positioned on the southwestern

edge of the Quaternary basin. Therefore, the northward drainage direction that has dominated throughout much of the Quaternary, and documented in this study (Chapter 3), is to be expected. The basin has experienced multiple phases of glaciation during the Pleistocene, resulting in dramatic changes in landscape ranging from subglacial to periglacial to marine. Multiple major river systems drained into the basin during the Pleistocene, which extended northwards from the UK and continental Europe (Funnell, 1996; Hijma et al., 2012). Before the Middle Pleistocene, sediment supply outpaced subsidence leading to non-marine conditions. Subsequently, rates of accommodation increase have outpaced sediment supply, and due to rapid rates of relative sea-level rise and continued thermal subsidence multiple periods of marine transgression have been preserved (Cohen et al., 2014).

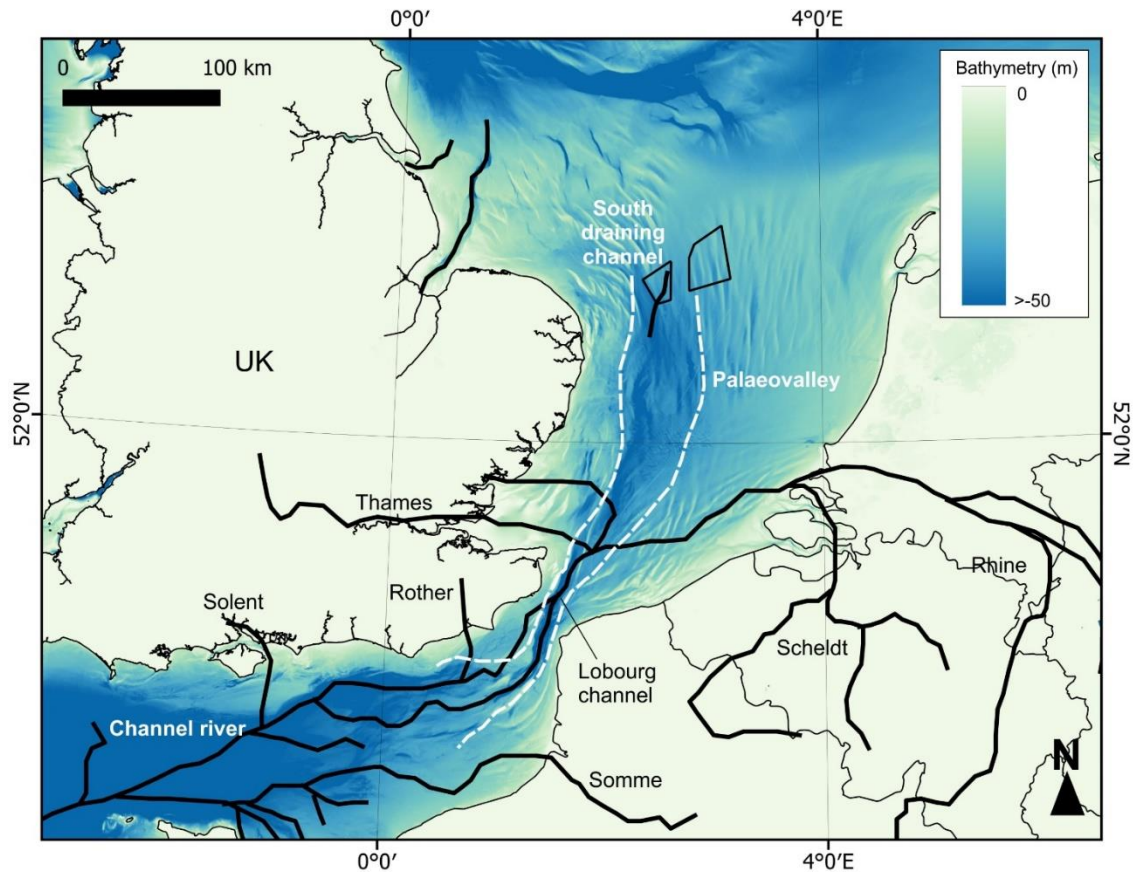


**Figure 6.5. Present-thickness maps of compacted Quaternary stratigraphy. A) 1.94 to 1.09 Ma. B) 1.09-0 Ma. Throughout the Quaternary the North Sea depocenter moved progressively northwards. The study area sits on the southwestern edge of the North Sea basin. Thickness maps adapted from Lamb et al. (2018).**

This study has documented switches in principal drainage direction in the southern North Sea. From approximately MIS 19 to 13, the principal drainage direction was northwards, over a delta plain that extended over the southern North Sea region (Figure 6.2). The switch to southwards draining during MIS 12 (Figure 6.3, Chapter 3) was in response to the development of the Anglian ice sheet, and the formation of a proglacial lake that extended over the southern North Sea region. During this period,

subglacial meltwater channels (tunnel valleys) formed that drained southwards into a proglacial lake. Rivers from south eastern England and continental Europe that previously flowed northwards over the North Sea shelf would have terminated at the proglacial lake. Overspill and drainage from the proglacial lake would have been southwards (Figure 6.3) through the Dover Strait and into the English Channel (Gibbard, 2007; Gupta et al., 2017). This change in drainage may have been influenced by changes in slope in response to flexure by ice sheet loading (Kiden et al., 2002). Following the Anglian glaciation, the study area was transgressed (Eemian interglacial), followed by regression leading up to LGM. The principal drainage direction both in the study area and the southern North Sea region remained southwards following the LGM. Gupta et al. (2017) proposed a series of megafloods that led to the breaching and rerouting of drainage network through the Dover Strait, and into the English Channel (Figure 6.6). Initial breaching of the Dover Strait occurred during the Anglian glaciation as overspill from a proglacial lake that covered the southern North Sea region. During the Saalian (MIS 6) a second megaflood has been postulated that led to the complete breach of the Dover Straits and a subsequent catastrophic flood event, draining proglacial lakes to the northeast (Gibbard et al., 2015). The Lobourg channel and its extension north-eastwards into the southern North Sea Basin (Figure 6.6) are considered by Gupta et al. (2017) to originate from mega flood events. These over deepened channel systems, in combination with crustal subsidence in the southern North Sea following deglaciation (Kiden et al., 2002) provide a mechanism to drive the change to the southwards drainage direction, and development of a cryptic drainage divide to the north of the study area.





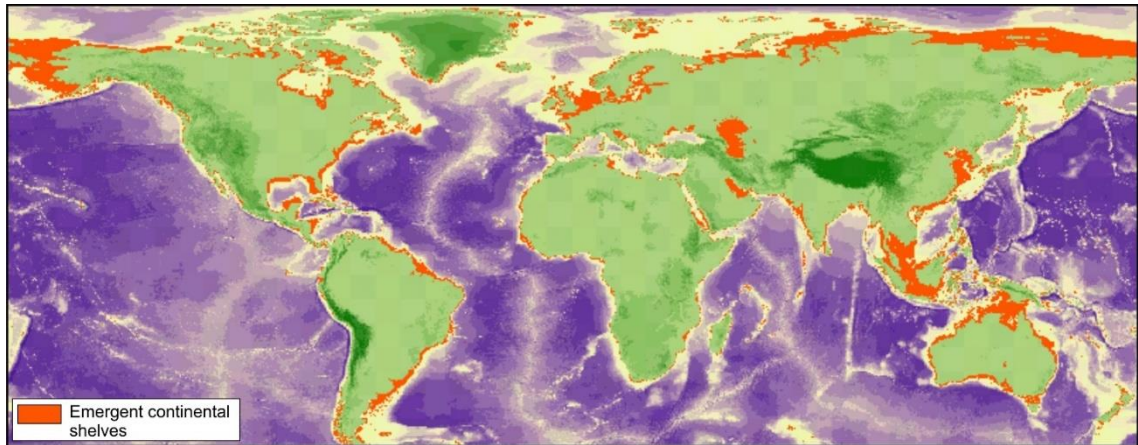
**Figure 6.6. The southern North Sea and English Channel drainage networks following the LGM. South-eastern England and continental European rivers drained southwards through the Dover Strait into the Atlantic. A palaeovalley has been extended northwards from the English Channel (based on bathymetric interpretation) that drained rivers identified in this study. A series of megafloods during the Anglian/Elsterian glaciation and again during the Wolstonian/Saalian lead to a breach of the land-bridge between England and continental Europe (Dover Strait), and subsequent diversion of rivers southwards into the Atlantic. River networks (black lines) adapted from Gibbard (2007) and Gupta et al. (2017)**

The opposing drainage directions documented in this study that occurred over a time period spanning approximately 700 ka are strongly influenced by the low relief shelf setting that is a distinctive and unusual aspect to the southern North Sea region. Where changes in drainage direction have been documented in other studies, they typically document changes from axial (longitudinal) to transverse drainage with respect to tectonic structures (Gawthorpe et al., 1993; Cullen et al., 2020). For the most part, continental shelves are steeper (Green, 2009) than those seen in the southern North Sea region, and face oceanic systems that have a strong and persistent control on drainage directions. Therefore, the abrupt changes in the principal drainage direction documented here over a relatively short periods are likely unusual in the geological record. However, there may be similar examples in ancient epeiric sea settings.

Similarities can be seen between the Carboniferous and Quaternary, with Carboniferous stratigraphy recording significant transgressions of largely nonmarine environments. Furthermore, glacial periods during the Carboniferous provided a mechanisms for generating higher-magnitude and higher-frequency sea-level changes as ice sheets waxed and waned (Tyrrell et al., 2006; Davies, 2008). The North Sea region can provide a useful analogue to interpret abrupt changes in palaeoflow, where tectonic influences cannot be ascribed.

## **6.2. Are buried and submerged postglacial peats a carbon sink or source, and should they be a consideration in carbon stock estimates?**

Throughout the 20<sup>th</sup> Century, sea levels have risen over the northwest European shelf by an average of 0.1-0.2 cm year<sup>-1</sup> (Horsburgh et al., 2013), with rates of sea-level rise expected to increase over the coming decade (IPCC, 2013). The impact of sea-level rise is likely to affect over 70% of coastal wetlands worldwide (Nicholls, 2004), which will have a detrimental effect on the ability of coastal wetlands to absorb and store atmospheric carbon due to increased erosion, drowning and loss of habitats (Legge et al., 2020). During the Early Holocene, relative sea-level rise was more than an order of magnitude greater than that projected for the future (Henman et al., 2008). The present-day processes leading to loss of coastal wetlands as a consequence of sea-level rise offer valuable insights into the processes that ultimately led to the submergence, degradation/erosion, and burial of Late Devensian to Early Holocene peats (Figure 6.7). Whilst at the same time, the present-day configuration of buried peats and their ongoing vulnerability offer a glimpse of the fates of many present-day coastal wetlands.



**Figure 6.7. Map illustrating the emergent parts of the continental shelves worldwide during the last glacial maximum. An assumed glacial eustatic lowstand of 120m below present sea level, with no glacially induced flexural uplift in high-latitude regions adjacent to large ice sheets or neotectonic (Holocene) uplift or subsidence taken into account (from Fitch et al., 2007).**

The coastal plain landscape that characterised the southern North Sea following the LGM was predominantly a wetland environment, where major peat deposits accumulated. These peats have been documented in this study, and in numerous other studies (e.g. Ward et al., 2006; Hazell, 2008; Missiaen et al., 2020). These coastal wetlands would have acted as a major carbon sink for atmospheric carbon, with examples from modern analogues storing more carbon per unit area than other coastal habitats (e.g. mud and sand flats). As the climate warmed in the period following the LGM, the effectiveness of these coastal wetlands to store atmospheric carbon would have increased (through plant growth). However, due to an increase in precipitation during this period (Emery et al., 2020), discharge through rivers would have increased leading to increased erosion of the wetland landscape. The documented fluvial networks in this study (Chapter 6.4), and those throughout the southern North Sea, support an increase in fluvial activity following LGM, and a consequent conversion of some coastal wetlands into a carbon source through increased erosion. The dissection, degradation and erosion of the coastal wetlands would have continued, and likely increased, with relative sea-level rise. Relict tidal channels and ponds identified in this study support a marked change in coastal processes in response to sea-level rise, with degradation of the marsh environment, through an inability to keep pace with sea-level rise, and consequent reduction in atmospheric carbon uptake due to marine inundation. The low relief shelf configuration and slow subsidence of the southern North Sea was likely the primary factor leading to preservation of Late Devensian/Early Holocene peats, given that a steeper shelf would have led to more erosion of soils and sediments during marine transgression (Green et al., 2018), and a consequent redistribution and

degradation of organic carbon. With inundation of the southern North Sea shelf (~8 ka), peats that survived the transgression were buried by shallow marine sands. With transgression and full marine conditions, a tidal system was established leading to erosive tidal processes. A number of tidal indicators, over a range of scales have been documented in the study area (Chapter 4 - furrows, ridges, sand banks), supporting a strong tidal influence. Multiple sand banks extend in a north-south orientation through the study area on the modern seabed. These sand banks are superimposed with sediment waves (Chapter 3). In the Boreas area, the trough between these sand banks incises into the underlying preglacial sediments, and seismic reflection data reveals truncation of postglacial peat on the margins of these troughs. In the Norfolk Vanguard West area, a bathymetric low extending north-south along the eastern margin and considered to be related to a large palaeovalley (extending southwest towards the Dover Strait, Figure 6.6), is characterised by truncated seismic reflectors of pre- and postglacial sediments (peats and Brown Bank Fm.). Furthermore, scour pits on the lee side of large submarine dunes (Chapter 3), which are interpreted to originate during marine transgression (Van Landeghem, et al., 2009), incise down into both postglacial peats and preglacial sediments. These features support continued erosion of postglacial peats following marine transgression, with erosive forces primarily driven by tidal processes. Repeat bathymetry surveys over the study area support a mobile seabed with net migration of sediment towards the north. In addition, sediment can be periodically remobilised during exceptional storm events (Van Der Molen et al., 2001; Ferret et al., 2010), which can lead to exposure or erosion of underlying postglacial peat deposits.

The stratigraphic and geomorphological features presented in this study clearly demonstrate degradation and erosion of a coastal wetland environment in response to relative sea-level rise following the LGM, and continued erosion during and after transgression (Chapter 4 and 5). Degradation and erosion would reduce the wetlands efficiency as a carbon sink, as well as liberating organic material. The fate of organic carbon associated with eroded peats is not clear. However, present-day analogues infer multiple mechanisms leading to either continued geological storage (sink) or liberation into marine or atmospheric environments (Henman et al., 2008). These include export via river systems to the ocean (long-term carbon storage), retainment of carbon in river and estuarine systems (sediments), and oxidization and outgassing as CO<sub>2</sub>. In addition, liberation of carbon from wetlands into the atmosphere or estuarine systems may have begun early (prior to marine influence), due to increased temperature and precipitation (Freeman et al., 2001; Freeman et al., 2004) associated

with interglacial conditions. The loss of carbon can be exacerbated by increased salt stress and subsequent decomposition associated with sea-level rise (Henman et al., 2008).

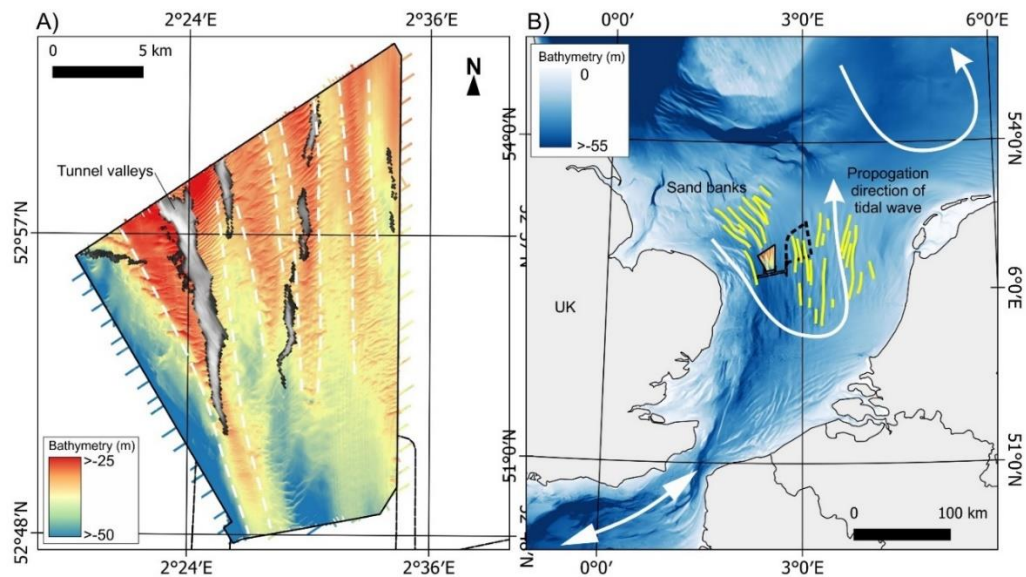
Presently, buried peats are not considered in the UK carbon capital (Office for National Statistics, 2016). The carbon capital accounts for carbon stocks held in the geosphere (oil, gas, coal resources, rocks (primarily limestone), and minerals, e.g. carbonate rocks) and biosphere (carbon in soil, plants, animals, and other life forms (living and dead)), are considered. The high commercial interest in certain forms of geocarbon (fossil fuels) has meant that data availability is good relative to other carbon stock categories. However, accounting for carbon stocks held within buried peats in the offshore environment has not been considered. This is largely due to land-use (seabed) practises, whereby subsurface data acquired offshore was focused on deeper geological features for fossil fuel exploration and production, therefore by-passing the shallow subsurface containing buried peats. With changes in land-use (seabed for offshore renewables), the characterisation of shallow buried peats has improved, providing an opportunity to better understand the carbon stocks associated with them. The need to understand carbon stocks associated with fossil fuels is clear, given the well documented link between fossil fuel use and climate change (Blanco et al., 2014). The link with buried peats has not been considered explicitly. Present-day peatlands in the UK occupies around 12 % of the land area (Office for National Statistics, 2019), and are recognised as important carbon sequestration stores (Mitsch et al., 2013). Globally, wetlands are under threat from anthropogenic contributions to climate change and land use changes. Coastal wetlands are under threat from rising sea levels (Grenfell et al., 2019), with estimates that up to 22 % could be lost by the 2080s (Nicholls et al., 1999). Infrastructure projects such as development of onshore windfarms have a range of negative impacts on peatlands, making the balance between carbon savings and loss challenging (Office for National Statistics, 2019). These same issues of 'change of land-use' have potentially negative consequences for the offshore domain. With increase in demand for renewable energy, the seabed environment and shallow subsurface are undergoing major change. The placement of wind turbines has a direct impact on the hydrodynamic environment around the base of a turbine, leading to significant scour (Ma et al., 2018). Considering this, the placement of wind turbines, particularly in the southern North Sea region, may lead to changing sediment mobility and increased erosion of postglacial peats, with implications for carbon stocks and future projections.

The postglacial peats identified in this study have undergone a complex evolution, with a shifting balance between carbon sinks and sources. Estimates for the southern North Sea region based on peats identified in this study suggest that currently undiscovered postglacial peats account for approximately 6 times the UK's annual greenhouse emissions (Chapter 5). The fate of the liberated carbon throughout wetland evolution is not clear. The flux of organic carbon in peatlands as a result of climate driven processes remain poorly understood (Limpens et al., 2008), and the extent to which the continued development of the offshore environment will impact carbon stocks held in buried peats remain unclear. Significant loss of CO<sub>2</sub> from modern coastal systems resulting from disturbance and oxidation of soils/sediments caused by anthropogenic activity have been documented (Lovelock et al., 2017). The loss of vegetation cover due to anthropogenic or changing environmental processes generally leads to an increase of microbial activity, as decomposers continue to mineralise organic stores. In the event that anoxic conditions prevail, decomposition of remaining organic stores will remain low. Furthermore, loss of vegetation cover alters sediment properties, potentially exposing sediments to enhanced erosion (Lovelock et al., 2017). The complexity of coastal systems with respect to processes impacting the flux of carbon (carbon stocks) across sediments and soils means further work is required. It is still not clear if exposure of peats to marine conditions following erosion will lead to an increase in oxidation of carbon stocks. Understanding these processes are highly pertinent given the acceleration in the expansion of infrastructure in the offshore environment for renewable energy.

### **6.3. How does inherited stratigraphic architecture influence present-day seabed sediment and bedform configuration in the southern North Sea?**

Inherited topography and substrate heterogeneity are known to control sediment distribution, supply, and morphology. On a coastal plain setting, the character (orientation, gradient etc.) of the antecedent topography can influence the erosional and depositional patterns during marine transgression (Green et al., 2018). Slope gradient has important connotations for the interaction between the palaeo-shelf/coastal plain and the rising wave bases during transgression (Cattaneo et al., 2003). On steeper shelves exposed for the same unit of time of relative sea-level rise, the effects of erosion are far greater than on gentler sloping shelves. The effects of antecedent topography on sediment supply and the preservation of depositional environments have been investigated by many authors (Emery et al., 2019; Green et al., 2018; Dillenburg et al., 2000). In contrast, the effect of heterogeneous substrates is poorly studied in siliciclastic

systems. The southern North Sea offers an opportunity to investigate how antecedent topography and/or substrate have influenced sediment distribution and morphology, in a transgressive, low relief shelf environment from Middle Pleistocene to present-day.



**Figure 6.8. Position and orientation of Holocene sandbanks and Anglian/Elsterian tunnel valleys, and propagation direction of southern North Sea tidal regime. A) Approximately north-south trending sandbanks (red) overlain by older tunnel valleys. The position, extent, and orientation of the sand banks and tunnel valleys is very similar. B) Present-day bathymetry with position and orientation of sand banks, and present-day propagation direction of tidal wave in the southern North Sea.**

The alignment of tunnel valley-fills and sand banks on the modern sea floor in terms of orientation, location and scale is striking (Figure 6.8 A, Chapter 3 and 4). Both tunnel valleys and sand banks are orientated approximately northeast-southwest. This may be coincidental. However, antecedent topography related to basin configuration can be a forcing factor in controlling the orientation of these features, and/or localised antecedent topography or substrate variability. Tunnel valleys in the southern North Sea formed as meltwater conduits that drained to the south, and then infilled as the ice sheet retreated northwards (Praeg, 2003). If the primary direction of ice sheet retreat, as well as the regional drainage paths are controlled by basin configuration (Bradwell et al., 2008), it is reasonable to conclude that tunnel valley orientation is also controlled by basin configuration. The origin of sand-banks identified here and across the southern North Sea (Dyer et al., 1999) is not clear. However, a number of possible origins have been presented in the published literature. Theories of sand bank origin in the southern North Sea include being relict features that developed during sea-level

rise, or that they are dynamic features that formed in response to modern shelf processes. Sand banks may lose the evidence of their inception once the initial sediment source is removed, and will tend to converge on an equilibrium with the tidal hydrodynamics that characterises the present-day seabed (Dyer et al., 1999, Figure 6.8 B). With the origin of sand banks remaining unclear, it is difficult to confidently link tunnel valley and sand banks. However, it is conceivable that the common orientation of both tunnel valleys and sand banks are strongly linked to a shared basin configuration (topography), regardless of later sand bank reworking by tidal hydrodynamics. The tunnel valley-fills are overlain by fine-grained marine sediments (Brown Bank Fm., Chapter 3). Localised topography associated with the upper boundary of the tunnel valley-fills due to differential compaction may have provided subtle nucleation points that influenced Holocene seabed hydrodynamics. However, there is no direct evidence to support this observed in the study area and the position and orientation of the younger sand banks are not considered to be controlled by tunnel valley-fill substrate.

The seabed within the northern parts of Norfolk Vanguard West and Boreas are characterised by sediment waves that are either superimposed on north-south trending sand banks or are within the trough of the sand banks (Chapter 4). In the south of Norfolk Vanguard West and Boreas, the Holocene marine sediments (excluding sand banks) are thinner, with only a thin veneer (< 0.4 m) present. The distribution of Holocene marine sediments over the study areas correlates with the distribution of postglacial peats. The postglacial peats are found within the northern half of the study areas with the exception of peats associated with the channel margins of the post glacial fluvial network (Chapter 4). The distribution of peats and sediment waves may be controlled by the underlying antecedent substrate (top peat surface), but this is unlikely to be the only factor governing the present-day distribution of the sediment waves. The patterns of distribution and bedform type are more likely controlled by multiple elements in the system. Bedform fields result from interactions between individual bedforms, giving rise to field scale patterns. This self-organisation is a characteristic of complex systems, which are typically dissipative, and involving a large number of components governed by non-linear dynamics (Kocurek et al., 2009). Given that the sand banks underlie large parts of the sediment wave field, it is unlikely that postglacial peats played a key role driving distribution of sediment waves, given they largely lack a direct interface with the peats. It is more feasible that the sand bank distribution, supply of sediment, and regional hydrodynamics are more critical components driving sediment wave distribution.



#### **6.4. How do low relief landscapes respond to and record changes in relative sea-level?**

Submerged and preserved coastal plain landscapes can provide insights into future coastal responses to relative sea-level change. The preservation of geomorphological features and their continued evolution in relation to antecedent topography (Green et al., 2018), and sediment supply (Mellett et al., 2012), record important information on coastal evolution in time and space in the context of postglacial sea-level change. The preservation potential of geomorphological features that record landscape evolution in response to relative sea-level rise is often complicated. The effect of eustatic sea level on low relief coastal plains is often compounded by effects of subsidence (Davis, 1987), and the way in which a coastal landscape responds to relative sea-level change is often highly dependent on sediment supply. Fluvially influenced coastal plains may expect to receive sufficient sediment to keep pace with relative sea-level rise, but those that have little sediment supply will often degrade (Reed, 1990). However, coastal processes are often more complex, with rapid relative sea-level rise often associated with an increase in deposition of organic sediments, and slow sea-level rise associated with decreased sedimentation (Mudd et al., 2009). In addition, the gradient of shelf landscapes has implications for glacial process, given that erosive processes are often selective (along valleys) on high relief terrain, and less erosive on low relief surfaces (Sugden, 1968; Hall et al., 2013), and understanding the relationship between process response and shelf gradient can inform ice sheet models. Investigation of the preserved stratigraphic record of the low relief southern North Sea shelf offers the opportunity to investigate the evolution of geomorphological features in the context of future sea-level rise with the potential to inform climate driven processes such as ice sheet dynamics.

Multiple cycles of relative sea-level rise and fall characterise the Middle to Late Pleistocene. Distinct geomorphological features preserved in the stratigraphic record support marked changes in sedimentary process over a low relief landscape, responding to changes in sea level. The valley-fill seismic architecture recorded in the Yarmouth Roads Fm. stratigraphy support a shift in depositional process, from terrestrial to marginal marine (Chapter 3). The lack of chronological constraints limits control on age relationships between the valleys, but preservation of the valley-fills supports an origin in the latter stages of the Cromerian stage, over a relatively short time period. With sediment supply outpacing isostatic subsidence during this time, the delta plain configuration would have been shallow, with relatively minor changes in relative sea level leading to marked changes in shoreline position and depositional

processes. The change in shoreline position would have driven changes in the drainage system that is reflected in the different valley-fills observed in the study area.

Dune-scale bedforms identified within the Brown Bank Fm., that formed during an overall regressive phase leading up to the Devensian glaciation, support fluctuations in sea level during this time, driving changes in sedimentary process (Chapter 3). The relative sea level history within the study area remains unclear without more chronostratigraphic and palaeoenvironmental data. However, the presence of dune-scale bedforms supports the introduction of higher energy tidal process at the location, resulting from coastal realignment through either relative sea level fall or rise. The preservation of the dunes, and capping by fine-grained marine sediments, favours two processes: 1) an abrupt cessation in tidal currents, or 2) enlargement or reduction in the water body. The instigation of either process over relatively short periods of time is enhanced by the low relief shelf setting, whereby minor changes in relative sea level culminate in significant lateral transgression or regression.

Postglacial marine transgression following the LGM led to the evolution of the study area from freshwater coastal plain, through marginal marine, to fully marine. The marine transgression saw fluvial channels repurposed as tidal drainage channels and estuaries, with accumulation of marine sediment (Chapter 4). Several origins have been put forward to account for the incisional features (Chapter 4) identified across the study areas. These include the formation of tidal drainage networks that extended inland with continued transgression. These drainage channels would then be either eroded and/or filled and buried, thus accounting for the lack of connectivity between the features and a planimetric form not typical of channels. These features can also represent tidal ponds that formed in response to sea-level rise, as the marsh surface failed to keep pace with the rising sea level. Tidal ponds origin would account for the isolated nature of the features and the planimetric form.

The absence of preserved barrier systems is notable as these features have been documented at a number of locations in the southern North Sea and English Channel (Mellett et al., 2012; Mellett and Plater, 2018; Emery, et al., 2019). Their absence reflects the complex interplay between the rate of RSL rise, sediment availability, coastal hydrodynamic regime, and low relief topography (Cowell and Thom, 1994; Roy et al., 1994; Emery, et al., 2019) that controls barrier evolution and ultimate preservation. The absence of clear barrier environments supports complete reworking during rollover, and redistribution of sediment (Cooper et al., 2018).

## **6.5. Application of research**

### **6.5.1. Offshore wind farms**

Large and comprehensive data sets are acquired by wind farm developers to access the subsurface and seabed conditions to determine site suitability and the correct engineering solution for the development. Often the data acquisition programs are designed to ensure an efficient and optimum recovery of data, as well as an even spread of sample points across the survey area, whilst also being constrained by budget. This approach means that often critical stratigraphic and geomorphological features are left untested. The approach of this research has been to develop a stratigraphic framework for the working area, through characterisation of stratigraphic units and surfaces and the assignment of depositional environments, which then have enabled these units to be placed in regional context within the previously defined formal lithostratigraphic framework (Chapter 3). Through detailed seismic facies analysis, integration with core and geotechnical logs and characterisation of geomorphological features within the stratigraphic units, a detailed understanding of depositional environments and palaeogeographies can be constructed. This approach can be capitalised on by the offshore wind farm developers, by offering predictive tools to help capture important lateral changes in the subsurface conditions, that would then directly feed into ground models. Wind turbine placement could then be refined through acquisition of additional intrusive measurements (CPTs, boreholes, vibrocores) at locations deemed geologically unusual (e.g. Tunnel Valleys and channels (Chapter 3 and 4), relict bedforms (Chapter 3)) within the context of the wider development area. The gaps in the geotechnical understanding of ground conditions may lead to incorrect prognosis of the subsurface, and consequently incorrect selection of wind turbine foundation type.

### **6.5.2. National carbon capital**

Given that the Early Holocene relative sea-level rise was more than an order of magnitude greater than that projected for the future (Henman et al., 2008), submerged and buried Early Holocene coastal plain landscapes offer a valuable analogue through which to understand and plan for the future landscape changes brought on by relative sea-level rise. In particular, understanding the erosive and degradational processes that led to and continue to impact the present-day configuration of buried peats will help understand the risk of carbon stocks held in modern coastal wetlands, and also the importance of buried peat carbon stocks. Buried peats are not presently considered in the national carbon capital (Office for National Statistics, 2016), but with more

detailed studies of buried peat carbon stocks, similar to those done here (Chapter 5), as a consequence of more offshore development projects, a case for their inclusion in the national carbon capital can be considered.

## **6.6. Future work**

### **6.6.1. Peat thickness classification using CPTs – pitfalls and limitations.**

Peats are often easily recognised in the subsurface, a result of its contrasting properties compared to the sediments overlying and underlying it. Peats identified in this study have been characterised in the seismic data by high amplitude seismic reflectors, that are tabular and laterally discontinuous. In CPTs they are characterised by a high friction ratio, compared with underlying silts and overlying sands which have comparatively low friction ratios. Given the relative ease of peat identification, the thickness of peat deposits defined using seismic data or CPTs is often exaggerated when compared to peat thicknesses measured in sediment cores (Chapter 5). As found in this study, peats are often associated with organic-rich sediments of fluvial and/or estuarine origin. These organic-rich sediments often exhibit the same response in seismic and CPTs as peat and therefore lead to over estimation of peat thickness. Sediment cores enable a more exact estimate of peat thickness, however, can also lead to overestimates of peat thickness, depending on how peats are classified; through visual inspection or using % organic carbon (Chapter 5). With large areas of the southern North Sea likely to contain peats of postglacial origin (Chapter 4 and 5), and the number of offshore engineering projects increasing as a result of increase in demand for renewable energy, understanding the vulnerability of buried peats through erosion as a consequence of offshore developments is increasingly important. This is compounded by future projections of sea-level rise (IPCC, 2013) that may lead to changes in the southern North Sea hydrodynamic regime and increased erosion of the seabed and underlying sediments. With CPTs being the most common means of geotechnically characterising the subsurface in the Southern North Sea, as well as effective peat indicators, estimates of regional peat distribution can be made, and then thickness estimated based on CPTs be refined through integration of sediment core data were available, leading to more meaningful estimates of carbon stocks associated with postglacial peats.

### **6.6.2. Provenance of Middle Pleistocene fluvial channel fills**

The offshore extension of fluvial drainage networks northwards into the southern North Sea during the Middle Pleistocene is widely recognised (Cameron et al., 1987;

Cameron et al., 1992; Funnell, 1996; Eaton et al., 2020), however the origin and provenance of channels morphologies and fills is poorly understood. The origin and provenance of channels has remained a point of debate (Gibbard, 1988) as no direct sampling of channel fill lithofacies has been achieved. This is largely due to the depth at which these channel fills are found, typically beyond the reach of vibrocores, and often missed by boreholes that do not directly target them. Sediment samples from channel fills would help with provenance and inform palaeogeographical constructions. With an increasing number of wind farm data sets being acquired, that often include deep boreholes it may be possible to place channel fills in a chronostratigraphic framework and also to trace back channel systems to near onshore using multiple seismic surveys, in particular cable route seismic surveys, that bridge the onshore to offshore environments.

## **6.7. Conclusions**

### **6.7.1. How does integrated subsurface data required for offshore windfarms improve understanding of Quaternary palaeo-drainage networks feeding into the southern North Sea basin?**

Middle to Late Pleistocene drainage networks have been discussed in chapters 3 and 4. The study has shown that over the course of the Middle to Late Pleistocene and including a period in the Late Devensian and Early Holocene, drainage networks feeding into and within the southern North Sea basin have been dynamic and highly responsive to change, including changes that are related to regional tectonics and those that are climatically driven. Interpretation of drainage features at multiple stratigraphic levels has only been possible due to the high resolution of data available to this study. These interpretations have then been placed in the regional framework, previously defined using sparser and lower resolution data than used here, to improve regional scale understanding of Quaternary palaeo-drainage networks feeding into the North Sea basin.

Between ~MIS 19 to 13 drainage into and within the study area were predominantly from the south and south west, with river systems from mainland Europe such as the Rhine-Meuse and from south-eastern England such as the Thames and Bytham, being the primary drainage routes. Progradation of the Ur-Frisia Delta into the North Sea Basin controlled the northward extension of drainage networks. The fills associated with these drainage systems has remains largely uncharacterised in terms of provenance due to a lack of core samples. However, seismic stratigraphic

interpretation and facies analysis of valley fills, as documented in this study, support a marked change in environment of deposition, characteristic of a drainage system responding to changes in relative sea levels, driven by glacial-interglacial cycles. With the onset of the Anglian glaciation (~MIS 12) drainage networks that previously extended northwards into the North Sea basin retreated and instead most likely drained into a large proglacial lake, dammed to the north by the Anglian ice sheet. Overspill from this proglacial lake drained southwards through the channel. In addition to northwards drainage into the proglacial lake, tunnel valley of Anglian age support subglacial drainage southward towards the ice-margin. Following the Late Glacial Maximum, drainage in the study area switched to southwards draining, likely in part controlled by antecedent topography created in response to the breaching of the Dover Strait. These drainage channels only reflect the semi regional drainage patterns, with drainage patterns over the southern North Sea region being more complex and driven by a range of factors, including deglaciation and topographic configuration of the shelf

#### **6.7.2. Are buried and submerged postglacial peats a carbon sink or source, and should they be a consideration in carbon stock estimates?**

Extensive postglacial peat deposits have been documented across the study area. These peats developed in a coastal plain wetland environment and would have acted as a major sink for atmospheric carbon. With the onset of the Holocene interglacial period following the Late Glacial Maximum, the effectiveness of the wetland environment to absorb carbon would have increased initially though plant growth. However, documented fluvial channels and deposits support a landscape dominated by fluvial activity during this period, this would have led to increased erosion of the wetlands, with destruction of peats and conversion of some areas of wetlands from carbon sink to source. With sea levels continuing to rise, the dissection, erosion and degradation of coastal wetlands and associated deposits would have increased. Incisional features with origins as tidal channels and/or tidal ponds support this marked change in environmental, and the decrease in effectiveness of the wetland as a carbon sink. The burial and preservation, aided by the low relief shelf and slow subsidence of the southern North Sea, led to stabilisation of the peat deposits and a slowing in the rate of carbon loss. However, with establishment of full marine conditions over the study area, a tidal system was established with associated erosive tidal processes. Peats that were buried under shallow marine sands were subjected to scour processes, and consequent excavation. Mobile seabed sediments, documented using repeat bathymetric surveys, support the continued erosion of the seabed and the underlying peat deposits, and conversion of peat deposits from carbon sink to source.

With a change of land-use in offshore environments driven by increased activity in the offshore renewable energy sector, understanding the distribution and carbon value of buried peats is becoming increasingly important. The increase in availability of high resolution shallow subsurface data has enabled the identification and characterisation of these peats and improved understanding of the carbon stocks associated with them. With a clearer understanding of the impacts that renewable energy infrastructure has on habitats, such as erosional scour, it becomes increasingly important that carbon stocks associated with buried peats be considered in national carbon inventories and in planning for future developments.

### **6.7.3. How does inherited stratigraphic architecture influence present-day seabed sediment and bedform configuration in the southern North Sea?**

The similar orientation and position of Anglian tunnel valleys and Holocene sand banks are considered here to be primarily controlled by basin configuration as opposed to antecedent topography or substrate related to tunnel valley origin. A controlling factor on Anglian ice sheet advance southwards was the configuration of the North Sea basin, with ice flow guided by basin topography. Similarly, sand banks which formed in response to the establishment of a tidal regime are more strongly influenced by basin configuration in terms of their orientation and position, as opposed to tunnel valley fills, given regional tidal regimes are strongly influenced by basin configuration. Rather than antecedent topography and substrate acting as controls of orientation and position of these features, it is more plausible that the basin configuration shared by both features has led to their common attributes.

The present-day distribution of sediment waves and postglacial peats show similar relationship in terms of spatial distribution. However, no supporting evidence has been found to establish a link between sediment wave spatial distribution and antecedent topography and/or substrate associated with postglacial peats. A preferred explanation is that the current sediment waves distribution and position is controlled by multiple elements in the environment that give rise to complex interactions between bedforms and the establishment of field-scale patterns. These elements include sand bank distribution, sediment supply and regional hydrodynamics.

### **6.7.4. How do low relief landscapes respond to/record changes in relative sea-level changes?**

Throughout the Quaternary period high levels of sediment supply into the North Sea basin and comparatively low subsidence rates have engendered a consistently low

relief shelf environment. Consequently, a range of stratigraphic and geomorphological features are preserved that record the landscape and sedimentary processes response to relative sea-level change over a low relief landscape.

The valley-fill architecture recorded in the Yarmouth Roads Fm. stratigraphy support a change in sedimentological process, from terrestrial to marginal marine (Chapter 3). This shallow shelf, over which the valley formed, and fills were deposited was sensitive to minor changes in relative sea-level, with small rises or falls in sea level resulting in large shifts in shoreline position. The change in depositional process associated with shifts in shoreline position are recorded in the valley-fill architecture, interpreted as switches in depositional environment from terrestrial to marginal marine.

During an overall regressive phase, leading up to the Devensian glaciation, fluctuations in relative sea level are recorded in the stratigraphy by dune-scale bedforms. Although the relative sea level history remains unclear in the area, the presence of dune-scale bedforms of tidal origin, supports the introduction of higher energy tidal processes, resulting from shoreline migration and coastal realignment through relative sea-level fall or rise. This marked change in coastal configuration is possible due to the low relief shelf setting, whereby minor changes in relative sea level impart significant lateral migration of shoreline position and complex flooding patterns.

The transgression of the southern North Sea region during the Holocene is recorded in the postglacial stratigraphy. Fluvial channels that dominated the postglacial landscape were repurposed as tidal drainage channels and this is supported by sediment fill of marine origin within a previously freshwater channel. Incisional features either represent relict tidal drainage channels or tidal ponds, both forming in response to relative sea-level rise. The absence of barrier deposits is notable and may reflect the low relief shelf setting, whereby complete reworking during rollover, led to redistribution of sediment.

#### **6.7.5. Concluding statement**

The preserved stratigraphy and geomorphologies at the location of this study provide useful insights into how landscapes have evolved in response to a changing climate from Middle Pleistocene to present day. The unique configuration of the southern North Sea Basin and its proximity to ice sheets from Middle Pleistocene has led to meaningful insights into the evolution of drainage networks over multiple glacial interglacial cycles. Dramatic switches in the regional drainage directions have been documented that are strongly related to the low relief shelf configuration that has



characterised the southern North Sea throughout the Quaternary. From Middle Pleistocene to present day the sedimentary archive has recorded the landscape response to changes in relative sea level in a low relief shelf setting. Valley-fills deposited in the Middle Pleistocene record dramatic shift in shoreline position. This was followed by subglacial conditions and a reversal in drainage direction. The postglacial stratigraphy following LGM record changes detailed changes in sedimentary process as coastal landscapes evolve from terrestrial to fully marine. Extensive postglacial peats deposits preserved in the study area not only enable detailed reconstruction of coastal evolution during a marine transgressive phase but also give valuable insights into the carbon stocks associated with buried peats and the long-term storage potential.

Furthermore, the ground conditions at the study area location are now better constrained as a result of the work done during this PhD research. This can provide valuable information for development of offshore wind farms and help to minimise costs. Through this PhD research, the potential for research using industry datasets has been shown and highlights the importance for collaboration between industry and academia.

## Reference

- Adam, P. 2002. Saltmarshes in a time of change. *Environmental Conservation*. [Online]. **29**(1),pp.39–61. Available from: <https://www.jstor.org/stable/44520561>.
- Ainsworth, R.B., Vakarelov, B.K., MacEachern, J.A., Rarity, F., Lane, T.I. and Nanson, R.A. 2017. Anatomy of a shoreline regression: Implications for the high-resolution stratigraphic architecture of Deltas *In: Journal of Sedimentary Research* [Online]. GeoScienceWorld, pp. 425–459. Available from: <https://doi.org/10.2110/jsr.2017.26%0A>.
- Allen, J.R.L. 1989. Evolution of salt-marsh cliffs in muddy and sandy systems: A qualitative comparison of British West-Coast estuaries. *Earth Surface Processes and Landforms*. **14**(1),pp.85–92.
- Allen, J.R.L. 2000. Morphodynamics of Holocene salt marshes: A review sketch from the Atlantic and Southern North Sea coasts of Europe. *Quaternary Science Reviews*. [Online]. **19**(12),pp.1155–1231. Available from: [https://doi.org/10.1016/S0277-3791\(99\)00034-7](https://doi.org/10.1016/S0277-3791(99)00034-7).
- Ashley, G.M. 1990. Classification of Large-Scale Subaqueous Bedforms: A New Look at an Old Problem-SEPM Bedforms and Bedding Structures. *Journal of Sedimentary Research*. [Online]. **60**(1),pp.160–172. Available from: <http://archives.datapages.com/data/sepm/journals/v59-62/data/060/060001/0160.htm?doi=10.1306/212F9138-2B24-11D7-8648000102C1865D>.
- van Asselen, S., Cohen, K.M. and Stouthamer, E. 2017. The impact of avulsion on groundwater level and peat formation in delta floodbasins during the middle-Holocene transgression in the Rhine-Meuse delta, The Netherlands. *Holocene*. **27**(11),pp.1694–1706.
- Baeteman, C., Waller, M. and Kiden, P. 2011. Reconstructing middle to late Holocene sea-level change: A methodological review with particular reference to ‘A new Holocene sea-level curve for the southern North Sea’ presented by K.-E. Behre. *Boreas*. **40**(4),pp.557–572.

- Ballin, T.B. 2017. Rising waters and processes of diversification and unification in material culture: the flooding of Doggerland and its effect on north-west European prehistoric populations between ca. 13 000 and 1500 cal BC. *Journal of Quaternary Science*. [Online]. **32**(2),pp.329–339. Available from: <https://doi.org/10.1002/jqs.2834>.
- Balson, P.S. and Jeffery, D.H. 1990. The glacial sequence of the southern North Sea *In: J. Ehlers, P. Gibbard and J. Rose, eds. Glacial Deposits in Great Britain and Ireland*. Balkema, Rotterdam, pp. 245–253.
- Bassinot, F.C., Labeyrie, L.D., Vincent, E., Quidelleur, X., Shackleton, N.J. and Lancelot, Y. 1994. The astronomical theory of climate and the age of the Brunhes-Matuyama magnetic reversal. *Earth and Planetary Science Letters*. [Online]. **126**(1–3),pp.91–108. Available from: [https://doi.org/10.1016/0012-821X\(94\)90244-5](https://doi.org/10.1016/0012-821X(94)90244-5).
- Bateman, M.D. 1998. The origin and age of coversand in North Lincolnshire, UK. *Permafrost and Periglacial Processes*. [Online]. **9**(4),pp.313–325. Available from: [https://doi.org/10.1002/\(SICI\)1099-1530\(199810/12\)9:4%3C313::AID-PPP297%3E3.0.CO;2-P](https://doi.org/10.1002/(SICI)1099-1530(199810/12)9:4%3C313::AID-PPP297%3E3.0.CO;2-P).
- Bateman, M.D., Hitchens, S., Murton, J.B., Lee, J.R. and Gibbard, P.L. 2014. The evolution of periglacial patterned ground in East Anglia, UK. *Journal of Quaternary Science*. [Online]. **29**(4),pp.301–317. Available from: <https://doi.org/10.1002/jqs.2704>.
- Baustian, J.J., Mendelssohn, I.A. and Hester, M.W. 2012. Vegetation's importance in regulating surface elevation in a coastal salt marsh facing elevated rates of sea level rise. *Global Change Biology*. **18**(11),pp.3377–3382.
- Beets, D.J., Meijer, T., Beets, C.J., Cleveringa, P., Laban, C. and van der Spek, A.J.F. 2005. Evidence for a Middle Pleistocene glaciation of MIS 8 age in the southern North Sea. *Quaternary International*. [Online]. **133–134**,pp.7–19. Available from: <https://doi.org/10.1016/j.quaint.2004.10.002>.

- Beets, D.J. and Van Der Spek, A.J.F. 2000. The Holocene evolution of the barrier and the back-barrier basins of Belgium and the Netherlands as a function of late Weichselian morphology, relative sea-level rise and sediment supply. *Netherlands Journal of Geosciences*. [Online]. **79**(1),pp.3–16. Available from: <https://doi.org/10.1017/S0016774600021533>.
- Behre, k. H. 2007. A new Holocene sea-level curve for the southern North Sea. *Boreas*. **36**(1),pp.82–102.
- Bicket, A. and Tizzard, L. 2015. A review of the submerged prehistory and palaeolandscapes of the British Isles. *Proceedings of the Geologists' Association*. [Online]. **126**,pp.643–663. Available from: <https://doi.org/10.1016/j.pgeola.2015.08.009>.
- Blanco, G., Gerlagh, R., Suh, S., Barrett, J., de Coninck, H., Diaz Morejon, C., Mathur, R., Nakicenovic, N., Ofosu-Ahenkora, A., Pan, J., Pathak, H., Rice, J., Richels, R., Smith, S., Stern, D., Toth, F. and Zhou, P. 2014. *Drivers, Trends and Mitigation*. In: *Climate Change: Mitigation of Climate Change. Contribution of Working Group III to the Fifth Assessment Report of the Intergovernmental Panel on Climate Change*.
- Bogemans, F., Roe, H.M. and Baeteman, C. 2016. Incised Pleistocene valleys in the Western Belgium coastal plain: Age, origins and implications for the evolution of the Southern North Sea Basin. *Palaeogeography, Palaeoclimatology, Palaeoecology*. [Online]. **456**,pp.46–59. Available from: <http://dx.doi.org/10.1016/j.palaeo.2016.04.047>.
- Bourillet, J.F., Reynaud, J.Y., Baltzer, A. and Zaragosi, S. 2003. The 'Fleuve Manche': The submarine sedimentary features from the outer shelf to the deep-sea fans. *Journal of Quaternary Science*. **18**(3–4),pp.261–282.
- Bowen, D.Q., Rose, J., McCabe, A.M. and Sutherland, D.G. 1986. Correlation of quaternary glaciations in England, Ireland, Scotland and Wales. *Quaternary Science Reviews*. [Online]. **5**(C),pp.299–340. Available from: [http://dx.doi.org/10.1016/0277-3791\(86\)90194-0](http://dx.doi.org/10.1016/0277-3791(86)90194-0).
- Bowler, M. and Bradshaw, R. 1985. Recent Accumulation and Erosion of Blanket Peat in the Wicklow Mountains, Ireland. *New Phytologist*. [Online]. **101**(3),pp.543–550. Available from: <https://doi.org/10.1111/j.1469-8137.1985.tb02859.x>.

- Bradwell, T., Stoker, M.S., Golledge, N.R., Wilson, C.K., Merritt, J.W., Long, D., Everest, J.D., Hestvik, O.B., Stevenson, A.G., Hubbard, A.L., Finlayson, A.G. and Mathers, H.E. 2008. The northern sector of the last British Ice Sheet: Maximum extent and demise. *Earth-Science Reviews*. [Online]. **88**(3–4),pp.207–226. Available from: <https://doi.org/10.1016/j.earscirev.2008.01.008>.
- Brew, D.S. 1996. Late Weichselian to early Holocene subaqueous dune formation and burial off the North Sea Northumberland coast. *Marine geology*. [Online]. **134**,pp.203–211. Available from: [https://doi.org/10.1016/0025-3227\(96\)00045-X](https://doi.org/10.1016/0025-3227(96)00045-X).
- Briant, R.M., Coope, G.R., Preece, R.C., Keen, D.H., Boreham, S., Griffiths, H.I., Seddon, M.B. and Gibbard, P.L. 2004. Fluvial system response to Late Devensian ( Weichselian ) aridity , Baston , Lincolnshire , England. *Journal of Quaternary Science*. **19**(5),pp.479–495.
- Briant, R.M., Gibbard, P.L. and Preece, R.C. 2004. Evidence for early Devensian (Weichselian) fluvial sedimentation: Geochronological and palaeoenvironmental data from the Upper Pleistocene deposits at Deeping St James, Lincolnshire, England. *Quaternaire*. **15**(1–2),pp.5–15.
- Bridgland, D.R. 2002. Fluvial deposition on periodically emergent shelves in the Quaternary : example records from the shelf around Britain. *Quaternary International*. [Online]. **92**,pp.25–34. Available from: [https://doi.org/10.1016/S1040-6182\(01\)00112-4](https://doi.org/10.1016/S1040-6182(01)00112-4).
- Bridgland, D.R. and D'Olier, B. 1995. The Pleistocene evolution of the Thames and Rhine drainage systems in the southern North Sea Basin. *Island Britain: a Quaternary perspective. Geological society Special Publication*. [Online]. (96),pp.27–45. Available from: <https://doi.org/10.1144/GSL.SP.1995.096.01.04>.
- Briggs, K., Thomson, K. and Gaffney, V. 2007. A Geomorphological Investigation of Submerged Depositional Features within the Outer Silver Pit, Southern North Sea *In: Mapping Doggerland. The Mesolithic Landscapes of the Southern North Sea*. Archaeopress (Oxford), pp. 43–59.
- Brown, A., Russell, J., Scaife, R., Tizzard, L., Whittaker, J. and Wyles, S.F. 2018. Lateglacial/early Holocene palaeoenvironments in the southern North Sea Basin: new data from the Dudgeon offshore wind farm. *Journal of Quaternary Science*. **33**(6),pp.597–610.

- Bruno, L., Campo, B., Di Martino, A., Hong, W. and Amorosi, A. 2019. Peat layer accumulation and post-burial deformation during the mid-late Holocene in the Po coastal plain (Northern Italy). *Basin Research*. **31**(3),pp.621–639.
- Bull, S. 2019. Offshore wind's key role in the global energy transition. *First Break*. [Online]. **37**(7),pp.47–49. Available from: <https://doi.org/10.3997/1365-2397.n0037>.
- Burrows, M.T., Hughes, D.J., Austin, W.E.N., Smeaton, C., Hicks, N., Howe, J.A., Allen, C., Taylor, P. and Vare, L.L. 2017. *Assessment of Blue Carbon Resources in Scotland 's Inshore Marine Protected Area Network*.
- Burrows, M.T., Kamenos, N.A., Hughes, D.J., Stahl, H., Howe, J.A. and Tett, P. 2014. *Assessment of carbon budgets and potential blue carbon stores in Scotland's coastal and marine environment, Scottish Natural Heritage Commissioned Report No. 761*.
- Busschers, F.S., Van Balen, R.T., Cohen, K.M., Kasse, C., Weerts, H.J.T., Wallinga, J. and Bunnik, F.P.M. 2008. Response of the Rhine-Meuse fluvial system to Saalian ice-sheet dynamics. *Boreas*. **37**(3),pp.377–398.
- Busschers, F.S., Kasse, C., van Balen, R.T., Vandenberghe, J., Cohen, K.M., Weerts, H.J.T., Wallinga, J., Johns, C., Cleveringa, P. and Bunnik, F.P.M. 2007. Late Pleistocene evolution of the Rhine-Meuse system in the southern North Sea basin: imprints of climate change, sea-level oscillation and glacio-isostasy. *Quaternary Science Reviews*. [Online]. **26**(25–28),pp.3216–3248. Available from: <https://doi.org/10.1016/j.quascirev.2007.07.013>.
- Cameron, T.D.J., Bulat, J. and Mesdag, C.S. 1993. High resolution seismic profile through a Late Cenozoic delta complex in the southern North Sea. *Marine and Petroleum Geology*. [Online]. **10**(6),pp.591–599. Available from: <http://www.sciencedirect.com/science/article/pii/026481729390061V>.
- Cameron, T.D.J., Crosby, A., Balsonn, P.S., Jefferey, D.H., Lott, G.K., Bulat, J. and Harrison, D.J. 1992. *United Kingdom offshore regional report: the geology of the southern North Sea*. London.

- Cameron, T.D.J., Laban, C. and Schuttenhelm, R.T.E. 1989. Upper Pliocene and Lower Pleistocene stratigraphy in the Southern Bight of the North Sea *In*: J. P. Henriët and G. De Moor, eds. *The Quaternary and Tertiary geology of the Southern Bight, North Sea*. Ministry of Economic Affairs - Belgian Geological Survey, pp. 97–110.
- Cameron, T.D.J., Stoker, M.S. and Long, D. 1987. The history of Quaternary sedimentation in the UK sector of the North Sea Basin. *Journal of the Geological Society*. [Online]. **144**(1),pp.43–58. Available from: <https://doi.org/10.1144/gsjgs.144.1.0043>.
- Carniello, L., Defina, A. and D'Alpaos, L. 2009. Morphological evolution of the Venice lagoon: Evidence from the past and trend for the future. *Journal of Geophysical Research: Earth Surface*. [Online]. **114**(4),pp.1–10. Available from: <https://doi.org/10.1029/2008JF001157>.
- Carr, S.J. 2004. The North Sea basin *In*: J. Ehlers and P. L. Gibbard, eds. *Quaternary Glaciations--Extent and Chronology, Part*. Elsevier, pp. 47–82.
- Carr, S.J., Holmes, R., van der Meer, J.J.M. and Rose, J. 2006. The Last Glacial Maximum in the North Sea Basin: Micromorphological evidence of extensive glaciation. *Journal of Quaternary Science*. **21**(2),pp.131–153.
- Castelltort, S. and Van Den Driessche, J. 2003. How plausible are high-frequency sediment supply-driven cycles in the stratigraphic record? *Sedimentary Geology*. [Online]. **157**(1–2),pp.3–13. Available from: [https://doi.org/10.1016/S0037-0738\(03\)00066-6](https://doi.org/10.1016/S0037-0738(03)00066-6).
- Cattaneo, A. and Steel, R.J. 2003. Transgressive deposits: A review of their variability. *Earth-Science Reviews*. **62**(3–4),pp.187–228.
- Chambers, F.M., Beilman, D.W. and Yu, Z. 2011. Methods for determining peat humification and for quantifying peat bulk density, organic matter and carbon content for palaeostudies of climate and peatland carbon dynamics. *Mires and Peat*. [Online]. **7**(7),pp.1–10. Available from: <http://www.mires-and-peat.net/pages/volumes/map07/map0707.php>.

- Chambers, L.G., Davis, S.E., Troxler, T., Boyer, J.N., Downey-Wall, A. and Scinto, L.J. 2014. Biogeochemical effects of simulated sea level rise on carbon loss in an Everglades mangrove peat soil. *Hydrobiologia*. [Online]. **726**(1),pp.195–211. Available from: <https://doi.org/10.1007/s10750-013-1764-6>.
- Charman, D.J., Beilman, D.W., Blaauw, M., Booth, R.K., Brewer, S., Chambers, F.M., Christen, J.A., Gallego-Sala, A., Harrison, S.P., Hughes, P.D.M., Jackson, S.T., Korhola, A., Mauquoy, D., Mitchell, F.J.G., Prentice, I.C., Van Der Linden, M., De Vleeschouwer, F., Yu, Z.C., Alm, J., Bauer, I.E., Corish, Y.M.C., Garneau, M., Hohl, V., Huang, Y., Karofeld, E., Le Roux, G., Loisel, J., Moschen, R., Nichols, J.E., Nieminen, T.M., MacDonald, G.M., Phadtare, N.R., Rausch, N., Sillasoo, U., Swindles, G.T., Tuittila, E.S., Ukonmaanaho, L., Väliranta, M., Van Bellen, S., Van Geel, B., Vitt, D.H. and Zhao, Y. 2013. Climate-related changes in peatland carbon accumulation during the last millennium. *Biogeosciences*. [Online]. **10**(2),pp.929–944. Available from: <https://doi.org/10.5194/bg-10-929-2013>.
- Chmura, G.L. 2013. What do we need to assess the sustainability of the tidal salt marsh carbon sink? *Ocean and Coastal Management*. [Online]. **83**,pp.25–31. Available from: <https://doi.org/10.1016/j.ocecoaman.2011.09.006>.
- Clark, C., Evans, D., Khatwa, A., Bradwell, T., Jordan, C., Marsh, S., Mitchell, W. and Bateman, M. 2004. Map and GIS database of glacial landforms and features related to the last British Ice Sheet. *Boreas*. **33**(4),pp.359–375.
- Clark, C.D., Hughes, A.L.C., Greenwood, S.L., Jordan, C. and Sejrup, H.P. 2012. Pattern and timing of retreat of the last British-Irish Ice Sheet. *Quaternary Science Reviews*. [Online]. **44**,pp.112–146. Available from: <http://dx.doi.org/10.1016/j.quascirev.2010.07.019>.
- Cohen, K.M., Gibbard, P.L. and Busschers, F.S. 2005. *No Title* INQUA-SEQS. (A. Dehnert & F. Preusser, eds.). Bern.
- Cohen, K.M., Gibbard, P.L. and Weerts, H.J.T. 2014. North Sea palaeogeographical reconstructions for the last 1 Ma. *Netherlands Journal of Geosciences*. [Online]. **93**(1–2),pp.7–29. Available from: <https://doi.org/10.1017/njg.2014.12>.



- Cohen, K.M., MacDonald, K., Joordens, J.C.A., Roebroeks, W. and Gibbard, P.L. 2012. The earliest occupation of north-west Europe: A coastal perspective. *Quaternary International*. [Online]. **271**,pp.70–83. Available from: <https://doi.org/10.1016/j.quaint.2011.11.003>.
- Cohen, K.M., Westley, K., Erkens, G., Hijma, M.P. and Weerts, H.J.T. 2017. The North Sea *In*: N. C. Flemming, J. Harff, D. Moura, A. Burgess and G. N. Bailey, eds. *Submerged Landscapes of the European Continental Shelf - Volume 1 Quaternary Paleoenvironments* [Online]. New York: John Wiley & Sons Ltd., pp. 147–186. Available from: <https://onlinelibrary.wiley.com/doi/book/10.1002/9781118927823>.
- Coles, B.J. 1998. Doggerland: a speculative survey. *Proceedings of the Prehistoric Society*. [Online]. **64**,pp.45–81. Available from: <https://doi.org/10.1017/S0079497X00002176>.
- Colombera, L., Mountney, N.P. and Mccaffrey, W.D. 2013. A quantitative approach to fluvial facies models : Methods and example results. *Sedimentology*. **60**(6),pp.1526–1558.
- Coope, G.R., Gibbard, P.L., Hall, A.R., Preece, R.C., Robinson, J.E. and Sutcliffe, A.J. 1997. Climatic and environmental reconstructions based on fossil assemblages from Middle Devensian (Weichselian) deposits of the river Thames at South Kensington, Central London, UK. *Quaternary Science Reviews*. [Online]. **16**(10),pp.1163–1195. Available from: [https://doi.org/10.1016/S0277-3791\(97\)00025-5](https://doi.org/10.1016/S0277-3791(97)00025-5).
- Cooper, J.A.G., Green, A.N. and Loureiro, C. 2018. Geological constraints on mesoscale coastal barrier behaviour. *Global and Planetary Change*. [Online]. **168**(March),pp.15–34. Available from: <https://doi.org/10.1016/j.gloplacha.2018.06.006>.
- Cooper, J.A.G. and Lemckert, C. 2012. Extreme sea-level rise and adaptation options for coastal resort cities: A qualitative assessment from the Gold Coast, Australia. *Ocean & coastal management*. [Online]. **64**,pp.1–14. Available from: <https://doi.org/10.1016/j.ocecoaman.2012.04.001>.

- Cott, G.M., Jansen, M.A.K. and Chapman, D. V. 2012. Salt-Marshes on peat substrate: where blanket bogs encounter the marine environment. *Journal of Coastal Research*. [Online]. **28**(3),pp.700–706. Available from: <https://doi.org/10.2112/JCOASTRES-D-11-00108.1%0A>.
- Cotterill, C.J., Phillips, E., James, L., Forsberg, C.F., Tjelta, T.I., Carter, G. and Dove, D. 2017. The evolution of the Dogger Bank, North Sea: A complex history of terrestrial, glacial and marine environmental change. *Quaternary Science Reviews*. [Online]. **171**,pp.136–153. Available from: <https://doi.org/10.1016/j.quascirev.2017.07.006>.
- Cowell, P.J. and Thom, B.G. 1994. Morphodynamics of coastal evolution *In: Coastal evolution: Late Quaternary shoreline morphodynamics*. Cambridge University Press, Cambridge, United Kingdom and New York, NY, USA, p. 33.
- Crombé, P., Sergeant, J., Robinson, E. and De Reu, J. 2011. Hunter-gatherer responses to environmental change during the Pleistocene-Holocene transition in the southern North Sea basin: Final Palaeolithic-Final Mesolithic land use in northwest Belgium. *Journal of Anthropological Archaeology*. [Online]. **30**(3),pp.454–471. Available from: <https://doi.org/10.1016/j.jaa.2011.04.001>.
- Cullen, T.M., Collier, R.E.L., Gawthorpe, R.L., Hodgson, D.M. and Barrett, B.J. 2020. Axial and transverse deep-water sediment supply to syn-rift fault terraces: Insights from the West Xylokaastro Fault Block, Gulf of Corinth, Greece. *Basin Research*. [Online]. **32**(5),pp.1115–1149. Available from: <https://doi.org/10.1111/bre.12416>.
- Dadey, K.A., Janecek, T. and Klaus, A. 1992. Dry bulk density: its use and determination. *Proceedings of the Ocean Drilling Program, Scientific Results*. **126**,pp.551–554.
- Dargie, G.C., Lewis, S.L., Lawson, I.T., Mitchard, E.T.A., Page, S.E., Bocko, Y.E. and Ifo, S.A. 2017. Age, extent and carbon storage of the central Congo Basin peatland complex. *Nature Publishing Group*. [Online]. **542**,pp.86–90. Available from: <http://dx.doi.org/10.1038/nature21048>.
- Davies, B.J., Roberts, D.H., Bridgland, D.R., Cofaigh, C.Ó. and Riding, J.B. 2011. Provenance and depositional environments of Quaternary sediments from the western North Sea Basin. *Journal of Quaternary Science*. **26**(1),pp.59–75.

- Davies, B.J., Roberts, D.H., Bridgland, D.R., Ó Cofaigh, C., Riding, J.B., Demarchi, B., Penkman, K.E.H. and Pawley, S.M. 2012. Timing and depositional environments of a Middle Pleistocene glaciation of northeast England: New evidence from Warren House Gill, County Durham. *Quaternary Science Reviews*. [Online]. **44**,pp.180–212. Available from: <http://dx.doi.org/10.1016/j.quascirev.2010.02.003>.
- Davies, S.J. 2008. The record of Carboniferous sea-level change in low-latitude sedimentary successions from Britain and Ireland during the onset of the late Paleozoic ice age. *Special Paper of the Geological Society of America*. [Online]. **441**(13),pp.187–204. Available from: [https://doi.org/10.1130/2008.2441\(13\)](https://doi.org/10.1130/2008.2441(13)).
- Davis, G.H. 1987. Land subsidence and sea level rise on the Atlantic Coastal Plain of the United States. *Environmental Geology and Water Sciences*. **10**(2),pp.67–80.
- Díaz, H. and Guedes Soares, C. 2020. Review of the current status, technology and future trends of offshore wind farms. *Ocean Engineering*. [Online]. **209**(March),p.107381. Available from: <https://doi.org/10.1016/j.oceaneng.2020.107381>.
- Dillenburg, S.R., Roy, P.S., Cowell, P.J. and Tomazelli, L.J. 2000. Influence of antecedent topography on coastal evolution as tested by the shoreface translation-barrier model (STM). *Journal of Coastal Research*. [Online]. **16**(1),pp.71–81. Available from: <https://www.jstor.org/stable/4300012>.
- Dove, D., Evans, D.J.A., Lee, J.R., Roberts, D.H., Tappin, D.R., Mellett, C.L., Long, D. and Callard, S.L. 2017. Phased occupation and retreat of the last British–Irish Ice Sheet in the southern North Sea; geomorphic and seismostratigraphic evidence of a dynamic ice lobe. *Quaternary Science Reviews*. [Online]. **163**,pp.114–134. Available from: <http://dx.doi.org/10.1016/j.quascirev.2017.03.006>.
- Du, J., Shen, J., Zhang, Y.J., Ye, F., Liu, Z., Wang, Z., Wang, Y.P., Yu, X., Sisson, M. and Wang, H. V. 2018. Tidal Response to Sea-Level Rise in Different Types of Estuaries: The Importance of Length, Bathymetry, and Geometry. *Geophysical Research Letters*. [Online]. **45**(1),pp.227–235. Available from: <https://doi.org/10.1002/2017GL075963>.
- Duarte, C., Middelburg, J. and Caraco, N. 2005. Major role of marine vegetation on the oceanic carbon cycle. *Biogeosciences*. [Online]. **1**,pp.1–8. Available from: [www.biogeosciences.net/bg/2/1/](http://www.biogeosciences.net/bg/2/1/).

- Dyer, K.R. and Huntley, D.A. 1999. The origin , classification and modelling of sand banks and ridges. *Continental Shelf Research*. [Online]. **19**(10),pp.1285–1330. Available from: [https://doi.org/10.1016/S0278-4343\(99\)00028-X](https://doi.org/10.1016/S0278-4343(99)00028-X).
- Eaton, S., Hodgson, D.M., Barlow, N.L.M., Mortimer, E. and Mellett, C.L. 2020. Palaeogeographic changes in response to glacial-interglacial cycles, as recorded in Middle and Late Pleistocene seismic stratigraphy, southern North Sea. *Journal of Quaternary Science*. **35**(6),pp.760–775.
- Ehlers, J. 1990. Reconstructing the dynamics of the North-west European Pleistocene ice sheets. *Quaternary Science Reviews*. [Online]. **9**(1),pp.71–83. Available from: [https://doi.org/10.1016/0277-3791\(90\)90005-U](https://doi.org/10.1016/0277-3791(90)90005-U).
- Ehlers, J. and Gibbard, P. 2008. Extent and chronology of Quaternary glaciation. *Episodes*. **31**(2),pp.211–218.
- Ehlers, J. and Gibbard, P.L. 2007. The extent and chronology of Cenozoic Global Glaciation. *Quaternary International*. [Online]. **164**,pp.6–20. Available from: <https://doi.org/10.1016/j.quaint.2006.10.008>.
- Ehlers, J. and Wingfield, R. 1991. The extension of the Late Weichselian/Late Devensian ice sheets in the North Sea Basin. *Journal of Quaternary Science*. **6**(4),pp.313–326.
- Emery, A., Hodgson, D., Barlow, N., Carrivick, J., Cotterill, C., Mellett, C. and Booth, A. 2019. Topographic and hydrodynamic controls on barrier retreat and preservation: an example from Dogger Bank, North Sea. *Marine Geology*. [Online]. **416**,p.105981. Available from: <https://doi.org/10.1016/j.margeo.2019.105981>.
- Emery, A., Hodgson, D., Barlow, N., Carrivick, J., Cotterill, C. and Phillips, E. 2019. Left high and dry: deglaciation of Dogger Bank, North Sea, recorded in proglacial lake evolution. *Frontiers in Earth Science*. [Online]. **7**,p.234. Available from: <https://doi.org/10.3389/feart.2019.00234>.
- Emery, A., Hodgson, D., Barlow, N., Carrivick, J., Cotterill, C., Richardson, J., Ivanovic, R. and Mellett, C. 2020. Ice sheet and palaeoclimate controls on drainage network evolution: an example from Dogger Bank, North Sea. *Earth Surface Dynamics Discussion*. [Online]. **8**(4),pp.869–891. Available from: <https://doi.org/10.5194/esurf-8-869-2020>.

- EMODnet Bathymetry Consortium 2018. EMODnet Bathymetry Consortium (2018). EMODnet Digital Bathymetry (DTM 2018). Available from: <https://doi.org/10.12770/18ff0d48-b203-4a65-94a9-5fd8b0ec35f6>.
- Ferret, Y., Le Bot, S., Tessier, B., Garlan, T. and Lafite, R. 2010. Migration and internal architecture of marine dunes in the eastern English Channel over 14 and 56 year intervals : the influence of tides and decennial storms. *Earth Surface Processes and Landforms*. **35**(12),pp.1480–1493.
- Fitch, S., Gaffney, V. and Thomson, K. 2007. In Sight of Doggerland: From speculative survey to landscape exploration. *Internet Archaeology*. [Online]. Available from: <https://doi.org/10.11141/ia.22.3>.
- Fitch, S., Thomson, K. and Gaffney, V. 2005a. Late Pleistocene and Holocene depositional systems and the palaeogeography of the Dogger Bank, North Sea. *Quaternary Research*. **64**(2),pp.185–196.
- Fitch, S., Thomson, K. and Gaffney, V. 2005b. Late Pleistocene and Holocene depositional systems and the palaeogeography of the Dogger Bank, North Sea. *Quaternary Research*. [Online]. **64**(2),pp.185–196. Available from: <https://doi.org/10.1016/j.yqres.2005.03.007>.
- Forbes, D.L., Manson, G.K., Whalen, D.J.R., Couture, N.J. and Hill, P.R. 2014. Coastal products of marine transgression in cold-temperate and high-latitude coastal-plain settings: Gulf of St Lawrence and Beaufort Sea. *Geological Society Special Publication*. [Online]. **388**(1),pp.131–163. Available from: <https://doi.org/10.1144/SP388.18>.
- Freeman, C., Evans, C.D., Monteith, D.T., Reynolds, B. and Fenner, N. 2001. Export of organic carbon from peat soils. *Nature*. [Online]. **412**(6849),pp.785–786. Available from: <https://doi.org/10.1038/35090628>.
- Freeman, C., Fenner, N., Ostle, N.J., Kang, H., Dowrick, D.J., Reynolds, B., Lock, M.A., Sleep, D., Hughes, S. and Hudson, J. 2004. Export of dissolved organic carbon from peatlands under elevated carbon dioxide levels. *Nature*. [Online]. **430**(6996),pp.195–198. Available from: <https://doi.org/10.1038/nature02707>.
- Frey, R.W. and Basan, P.B. 1978. Coastal salt marshes *In*: R. A. Davis, ed. *Coastal sedimentary environments*. Springer, pp. 101–169.

- Fugro 2017. *Norfolk Boreas Offshore Wind Farm Geophysical Investigation Report*.
- Fugro 2016. *Norfolk Vanguard Offshore Wind Farm Geophysical Investigation Report GEO50-R1 Volumes 1-3*.
- Funnell, B.M. 1996. Plio-Pleistocene Palaeogeography of the southern North Sea basin (3.75-0.60 Ma). *Quaternary International*. [Online]. **15**(5–6),pp.391–405. Available from: [https://doi.org/10.1016/0277-3791\(96\)00022-4](https://doi.org/10.1016/0277-3791(96)00022-4).
- Gaffney, V.L., Thomson, K. and Fitch, S. 2007. *Mapping Doggerland: the Mesolithic landscapes of the southern North Sea*. Archaeopress.
- Galloway, W.E. 1976. Copper River Fan-Delta. *Journal of Sedimentary Petrology*. [Online]. **46**(3),pp.726–737. Available from: <https://doi.org/10.1306/212F703B-2B24-11D7-8648000102C1865D%0A>.
- Gatliff, R.W., Richards, P.C., Smith, K., Graham, C.C., McCormac, M., Smith, N.J.P., Long, D., Cameron, T.D.J., Evans, D., Stevenson, A.G., Bulat, J. and Ritchie, J.D. 1994. *United Kingdom offshore regional report: the geology of the central North Sea*. London.
- Gawthorpe, R.L. and Hurst, J.M. 1993. Transfer zones in extensional basins: their structural style and influence on drainage development and stratigraphy. *Journal - Geological Society (London)*. [Online]. **150**(6),pp.1137–1152. Available from: <https://doi.org/10.1144/gsjgs.150.6.1137>.
- Gibbard, P.L. 2007. Europe cut adrift. *Nature*. [Online]. **448**(July),p.259,260. Available from: <https://doi.org/10.1038/448259a>.
- Gibbard, P.L. 1988. The history of the great northwest European rivers during the past three million years. *Philosophical Transactions of the Royal Society of London. B, Biological Sciences*. [Online]. **318**(1191),pp.559–602. Available from: <https://doi.org/10.1098/rstb.1988.0024>.
- Gibbard, P.L. and Cohen, K.M. 2008. Global chronostratigraphical correlation table for the last 2.7 million years. *Episodes*. [Online]. **31**(2),pp.243–247. Available from: <https://doi.org/10.1016/j.quaint.2019.03.009>.

- Gibbard, P.L. and Cohen, K.M. 2015. Quaternary evolution of the North Sea and the English Channel. *Proceedings of the Open University Geological Society*. [Online]. **1**,pp.63–74. Available from: <https://dspace.library.uu.nl/handle/1874/309055>.
- Gibbard, P.L., Pasanen, A.H., West, R.G., Lunkka, J.P., Boreham, S., Cohen, K.M. and Rolfe, C. 2009. Late Middle Pleistocene glaciation in East Anglia, England. *Boreas*. **38**(3),pp.504–528.
- Glennie, K.W. and Underhill, J.R. 1998. Origin, development and evolution of structural styles. In: K. . Glennie, ed. *Petroleum Geology of the North Sea: Basin Concepts and Recent Advances*. Blackwell Science Ltd., Oxford, pp. 42–84.
- Government, U.K. 2019. *2019 UK greenhouse gas emissions, provisional figures* [Online]. Available from: [https://assets.publishing.service.gov.uk/government/uploads/system/uploads/attachment\\_data/file/875485/2019\\_UK\\_greenhouse\\_gas\\_emissions\\_provisional\\_figures\\_statistical\\_release.pdf](https://assets.publishing.service.gov.uk/government/uploads/system/uploads/attachment_data/file/875485/2019_UK_greenhouse_gas_emissions_provisional_figures_statistical_release.pdf).
- Graham, A.G.C., Lonergan, L. and Stoker, M.S. 2007. Evidence for Late Pleistocene ice stream activity in the Witch Ground Basin, central North Sea, from 3D seismic reflection data. *Quaternary Science Reviews*. [Online]. **26**(5–6),pp.627–643. Available from: <https://doi.org/10.1016/j.quascirev.2006.11.004>.
- Graham, A.G.C., Stoker, M.S., Lonergan, L., Bradwell, T. and Stewart, M.A. 2011. The pleistocene glaciations of the North Sea basin. *Developments in Quaternary Science*. [Online]. **15**,pp.261–278. Available from: <https://doi.org/10.1016/B978-0-444-53447-7.00021-0>.
- Green, A.N. 2009. Palaeo-drainage, incised valley fills and transgressive systems tract sedimentation of the northern KwaZulu-Natal continental shelf, South Africa, SW Indian Ocean. *Marine Geology*. [Online]. **263**(1–4),pp.46–63. Available from: <http://dx.doi.org/10.1016/j.margeo.2009.03.017>.
- Green, A.N., Cooper, J.A.G. and Salzmann, L. 2018. The role of shelf morphology and antecedent setting in the preservation of palaeo-shoreline (beachrock and aeolianite) sequences: the SE African shelf. *Geo-Marine Letters*. [Online]. **38**(1),pp.5–18. Available from: <https://doi.org/10.1007/s00367-017-0512-8>.

- Grenfell, S.E., Fortune, F., Mamphoka, M.F. and Sanderson, N. 2019. Coastal wetland resilience to climate change: modelling ecosystem response to rising sea level and salinity in a variable climate. *Anthropocene Coasts*. [Online]. **2**(1),pp.1–20. Available from: <https://doi.org/10.1139/anc-2018-0004>.
- Grossman, E.E., Barnhardt, W.A., Hart, P., Richmond, B.M. and Field, M.E. 2006. Shelf stratigraphy and the influence of antecedent substrate on Holocene reef development, south Oahu, Hawaii. *Marine Geology*. [Online]. **226**(1–2),pp.97–114. Available from: <https://doi.org/10.1016/j.margeo.2005.09.012>.
- Guiot, J., Pons, A., de Beaulieu, J.L. and Reille, M. 1989. A 140,000-year continental climate reconstruction from two European pollen records. *Nature*. [Online]. **338**(6213),pp.309–313. Available from: <https://doi.org/10.1038/338309a0>.
- Gulliford, A.R., Flint, S.S. and Hodgson, D.M. 2014. Testing applicability of models of distributive fluvial systems or trunk rivers in ephemeral systems: reconstructing 3-D fluvial architecture in the Beaufort Group, South Africa. *Journal of Sedimentary Research*. [Online]. **84**(12),pp.1147–1169. Available from: <https://doi.org/10.2110/jsr.2014.88%0A>.
- Gupta, S., Collier, J.S., Garcia-Moreno, D., Oggioni, F., Trentesaux, A., Vanneste, K., De Batist, M., Camelbeeck, T., Potter, G., Van Vliet-Lanoë, B. and Arthur, J.C.R. 2017. Two-stage opening of the Dover Strait and the origin of island Britain. *Nature Communications*. [Online]. **8**(1),pp.1–12. Available from: <https://doi.org/10.1038/ncomms15101>.
- Hall, A.M., Ebert, K., Kleman, J., Nesje, A. and Ottesen, D. 2013. Selective glacial erosion on the Norwegian passive margin. *Geology*. [Online]. **41**(12),pp.1203–1206. Available from: <https://doi.org/10.1130/G34806.1%0A>.
- Hartley, A.J., Weissmann, G.S., Nichols, G.J. and Warwick, G.L. 2010. Large distributive fluvial systems: characteristics, distribution, and controls on development. *Journal of Sedimentary Research*. [Online]. **80**(2),pp.167–183. Available from: <https://doi.org/10.2110/jsr.2010.016%0A>.
- Hazell, Z.J. 2008. Offshore and intertidal peat deposits, England - a resource assessment and development of a database. *Environmental Archaeology*. [Online]. **13**(2),pp.101–110. Available from: <https://doi.org/10.1179/174963108X343227>.



- Head, M.J. and Gibbard, P.L. 2015. Early-Middle Pleistocene transitions: Linking terrestrial and marine realms. *Quaternary International*. [Online]. **389**,pp.7–46. Available from: <http://dx.doi.org/10.1016/j.quaint.2015.09.042>.
- Hede, M.U., Sander, L., Clemmensen, L.B., Kroon, A., Pejrup, M. and Nielsen, L. 2015. Changes in Holocene relative sea-level and coastal morphology: A study of a raised beach ridge system on Samsø, southwest Scandinavia. *The Holocene*. [Online]. **25**(9),pp.1402–1414. Available from: <https://doi.org/10.1177/0959683615585834>.
- Henman, J. and Poulter, B. 2008. Inundation of freshwater peatlands by sea level rise: Uncertainty and potential carbon cycle feedbacks. *Journal of Geophysical Research: Biogeosciences*. [Online]. **113**(1),pp.1–11. Available from: <https://doi.org/10.1029/2006JG000395>.
- Hepp, D.A., Hebbeln, D., Kreiter, S., Keil, H., Bathmann, C., Ehlers, J. and M??rz, T. 2012. An east-west-trending Quaternary tunnel valley in the south-eastern North Sea and its seismic-sedimentological interpretation. *Journal of Quaternary Science*. **27**(8),pp.844–853.
- Hepp, D.A., Romero, O.E., M??rz, T., de Pol-Holz, R. and Hebbeln, D. 2019. How a river submerges into the sea: a geological record of changing a fluvial to a marine paleoenvironment during early Holocene sea level rise. *Journal of Quaternary Science*. [Online]. **34**(7),pp.581–592. Available from: <http://dx.doi.org/10.1002/jqs.3147>.
- Van Heteren, S., Meekes, J.A.C., Bakker, M.A.J., Gaffney, V., Fitch, S., Gearey, B.R. and Paap, B.F. 2014. Reconstructing North Sea palaeolandscapes from 3D and high-density 2D seismic data: An overview. *Geologie en Mijnbouw/Netherlands Journal of Geosciences*. [Online]. **93**(1–2),pp.31–42. Available from: <https://doi.org/10.1017/njg.2014.4>.
- Hijma, M.P. and Cohen, K.M. 2011. Holocene transgression of the Rhine river mouth area, The Netherlands/Southern North Sea: Palaeogeography and sequence stratigraphy. *Sedimentology*. **58**(6),pp.1453–1485.
- Hijma, M.P. and Cohen, K.M. 2010. Timing and magnitude of the sea-level jump precluding the 8200 yr event. *Geology*. [Online]. **38**(3),pp.275–278. Available from: <https://doi.org/10.1130/G30439.1%0A>.

- Hijma, M.P., Cohen, K.M., Roebroeks, W., Westerhoff, W.E. and Busschers, F.S. 2012. Pleistocene Rhine-Thames landscapes: Geological background for hominin occupation of the southern North Sea region. *Journal of Quaternary Science*. **27**(1),pp.17–39.
- Hinestrosa, G., Webster, J.M. and Beaman, R.J. 2016. Postglacial sediment deposition along a mixed carbonate-siliciclastic margin: New constraints from the drowned shelf-edge reefs of the Great Barrier Reef, Australia. *Palaeogeography, Palaeoclimatology, Palaeoecology*. [Online]. **446**,pp.168–185. Available from: <http://dx.doi.org/10.1016/j.palaeo.2016.01.023>.
- Horsburgh, K. and Lowe, J. 2013. Impacts of climate change on sea level. *Marine Climate Change Impacts Partnership: Science Review*. (June),pp.27–33.
- Huijzer, A.S. and Isarin, R.F.B. 1997. The reconstruction of past climates using multi-proxy evidence: an example of the Weichselian Pleniglacial in northwest and central Europe. *Quaternary Science Reviews*. [Online]. **16**(6),pp.513–533. Available from: [https://doi.org/10.1016/S0277-3791\(96\)00080-7](https://doi.org/10.1016/S0277-3791(96)00080-7).
- Van Huissteden, J. and Kasse, C. 2001. Detection of rapid climate change in Last Glacial fluvial successions in the Netherlands. *Global and Planetary Change*. [Online]. **28**(1–2),pp.319–339. Available from: [https://doi.org/10.1016/S0921-8181\(00\)00082-5](https://doi.org/10.1016/S0921-8181(00)00082-5).
- Huuse, M. and Lykke-Andersen, H. 2000. Overdeepened Quaternary valleys in the eastern Danish North Sea: Morphology and origin. *Quaternary Science Reviews*. [Online]. **19**(12),pp.1233–1253. Available from: [https://doi.org/10.1016/S0277-3791\(99\)00103-1](https://doi.org/10.1016/S0277-3791(99)00103-1).
- IPCC 2013. *Climate Change 2013: The Physical Science Basis. Contribution of Working Group I to the Fifth Assessment Report of the Intergovernmental Panel on Climate Change* (T. F. Stocker, D. Qin, G.-K. Plattner, M. Tignor, S. K. Allen, J. Boschung, A. Nauels, Y. Xia, V. Bex, & P. M. Midgley, eds.). United Kingdom and New York, NY, USA: Cambridge University Press.
- Jelgersma, S. 1961. Holocene sea-level changes in the Netherlands. *Ph. D. dissertation, Leiden Univ.*

- Kalbitz, K. and Geyer, S. 2002. Different effects of peat degradation on dissolved organic carbon and nitrogen. *Organic Geochemistry*. [Online]. **33**(3),pp.319–326. Available from: [https://doi.org/10.1016/S0146-6380\(01\)00163-2](https://doi.org/10.1016/S0146-6380(01)00163-2).
- Kearney, M.S., Grace, R.E. and Stevenson, J.C. 1988. Marsh Loss in Nanticoke Estuary , Chesapeake Bay. *Geographical Review*. [Online]. **78**(2),pp.205–220. Available from: <https://doi.org/10.2307/214178>.
- Kennish, M.J. 2001. Coastal salt marsh systems in the U.S.: A review of anthropogenic impacts. *Journal of Coastal Research*. **17**(3),pp.731–748.
- Kerney, M.P., Gibbard, P.L., Hall, A.R. and Robinson, J.E. 1982. Middle Devensian river deposits beneath the ‘upper floodplain’ terrace of the river Thames at Isleworth, west London. *Proceedings of the Geologists’ Association*. [Online]. **93**(4),pp.385–393. Available from: [https://doi.org/10.1016/S0016-7878\(82\)80023-0](https://doi.org/10.1016/S0016-7878(82)80023-0).
- Kiden, P., Denys, L. and Johnston, P. 2002. Late Quaternary sea-level change and isostatic and tectonic land movements along the Belgian-Dutch North Sea coasts: Geological data and model results. *Journal of Quaternary Science*. **17**(5–6),pp.535–546.
- Kocurek, G., Ewing, R. and Mohrig, D. 2009. How do bedform patterns arise? New views on the role of bedform interactions within a set of boundary. *Earth Surface Processes and Landforms*. [Online]. **35**(March),pp.51–63. Available from: <http://doi.wiley.com/10.1002/esp.1730>.
- Van Kolfschoten, T. and Laban, C. 1995. Pleistocene terrestrial mammal faunas from the North Sea. *Mededelingen - Rijks Geologische Dienst*. [Online]. **52**,pp.135–151. Available from: <https://hdl.handle.net/1887/10035>.
- Kolstrup, E. 1986. Reappraisal of the upper weichselian periglacial environment from Danish frost wedge casts. *Palaeogeography, Palaeoclimatology, Palaeoecology*. [Online]. **56**(3–4),pp.237–249. Available from: [https://doi.org/10.1016/0031-0182\(86\)90096-9](https://doi.org/10.1016/0031-0182(86)90096-9).
- Konradi, P.B., Larsen, B. and Sørensen, A.B. 2005. Marine Eemian in the Danish eastern North Sea. *Quaternary International*. [Online]. **133**,pp.21–31. Available from: <https://doi.org/10.1016/j.quaint.2004.10.003>.

- Koop-Jakobsen, K. and Gutbrod, M.S. 2019. Shallow Salt Marsh Tidal Ponds—An Environment With Extreme Oxygen Dynamics. *Frontiers in Environmental Science*. [Online]. **7**(October). Available from: <https://doi.org/10.3389/fenvs.2019.00137>.
- Kristensen, T.B., Huuse, M., Piotrowski, J. a and Clausen, O.R. 2007. A morphometric analysis of tunnel valleys in the eastern North Sea based on 3D seismic data. *Journal of Quaternary Science*. [Online]. **22**(8),pp.801–815. Available from: <http://dx.doi.org/10.1002/jqs.1123>.
- Laban, C. 1995. The Pleistocene glaciations in the Dutch sector of the North Sea: A synthesis of sedimentary and seismic data. Available from: <https://hdl.handle.net/11245/1.119444>.
- Laban, C. and van der Meer, J.J.M. 2004. Chapter 20 - Pleistocene Glaciation in The Netherlands *In: J. Ehlers and P. L. Gibbard, eds. Quaternary Glaciations / Extent and Chronology: Part 1: Europe* [Online]. Elsevier, pp. 251–260. Available from: <https://doi.org/10.1016/B978-0-444-53447-7.00020-9>.
- Lamb, R.M., Harding, R., Huuse, M., Stewart, M. and Brocklehurst, S.H. 2018. The early Quaternary North Sea Basin. *Journal of the Geological Society*. [Online]. **175**(2),pp.275–290. Available from: <https://doi.org/10.1144/jgs2017-057>.
- Lamb, R.M., Huuse, M. and Stewart, M. 2017. Early Quaternary sedimentary processes and palaeoenvironments in the central North Sea. *Journal of Quaternary Science*. **32**(2),pp.127–144.
- Van Landeghem, K.J.J., Uehara, K., Wheeler, A.J., Mitchell, N.C. and Scourse, J.D. 2009. Post-glacial sediment dynamics in the Irish Sea and sediment wave morphology: Data-model comparisons. *Continental Shelf Research*. [Online]. **29**(14),pp.1723–1736. Available from: <https://doi.org/10.1016/j.csr.2009.05.014>.
- Van Landeghem, K.J.J., Wheeler, A.J., Mitchell, N.C. and Sutton, G. 2009. Variations in sediment wave dimensions across the tidally dominated Irish Sea, NW Europe. *Marine Geology*. [Online]. **263**(1–4),pp.108–119. Available from: <http://dx.doi.org/10.1016/j.margeo.2009.04.003>.

- Lee, J.R., Rose, J., Candy, I.A.N. and Barendregt, R.W. 2006. Sea-level changes , river activity , soil development and glaciation around the western margins of the southern North Sea Basin during the Early and early Middle Pleistocene : evidence from Pakefield , Suffolk , UK. *Journal of Quaternary Science*. **21**(2),pp.155–179.
- Legge, O., Johnson, M., Hicks, N., Jickells, T., Diesing, M., Aldridge, J., Andrews, J., Artioli, Y., Bakker, D.C.E., Burrows, M.T., Carr, N., Cripps, G., Felgate, S.L., Fernand, L., Greenwood, N., Hartman, S., Kröger, S., Lessin, G., Mahaffey, C., Mayor, D.J., Parker, R., Queirós, A.M., Shutler, J.D., Silva, T., Stahl, H., Tinker, J., Underwood, G.J.C., Van Der Molen, J., Wakelin, S., Weston, K. and Williamson, P. 2020. Carbon on the Northwest European Shelf: Contemporary Budget and Future Influences. *Frontiers in Marine Science*. [Online]. **7**,p.143. Available from: <https://doi.org/10.3389/fmars.2020.00143>.
- Lengkeek, H.J., de Greef, J. and Joosten, S. 2018. CPT based unit weight estimation extended to soft organic soils and peat. *Cone Penetration Testing 2018 - Proceedings of the 4th International Symposium on Cone Penetration Testing, CPT 2018*. (January 2018),pp.389–394.
- Limpenny, S.E., Barrio Frojan, C., Cotterill, C., Foster-Smith, R.L., Pearce, B., Tizzard, L., Limpenny, D.L., Long, D., Walmsley, S., Kirby, S., Baker, K., Meadows, W.J., Rees, J., Hill, J., Wilson, C., Leivers, M., Churchley, S., Russell, J., Birchenough, A.C., Green, S.L. and Law, R.J. 2011. *The East Coast Regional Environmental Characterisation*.
- Limpens, J., Berendse, F., Blodau, C., Canadell, J.G., Freeman, C., Holden, J., Roulet, N., Rydin, H. and Schaepman-Strub, G. 2008. Peatlands and the carbon cycle: from local processes to global implications—a synthesis. *Biogeosciences*. [Online]. **5**(5),pp.1475–1491. Available from: <https://doi.org/10.5194/bg-5-1475-2008>.
- Liu, Z., Berne, S., Saito, Y., Yu, H., Trentesaux, A., Uehara, K., Yin, P., Paul Liu, J., Li, C., Hu, G. and Wang, X. 2007. Internal architecture and mobility of tidal sand ridges in the East China Sea. *Continental Shelf Research*. [Online]. **27**(13),pp.1820–1834. Available from: <https://doi.org/10.1016/j.csr.2007.03.002>.

- Long, A.J., Barlow, N.L.M., Busschers, F.S., Cohen, K.M., Gehrels, W.R. and Wake, L.M. 2015. Near-field sea-level variability in northwest Europe and ice sheet stability during the last interglacial. *Quaternary Science Reviews*. [Online]. **126**,pp.26–40. Available from: <http://dx.doi.org/10.1016/j.quascirev.2015.08.021>.
- Long, A.J., Waller, M.P. and Stupples, P. 2006. Driving mechanisms of coastal change: Peat compaction and the destruction of late Holocene coastal wetlands. *Marine Geology*. [Online]. **225**(1–4),pp.63–84. Available from: <https://doi.org/10.1016/j.margeo.2005.09.004>.
- Long, D., Laban, C., Streif, H., Cameron, T.D.J. and Schuttenhelm, R.T.E. 1988. The sedimentary record of climatic variations in the southern North Sea. *Philosophical Transactions of the Royal Society*. [Online]. **318**(1191),pp.523–537. Available from: <https://doi.org/10.1098/rstb.1988.0022>.
- Lovelock, C.E., Fourqurean, J.W. and Morris, J.T. 2017. Modeled CO<sub>2</sub> emissions from coastal wetland transitions to other land uses: Tidal marshes, mangrove forests, and seagrass beds. *Frontiers in Marine Science*. **4**(MAY),pp.1–11.
- Lowe, J.J., Birks, H.H., Brooks, S.J., Coope, G.R., Harkness, D.D., Mayle, F.E., Sheldrick, C., Turney, C.S.M. and Walker, M.J.C. 1999. The chronology of palaeoenvironmental changes during the last Glacial-Holocene transition: towards an event stratigraphy for the British Isles. *Journal of the Geological Society*. [Online]. **156**(2),pp.397–410. Available from: <https://doi.org/10.1144/gsjgs.156.2.0397>.
- Lunne, T., Powell, J.J.M. and Robertson, P.K. 2002. *Cone penetration testing in geotechnical practice*. CRC Press.
- Ma, H., Yang, J. and Chen, L. 2018. Effect of scour on the structural response of an offshore wind turbine supported on tripod foundation. *Applied Ocean Research*. [Online]. **73**,pp.179–189. Available from: <https://doi.org/10.1016/j.apor.2018.02.007>.

- Macreadie, P.I., Anton, A., Raven, J.A., Beaumont, N., Connolly, R.M., Friess, D.A., Kelleway, J.J., Kennedy, H., Kuwae, T., Lavery, P.S., Lovelock, C.E., Smale, D.A., Apostolaki, E.T., Atwood, T.B., Baldock, J., Bianchi, T.S., Chmura, G.L., Eyre, B.D., Fourqurean, J.W., Hall-Spencer, J.M., Huxham, M., Hendriks, I.E., Krause-Jensen, D., Laffoley, D., Luisetti, T., Marbà, N., Masque, P., McGlathery, K.J., Megonigal, J.P., Murdiyarso, D., Russell, B.D., Santos, R., Serrano, O., Silliman, B.R., Watanabe, K. and Duarte, C.M. 2019. The future of Blue Carbon science. *Nature Communications*. **10**(1),pp.1–13.
- Marren, P.M. and Toomath, S.C. 2014. Channel pattern of proglacial rivers: Topographic forcing due to glacier retreat. *Earth Surface Processes and Landforms*. **39**(7),pp.943–951.
- McGowan, S.A. and Baker, R.G.V. 2014. How past sea-level changes can inform future planning: A case study from the Macleay River estuary, New South Wales, Australia. *The Holocene*. [Online]. **24**(11),pp.1591–1601. Available from: <https://doi.org/10.1177/0959683614544055>.
- McLeod, E., Chmura, G.L., Bouillon, S., Salm, R., Björk, M., Duarte, C.M., Lovelock, C.E., Schlesinger, W.H. and Silliman, B.R. 2011. A blueprint for blue carbon: Toward an improved understanding of the role of vegetated coastal habitats in sequestering CO<sub>2</sub>. *Frontiers in Ecology and the Environment*. [Online]. **9**(10),pp.552–560. Available from: <https://doi.org/10.1890/110004>.
- Meadows, M.E. 2012. Quaternary environments: Going forward, looking backwards? *Progress in Physical Geography*. [Online]. **36**(4),pp.539–547. Available from: <https://doi.org/10.1177/0309133312438907>.
- Mellett, C.L., Hodgson, D.M., Lang, A., Mauz, B., Selby, I. and Plater, A.J. 2012. Preservation of a drowned gravel barrier complex: A landscape evolution study from the north-eastern English Channel. *Marine Geology*. [Online]. **315–318**,pp.115–131. Available from: <http://dx.doi.org/10.1016/j.margeo.2012.04.008>.
- Mellett, C.L., Hodgson, D.M., Plater, A.J., Mauz, B., Selby, I. and Lang, A. 2013. Denudation of the continental shelf between Britain and France at the glacial-interglacial timescale. *Geomorphology*. [Online]. **203**,pp.79–96. Available from: <https://doi.org/10.1016/j.geomorph.2013.03.030>.

- Mellett, C.L., Phillips, E.R., Lee, J.R., Cotterill, C.J., Tjelta, T.I., James, L. and Duffy, C. 2019. Elsterian ice sheet retreat in the southern North 1 Sea: antecedent controls on large-scale glacetectonics and subglacial bed conditions. *Boreas*. **49**(1),pp.129–151.
- Mellett, C.L. and Plater, A.J. 2018. Drowned barriers as archives of coastal-response to sea-level rise *In: Barrier dynamics and response to changing climate* [Online]. Springer, pp. 57–89. Available from: [https://doi.org/10.1007/978-3-319-68086-6\\_2](https://doi.org/10.1007/978-3-319-68086-6_2).
- Ménot, G., Bard, E., Rostek, F., Weijers, J.W.H., Hopmans, E.C., Schouten, S. and Damsté, J.S.S. 2006. Early reactivation of European rivers during the last deglaciation. *Science*. [Online]. **313**(5793),pp.1623–1625. Available from: <https://doi.org/10.1126/science.1130511>.
- Millette, T.L., Argow, B.A., Marcano, E., Hayward, C., Hopkinson, C.S. and Valentine, V. 2010. Salt Marsh Geomorphological Analyses via Integration of Multitemporal Multispectral Remote Sensing with LIDAR and GIS. *Journal of Coastal Research*. [Online]. **26**(5 (265)),pp.809–816. Available from: <https://doi.org/10.2112/JCOASTRES-D-09-00101.1>.
- Milner, A.M., Baird, A.J., Green, S.M., Swindles, G.T., Young, D.M., Sanderson, N.K., Timmins, M.S.I. and Galka, M. 2021. A regime shift from erosion to carbon accumulation in a temperate northern peatland. *Journal of Ecology*. [Online]. **109**(1),pp.125–138. Available from: <https://doi.org/10.1111/1365-2745.13453>.
- Missiaen, T., Fitch, S., Muru, M., Harding, R., Fraser, A. and De, M. 2020. Targeting the mesolithic: Interdisciplinary approaches to archaeological prospection in the Brown Bank area, southern North Sea. *Quaternary International*. [Online]. Available from: <https://doi.org/10.1016/j.quaint.2020.05.004>.
- Missiaen, T., Jongepier, I., Heirman, K., Soens, T., Gelorini, V., Verniers, J., Verhegge, J. and Crombé, P. 2017. Holocene landscape evolution of an estuarine wetland in relation to its human occupation and exploitation: Waasland Scheldt polders, northern Belgium. *Netherlands Journal of Geosciences*. [Online]. **96**(1),pp.35–62. Available from: <https://doi.org/10.1017/njg.2016.24>.



- Mitchum Jr., R.M. 1977. Seismic Stratigraphy and Global Changes of Sea Level: Part 6. Stratigraphic Interpretation of Seismic Reflection Patterns in Depositional Sequences: Section 2. Application of Seismic Reflection Configuration to Stratigraphic Interpretation *In*: C. E. Payton, ed. *APG Memoire 26: Seismic Stratigraphy--Applications to Hydrocarbon Exploration*. American Association of Petroleum Geologists, pp. 117–133.
- Mitchum, R.M. and Vail, P.R. 1977. Seismic Stratigraphy and Global Changes of Sea Level: Part 7. Seismic Stratigraphic Interpretation Procedure: Section 2. Application of Seismic Reflection Configuration to Stratigraphic Interpretation *In: M 26: Seismic Stratigraphy--Applications to Hydrocarbon Exploration.*, pp. 135–143.
- Mitsch, W.J., Bernal, B., Nahlik, A.M., Mander, Ü., Zhang, L., Anderson, C.J., Jørgensen, S.E. and Brix, H. 2013. Wetlands, carbon, and climate change. *Landscape Ecology*. [Online]. **28**(4),pp.583–597. Available from: <https://doi.org/10.1007/s10980-012-9758-8>.
- Van Der Molen, J. and de Swart, H.E. 2001. Holocene wave conditions and wave-induced sand transport in the southern North Sea. *Continental Shelf Research*. [Online]. **21**(16–17),pp.1723–1749. Available from: [https://doi.org/10.1016/S0278-4343\(01\)00018-8](https://doi.org/10.1016/S0278-4343(01)00018-8).
- Montenegro, A., Eby, M., Kaplan, J.O., Meissner, K.J. and Weaver, A.J. 2006. Carbon storage on exposed continental shelves during the glacial-interglacial transition. *Geophysical Research Letters*. [Online]. **33**(8),pp.6–8. Available from: <https://doi.org/10.1029/2005GL025480>.
- Moorlock, B.S.P., Riding, J.B., Hamblin, R.J.O., Allen, P. and Rose, J. 2002. The Pleistocene College Farm Silty Clay at Great Blakenham, Suffolk, England—additional information on the course of the early River Thames. *Netherlands Journal of Geosciences*. [Online]. **81**(1),pp.9–17. Available from: <https://doi.org/10.1017/S0016774600020527>.
- Moreau, J., Huuse, M., Janszen, A. and van der Vegt, P. 2012. The glaciogenic unconformity of the southern North Sea. *Glaciogenic Reservoirs and Hydrocarbon Systems*. [Online]. **368**(1),pp.99–110. Available from: <https://doi.org/10.1144/SP368.5>.

- Mudd, S.M., Howell, S.M. and Morris, J.T. 2009. Impact of dynamic feedbacks between sedimentation, sea-level rise, and biomass production on near-surface marsh stratigraphy and carbon accumulation. *Estuarine, Coastal and Shelf Science*. [Online]. **82**(3),pp.377–389. Available from: <http://dx.doi.org/10.1016/j.ecss.2009.01.028>.
- Mueller, J.E. 1968. An introduction to the hydraulic and topographic sinuosity indexes. *Annals of the Association of American Geographers*. [Online]. **58**(2),pp.371–385. Available from: <https://doi.org/10.1111/j.1467-8306.1968.tb00650.x>.
- Murton, D.K. and Murton, J.B. 2012. Middle and Late Pleistocene glacial lakes of lowland Britain and the southern North Sea Basin. *Quaternary International*. [Online]. **260**,pp.115–142. Available from: <https://doi.org/10.1016/j.quaint.2011.07.034>.
- Murton, J.B., Bateman, M.D., Baker, C.A., Knox, R. and Whiteman, C.A. 2003. The Devensian periglacial record on Thanet, Kent, UK. *Permafrost and Periglacial Processes*. **14**(3),pp.217–246.
- Nelleman, C., Corcoran, E., Duarte, C.M., DeYoung, C., Fonseca, L. and Grimsditch, G. 2009. *Blue carbon. A rapid response assessment*. UN Environment, GRID-Arendal.
- NGICP 2004. High resolution record of Northern Hemisphere climate extending into the last interglacial period. *Nature*. [Online]. **431**(7005),pp.147–151. Available from: <https://doi.org/10.1038/nature02805>.
- Nicholls, R.J. 2004. Coastal flooding and wetland loss in the 21st century: Changes under the SRES climate and socio-economic scenarios. *Global Environmental Change*. [Online]. **14**(1),pp.69–86. Available from: <https://doi.org/10.1016/j.gloenvcha.2003.10.007>.
- Nicholls, R.J., Hoozemans, F.M.J. and Marchand, M. 1999. Increasing flood risk and wetland losses due to global sea-level rise: regional and global analyses. *Global Environmental Change*. [Online]. **9**,pp.S69--S87. Available from: [https://doi.org/10.1016/S0959-3780\(99\)00019-9](https://doi.org/10.1016/S0959-3780(99)00019-9).

- Nyman, J.A., Delaune, R.D., Roberts, H.H. and Patrick, W.H. 1993. Relationship between vegetation and soil formation in a rapidly submerging coastal marsh. *Marine Ecology Progress Series*. [Online]. **96**,pp.269–279. Available from: <https://www.jstor.org/stable/24833555>.
- O’Cofaigh, C. 1996. Tunnel valley genesis. *Progress in Physical Geography*. [Online]. **20**(1),pp.1–19. Available from: <https://doi.org/10.1177/030913339602000101>.
- Office for National Statistics 2016. *UK Natural Capital: Experimental carbon stock accounts, preliminary estimates. Statistical bulletin*.
- Office for National Statistics 2019. *UK natural capital: peatlands. Statistical bulletin*.
- Ottesen, D., Stewart, M., Brønner, M. and Batchelor, C.L. 2020. Tunnel valleys of the central and northern North Sea (56°N to 62°N): Distribution and characteristics. *Marine Geology*. [Online]. **425**(April),p.106199. Available from: <https://doi.org/10.1016/j.margeo.2020.106199>.
- Overeem, I., Weltje, G.J., Bishop-Kay, C. and Kroonenberg, S.B. 2001. The Late Cenozoic Eridanos delta system in the Southern North Sea Basin: A climate signal in sediment supply? *Basin Research*. [Online]. **13**(3),pp.293–312. Available from: <https://doi.org/10.1046/j.1365-2117.2001.00151.x>.
- Parfitt, S.A., Ashton, N.M., Lewis, S.G., Abel, R.L., Coope, G.R., Field, M.H., Gale, R., Hoare, P.G., Larkin, N.R., Lewis, M.D., Karloukovski, V., Maher, B.A., Peglar, S.M., Preece, R.C., Whittaker, J.E. and Stringer, C.B. 2010. Early pleistocene human occupation at the edge of the boreal zone in northwest Europe. *Nature*. [Online]. **466**(7303),pp.229–233. Available from: <https://doi.org/10.1038/nature09117>.
- Passchier, S. and Kleinhans, M.G. 2005. Observations of sand waves, megaripples, and hummocks in the Dutch coastal area and their relation to currents and combined flow conditions. *Journal of Geophysical Research: Earth Surface*. [Online]. **110**(F4),pp.1–15. Available from: <https://doi.org/10.1029/2004JF000215>.
- Pawley, S.M., Bailey, R.M., Rose, J., Moorlock, B.S.P., Hamblin, R.J.O. and Booth, Steven J.Lee, J.R. 2008. Age limits on Middle Pleistocene glacial sediments from OSL dating, north Norfolk, UK. *Quaternary Science Reviews*. [Online]. **27**(13–14),pp.1363–1377. Available from: <https://doi.org/10.1016/j.quascirev.2008.02.013>.

- Payette, S. 1988. Late-Holocene development of subarctic ombrotrophic peatlands: allogenic and autogenic succession. *Ecology*. [Online]. **69**(2),pp.516–531. Available from: <https://doi.org/10.2307/1940450>.
- Pearsall, S.H. and Poulter, B. 2005. Adapting coastal lowlands to rising seas. *In*: M. J. Groom, G. K. Meffe and C. R. Carroll, eds. *Principles of conservation biology*. MA: Sinauer Associates, pp. 366–370.
- Peeters, J. 2018. The Last Interglacial Rhine estuary: Sedimentary architecture, chronostratigraphy, preservation and analogue potential. Available from: <https://dspace.library.uu.nl/handle/1874/373080>.
- Peeters, J., Busschers, F.S. and Stouthamer, E. 2015. Fluvial evolution of the Rhine during the last interglacial-glacial cycle in the southern North Sea basin: A review and look forward. *Quaternary International*. [Online]. **357**,pp.176–188. Available from: <https://doi.org/10.1016/j.quaint.2014.03.024>.
- Peeters, J., Busschers, F.S., Stouthamer, E., Bosch, J.H.A. and Berg, M.W. Van Den 2016. Sedimentary architecture and chronostratigraphy of a late Quaternary incised-valley fill: A case study of the late Middle and Late Pleistocene Rhine system in the Netherlands. *Quaternary Science Reviews*. [Online]. **131**,pp.211–236. Available from: <http://dx.doi.org/10.1016/j.quascirev.2015.10.015>.
- Peltier, W.R. 2005. On the hemispheric origins of meltwater pulse 1a. *Quaternary Science Reviews*. [Online]. **24**(14–15),pp.1655–1671. Available from: <https://doi.org/10.1016/j.quascirev.2004.06.023>.
- Pendleton, L., Donato, D.C., Murray, B.C., Crooks, S., Jenkins, W.A., Sifleet, S., Craft, C., Fourqurean, J.W., Kauffman, J.B., Marbà, N., Megonigal, P., Pidgeon, E., Herr, D., Gordon, D. and Baldera, A. 2012. Estimating Global ‘Blue Carbon’ Emissions from Conversion and Degradation of Vegetated Coastal Ecosystems. *PLoS ONE*. [Online]. **7**(9),p.43542. Available from: <https://doi.org/10.1371/journal.pone.0043542>.
- Pissart, A. 1987. Weichselian periglacial structures and their environmental significance: Belgium, the Netherlands and northern France *In*: *Periglacial processes and landforms in Britain and Ireland* [Online]. Cambridge University Press, pp. 77–85. Available from: <http://hdl.handle.net/2268/250023>.

- van de Plassche, O. 1995. Evolution of the intra-coastal tidal range in the Rhine-Meuse delta and Flevo Lagoon, 5700-3000 yrs cal BC. *Marine Geology*. [Online]. **124**(1–4),pp.113–128. Available from: [https://doi.org/10.1016/0025-3227\(95\)00035-W](https://doi.org/10.1016/0025-3227(95)00035-W).
- van de Plassche, O. 1982. Sea-level change and water-level movements in the Netherlands during the Holocene. *Ph. D. dissertation, Vrije Universiteit Amsterdam*.
- Plets, R., Dix, J., Bastos, A. and Best, A. 2007. Characterization of Buried Inundated Peat on Seismic (Chirp) Data, Inferred from Core Information. *Archaeological Prospection*. **14**(4),pp.261–272.
- Praeg, D. 1996. Morphology, stratigraphy and genesis of buried Mid-Pleistocene Tunnel-valleys in the southern north Sea basin.
- Praeg, D. 2003. Seismic imaging of mid-Pleistocene tunnel-valleys in the North Sea Basin-high resolution from low frequencies. *Journal of Applied Geophysics*. [Online]. **53**(4),pp.273–298. Available from: <https://doi.org/10.1016/j.jappgeo.2003.08.001>.
- Prins, L.T. and Andresen, K.J. 2019. Buried late Quaternary channel systems in the Danish North Sea – Genesis and geological evolution. *Quaternary Science Reviews*. [Online]. **223**,p.105943. Available from: <https://doi.org/10.1016/j.quascirev.2019.105943>.
- QGIS Development Team 2020. QGIS Geographic Information System. Open Source Geospatial Foundation Project. Available from: <http://qgis.osgeo.org>.
- Raposa, K.B., Weber, R.L.J., Ekberg, M.C. and Ferguson, W. 2017. Vegetation Dynamics in Rhode Island Salt Marshes During a Period of Accelerating Sea Level Rise and Extreme Sea Level Events. *Estuaries and Coasts*. [Online]. **40**(3),pp.640–650. Available from: <https://doi.org/10.1007/s12237-015-0018-4>.
- Reed, D.J. 1990. The impact of sea-level rise on coastal salt marshes. *Progress in Physical Geography*. [Online]. **14**(4),pp.465–481. Available from: <https://doi.org/10.1177/030913339001400403>.

- Reimer, P.J., Edouard Bard, B., Alex Bayliss, B., Warren Beck, B.J., Paul Blackwell, B.G. and Christopher Bronk Ramsey, B. 2013. Intcal13 and Marine13 Radiocarbon Age Calibration Curves 0–50,000 Years Cal Bp. *Radiocarbon*. **55**(4),pp.1869–1887.
- Rieu, R., van Heteren, S., van der Spek, A. and De Boer, P. 2005. Development and preservation of a mid-Holocene tidal-channel network offshore the western Netherlands. *Journal of Sedimentary Research*. [Online]. **75**(3),pp.409–415. Available from: <https://doi.org/10.2110/jsr.2005.032%0A>.
- Roberts, D.H., Evans, D.J.A., Callard, S.L., Clark, C.D., Bateman, M.D., Medialdea, A., Dove, D., Cotterill, C.J., Saher, M., Cofaigh, C., Chiverrell, R.C., Moreton, S.G., Fabel, D. and Bradwell, T. 2018. Ice marginal dynamics of the last British-Irish Ice Sheet in the southern North Sea: Ice limits, timing and the influence of the Dogger Bank. *Quaternary Science Reviews*. [Online]. **198**,pp.181–207. Available from: <https://doi.org/10.1016/j.quascirev.2018.08.010>.
- Robertson, P.K. 1990. Soil classification using the cone penetration test. *Canadian Geotechnical Journal*. **27**(1),pp.151–158.
- Robertson, P.K., Campanella, R.G., Gillespie, D. and Greig, J. 1986. Use of piezometer cone data *In: Use of in situ tests in geotechnical engineering.*, pp. 1263–1280.
- Romans, B.W., Castelltort, S., Covault, J.A., Fildani, A. and Walsh, J.P. 2016. Environmental signal propagation in sedimentary systems across timescales. *Earth-Science Reviews*. [Online]. **153**,pp.7–29. Available from: <http://dx.doi.org/10.1016/j.earscirev.2015.07.012>.
- Rose, J. 1994. Major river systems of central and southern Britain during the Early and Middle Pleistocene. *Terra Nova*. **6**(5),pp.435–443.
- Roy, P.S., Cowell, P.J., Ferland, M.A. and Thom, B.G. 1994. Wave-dominated coasts *In: R. W. G. Carter and C. D. Woodroffe, eds. Coastal evolution: Late Quaternary shoreline morphodynamics*. Cambridge University Press, pp. 121–186.
- Sadler, P.M. and Jerolmack, D.J. 2015. Scaling laws for aggradation, denudation and progradation rates: The case for time-scale invariance at sediment sources and sinks. *Geological Society Special Publication*. [Online]. **404**(1),pp.69–88. Available from: <https://doi.org/10.1144/SP404.7>.

- Sander, L., Hede, M.U., Fruergaard, M., Nielsen, L., Clemmensen, L.B., Kroon, A., Johannessen, P.N., Nielsen, L.H. and Pejrup, M. 2016. Coastal lagoons and beach ridges as complementary sedimentary archives for the reconstruction of Holocene relative sea-level changes. *Terra Nova*. **28**(1),pp.43–49.
- Schepers, L., Kirwan, M., Guntenspergen, G. and Temmerman, S. 2017. Spatio-temporal development of vegetation die-off in a submerging coastal marsh. *Limnology and Oceanography*. [Online]. **62**(1),pp.137–150. Available from: <https://doi.org/10.1002/lno.10381>.
- Scourse, J.D., Ansari, M.H., Wingfield, R.T.R., Harland, R. and Balson, P.S. 1998. A middle pleistocene shallow marine interglacial sequence, inner silver pit, Southern North Sea: Pollen and dinoflagellate cyst stratigraphy and sea-level history. *Quaternary Science Reviews*. [Online]. **17**(9–10),pp.871–900. Available from: [https://doi.org/10.1016/S0277-3791\(98\)00023-7](https://doi.org/10.1016/S0277-3791(98)00023-7).
- Shaw, J. 2005. Geomorphic evidence of postglacial terrestrial environments on Atlantic Canadian continental shelves. *Géographie physique et Quaternaire*. [Online]. **59**(2–3),pp.141–154. Available from: <https://doi.org/10.7202/014752ar>.
- Shennan, I., Lambeck, K., Flather, R., Horton, B., McArthur, J., Innes, J., Lloyd, J., Rutherford, M. and Wingfield, R. 2000. Modelling western North Sea paleogeographies and tidal changes during the Holocene. *Holocene Land-Ocean Interaction and Environmental Change around the North Sea*. [Online]. **166**(1),pp.299–319. Available from: <https://doi.org/10.1144/GSL.SP.2000.166.01.15>.
- Shennan, I., Milne, G. and Bradley, S. 2009. Late Holocene relative land- and sea-level changes: Providing information for stakeholders. *GSA Today*. **19**(9),pp.52–53.
- Siddall, M., Rohling, E.J., Almogi-Labin, A., Hemleben, C., Meischner, D., Schmelzer, I. and Smeed, D.A. 2003. Sea-level fluctuations during the last glacial cycle. *Nature*. [Online]. **423**(6942),pp.853–858. Available from: <https://doi.org/10.1038/nature01690>.
- Sim, T.G., Swindles, G.T., Morris, P.J., Gaika, M., Mullan, D. and Galloway, J.M. 2019. Pathways for Ecological Change in Canadian High Arctic Wetlands Under Rapid Twentieth Century Warming. *Geophysical Research Letters*. [Online]. **46**(9),pp.4726–4737. Available from: <https://doi.org/10.1029/2019GL082611>.

- Sloss, C.R., Nothdurft, L., Hua, Q., O'Connor, S.G., Moss, P.T., Rosendahl, D., Petherick, L.M., Nanson, R.A., Mackenzie, L.L., Sternes, A., Jacobsen, G.E. and Ulm, S. 2018. Holocene sea-level change and coastal landscape evolution in the southern Gulf of Carpentaria, Australia. *Holocene*. [Online]. **28**(9),pp.1411–1430. Available from: <https://doi.org/10.1177/0959683618777070>.
- Smeaton, C. and Austin, W.E.N. 2019. Where's the Carbon: Exploring the Spatial Heterogeneity of Sedimentary Carbon in Mid-Latitude Fjords. *Frontiers in Earth Science*. **7**(October),pp.1–16.
- Smeaton, C., Austin, W.E.N., Davies, A.L., Baltzer, A., Abell, R.E. and Howe, J.A. 2016. Substantial stores of sedimentary carbon held in mid-latitude fjords. *Biogeosciences*. [Online]. **13**(20),pp.5771–5787. Available from: <https://doi.org/10.5194/bg-13-5771-2016>.
- Smeaton, C., Austin, W.E.N., Davies, A.L., Baltzer, A., Howe, J.A. and Baxter, J.M. 2017. Scotland ' s forgotten carbon : a national assessment of mid-latitude fjord sedimentary carbon stocks. *Biogeosciences*. [Online]. **14**(24),pp.5663–5674. Available from: <https://doi.org/10.5194/bg-14-5663-2017>.
- Smeaton, C., Hunt, C.A., Turrell, W.R. and Austin, W.E.N. 2021. *Sediment type and surficial sedimentary carbon stocks across the United Kingdom's Exclusive Economic Zone and the territorial waters of the Isle of Man and the Chanel Islands*. [Online]. Available from: <https://doi.org/10.7489/12354-1>.
- Smith, D.E., Harrison, S., Firth, C.R. and Jordan, J.T. 2011. The early Holocene sea level rise. *Quaternary Science Reviews*. **30**(15–16),pp.1846–1860.
- Smith, R.W., Bianchi, T.S., Allison, M., Savage, C. and Galy, V. 2015. High rates of organic carbon burial in fjord sediments globally. *Nature Geoscience*. **8**(6),pp.450–453.
- Spratt, R.M. and Lisiecki, L.E. 2016. A Late Pleistocene sea level stack. *Climate of the Past*. [Online]. **12**(4),pp.1079–1092. Available from: <https://doi.org/10.5194/cp-12-1079-2016>.
- Stephenson, M.H., Ringrose, P., Geiger, S., Bridden, M. and Schofield, D. 2019. Geoscience and decarbonization: Current status and future directions. *Petroleum Geoscience*. [Online]. **25**(4),pp.501–508. Available from: <https://doi.org/10.1144/petgeo2019-084>.



- Stevenson, J.C., Kearney, M.S. and Pendleton, E.C. 1985. Sedimentation and erosion in a Chesapeake Bay brackish marsh system. *Marine Geology*. [Online]. **67**(3–4),pp.213–235. Available from: [https://doi.org/10.1016/0025-3227\(85\)90093-3](https://doi.org/10.1016/0025-3227(85)90093-3).
- Stewart, M., Lonergan, L. and Hampson, G. 2012. 3D seismic analysis of buried tunnel valleys in the Central North Sea: tunnel valley fill sedimentary architecture. *Geological Society Special Publication*. [Online]. **368**(1),pp.173–184. Available from: <https://doi.org/10.1144/SP368.9>.
- Stewart, M.A., Lonergan, L. and Hampson, G. 2013. 3D seismic analysis of buried tunnel valleys in the central North Sea: Morphology, cross-cutting generations and glacial history. *Quaternary Science Reviews*. [Online]. **72**,pp.1–17. Available from: <https://doi.org/10.1016/j.quascirev.2013.03.016>.
- Stoker, M., Balson, P.S., Long, D. and Tappin, D.R. 2011. An overview of the lithostratigraphical framework for the Quaternary deposits on the United Kingdom continental shelf. *British Geological Survey Research Report*. [Online]. **RR/11/03**,p.40. Available from: <http://nora.nerc.ac.uk/id/eprint/15939>.
- Storms, J.E.A., Weltje, G.J., Terra, G.J., Cattaneo, A. and Trincardi, F. 2008. Coastal dynamics under conditions of rapid sea-level rise: Late Pleistocene to Early Holocene evolution of barrier-lagoon systems on the northern Adriatic shelf (Italy). *Quaternary Science Reviews*. [Online]. **27**(11–12),pp.1107–1123. Available from: <https://doi.org/10.1016/j.quascirev.2008.02.009>.
- Stouthamer, E., Cohen, K.M. and Gouw, M.J.P. 2011. Avulsion and its Implications for Fluvial-Deltaic Architecture: Insights from the Holocene Rhine–Meuse Delta. *SEPM Special Publication*. [Online]. **97**,pp.215–231. Available from: <https://doi.org/10.2110/sepmsp.097.215>.
- Streif, H. 2004. Sedimentary record of Pleistocene and Holocene marine inundations along the North Sea coast of Lower Saxony, Germany. *Quaternary International*. [Online]. **112**(1),pp.3–28. Available from: [https://doi.org/10.1016/S1040-6182\(03\)00062-4](https://doi.org/10.1016/S1040-6182(03)00062-4).
- Stuiver, M., Reimer, P.J. and Reimer, R.W. 2020. CALIB 8.2 [WWW program]. Available from: <http://calib.org>.

- Sturt, F., Garrow, D. and Bradley, S. 2013. New models of North West European Holocene palaeogeography and inundation. *Journal of Archaeological Science*. [Online]. **40**(11),pp.3963–3976. Available from: <http://dx.doi.org/10.1016/j.jas.2013.05.023>.
- Sugden, D.E. 1968. The Selectivity of Glacial Erosion in the Cairngorm Mountains, Scotland. *Transactions of the Institute of British Geographers*. [Online],pp.79–92. Available from: <https://doi.org/10.2307/621394>.
- Tappin, D.R., Pearce, B., Fitch, S., Dove, D., Gearey, B., Hill, J.M., Chambers, C., Bates, R., Pinnion, J., Diaz Doce, D. and others 2011. *The Humber regional environmental characterisation* [Online]. Marine Aggregate Levy Sustainability Fund. Available from: <http://www.cefas.defra.gov.uk/alsf.aspx>.
- Tarnocai, C., Kuhry, P., Broll, G., Ping, C.L. and Brown, J. 2012. Peatlands and their carbon dynamics: Comment on ‘peatlands and their role in the global carbon cycle’. *Eos*. **93**(3),p.31.
- Temmerman, S., Moonen, P., Schoelynck, J., Govers, G. and Bouma, T.J. 2012. Impact of vegetation die-off on spatial flow patterns over a tidal marsh. *Geophysical Research Letters*. [Online]. **39**(3),pp.1–5. Available from: <https://doi.org/10.1029/2011GL050502>.
- Tizzard, L., Bicket, A.R., Benjamin, J. and Loecker, D. De 2014. A Middle Palaeolithic site in the southern North Sea: Investigating the archaeology and palaeogeography of Area 240. *Journal of Quaternary Science*. **29**(7),pp.698–710.
- Toucanne, S., Zaragosi, S., Bourillet, J.F., Cremer, M., Eynaud, F., Van Vliet-Lanoë, B., Penaud, A., Fontanier, C., Turon, J.L., Cortijo, E. and Gibbard, P.L. 2009. Timing of massive ‘Fleuve Manche’ discharges over the last 350 kyr: insights into the European ice-sheet oscillations and the European drainage network from MIS 10 to 2. *Quaternary Science Reviews*. [Online]. **28**(13–14),pp.1238–1256. Available from: <https://doi.org/10.1016/j.quascirev.2009.01.006>.

- Treat, C.C., Kleinen, T., Broothaerts, N., Dalton, A.S., Dommaine, R., Douglas, T.A., Drexler, J.Z., Finkelstein, S.A., Grosse, G., Hope, G., Hutchings, J., Jones, M.C., Kuhry, P., Lacourse, T., Lähteenoja, O., Loisel, J., Notebaert, B., Payne, R.J., Peteet, D.M., Sannel, A.B.K., Stelling, J.M., Strauss, J., Swindles, G.T., Talbot, J., Tarnocai, C., Verstraeten, G., Williams, C.J., Xia, Z., Yu, Z., Väiliranta, M., Hättestrand, M., Alexanderson, H. and Brovkin, V. 2019. Widespread global peatland establishment and persistence over the last 130,000 y. *Proceedings of the National Academy of Sciences of the United States of America*. **116**(11),pp.4822–4827.
- Trenhaile, A.S. 2010. The effect of Holocene changes in relative sea level on the morphology of rocky coasts. *Geomorphology*. **114**(1–2),pp.30–41.
- Tyrrell, S., Houghton, P.D.W., Daly, J.S., Kokfelt, T.F. and Gagnevin, D. 2006. The use of the common Pb isotope composition of detrital K-feldspar grains as a provenance tool and its application to Upper Carboniferous paleodrainage, northern England. *Journal of Sedimentary Research*. [Online]. **76**(2),pp.324–345. Available from: <https://doi.org/10.2110/jsr.2006.023%0A>.
- Uehara, K., Scourse, J.D., Horsburgh, K.J., Lambeck, K. and Purcell, A.P. 2006. Tidal evolution of the northwest European shelf seas from the Last Glacial Maximum to the present. *Journal of Geophysical Research: Oceans*. [Online]. **111**(9),pp.1–15. Available from: <http://dx.doi.org/10.1029/2006JC003531>; doi:10.102.
- UN 2015. Adoption of the Paris agreement. *Framework Convention on Climate Change*,pp.1–40.
- University of Birmingham 2011. North Sea Palaeolandscape project [data-set]. *York: Archaeology Data Services*. [Online]. Available from: <https://doi.org/10.5284/1000397>.
- Vandenbergh, D.A.G., Derese, C., Kasse, C. and Den, P. Van 2013. Late Weichselian (fluvio-)aeolian sediments and Holocene drift-sands of the classic type locality in Twente (E Netherlands): a high-resolution dating study using optically stimulated luminescence. *Quaternary Science Reviews*. [Online]. **68**,pp.96–113. Available from: <http://dx.doi.org/10.1016/j.quascirev.2013.02.009>.

- Vandenberghe, J. 1985. Paleoenvironment and Stratigraphy during the Last Glacial in the Belgian-Dutch Border Region. *Quaternary Research*. [Online]. **24**(1),pp.23–38. Available from: [https://doi.org/10.1016/0033-5894\(85\)90081-X](https://doi.org/10.1016/0033-5894(85)90081-X).
- Vandenberghe, J. 1995. Timescales, climate and river development. *Quaternary Science Reviews*. [Online]. **14**(6),pp.631–638. Available from: [https://doi.org/10.1016/0277-3791\(95\)00043-O](https://doi.org/10.1016/0277-3791(95)00043-O).
- Vegt, V. Der, Janszen, A. and Moscariello, A. 2012. Tunnel valleys: Current knowledge and future perspectives. *Geological Society Special Publication*. [Online]. **368**(1),pp.75–97. Available from: <https://doi.org/10.1144/SP368.13>.
- Waelbroeck, C., Labeyrie, L., Michel, E., Duplessy, J.C., McManus, J.F., Lambeck, K., Balbon, E. and Labracherie, M. 2002. Sea-level and deep water temperature changes derived from benthic foraminifera isotopic records. *Quaternary Science Reviews*. [Online]. **21**(1–3),pp.295–305. Available from: [https://doi.org/10.1016/S0277-3791\(01\)00101-9](https://doi.org/10.1016/S0277-3791(01)00101-9).
- Waller, M. and Kirby, J. 2020. Coastal peat-beds and peatlands of the southern North Sea: their past, present and future. *Biological Reviews*. **4**.
- Ward, I., Larcombe, P. and Lillie, M. 2006. The dating of Doggerland – post-glacial geochronology of the southern North Sea. *Environmental Archaeology*. [Online]. **11**(2),pp.207–218. Available from: <https://doi.org/10.1179/174963106x123214>.
- Warner B G 2005. Canadian Peatlands. *Mires, from Siberia to Tierra del Fuego*. **35**,pp.353–372.
- Warnke, U. 2015. Die Nordsee. Ein archäologisches Archiv der Neuzeit. *Mitteilungen der Deutschen Gesellschaft für Archäologie des Mittelalters und der Neuzeit*. **30**(28),pp.37–46.
- Wessex Archaeology 2019a. *Norfolk Boreas Offshore Wind Farm, Appendix 17.7 - Stage 3 Geoarchaeological Assessment*.
- Wessex Archaeology 2019b. *Norfolk Boreas Offshore Wind Fram, Stage 4 Palaeoenvironmental Analysis*.

- Wessex Archaeology 2019c. *Norfolk Vanguard Offshore Wind Farm, Stage 4 Paaeoenvironmental Assessment* [Online]. Available from: <https://corporate.vattenfall.co.uk/globalassets/uk/projects/norfolk-vanguard/en010079-000022-scoping-report-6.pdf>.
- Wessex Archaeology 2018. *Norfolk Vanguard Offshore Wind Farm Stage 3 Geoarchaeological Sampling and Assessment* [Online]. Available from: <https://corporate.vattenfall.co.uk/globalassets/uk/projects/norfolk-vanguard/en010079-000022-scoping-report-6.pdf>.
- Whittle, A. and Gallego-Sala, A. V. 2016. Vulnerability of the peatland carbon sink to sea-level rise. *Scientific Reports*. [Online]. **6**(March),pp.1–11. Available from: <http://dx.doi.org/10.1038/srep28758>.
- Wilson, K.R., Kelley, J.T., Croitoru, A., Dionne, M., Belknap, D.F. and Steneck, R. 2009. Stratigraphic and Ecophysical Characterizations of Salt Pools: Dynamic Landforms of the Webhannet Salt Marsh, Wells, ME, USA. *Estuaries and Coasts*. [Online]. **32**(5),pp.855–870. Available from: <https://doi.org/10.1007/s12237-009-9203-7>.
- Wilson, K.R., Kelley, J.T., Tanner, B.R. and Belknap, D.F. 2010. Probing the Origins and Stratigraphic Signature of Salt Pools from North-Temperate Marshes in Maine, U.S.A. *Journal of Coastal Research*. [Online]. **26**(6),pp.1007–1026. Available from: <https://doi.org/10.2112/JCOASTRES-D-10-00007.1>.
- Wingfield, R. 1990. The origin of major incisions within the Pleistocene deposits of the North Sea. *Marine Geology*. [Online]. **91**(1–2),pp.31–52. Available from: [https://doi.org/10.1016/0025-3227\(90\)90131-3](https://doi.org/10.1016/0025-3227(90)90131-3).
- Yu, Z., Loisel, J., Brosseau, D.P., Beilman, D.W. and Hunt, S.J. 2010. Global peatland dynamics since the Last Glacial Maximum. *Geophysical Research Letters*. [Online]. **37**(13),pp.1–5. Available from: <https://doi.org/10.1029/2010GL043584>.
- Zagwijn, W.H. 1983. Sea-level changes in the Netherlands during the Eemian. *Geologie en Mijnbouw*. [Online]. **62**(3),pp.437–450. Available from: <http://pascal-francis.inist.fr/vibad/index.php?action=getRecordDetail&idt=9542518>.

- Zagwijn, W.H. 1974. The palaeogeographic evolution of the Netherlands during the Quaternary. *Quaternary Geology*. [Online]. **53**,pp.369–385.
- Zanella, E. and Coward, M.P. 2003. Structural framework *In*: D. Evans, C. Graham, A. Atmour and P. Bathurst, eds. *The Millenium Atlas: Petroleum Geology of the Central and Northern North Sea*. London: The Geological Society of London, pp. 45–59.
- Zeff, M.L. 1999. Salt marsh tidal channel morphometry: Applications for wetland creation and restoration. *Restoration Ecology*. **7**(2),pp.205–211.
- Ziegler, P.A. 1992. North Sea rift system. *Geodynamics of Rifting*. [Online]. **208**(1–3),pp.55–75. Available from: [https://doi.org/10.1016/0040-1951\(92\)90336-5](https://doi.org/10.1016/0040-1951(92)90336-5).

## Appendix 1 – Bulk density analysis data

Core	Sample ID	Depth below seabed	Tin weight grams	Tin + sample weight grams	Wet weight grams	Wet bulk density g/cm <sup>3</sup>	Dried weight g/cm <sup>3</sup>	Dry bulk density g/cm <sup>3</sup>
VC085	110957	1.8	1.297	4.327	3.03	1.515	2.319	1.1595
VC085	110958	1.85	1.309	4.206	2.897	1.4485	2.113	1.0565
VC085	110959	1.9	1.297	4.202	2.905	1.4525	2.163	1.0815
VC085	110960	1.95	1.297	4.036	2.739	1.3695	1.97	0.985
VC085	110961	2	1.298	4.156	2.858	1.429	1.992	0.996
VC085	110962	2.05	1.299	3.994	2.695	1.3475	2.019	1.0095
VC085	110963	2.1	1.307	4.376	3.069	1.5345	2.494	1.247
VC085	110964	2.2	1.296	4.74	3.444	1.722	2.997	1.4985
VC085	110965	2.3	1.301	5.882	4.581	2.2905	4.701	2.3505
VC085	110966	2.4	1.307	5.616	4.309	2.1545	4.346	2.173
VC085	110967	2.5	1.307	5.931	4.624	2.312	4.781	2.3905
VC085	110968	2.6	1.3	5.192	3.892	1.946	4.537	2.2685
VC085	110969	2.7	1.306	5.695	4.389	2.1945	5.088	2.544
VC074	110970	0.85	1.295	4.895	3.6	1.8	3.451	1.7255
VC074	110971	0.9	1.303	4.503	3.2	1.6	2.693	1.3465
VC074	110972	0.95	1.311	4.091	2.78	1.39	1.979	0.9895
VC074	110973	1	1.304	4.165	2.861	1.4305	2.083	1.0415
VC074	110974	1.05	1.303	4.078	2.775	1.3875	2.127	1.0635
VC074	110975	1.1	1.303	4.196	2.893	1.4465	2.184	1.092
VC074	110976	1.15	1.304	4.126	2.822	1.411	2.106	1.053
VC074	110977	1.2	1.309	4.2	2.891	1.4455	2.301	1.1505
VC074	110978	1.25	1.311	4.532	3.221	1.6105	3.527	1.7635
VC074	110979	1.3	1.31	4.331	3.021	1.5105	3.481	1.7405
VC074	110980	1.35	1.307	4.149	2.842	1.421	2.378	1.189
VC074	110981	1.4	1.306	4.045	2.739	1.3695	2.707	1.3535
VC074	110982	1.45	1.308	4.426	3.118	1.559	2.628	1.314
VC074	110983	1.5	1.308	4.892	3.584	1.792	3.188	1.594
VC074	110984	1.55	1.307	4.119	2.812	1.406	2.183	1.0915
VC074	110985	1.6	1.306	5.52	4.214	2.107	5.009	2.5045
VC076	110986	3.7	1.305	4.083	2.778	1.389	2.135	1.0675
VC076	110987	3.75	1.307	5.483	4.176	2.088	4.364	2.182
VC076	110988	3.8	1.303	5.76	4.457	2.2285	4.806	2.403
VC076	110989	3.9	1.304	5.7	4.396	2.198	5.132	2.566
VC075	110990	4.4	1.302	4.184	2.882	1.441	2.276	1.138
VC075	110991	4.45	1.302	3.518	2.216	1.108	1.945	0.9725
VC075	110992	4.5	1.303	4.484	3.181	1.5905	2.782	1.391
VC075	110993	4.55	1.303	3.916	2.613	1.3065	2.003	1.0015
VC075	110994	4.6	1.304	3.719	2.415	1.2075	1.986	0.993
VC075	110995	4.65	1.303	3.942	2.639	1.3195	2.083	1.0415
VC075	110996	4.7	1.31	5.597	4.287	2.1435	4.439	2.2195
VC039	110997	2.925	1.305	6.207	4.902	2.451	5.161	2.5805
VC039	110998	3	1.303	4.122	2.819	1.4095	2.226	1.113
VC039	110999	3.05	1.303	4.073	2.77	1.385	2.224	1.112
VC039	111000	3.1	1.311	5.062	3.751	1.8755	3.36	1.68
VC039	111001	3.15	1.307	5.014	3.707	1.8535	3.458	1.729
VC039	111002	3.2	1.306	5.178	3.872	1.936	3.653	1.8265
VC039	111003	3.25	1.306	5.434	4.128	2.064	3.961	1.9805
VC039	111004	3.3	1.308	5.695	4.387	2.1935	4.879	2.4395
VC028	111005	2.3	1.294	5.556	4.262	2.131	5.106	2.553
VC028	111006	2.4	1.293	4.234	2.941	1.4705	2.398	1.199
VC028	111007	2.5	1.307	4.201	2.894	1.447	2.246	1.123
VC028	111008	2.55	1.29	4.106	2.816	1.408	2.169	1.0845
VC028	111009	2.6	1.291	3.906	2.615	1.3075	2.15	1.075
VC028	111010	2.65	1.292	4.525	3.233	1.6165	2.904	1.452
VC028	111011	2.75	1.286	5.393	4.107	2.0535	4.864	2.432
VC032	111012	3.78	1.288	4.808	3.52	1.76	3.091	1.5455
VC032	111013	3.83	1.297	3.635	2.338	1.169	1.945	0.9725
VC032	111014	3.88	1.29	3.932	2.642	1.321	2.089	1.0445
VC032	111015	3.93	1.289	3.931	2.642	1.321	2.094	1.047
VC032	111016	3.98	1.306	3.988	2.682	1.341	2.108	1.054
VC032	111017	4.03	1.308	3.819	2.511	1.2555	2.179	1.0895
VC032	111018	4.08	1.304	4.07	2.766	1.383	2.283	1.1415
VC032	111019	4.13	1.3	5.269	3.969	1.9845	3.889	1.9445
VC032	111020	4.2	1.297	5.77	4.473	2.2365	5.144	2.572
VC016	111021	0.2	1.307	6.558	5.251	2.6255	5.821	2.9105
VC047	111022	2.4	1.298	6.525	5.227	2.6135	5.975	2.9875

## Appendix 2 – Total carbon analysis data

Elementar vario micro

24th Sept 2019

DJA

No.	Weight [mg]	Name	NArea	CArea	HArea	N [%]	C [%]	H [%]	C/N ratio	C/H ratio	Method	Date Time
1	1.000	RunIn	8	17	170	0.17	0.00	0.41	0.0000	0.0000	9mgPlant90s	13.09.2019 10:39
2	0.508	sulfamilic acid	1457	5365	1715	8.18	41.73	4.19	5.0986	9.9603	9mgPlant90s	-----
3	0.982	sulfamilic acid	2819	10395	3396	8.05	41.61	4.08	5.1670	10.2127	9mgPlant90s	-----
4	2.054	sulfamilic acid	5976	21765	7190	8.08	41.53	4.01	5.1400	10.3690	9mgPlant90s	-----
5	2.920	sulfamilic acid	8531	31041	10511	8.09	41.63	4.08	5.1449	10.1932	9mgPlant90s	-----
6	3.963	sulfamilic acid	11586	42138	14299	8.08	41.62	4.07	5.1487	10.2155	9mgPlant90s	-----
7	4.994	sulfamilic acid	14635	53096	18058	8.10	41.61	4.07	5.1397	10.2187	9mgPlant90s	13.09.2019 11:29
8	1.203	1drift	3456	12811	4338	8.03	41.82	4.20	5.2067	9.9602	9mgPlant90s	13.09.2019 11:37
9	2.510	1drift	7363	26837	9059	8.13	41.89	4.11	5.1499	10.1979	9mgPlant90s	13.09.2019 11:46
10	0.000	blank	0	31	212	0.00	0.00	0.00	0.0000	0.0000	9mgPlant90s	13.09.2019 11:54
207	0.000	blank	9	19	186	0.00	0.00	0.00	0.0000	0.0000	9mgPlant90s	16.09.2019 20:00
208	8.129	b2150X	1483	12892	10335	0.52	6.86	1.47	13.2000	4.6853	9mgPlant90s	19.09.2019 15:38
209	8.023	B2152X	350	3279	2600	0.14	1.80	0.41	12.8857	4.4000	9mgPlant90s	19.09.2019 15:46
210	4.133	110957	1736	25098	12439	1.20	26.20	3.45	21.8350	7.5992	9mgPlant90s	19.09.2019 15:54
211	4.016	110958	2240	31235	15764	1.58	33.54	4.47	21.2272	7.5015	9mgPlant90s	19.09.2019 16:03
212	3.911	110959	1831	26840	13065	1.33	29.60	3.82	22.2564	7.7449	9mgPlant90s	19.09.2019 16:11
213	3.909	110960	2579	35799	17405	1.86	39.47	5.06	21.2194	7.7985	9mgPlant90s	19.09.2019 16:19
214	3.912	110961	2588	35913	17318	1.86	39.57	5.03	21.2726	7.8631	9mgPlant90s	19.09.2019 16:28
215	4.008	110962	2695	35513	17165	1.89	38.19	4.87	20.2074	7.8439	9mgPlant90s	19.09.2019 16:36
216	4.133	110963	1381	19890	11063	0.96	20.78	3.08	21.6448	6.7530	9mgPlant90s	19.09.2019 16:45
217	4.038	110964	724	10526	5656	0.53	11.30	1.66	21.3151	6.8136	9mgPlant90s	19.09.2019 16:53
218	4.016	110965	170	2422	1859	0.16	2.68	0.61	16.7750	4.3713	9mgPlant90s	19.09.2019 17:01
219	3.979	110966	242	3501	2219	0.21	3.87	0.72	18.4381	5.3778	9mgPlant90s	19.09.2019 17:09
220	3.970	110967	102	2281	1368	0.11	2.56	0.48	23.3000	5.3064	9mgPlant90s	19.09.2019 17:17
221	3.914	110968	35	1331	734	0.07	1.55	0.31	22.1571	5.0032	9mgPlant90s	19.09.2019 17:25
222	3.920	110969	21	972	894	0.06	1.16	0.36	19.2500	3.2535	9mgPlant90s	19.09.2019 17:33
223	1.276	2drift	3692	13489	4505	8.09	41.59	4.24	5.1409	9.8043	9mgPlant90s	19.09.2019 17:41
224	2.652	2drift	7614	27872	9301	7.96	41.21	4.06	5.1771	10.1628	9mgPlant90s	19.09.2019 17:49
225	0.000	blank	0	29	209	0.00	0.00	0.00	0.0000	0.0000	9mgPlant90s	19.09.2019 17:57
226	4.065	110970	321	5557	2535	0.26	5.97	0.79	22.9731	7.5417	9mgPlant90s	19.09.2019 18:05
227	3.933	110971	483	7799	3601	0.38	8.62	1.12	22.6947	7.7000	9mgPlant90s	19.09.2019 18:13



228	4.028	110972	1935	27227	13157	1.36	29.16	3.74	21.4419	7.8033	9mgPlant90s	19.09.2019 18:22
229	3.989	110973	1050	30777	14486	0.77	33.26	4.14	43.2000	8.0270	9mgPlant90s	19.09.2019 18:30
230	3.963	110974	1723	23367	11962	1.24	25.44	3.46	20.5185	7.3492	9mgPlant90s	19.09.2019 18:39
231	3.983	110975	1961	27855	13446	1.40	30.16	3.86	21.5443	7.8160	9mgPlant90s	19.09.2019 18:47
232	3.959	110976	1967	28013	13382	1.41	30.51	3.87	21.6411	7.8950	9mgPlant90s	19.09.2019 18:55
233	4.078	110977	1431	22540	10025	1.01	23.86	2.84	23.6228	8.4159	9mgPlant90s	19.09.2019 19:04
234	4.000	110978	139	2978	1567	0.14	3.29	0.54	23.4929	6.1477	9mgPlant90s	19.09.2019 19:12
235	4.036	110979	128	2969	1480	0.13	3.26	0.51	25.0462	6.4348	9mgPlant90s	19.09.2019 19:20
236	3.969	110980	505	8137	3759	0.39	8.91	1.15	22.8462	7.7210	9mgPlant90s	19.09.2019 19:28
237	3.983	110981	1017	16634	7445	0.74	18.05	2.18	24.3932	8.2765	9mgPlant90s	19.09.2019 19:36
238	4.081	110982	652	9612	4524	0.48	10.22	1.33	21.2896	7.6719	9mgPlant90s	19.09.2019 19:44
239	4.082	110983	541	7908	3845	0.41	8.42	1.15	20.5244	7.3429	9mgPlant90s	19.09.2019 19:53
240	4.029	110984	1801	23750	11483	1.27	25.44	3.27	20.0339	7.7736	9mgPlant90s	19.09.2019 20:01
241	1.245	3drift	3574	13257	4482	8.03	41.89	4.33	5.2167	9.6811	9mgPlant90s	19.09.2019 20:09
242	2.471	3drift	7075	25832	8653	7.95	41.00	4.06	5.1572	10.0960	9mgPlant90s	19.09.2019 20:18
243	0.000	blank	0	34	178	0.00	0.00	0.00	0.0000	0.0000	9mgPlant90s	19.09.2019 20:26
244	3.982	110985	28	254	416	0.06	0.36	0.22	6.0500	1.6884	9mgPlant90s	19.09.2019 20:33
245	4.000	110986	1364	36061	17478	0.98	38.85	4.97	39.6449	7.8236	9mgPlant90s	19.09.2019 20:42
246	3.959	110987	197	3016	1884	0.18	3.37	0.63	18.7000	5.3429	9mgPlant90s	19.09.2019 20:50
247	3.969	110988	39	895	757	0.07	1.07	0.31	15.2429	3.4199	9mgPlant90s	19.09.2019 20:58
248	3.927	110989	6	544	411	0.05	0.69	0.22	13.8600	3.1935	9mgPlant90s	19.09.2019 21:06
249	4.060	110990	1953	27572	13264	1.36	29.29	3.74	21.5390	7.8407	9mgPlant90s	19.09.2019 21:14
250	4.000	110991	2485	38598	18466	1.75	41.58	5.24	23.7600	7.9336	9mgPlant90s	19.09.2019 21:23
251	3.940	110992	616	9908	5517	0.47	10.90	1.66	23.1936	6.5669	9mgPlant90s	19.09.2019 21:31
252	4.070	110993	1811	38363	18168	1.27	40.62	5.07	31.9866	8.0140	9mgPlant90s	19.09.2019 21:39
253	4.036	110994	2827	41149	19455	1.97	43.93	5.47	22.3015	8.0362	9mgPlant90s	19.09.2019 21:48
254	3.975	110995	2748	39373	19019	1.94	42.68	5.43	22.0000	7.8615	9mgPlant90s	19.09.2019 21:56
255	4.020	110996	94	1567	1141	0.11	1.77	0.41	16.1000	4.2778	9mgPlant90s	19.09.2019 22:04
256	4.025	110997	75	3089	1095	0.09	3.39	0.40	37.6444	8.4489	9mgPlant90s	19.09.2019 22:12
257	4.067	110998	3000	36401	17046	2.07	38.58	4.77	18.6362	8.0942	9mgPlant90s	19.09.2019 22:21
258	3.923	110999	2488	35075	16045	1.79	38.54	4.66	21.5330	8.2766	9mgPlant90s	19.09.2019 22:29
259	1.233	4drift	3499	13039	4454	7.94	41.61	4.34	5.2406	9.5787	9mgPlant90s	19.09.2019 22:37
260	2.586	4drift	7480	27338	9183	8.03	41.45	4.11	5.1619	10.0901	9mgPlant90s	-----
261	0.000	blank	0	37	199	0.00	0.00	0.00	0.0000	0.0000	9mgPlant90s	19.09.2019 22:54
262	4.002	111000	670	14622	8278	0.50	15.81	2.40	31.6140	6.5780	9mgPlant90s	24.09.2019 14:58

263	4.096	111001	374	11393	3778	0.29	12.05	1.12	41.5345	10.7162	9mgPlant90s	24.09.2019 15:06
264	4.053	111002	323	10127	3342	0.26	10.84	1.02	41.6731	10.6644	9mgPlant90s	24.09.2019 15:14
265	4.014	111003	155	7366	2292	0.15	7.99	0.73	53.2400	10.8801	9mgPlant90s	24.09.2019 15:22
266	3.938	111004	28	2369	709	0.06	2.68	0.30	44.7333	8.9169	9mgPlant90s	24.09.2019 15:30
267	3.981	111005	38	431	458	0.07	0.56	0.23	8.0143	2.4714	9mgPlant90s	24.09.2019 15:38
268	4.039	111006	1591	18457	9580	1.13	19.75	2.74	17.4735	7.2062	9mgPlant90s	24.09.2019 15:46
269	3.930	111007	1766	19797	10504	1.28	21.76	3.08	16.9984	7.0689	9mgPlant90s	24.09.2019 15:54
270	4.039	111008	2000	34572	16101	1.40	36.89	4.54	26.3529	8.1300	9mgPlant90s	24.09.2019 16:03
271	4.029	111009	1683	32864	14768	1.19	35.17	4.18	29.5521	8.4111	9mgPlant90s	24.09.2019 16:12
272	4.049	111010	120	2009	1717	0.12	2.22	0.57	18.5167	3.8982	9mgPlant90s	24.09.2019 16:20
273	4.083	111011	16	233	733	0.05	0.33	0.30	6.6000	1.1111	9mgPlant90s	24.09.2019 16:27
274	3.782	111012	687	8918	5652	0.54	10.24	1.77	18.9648	5.7891	9mgPlant90s	24.09.2019 16:36
275	4.037	111013	2069	39120	16931	1.45	41.76	4.77	28.7972	8.7557	9mgPlant90s	24.09.2019 16:44
276	3.946	111014	2231	40102	17912	1.60	43.79	5.16	27.3694	8.4932	9mgPlant90s	24.09.2019 16:53
277	1.266	5drift	3576	13222	4583	7.90	41.09	4.34	5.2013	9.4590	9mgPlant90s	24.09.2019 17:01
278	2.557	5drift	7391	26927	9094	8.02	41.30	4.12	5.1496	10.0340	9mgPlant90s	24.09.2019 17:10
279	0.000	blank	0	36	271	0.00	0.00	0.00	0.0000	0.0000	9mgPlant90s	24.09.2019 17:17
280	4.084	111015	2811	40880	18175	1.93	43.13	5.05	22.3477	8.5340	9mgPlant90s	24.09.2019 17:26
281	4.012	111016	2931	40110	18991	2.05	43.08	5.37	21.0127	8.0201	9mgPlant90s	24.09.2019 17:35
282	3.975	111017	3349	36538	17295	2.36	39.62	4.95	16.7890	8.0109	9mgPlant90s	24.09.2019 17:43
283	3.970	111018	3090	36108	16649	2.18	39.20	4.77	17.9835	8.2171	9mgPlant90s	24.09.2019 17:52
284	4.058	111019	596	8052	4476	0.44	8.62	1.33	19.6000	6.5038	9mgPlant90s	24.09.2019 18:00
285	3.935	111020	7	1537	582	0.05	1.77	0.27	35.4200	6.6830	9mgPlant90s	24.09.2019 18:08
286	4.045	111021	44	2696	1652	0.07	2.96	0.55	42.2714	5.3508	9mgPlant90s	24.09.2019 18:16
287	4.041	111022	35	1487	840	0.06	1.67	0.33	27.8667	5.0821	9mgPlant90s	24.09.2019 18:24
288	4.087	110957*	1690	24172	11500	1.18	25.52	3.23	21.6271	7.8985	9mgPlant90s	24.09.2019 18:32
289	4.007	110969*	12	954	1037	0.05	1.11	0.39	22.2200	2.8708	9mgPlant90s	24.09.2019 18:40
290	4.081	110977*	1428	22121	9820	1.00	23.40	2.78	23.3970	8.4253	9mgPlant90s	24.09.2019 18:48
291	4.040	110991*	2544	38890	19052	1.77	41.48	5.35	23.4356	7.7520	9mgPlant90s	24.09.2019 18:57
292	4.034	111000*	600	14940	4482	0.45	16.02	1.34	35.5911	11.9880	9mgPlant90s	24.09.2019 19:05
293	4.079	111014*	2311	40732	19139	1.60	43.03	5.32	26.8950	8.0842	9mgPlant90s	24.09.2019 19:14
295	8.136	b2150x	1393	12906	9660	0.49	6.86	1.37	14.0082	5.0066	9mgPlant90s	24.09.2019 19:30
296	8.016	b2152x	350	3269	2602	0.14	1.80	0.41	12.8857	4.3893	9mgPlant90s	24.09.2019 19:38
297	1.281	6drift	3661	13420	4538	7.99	41.21	4.25	5.1577	9.6874	9mgPlant90s	24.09.2019 19:46
298	2.536	6drift	7305	26697	8962	7.99	41.28	4.09	5.1665	10.0880	9mgPlant90s	24.09.2019 19:55
299	0.000	blank	0	161	290	0.00	0.00	0.00	0.0000	0.0000	9mgPlant90s	24.09.2019 20:03
300	4.084	b2150x	694	6442	4867	0.51	6.88	1.42	13.4804	4.8279	9mgPlant90s	24.09.2019 20:11
301	4.026	b2150x	138	1611	1312	0.14	1.82	0.46	12.9643	3.9371	9mgPlant90s	24.09.2019 20:19

## Appendix 3 – Organic carbon analysis data

Checked	DJA	Elementar Vario micro cube																
		samples: dried in freeze drier. peak shapes symmetrical and easier to integrate. less residual water.																
No.	Weight [mg]	Name	NArea	CArea	HArea	N [%]	C [%]	H [%]	C/N ratio	C/H ratio	Method	N Factor	C Factor	H Factor	N Blank	C Blank	H Blank	Date Time
1	5.000	runin	342	0	40	0.13	0.00	0.00	0.0000	0.0000	9mgPlant90s	1	1	1	15	11	0	25.10.2019 10:53
2	0.465	sulfanilic acid	1482	5135	55	8.22	42.39	3.68	5.1548	11.5073	9mgPlant90s	1	1	1	15	11	0	25.10.2019 11:01
3	0.971	sulfanilic acid	2937	10298	67	8.08	41.26	3.89	5.1096	10.6102	9mgPlant90s	1	1	1	15	11	0	25.10.2019 11:10
4	1.909	sulfanilic acid	5656	20309	91	8.04	41.66	4.11	5.1816	10.1462	9mgPlant90s	1	1	1	15	11	0	25.10.2019 11:19
5	3.021	sulfanilic acid	9000	32095	121	8.14	41.71	4.26	5.1250	9.7815	9mgPlant90s	1	1	1	15	11	0	25.10.2019 11:27
6	4.116	sulfanilic acid	12072	43265	151	8.03	41.31	4.34	5.1418	9.5298	9mgPlant90s	1	1	1	15	11	0	25.10.2019 11:36
7	5.039	sulfanilic acid	14906	53522	158	8.12	41.77	3.79	5.1468	11.0092	9mgPlant90s	1	1	1	15	11	0	25.10.2019 11:44
8	1.281	1drift	3641	12834	86	7.64	39.08	5.42	5.1159	7.2179	9mgPlant90s	1	1	1	15	11	0	25.10.2019 11:53
9	2.588	1drift	7622	27453	110	8.03	41.61	4.26	5.1830	9.7770	9mgPlant90s	1	1	1	15	11	0	25.10.2019 12:02
10	0.000	blank	36	29	0	0.00	0.00	0.00	0.0000	0.0000	9mgPlant90s	1	1	1	36	29	0	25.10.2019 12:09
11	8.320	b2150	1621	13361	93	0.51	6.89	0.97	13.6354	7.0835	9mgPlant90s	1	1.1	1	15	11	0	25.10.2019 12:18
12	9.951	110957	4373	59021	179	1.19	25.66	2.27	21.6281	11.2943	9mgPlant90s	1	1.1	1	15	11	0	25.10.2019 12:26
13	9.311	110958	5290	70435	190	1.54	32.74	2.63	21.2614	12.4713	9mgPlant90s	1	1.1	1	15	11	0	25.10.2019 12:35
14	9.935	110959	4551	61261	169	1.24	26.68	2.11	21.5541	12.6236	9mgPlant90s	1	1.1	1	15	11	0	25.10.2019 12:43
15	10.212	110960	6822	90721	211	1.82	38.47	2.74	21.1564	14.0334	9mgPlant90s	1	1.1	1	15	11	0	25.10.2019 12:52
16	9.382	110961	6386	84319	198	1.85	38.91	2.76	21.0240	14.1151	9mgPlant90s	1	1.1	1	15	11	0	25.10.2019 13:00
17	10.465	110962	7335	92733	223	1.91	38.37	2.87	20.0927	13.3513	9mgPlant90s	1	1.1	1	15	11	0	25.10.2019 13:09
18	10.268	110963	3745	50329	147	0.98	11.20	1.69	21.6129	12.5778	9mgPlant90s	1	1.1	1	15	11	0	25.10.2019 13:18
19	9.335	110964	1975	24986	114	0.56	11.54	1.25	20.7933	9.2508	9mgPlant90s	1	1.1	1	15	11	0	25.10.2019 13:26
20	9.671	110965	648	5602	71	0.16	2.45	0.46	15.6115	5.3141	9mgPlant90s	1	1.1	1	15	11	0	25.10.2019 13:34
21	10.434	110966	888	7922	54	0.21	3.24	0.15	15.4647	22.1334	9mgPlant90s	1	1.1	1	15	11	0	25.10.2019 13:43
22	9.951	110967	472	3117	39	0.10	1.30	0.00	12.5066	0.0000	9mgPlant90s	1	1.1	1	15	11	0	25.10.2019 13:51
23	10.674	110968	290	2226	34	0.05	0.85	0.00	17.0641	0.0000	9mgPlant90s	1	1.1	1	15	11	0	25.10.2019 13:59
24	10.823	110969	262	1051	27	0.04	0.37	0.00	8.7639	0.0000	9mgPlant90s	1	1.1	1	15	11	0	25.10.2019 14:07
25	9.882	110970	1103	13392	83	0.28	5.82	0.65	20.7079	8.8940	9mgPlant90s	1	1.1	1	15	11	0	25.10.2019 14:16
26	1.272	2drift	3453	11995	65	7.28	36.76	2.70	5.0461	13.6170	9mgPlant90s	1	1	1	15	11	0	25.10.2019 14:24
27	2.659	2drift	7863	28220	105	8.06	41.64	3.83	5.1633	10.8854	9mgPlant90s	1	1	1	15	11	0	25.10.2019 14:33
28	0.000	blank	35	35	0	0.00	0.00	0.00	0.0000	0.0000	9mgPlant90s	1	1	1	35	35	0	25.10.2019 14:41
29	10.388	110971	1671	21352	96	0.42	8.86	0.84	21.1718	10.5829	9mgPlant90s	1	1.1	1	15	11	0	25.10.2019 14:50
30	4.830	110972	4849	64432	185	2.72	57.73	4.90	21.2498	11.7903	9mgPlant90s	1	1.1	1	15	11	0	25.10.2019 14:58
31	10.398	110973	2972	78751	206	0.76	32.79	2.61	42.9462	12.5504	9mgPlant90s	1	1.1	1	15	11	0	25.10.2019 15:07
32	10.407	110974	4746	60833	168	1.23	25.29	2.00	20.5038	12.6592	9mgPlant90s	1	1.1	1	15	11	0	25.10.2019 15:15
33	9.342	110975	4844	65247	168	1.40	30.23	2.22	21.5428	13.6462	9mgPlant90s	1	1.1	1	15	11	0	25.10.2019 15:24
34	10.150	110976	5376	71549	198	1.44	30.51	2.54	21.2454	12.0107	9mgPlant90s	1	1.1	1	15	11	0	25.10.2019 15:32
35	10.726	110977	4084	59595	189	1.03	24.04	0.20	23.4209	10.6215	9mgPlant90s	1	1.1	1	15	11	0	25.10.2019 15:41
36	10.686	110978	707	7786	57	0.16	3.10	0.26	19.7237	15.6917	9mgPlant90s	1	1.1	1	15	11	0	25.10.2019 15:49
37	10.650	110979	691	8265	59	0.15	3.31	0.23	21.5215	14.3195	9mgPlant90s	1	1.1	1	15	11	0	25.10.2019 15:57

38	9.519	110980	1552	20359	93	0.42	9.21	0.86	21.8455	10.7367	9mgPlant90s	1	1.1	1	15	11	0	25.10.2019 16:06
39	10.114	110981	2760	40941	125	0.73	17.50	1.34	24.0735	13.0917	9mgPlant90s	1	1.1	1	15	11	0	25.10.2019 16:15
40	9.444	110982	1680	21450	107	0.46	9.79	1.10	21.1567	8.8797	9mgPlant90s	1	1.1	1	15	11	0	25.10.2019 16:23
41	10.183	110983	1636	19879	85	0.42	8.41	0.66	20.1524	12.7030	9mgPlant90s	1	1.1	1	15	11	0	25.10.2019 16:32
42	10.177	110984	4698	59308	173	1.25	25.22	2.42	20.1992	11.8861	9mgPlant90s	1	1.1	1	15	11	0	25.10.2019 16:41
43	10.112	110985	140	584	14	0.01	0.19	0.00	16.4877	0.0000	9mgPlant90s	1	1.1	1	15	11	0	25.10.2019 16:49
44	1.230	3drift	3746	13057	64	8.19	41.42	2.59	5.0568	15.9823	9mgPlant90s	1	1	1	15	11	0	25.10.2019 16:58
45	2.611	3drift	7751	27664	100	8.10	41.57	3.56	5.1348	11.6916	9mgPlant90s	1	1	1	15	11	0	25.10.2019 17:06
46	0.000	blank	21	0	0	0.00	0.00	0.00	0.0000	0.0000	9mgPlant90s	1	1	1	21	0	0	25.10.2019 17:14
47	10.313	110986	2964	79390	861	0.77	33.33	13.35	43.4159	2.4968	9mgPlant90s	1	1.1	1	15	11	0	25.10.2019 17:26
48	10.262	110987	1085	18319	62	0.27	7.68	0.28	28.9357	27.9673	9mgPlant90s	1	1.1	1	15	11	0	25.10.2019 17:35
49	10.891	110988	316	2451	17	0.06	0.92	0.00	16.6699	0.0000	9mgPlant90s	1	1.1	1	15	11	0	25.10.2019 17:43
50	10.243	110989	232	949	20	0.04	0.34	0.00	9.5379	0.0000	9mgPlant90s	1	1.1	1	15	11	0	25.10.2019 17:51
51	9.507	110990	4433	59884	693	1.26	27.26	11.51	21.6433	2.3684	9mgPlant90s	1	1.1	1	15	11	0	25.10.2019 18:03
52	10.175	110991	6243	91268	974	1.67	38.84	15.41	23.2881	2.5205	9mgPlant90s	1	1.1	1	15	11	0	25.10.2019 18:16
53	10.505	110992	2371	35248	80	0.60	14.50	0.56	24.2551	26.0619	9mgPlant90s	1	1.1	1	15	11	0	25.10.2019 18:24
54	10.045	110993	4649	94255	207	1.25	40.63	2.72	32.4779	14.9354	9mgPlant90s	1	1.1	1	15	11	0	25.10.2019 18:33
55	10.390	110994	7326	103150	843	1.92	43.00	12.97	22.3797	3.3163	9mgPlant90s	1	1.1	1	15	11	0	25.10.2019 18:45
56	10.822	110995	7480	100445	965	1.88	40.20	14.35	21.3389	2.8021	9mgPlant90s	1	1.1	1	15	11	0	25.10.2019 18:56
57	10.460	110996	731	9064	36	0.17	3.70	0.00	22.1507	0.0000	9mgPlant90s	1	1.1	1	15	11	0	25.10.2019 19:05
58	9.550	110997	380	2879	66	0.08	1.25	0.38	15.2618	3.3237	9mgPlant90s	1	1.1	1	15	11	0	25.10.2019 19:13
59	9.355	110998	6707	77938	1005	1.95	36.07	17.32	18.4870	2.0830	9mgPlant90s	1	1.1	1	15	11	0	25.10.2019 19:25
60	9.473	110999	6486	88931	177	1.86	40.65	2.35	21.8259	17.2761	9mgPlant90s	1	1.1	1	15	11	0	25.10.2019 19:34
61	9.408	111000	1710	29470	121	0.47	13.52	1.37	28.5717	9.8619	9mgPlant90s	1	1.1	1	15	11	0	25.10.2019 19:42
62	1.320	4drift	3953	13995	81	8.07	41.39	4.57	5.1318	9.0538	9mgPlant90s	1	1	1	15	11	0	25.10.2019 19:51
63	2.566	4drift	7586	27207	104	8.06	41.59	3.88	5.1606	10.7311	9mgPlant90s	1	1	1	15	11	0	25.10.2019 20:00
64	0.000	blank	45	15	153	0.00	0.00	0.00	0.0000	0.0000	9mgPlant90s	1	1	1	45	15	153	26.10.2019 17:52
65	10.570	111001	1194	24534	122	0.29	10.01	1.23	34.9526	8.1672	9mgPlant90s	1	1.1	1	15	11	0	26.10.2019 18:00
66	10.531	111002	1032	21367	122	0.24	8.74	1.24	35.7085	7.0348	9mgPlant90s	1	1.1	1	15	11	0	26.10.2019 18:08
67	10.023	111003	715	7464	71	0.17	3.17	0.44	18.6409	7.2585	9mgPlant90s	1	1.1	1	15	11	0	26.10.2019 18:17
68	10.460	111004	227	1890	27	0.03	0.73	0.00	21.3248	0.0000	9mgPlant90s	1	1.1	1	15	11	0	26.10.2019 18:25
69	9.407	111005	51	282	0	0.00	0.07	0.00	0.0000	0.0000	9mgPlant90s	1	1.1	1	15	11	0	26.10.2019 18:33
70	10.637	111006	4405	48870	171	1.12	19.87	2.00	17.7657	9.9376	9mgPlant90s	1	1.1	1	15	11	0	26.10.2019 18:41
71	9.754	111007	4678	49275	170	1.30	21.85	2.16	16.8485	10.1262	9mgPlant90s	1	1.1	1	15	11	0	26.10.2019 18:49
72	9.678	111008	4970	82698	245	1.39	37.00	3.48	26.6112	10.6222	9mgPlant90s	1	1.1	1	15	11	0	26.10.2019 18:58
73	9.969	111009	4302	79076	229	1.16	34.34	3.11	29.4825	11.0409	9mgPlant90s	1	1.1	1	15	11	0	26.10.2019 19:07
74	10.644	111010	588	5463	59	0.13	2.17	0.23	17.0775	9.6006	9mgPlant90s	1	1.1	1	15	11	0	26.10.2019 19:15
75	9.564	111011	73	416	0	0.00	0.13	0.00	0.0000	0.0000	9mgPlant90s	1	1.1	1	15	11	0	26.10.2019 19:23
76	10.205	111012	2180	22766	123	0.56	9.62	1.30	17.0668	7.4093	9mgPlant90s	1	1.1	1	15	11	0	26.10.2019 19:31
77	10.291	111013	5443	99372	277	1.43	41.82	3.81	29.1517	10.9902	9mgPlant90s	1	1.1	1	15	11	0	26.10.2019 19:40

78	9.790	111014	5784	98477	252	1.60	43.56	3.56	27.1566	12.2354	9mgPlant90s	1	1.1	1	15	11	0	26.10.2019 19:49
79	10.640	111015	7177	104737	1173	1.84	42.63	17.89	23.2042	2.3837	9mgPlant90s	1	1.1	1	15	11	0	26.10.2019 20:01
80	1.294	5drift	4016	14157	51	8.36	42.72	0.84	5.1087	51.0932	9mgPlant90s	1	1	1	15	11	0	26.10.2019 20:10
81	2.582	5drift	7242	25833	104	7.64	39.24	3.87	5.1350	10.1512	9mgPlant90s	1	1	1	15	11	0	26.10.2019 20:19
82	1.000	blank	48	77	0	0.00	0.00	0.00	0.0000	0.0000	9mgPlant90s	1	1	1	48	77	0	26.10.2019 20:27
83	10.604	111016	8107	106644	287	2.09	43.56	3.85	20.8837	11.3225	9mgPlant90s	1	1.1	1	15	11	0	26.10.2019 20:36
84	9.476	111017	8337	87434	261	2.40	39.95	3.85	16.6390	10.3864	9mgPlant90s	1	1.1	1	15	11	0	26.10.2019 20:44
85	9.400	111018	7677	85531	241	2.23	39.40	3.52	17.6936	11.1945	9mgPlant90s	1	1.1	1	15	11	0	26.10.2019 20:53
86	9.565	111019	1641	19717	110	0.45	8.88	1.15	19.9226	7.7150	9mgPlant90s	1	1.1	1	15	11	0	26.10.2019 21:01
87	9.502	111020	71	933	10	0.00	0.36	0.00	0.0000	0.0000	9mgPlant90s	1	1.1	1	15	11	0	26.10.2019 21:09
88	10.013	111021	295	1510	33	0.05	0.60	0.00	10.9480	0.0000	9mgPlant90s	1	1.1	1	15	11	0	26.10.2019 21:18
89	9.309	111022	195	629	30	0.03	0.23	0.00	7.9320	0.0000	9mgPlant90s	1	1.1	1	15	11	0	26.10.2019 21:26
111	10.555	110957*	4618	62343	193	1.18	25.56	2.37	21.6111	10.7965	9mgPlant90s	1	1.1	1	15	11	0	---
112	10.663	110971*	1678	21075	110	0.41	8.52	1.03	20.8085	8.2666	9mgPlant90s	1	1.1	1	15	11	0	---
113	10.419	1109975*	47	429	0	0.00	0.12	0.00	0.0000	0.0000	9mgPlant90s	1	1.1	1	15	11	0	---
114	9.541	111000*	1719	30259	134	0.47	13.69	1.58	29.1782	8.6895	9mgPlant90s	1	1.1	1	15	11	0	---
115	10.452	111015*	7364	104224	615	1.92	43.19	9.20	22.4951	4.6933	9mgPlant90s	1	1.1	1	15	11	0	---
116	9.518	111022*	224	673	19	0.04	0.24	0.00	6.6828	0.0000	9mgPlant90s	1	1.1	1	15	11	0	---
117	7.937	b2150x	1560	12984	108	0.51	7.02	1.34	13.7983	5.2331	9mgPlant90s	1	1.1	1	15	11	0	---
118	8.019	b2152x	510	3412	46	0.14	1.77	0.02	12.4808	75.6598	9mgPlant90s	1	1.1	1	15	11	0	---
119	1.215	6drift	3608	12551	69	7.98	40.29	3.35	5.0492	12.0321	9mgPlant90s	1	1	1	15	11	0	---
120	2.445	6drift	7218	25773	121	8.04	41.34	5.25	5.1402	7.8714	9mgPlant90s	1	1	1	15	11	0	---